CHARACTERIZATION OF THE ENZYME-BOUND FORMS OF COBALAMINS USING SPECTROSCOPY AND COMPUTATIONS

by

Iván Guillermo Pallares

A dissertation submitted in partial fulfillment of
the requirements for the degree of

Doctor of Philosophy

(Chemistry)

at the

UNIVERSITY OF WISCONSIN–MADISON

2015

Date of final oral examination: 8/28/15

The dissertation is approved by the following members of the Final Oral Committee:

Thomas C. Brunold, Professor, Chemistry
Jorge C. Escalante-Semerena, Professor, Microbiology
Silvia Cavagnero, Professor, Chemistry
Clark R. Landis, Professor, Chemistry
Randall H. Goldsmith, Assistant Professor, Chemistry

To Consuela, you blue icy queen,
for blowing up at the worst possible time.
You had me really worried there.

ACKNOWLEDGMENTS

Much advice and support has been provided to me by many individuals. Thank you for making this work possible. For those involved, while I cannot properly acknowledge your contributions within these pages, I have not forgotten your help. My hope is that you approve of the final work, so read up. For those reading out of interest, I hope you find what you are looking for. Please enjoy.

To Thomas, I knew little about cobalamins before I joined your group, but I learned a lot from them and because of them. Thank you for entrusting me with this project, and for all of your help and patience with it. It will be hard forget the experience so long I still have my red trek to ride (the aero bars are great on it!). Your accomplishments in and out of lab are truly inspiring. I wish you success on the awesome work you have coming your way.

To my collaborators, Ted and Jorge, I am very much indebted to you. I enjoyed the days learning about protein preps, all of those meetings filled with B_{12} speak, and counting on you guys as friends. It was a truly unique experience with much more to come, as the B_{12} mystery is far from solved. Flavia, you are set to have a lot of fun.

To the Brunoldites, may we meet again. Please take care of Odie, Penny, and Icky for me in the meantime. Kiyoung, I can't recall exactly why I decided to join the group, but you mentorship had a lot to do with it. Chris and Beth, I'm happy to have my deskmate become a professor, and my GRS buddy become an esteemed scientist. We were by far the "funnest" wave to join the group. Kristine, thank you for the hat. It is truly an heirloom now (it will truly be a dark day when the streamers go down in the America room). Mickey, you were by far the nicest and most polite of everyone in the lab, I wish you success. Steph, I think you are now the "most-fit" group member, keep up the good work. May your love for the talking heads never wane. Nuru, don't tell anyone but you were my favorite lab member, even if you completely dozed off when I gave group meetings.

To the people of the department, your help as been tremendous. To the professors I bugged, thank you for your open door policies and thoughful explanations. The division coordinators, instrument techs, and the shops, what would we do without you? To Mark, teaching pchem lab was a great experience, thank you for hiring me. To Alan, thank you for letting us take care of Colt, he is a great thesis writing pal.

To my friends, you didn't just make the grad school experience bearable, you made it enjoyable. Special words go to old roomies and all those folks that have gone by the 313 N. Livingston. The personal value of my thesis is immeasurable compared to the memories I hold of our times together.

To my adopted U.S family (Ann, Walt, and Huntley), thank you for taking me in.

To Frank, I have learned a lot from you and I didn't even notice it. I got every ounce of craftiness and ourdoorsmanship I have from being on Creighton. I have used a lot of it while in Wisconsin.

A my Papá, Iválllri, y my familia al Sur, me gustaría mucho haber tenido tu presencia en my defensa. Los pienso mucho.

A my linda Mamá, gracias por todo lo que me has dado. He logrado mucho con tu alluda.

–Iván Guillermo

CONTENTS

LIST OF TABLES

LIST OF FIGURES

CHARACTERIZATION OF THE ENZYME-BOUND FORMS OF COBALAMINS USING SPECTROSCOPY AND COMPUTATIONS

Iván Guillermo Pallares

Under the supervision of Professor Thomas C. Brunold
At the University of Wisconsin-Madison

While structural information is available for many cobalamin-dependent enzymes, their catalytic mechanisms remain to be completely eludicated. Notably, specroscopic characterization of these enzymes in the presence of their B_{12} cofactors and corresponding substrates is lacking. Magnetic circular dichroism and electronic paramagnetic spectroscopies in particular provide a sensitive probe of cobalamins in their reduced states. As reduced cobalamins are required in the catalytic cycles of ACATs, spectroscopic methods employed in conjuncton with computational modeling provide novel insights into the mechanism of these enzymes.

Chapter 1 highlights the main aspects of cobalamin chemistry and summarize recent crystallographic efforts of B_{12}-dependent enzymes. Chapter 2 presents the spectroscopic characterization of nitrosylcobalamin (NOCbl), a recently crystallized form of cobalamin implicated in the nitric oxide cycle and in the inactivation of cobalamin-dependent enzymes. Chapter 3 presents the spectroscopic characterization of Co(II)rrinoids bound to the active site of the CobA ACAT, involved in scavenging and the *de novo* synthesis of AdoCbl in *Salmonella enterica*. Our spectroscopic methods allow for determination of the five-coordinate to four-coordinate Co(II)rrinoid equilibrium formed by various CobA variants. In conjunction with crystallographic data and computational modeling, our results provide molecular

level information on how CobA facilitates the formation of the Co(I)Cbl supernucleophile required in the catalytic cycle. Chapters 4 and 5 present spectroscopic characterization of the Co(II)Cbl in the active site of the EutT ACAT from *Salmonella enterica* involved in the catabolism of ethanolamine. EutT is purported to contain a divalent transition metal ion critical in maintaining catalytic function, however no crystal structure of this enzyme or related homologues is available. Specifically, chapter 4 presents spectroscopic studies of Co(II)Cbl in the presence of Fe^{2+} and Zn^{2+} containing forms of the wild-type EutT enzyme and selected variants, aimed at elucidating the role of specific amino acids in the putative metal binding site on the formation of Co(I)Cbl species. Chapter 5 presents the spectroscopic characterization of Co^{2+} containing EutT, disclosing the structure of the divalent metal binding site and the presence of protein-derived cysteine residues serving as ligands.

Thomas C. Brunold

ABSTRACT

Cobalamins and related B_{12} species are an important class of biological molecules involved in the functioning of various metabolic processes. These processes employ cobalamin-dependent enzymes to catalyze various life-sustaining chemical reactions. Examples of such enzymes in humans, such as methionine synthase (MetH), methylmalonyl Co-A mutase (MMCM), and adenosyltransferase enzymes (ACATs), have been under extensive study. The MetH enzyme is involved in the folate, methionine, and S-adenosylmethionine cycles. MMCM is important for the metabolism of fatty acids in the citric acid cycle, with the human ACAT (hATR) serving a critical role in maintaining the levels of the AdoCbl cofactor required by this enzyme. Additional cobalamin-dependent enzymes are also known in bacterial systems, involved in processes such as methanogenesis, biosynthesis of acetyl-CoA, and dehalorespiration.

While structural information is available for many cobalamin-dependent enzymes, their catalytic mechanisms remain to be completely eludicated. Notably, specroscopic characterization of these enzymes in the presence of their B_{12} cofactors and corresponding substrates is lacking. Magnetic circular dichroism and electronic paramagnetic spectroscopies in particular provide a sensitive probe of cobalamins in their reduced states. Particularly, as reduced cobalamins are required in the catalytic cycles of ACATs, spectroscopic methods employed in this work in conjuncton with computational modeling provide novel insights into the mechanism of these enzymes.

In this context, the following chapters present experimental results that ex-

pand upon previous work on a number of fronts. Chapter 1 highlights the main aspects of cobalamin chemistry and summarize recent crystallographic efforts of B_{12}-dependent enzymes. Chapter 2 presents the spectroscopic characterization of nitrosylcobalamin (NOCbl), a recently crystallized form of cobalamin implicated in the nitric oxide cycle and in the inactivation of cobalamin-dependent enzymes. Chapter 3 presents the spectroscopic characterization of Co(II)rrinoids bound to the active site of the CobA ACAT, involved in scavenging and the *de novo* synthesis of AdoCbl in *Salmonella enterica*. Our spectroscopic methods allow for determination of the five-coordinate to four-coordinate Co(II)rrinoid equilibrium formed by various CobA variants. In conjunction with crystallographic data and computational modeling, our results provide molecular level information on how CobA facilitates the formation of the Co(I)Cbl supernucleophile required in the catalytic cycle. Chapters 4 and 5 present spectroscopic characterization of the Co(II)Cbl in the active site of the EutT ACAT from *Salmonella enterica* involved in the catabolism of ethanolamine. EutT is purported to contain a divalent transition metal ion critical in maintaining catalytic function, however no crystal structure of this enzyme or related homologues is available. Chapter 4 presents spectroscopic studies of Co(II)Cbl in the presence of Fe^{2+} and Zn^{2+} containing forms of the wild-type EutT enzyme and selected variants, aimed at elucidating the role of specific amino acids in the putative metal binding site on the formation of Co(I)Cbl species. Chapter 5 presents the spectroscopic characterization of Co^{2+} containing EutT, disclosing the structure of the divalent metal binding site and the presence of protein-derived cysteine residues serving as ligands.

The spectroscopic and computational approach presented for the characterization of Co(II)rrinoids is a promising basis for the study of related cobalamin-dependent enzymes, many of which also require Co(II)rrinoids along their catalytic cycles. Structural and kinetic studies of these enzymes have been presented previously, however spectroscopic characterization of the generated Co(II)rrinoid species remains to be determined. The spectroscopic data obtained for these cobalamin species is also a useful benchmark for theoretical methods. Computational modeling of the electronic properties of Co(II)Cbls requires rigorous incorporation of correlation and spin-orbit coupling effects to accurately model observed spectroscopic properties. Spectroscopic data can thus be used to calibrate computational models of cobalamin-dependent enzymes and provide a novel approach for the study of their catalytic cycles, particularly with regards to reactive intermediates and transition states.

Chapter 1

Overview of Cobalamin Chemistry.

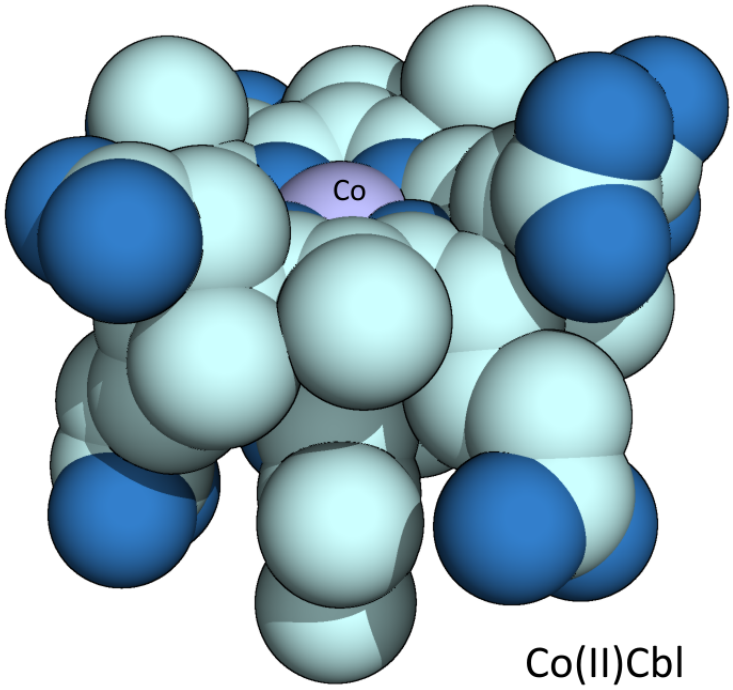

1.1 Introduction

Carbon is one of the fundamental building blocks of life. Alongside hydrogen, nitrogen, oxygen, and sulfur, it makes up the scaffold of many biomolecules such as proteins, nucleic acids, lipids and carbohydrates. Notably, as much as 99% of the body weight in humans can be accounted for by these four elements, in addition to small amounts of sodium, potassium, chlorine, calcium, and magnesium ions as well as phosphorus.[1] Additional trace metals constitute the remaining 1%, among these the transition metals. However, despite their low relatively availability, considerable interest has been drawn by trace elements and their roles in biological systems. In the context of human health for instance, the interplay between metals and the nervous system is currently a very active field particularly in relation to neurodegenerative diseases.[2, 3, 4] With regards to their interactions with biomolecules, estimates have suggested that about half of all proteins incorporate trace metals.[5] Transition metals in their ionized forms in particular are required cofactors for the activity of as many as 30% of all known enzymes.[6] These metal-containing "protein catalysts", or metalloenzymes, are responsible for facilitating some of the most important of life-sustaining chemical reactions.[7] For instance, the photo-catalyzed oxidation of water (H_2O) to yield hydrogen and oxygen gas (H_2 and O_2 respectively) is carried out by a manganese-oxo cluster (Mn_4Ca) in the oxygen evolving complex (OEC).[8, 9] The OEC is the source of the O_2 in the atmosphere that supports all aerobic life.[10] Various oxygenases use this molecular oxygen (O_2) to oxidize organic substrates, using activated O_2 species generated in

their active sites to functionalize even the most unreactive bonds.[11] For instance, the methane monoxygenases (MMO) are capable of carrying out the oxidation of the relatively inert C–H bonds of methane to produce methanol, employing bi-nuclear iron or copper cofactors.[7] Similarly, cytochrome-P450 enzymes, containing an iron-porphyrin cofactor, have been dubbed "nature's blowtorch" due to their combined high specificity and high reactivity towards substrates.[12] Various copper- and iron-containing metalloenzymes play an important role in facilitating these redox reactions, efficiently transferring electrons via changes in the oxidation state of their metal cofactors. These include blue-copper proteins, cytochromes and iron-sulfur proteins such as ferrodoxins and rubredoxins.[13, 14] Furthermore, the molecular oxygen involved in many biochemical reactions is solubilized and transported by metal containing proteins.[15] Most famously, the myoglobin and hemoglobin transport dioxygen across tissues in vertebrates via a prosthetic heme group. A similar task is carried out by hemerythrin, a bi-nuclear iron enzyme, in some marine invertebrates and by hemocyanin, with a bi-nuclear copper center, in mollusks and arthropods.[16, 17, 18] These oxygen transport enzymes reversibly bind oxygen and exhibit a distinct color change observable to the naked eye depending on the presence of oxygen. For instance, the binding of O_2 to the heme center in hemoglobin (Hb) results in a shift from the characteristic purple hue of deoxygenated-Hb to the red color of oxygenated-Hb. Similarly, hemerythrin and hemocyanin, colorless in the absence of oxygen, turn violet-pink and blue respectively when oxygen is bound to their metal centers, the latter giving rise to the âŁœblue bloodâŁž in horseshoe crabs and squid.[18, 19] While the previous

examples focus on reactions involving oxygen, reactions catalyzed by metalloenzymes in anaerobic organisms can also be noted. Nitrogenase enzymes carry out the difficult task of nitrogen fixation using unique iron-molybdenum (FeMo) or related cofactors to catalyze the reduction of nitrogen gas (N_2) to ammonia, enabling the bioavailability of nitrogen for other organisms.[20, 21] Alongside these, the Fe or Ni containing hydrogenase, carbon monoxide dehydrogenase (CODH), acetyl-SCoA synthase (ACS), and methyl-coenzyme M reductase (MCR) enzymes are involved in the processing of hydrogen, carbon dioxide, and carbon monoxide gases in various microorganisms, allowing them to thrive in the absence of solar energy.[22] Thermophillic methanogenic bacteria for instance, have been found to grow around hydrothermal vents, or "black smokers", at the bottom of the oceans, sustaining their metabolism via the oxidation of H_2 and reduction of CO to methane catalyzed by metalloenzymes.[23] The ecosystems supported by these vents are considered to be some of the most ancient biomes, possible dating back to the origin of life.[22]In the context of human technology, various biomimetic approaches aimed at understanding and replicating reactions catalyzed by metalloenzymes are currently being pursued.[24] Success in this area would achieve a "holy grail" for chemistry: cheap and efficient man-made catalysts that can be used in the context of "green" chemistry and biotechnology.[7]

The properties of transition metals that characterize their utility in metalloenzymes can be related to the properties of their chemically reactive, or valence, electrons.[25] Unlike other elements, the valence electrons of transition metals can be said to formally occupy a partially filled d-sub shell, and can readily accept or

donate electrons from/to other species. For instance, common forms of iron (Fe) and manganese ions (Mn) in the +2 oxidation state [Fe(II) and Mn(II)], described as d^6 and d^5 ions respectively where the superscripts note the number of electrons in the 3d sub-shell, are readily oxidized under certain conditions, resulting in formal loss of electrons. In the presence of dioxygen (O_2), oxidation results in formation of metal-oxo species, such as Fe_2O_3 (iron oxide, a component of rust, and a Fe(III), d_5 species) and MnO_2 (main component of pyrolusite, a naturally occurring ore, and a Mn(IV), d_3 species),[26] which can be reversed by the reduction of the metal center. Various transition metals complexes also have unique optical properties. Dissolved in aqueous solution many of these give rise to various colors depending on their oxidation state in the form of aqua cations, or $[M(H_2O)_6]^n$ (where M is the metal, present with six water molecules bound, and *n* refers to the overall charge of the complex), among others. Furthermore, the valence electrons of transition metals can form stable bonds with many side chain residues of proteins, leading to their incorporation into these biomolecules. In the context of coordination chemistry, metalloenzymes can thus be considered an elaborate metal complex where the metal center and bound amino acid side chains (serving as ligands) constitute the reactive prosthetic group where chemistry occurs—the enzyme active site.[27] The chemical properties of these metal centers are sensitive to the nature of the metal-ligand bonds present in the enzyme active site, partly as the coordination geometry of these sites directly affects the properties of the 3d valence electrons. Different geometries can result in various arrangements of electrons in the 3d shell, giving rise to different spin states (related to the number of unpaired electrons in

each configuration), thus altering the metal's electronic structure. Differences in spin state directly affect the magnetic properties of these sites as a function of the ligand environment. Changes to the electronic structure of the metal center can also result in modulation of its oxidation / reduction potential (related to the free energy required to accept or give up electrons) and optical properties. For instance, the color change observed in samples of hemoglobin and hemerythrin in the presence of oxygen is a direct reflection of a change in the electronic structure of the Fe center when bound to O_2.[19] Notably, with the exception of Zn(II) ions and similar d_{10} species present with a filled 3d shell, it is the optical and magnetic properties of transition metals complexes that make these amenable to study with a variety of physical methods.[13, 24, 27] Among these methods, absorption, resonance raman, magnetic circular dichroism, electron paramagnetic resonance spectroscopies and related techniques have been successfully applied to elucidate the nature of reactivity of various metal-containing systems. These spectroscopies are particularly sensitive to the optical and magnetic properties of transition metal ions, providing and experimental window into the electronic structure of these species.[5, 7, 24] In conjunction with structural information (from X-ray crystallography, or solution NMR techniques), computational approaches, and information from enzyme kinetics, spectroscopic techniques have afforded bountiful insights into the catalytic mechanism employed by many metalloenzymes. From this large body of work, an intimate relationship between geometric structure of a metalloenzyme active site and the electronic structure of its metal center has been observed, shown to be directly related to biological function.

1.2 Cobalt in Biological Systems

Cobalt (Co) is the 27th element in the periodic table, with the most abundant isotope being ^{59}Co. Historically, it has been used to give color in jewelry, paint, and ceramics, (particularly Chinese porcelain) in the form dyes, some as alumina salts ($CoAl_2O_4$). Before its discovery as an element by Georg Brandt in 1735, smelting of cobalt containing ores in search of more valuable metals yielded little material of value and instead resulting in the release of poisonous arsenic- and sulfur- containing oxides from the ore. Medieval miners referred to these as kobold ores due to their associated bad fortune, in reference to the creature from German folklore thought to inhabit the mines, and is purported to give rise to the element's name.

Relative to other transition metals, Co is of relatively low abundance in earth's crust and in seawater (Figure 1.1[1]).[28] Similarly, only a very small subset of metalloenzymes have been found to directly bind Co into their active sites, with some species capable of using other ions to sustain activity.[29, 30] Most of the biological requirements for Co in living systems instead stems from its use in the form of cobalamin and related species. Cobalamins belong to a class of molecules referred to as corrinoids, characterized by the presence of a highly modified tetrapyrrole macrocycle termed the coring ring, which serves as a tetradentate ligand to a bound Co ion (Figure 1.2).[?] The Co ion in this complex is redox active in biological systems, with +3 (oxidized), +2 (reduced), and +1 (supperreduced) oxidation states known. Notably, the oxidation estate of the Co ion modulates the presence of additional ligands bound to the available axial sites. In the superreduced state, the

[1] U.S Geological Survey Fact Sheet 087-02

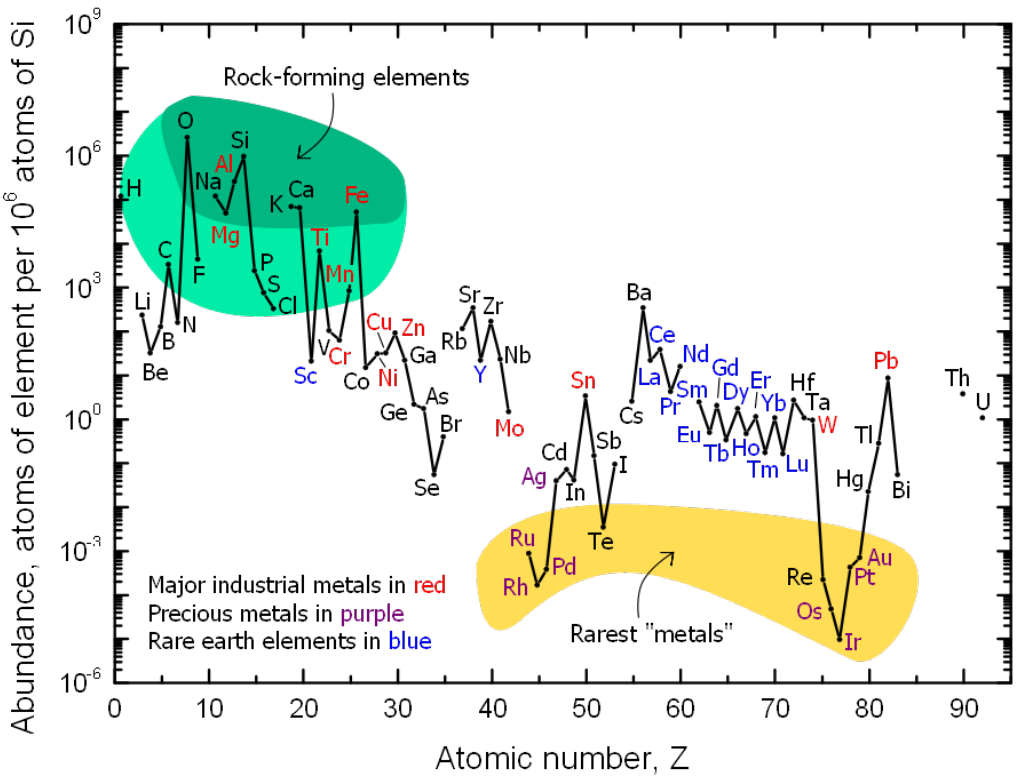

Figure 1.1: Relative abundance of the chemical elements relative to silicon in Earth's upper continental crust. The rarest elements in the crust are highlighted in yellow and common elements in green. From U.S. Geological Survey Fact Sheet 087-02.

axial ligand sites in corrinoids are vacant in aqueous solution. These species are among the strongest biological nucleophiles in alkylation reactions.[31, 32] In reduced cobalamins [or Co(II)Cbl], a dimethylbenzimidazole base at the terminal end of an intramolecular nucleotide loop attached to the corrin ring ligates to the Co ion at one of the axial positions available, noted as the "lower" Coα site. In the case of reduced cobinamides [or Co(II)Cbi$_+$], referring to incomplete corrinoids lacking the terminal DMB base and nucleotide loop, a solvent derived water molecule serves as the ligand at this site. A variety of related species have also been observed with

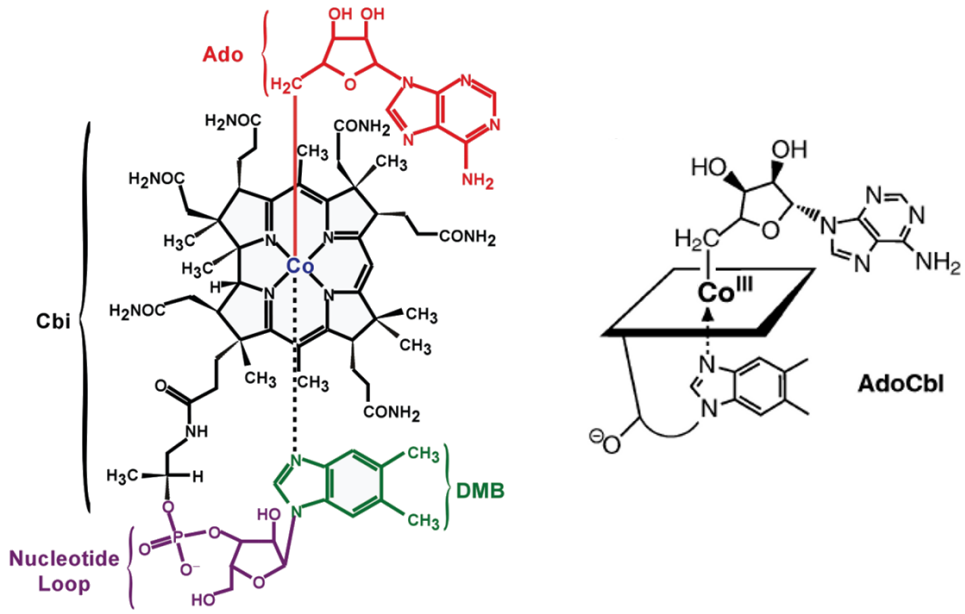

Figure 1.2: Chemical structure of adenosylcobalamin (AdoCbl), also known as coenzyme-B_{12} (left). Relevant structural motifs noted in the text are highlighted in color. Abbreviations refer to Ado, adenosyl; DMB, dimethylbenzimidazole; and Cbi, cobinamide. The condensed structure of AdoCbl is shown (right).[47]

different terminal bases, however the majority of enzymes that require the cobalt-corrin motif for activity predominately employ cobalamins.[33, 34] In their oxidized forms cobalamins are present with a variable ligand in the "upper" Coβ site, with the major forms encountered in biological systems containing hydroxyl– (OH), nitrosyl– (NO), gluthathionyl– (GS), methyl- (CH_3), and adenosyl– (Ado)moieties. These last two species in particular are required cofactors for the activity of various methyltransferase and B_{12}-dependent enzymes respectively.[34] Upon light exposure, the upper ligand of cobalamins can become photolyzed resulting in the formation of Co(II)Cbl and ligand-based radical.[35, 36] For instance, hydoxocobalamin (HOCbl) has been shown to produce hydroxyl radicals useful for DNA footprinting studies

upon light exposure (with wavelengths >300 nm). Oxidation of Co(II)Cbl in the presence of molecular oxygen regenerates HOCbl, thus making the overall process catalytic.[37, 38] Notably, photolysis of the upper ligand in the case AdoCbl and MeCbl cofactors results in inactivation of their respective enzymes.

Despite the prevalence of enzymes requiring cobalamin across many organisms, the complete enzymatic machinery necessary for the biosynthesis of this molecule is only found in some Bacteria and Archae.[39] Thus, many organisms intake this molecule in the form of vitamin-B_{12} (in reference to oxidized cobalamin species present without the Ado moiety attached), and are thus reliant on sufficient amounts being present in their diet. The growth of pythoplankton requires vitamin-B_{12} for instance, impacting food webs in marine ecosystems, and has been shown to rely on the availability of this vitamin from bacterial sources.[40] Specifically, animal derived foods are the most prevalent sources of B_{12} for humans. Ruminants in particular, which obtain this species from the bacteria in their digestive track, are a major source.[41] Significant stores of B_{12} are present in the liver, and only small dietary amounts are required (~3 μg DV), making deficiency rare in most communities except strict vegetarians (lacto- and ovo- vegetarians obtain enough vitamin from eggs and milk) and the elderly due to inefficient digestive uptake.[42] Non-animal sources of vitamin-B_{12} have been suggested in the form of soyweed-fermented and algae-derived foods.[43] Nori in sushi derived from *Porphyra yezoensis* was shown to contain B_{12}, which acquire it from symbiotic relationships with bacteria,[44, 45] however, its bioavailability has been debated.[46] Various enzymes are involved in the uptake of cobalamin from food in humans (and similarly in mammals),

starting in the oral cavity with the release of haptocorrin from salivary glands (Figure 1.3). Various other proteins (among these the transcobalamins and intrinsic

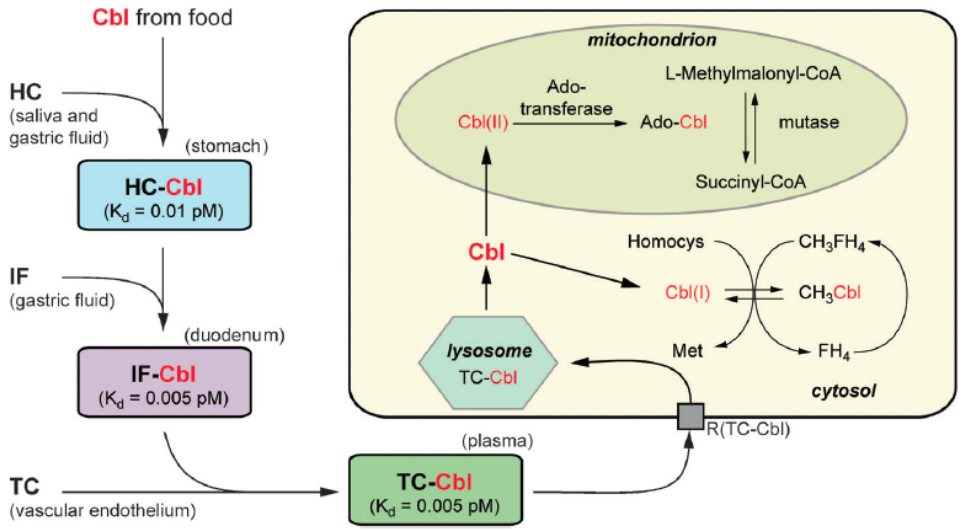

Figure 1.3: Schematic outline of cobalamin uptake and transport in mammals. Abbreviations refer to Cbl, cobalamin; TC, transcobalamin; HC, haptocorrin, IF, intrinsic factor; R(TC-Cbl), uptake receptor of the TC-Cbl complex; homocys, homocysteine; met, methionine; FH_4, tetrahydrofolate; and CH_3FH_4, methyltetrahydrofolate.[47]

factor) are involved in the trafficking of this vitamin from the digestive track to the bloodsteam. These cobalamin transport proteins exhibit such high affinity for cobalamins (K_d ~10-15 M) that proteolysis is required for its release.[47] At their final destination in cells, these protein-B_{12} complexes are internalized and degraded in lyzosomes, where further processing of the vitamin into its active forms occurs. In this process, the CblC enzyme is postulated to facilitate the formation of Co(II)Cbl species via removal of the upper axial ligand present in the various vitamin forms.[48] Conversion of Co(II)Cbl to AdoCbl is carried out by the human ATP:Co(I)rrinoid adenosyltransferase (hATR) enzyme followed by uptake by methylmalonyl-CoA

mutase (MMCM),[49] one the two AdoCbl-dependent enzymes in humans. The second enzyme, methionine synthase (MetH), employs MeCbl as its cofactor, and it is able to generate this species from Co(II)Cbl.[47] These enzymes are involved in the metabolism of fatty acids (MMCM), and of folate, S-adenosylmethionine, and the amino acids cysteine and methionine (MetH). Malfunctioning of MMCM, MetH, or in the cofactor trafficking systems, has been shown to result in various human diseases, ranging from methylmalonic academia to pernicious anemia, characterized by impaired DNA synthesis and neurological damage.[48, 50]

Two enzymatic pathways including over 20 enzymes have been identified in bacteria and archaea devoted to the complete biosynthesis of cobalamins. These convert a uroprophyrinogen-III (UroIII) precursor into AdoCbl, and differ at the point at which the cobalt ion is incorporated into the corrin macrocycle and whether they occur anaerobically (early insertion of Co) or aerobically (late insertion).[39, 51] The elucidation of these pathways is a highlight in enzymology, as the enzymes involved carry out many unique chemical steps. These include multiple methylations of the uroprophyrinogen-III scaffold, cobalt insertion, ring contraction via removal of a methylene moiety, and various side chain modifications. Addition of the axial ligand occurs via the synthesis and attachment of the nucleotide loop and terminal base a corrin ring sidechain, as well as adenosylation of the Co ion. In *Salmonella enterica*, this latter reaction is catalyzed by the CobA enzyme, an ATP:Co(I)rrinoid adenosyltransterase (ACAT). Although UroIII is a common tetrapyrrole primogenitor to other biologically synthesized macrocycles (including heme, chlorophyll and the nickel-containing F450 cofactor), it has been postulated that this precursor

original arose initially to serve B_{12} synthesis in the anaerobic, pre-oxygen, earth.[39] This idea has been supported by the asymmetry of UroIII, thought to be important

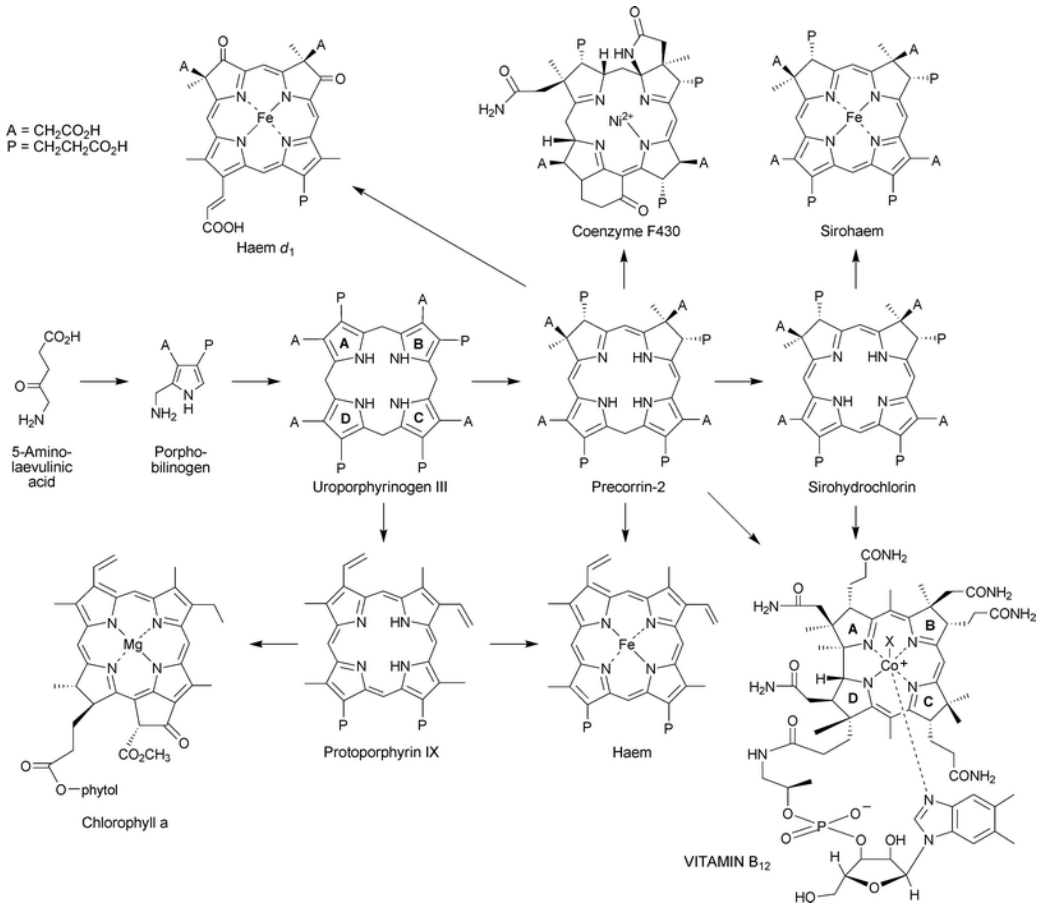

Figure 1.4: Summary of chemical intermediates observed in the biosysnthesis of various tetrapyrroles. Note the common Uroprophyrinogen III precursor in the various pathwys.[51]

for the ring contraction step that generated the corrin structure that is absent in the biosynthesis of the other biological macrocycles (Figure 1.4).[51] Furthermore, studies of the distribution of B_{12} across all life forms suggests that requirement of B_{12} is negatively correlated with the use of oxygen in metabolism.[39] Multicellular plants and fungi are not known to employ cobalamin in their metabolism, and

B_{12} auxotrophy in animals largely arises from the presence of MMCM and MetH in their genomes. In contrast, many examples of catalytic reactions employing cobalamins can be found, particularly in anaerobic bacteria and methanogens.[47, 52]

1.3 Cobalamin-Dependent Enzymes

Recent reviews are available that cover the detailed chemistry of cobalamin dependent enzymes.[47, 52, 53] Here these will only be summarized, instead focusing on the latest structural information obtained for the major types, and how it can be related to their biological function based on available spectroscopic evidence. The large variety of reactions catalyzed by the cobalamin cofactors can be contextualized by how the corresponding enzymes take advantage of the redox properties of this cofactor, specifically how they modulate the interaction between the cobalt ion and its axial ligands. Based on the cobalamins species generated in their catalytic cycles, these enzymes can be associated into four distinct groups, consisting of AdoCbl-dependent enzymes, methyltransferases, cobalamin-dependent dehalogenases, and the adenosyltransferase enzymes.

(i) AdoCbl-dependent enzymes: AdoCbl-dependent enzymes are characterized by the controlled homolytic cleavage of the Co–C(Ado) bond of AdoCbl in response to substrate binding. This process yields Co(II)Cbl and a reactive Ado-based (Ado•) radical, which is propagated to the enzyme substrate with a subsequent hydrogen abstraction to yield Ado–H. Radical mediated rearrangement of the substrate proceeds, followed by yield of the product after hydrogen abstraction of Ado–H to regenerate Ado•.[52, 53] This motif recombines with Co(II)Cbl at the end of the cycle

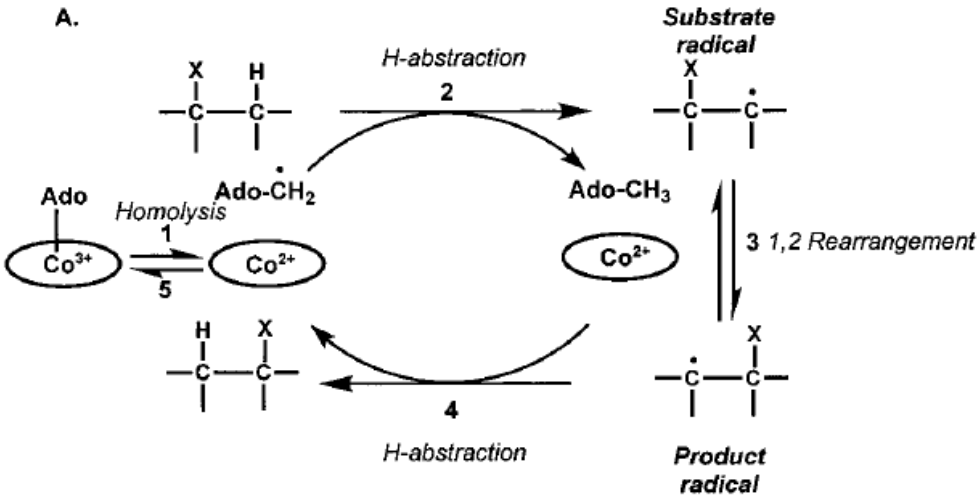

Figure 1.5: Generalized reaction cycle in AdoCbl-dependent enzymes. Various steps in the catalytic mechanism are highlighted with numbers. Although the lower axial ligand is not shown, this species remains bound to the Co ion along the catalytic cycle. Note that ribonucleotide reductases follow a different overall mechanism, but share the initial AdoCbl homolysis and final radical recombination steps (steps 1 and 5). The migrating group, X, can constitute carbon, hydroxyl, or amine moieties.[52]

to form AdoCbl (Figure 1.5). These enzymes have been historically subdivided into three families bases on the nature of the migrating group during the radical rearrangement, and catalyze a variety of reactions, such as dehydration or deamination of substrates to yield aldehydes (diol dehydratase, glycerol dehydratase, and ethanolamine ammonia lyase), the migration of primary amine groups (by D-ornithine 4,5-aminomutase and L-leucine 2,3-aminomutase) and various carbon skeleton rearrangements (methylmalonyl-CoA mutase (MMCM) and glutamate mutase (GM)).[54] Two additional sub-classes differing on the nature of the ligand present in the Coα site during turnover are also noted, Class I or Class II, depending on whether or not the DMB remains ligated to the Co ion during enzyme turnover.

Relative to other steps in the enzyme mechanism, a lot of attention has been devoted at elucidating the approach by which the enzymes facilitate the homolysis of the Co–C(Ado) bond. Notably, while the Co–C(Ado) bond of AdoCbl is relatively stable in solution (with an approximate bond dissociation energy of 31.5 kcal/mol, comparable to weak covalent bonds),[52] in the active sites of these enzymes a significant weakening of this bond occurs (by ~17 kcal/mol)[52, 45] resulting in acceleration of the homolytic cleavage rate of this bond by 12 orders of magnitude. The reverse reaction is essentially barrierless as it involves the recombination of two radical species to form a stable bond, thus the overall equilibrium between bound and dissociated states depends on their relative free energies. This observation suggested two possible approaches upon with bond homolysis can be favored in the presence of the enzyme, one case involving destabilization of the AdoCbl species, and another the stabilization of the dissociated products.[47]

In the case of MMCM and GM, crystallographic evidence have revealed that the AdoCbl cofactor is present in a unique conformation where the DMB is dissociated from the Co ion, and a protein-derived histidine residue occupies the lower axial site instead (described as a base-off/his-on conformation, and a defining feature of Class I enzymes).[55, 56] An aspartate residue interacts with the histidine moiety via a hydrogen bond. Alongside a downstream glycine moiety, these make up the characteristic DXHX2G catalytic triad of these enzymes (Figure 1.6).[47, 57] Spectroscopic studies of MMCM and GM indicate that the electronic structure of AdoCbl is largely unperturbed in the presence of the enzyme with substrate. Low-temperature absorption and magnetic circular dichroism spectroscopy do not

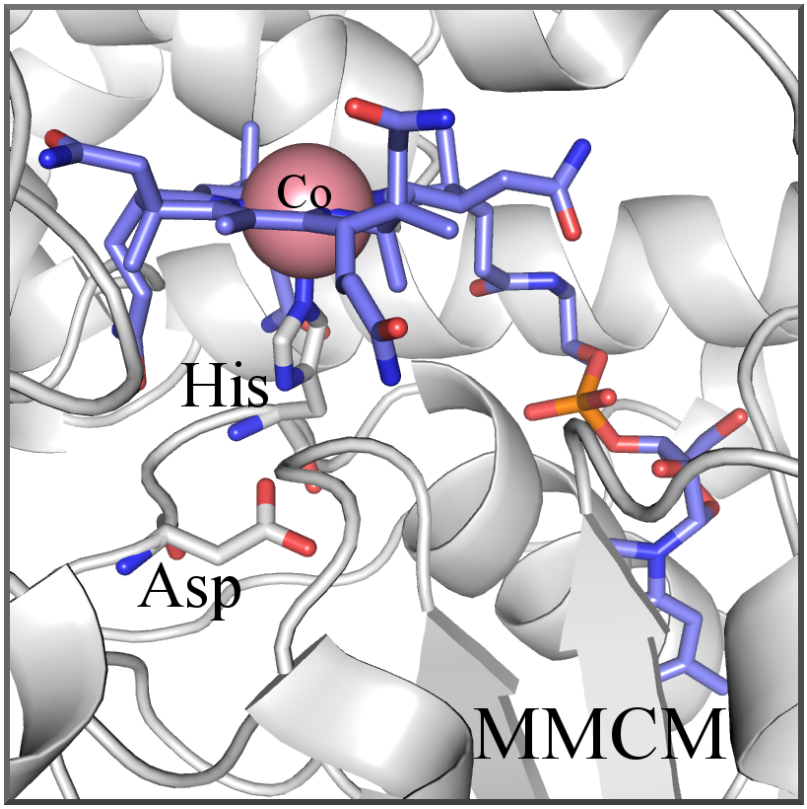

Figure 1.6: Crystallographic structure of the methylmalonyl-CoA mutase (MMCM) active site with Co(II)Cbl bound (blue sticks). Note the presence of a histidine moiety endogenous to the protein scaffold bound to the lower axial ligand side of Co(II)Cbl. The nearby glutamate residue which hydrogen bonds with histidine is also shown. Generated from PDB entry 2XIJ. Background protein structure is shown in white, relevant amino acid residues are highlighted as sticks, and the cobalt ion of cobalamin is shown as a purple sphere.

show significant differences from those of AdoCbl free in solution.[58] Furthermore, resonance Raman (rR) experiments of AdoCbl bound to MMCM with substrate did not indicate any changes consistent with weakening of the Co–C(Ado) bond.[59] However, analogous spectroscopic evidence of Co(II)Cbl bound to MMCM and GM noted significant changes to the electronic structure of this species relative

to free Co(II)Cbl, attributed to the stabilization of the enzyme-cofactor complex based on computational studies.[60, 61, 62] In the context of the crystal structure, these spectroscopic results suggest that the DXHX2G triad is involved in the stabilization of Co(II)Cbl possibly by modulation of the Co–N(His) interaction via changes to the protonation state of the His and Glu residues.[56] Additional experimental evidence for these enzymes, focusing on the interactions of the Ado• moiety with the enzyme active site, highlighted the role of polar interactions present in the Ado-binding pocket in stabilization the dissociated state in the presence of substrate. Thus, the overall experimental data available for Class I enzymes indicated that the stabilization of the post-homolysis products is critical contributor to the large enzymatic acceleration observed.

In the case of Class II enzymes, the AdoCbl cofactor bound in the enzyme active retains its DMB ligand. This class of enzymes includes ethanolamine ammonia lyase (EAL), which catalyzes the formation of acetaldehyde and ammonia from ethanolamine. The crystal structures of EAL highlights distinct structural differences from those of Class I enzymes, notwithstanding their difference in cofactor binding modes (Figure 1.7).[63, 64] Little spectroscopic information is available for these enzymes, and no structure is available with AdoCbl bound to the active site, however the absence of a DXHX2G indicate that different mechanism for the stabilization of Co(II)Cbl must occur, if present. The B_{12}-dependent ribonucleotide reductases (RNRs) are also included with Class II enzymes. RNRs share the initial AdoCbl homolysis step of other AdoCbl-dependent enzymes, but propagate the Ado radical to an enzyme-derived cysteine residue instead. The crystal structure

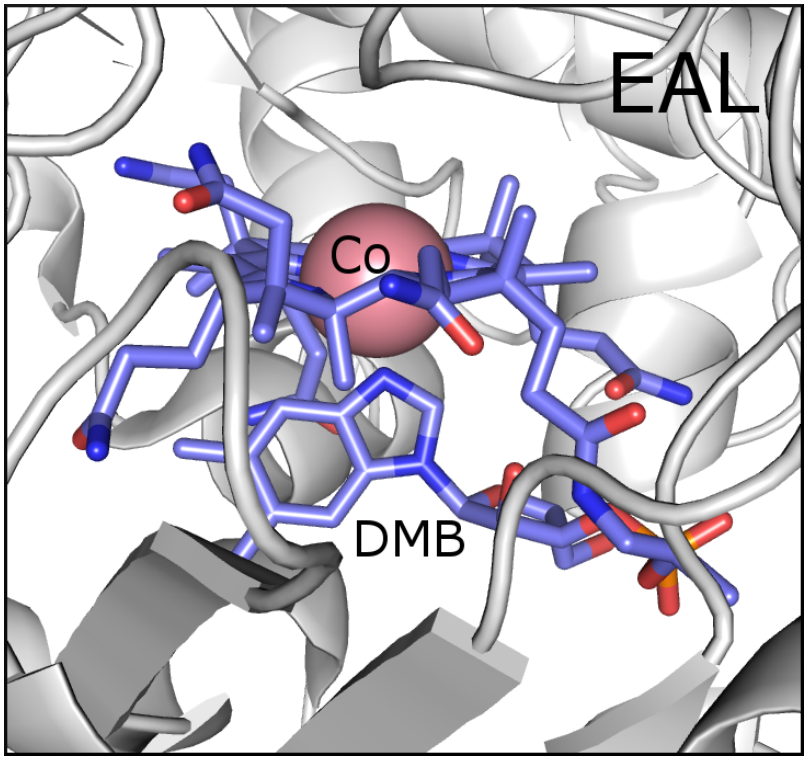

Figure 1.7: Crystallographic structure of the ethanolamine ammonia lyase (EAL) active site with Co(II)Cbl bound (blue sticks). Note the presence of DMB moiety bound to the lower axial ligand side of Co(II)Cbl. Generated from PDB entry 3ANY. Background protein structure is shown in white, and the cobalt ion of cobalamin is shown as a purple sphere.

of RNR from *Lactobacillus leichmannii* with AdoCbl bound confirmed its presence in a base-on conformation similar to other Class II enzymes. However, a unique lengthening of the Co–C(Ado) bond was observed, which at a distance of 2.7 Å is significantly longer than that found in the absence of enzyme (~2.0 Å).[65] This finding highlights an alternate approach by which bond homolysis of AdoCbl is promoted in Class II enzymes, possibly involving the destabilization of the AdoCbl species via a "mechanochemical" triggering mechanism.[47] However spectroscopic characterization of the relevant species remains to be reported. While crystal structures

of the aminomutases are available (which show AdoCbl binds in a base-off/his-on form similar to Class I enzymes), no spectroscopic information for these enzymes is available.[66]

(ii) Methyltransferases: Various B_{12}-dependent enzymes involved in the transfer of methyl groups have been identified in a variety of organisms. In comparison to AdoCbl-dependent enzymes, methyltransferases cycle between the Co(I) and Co(III) oxidation states of their cobalamin cofactors, concomitantly with changes in the coordination environment from hexacoordinate to tetracoordinate (Figure 1.8).[53] The most extensively studied enzyme in this class is methionine synthase (MetH), present in numerous organisms, including humans. This enzyme catalyzes the formation of methionine from homocysteine. Homocysteine is required in mammals for the biosynthesis of cysteine, mediated by Cystathionine β-synthase (CBS) and Cystathionine λ-lyase. Methionine is particularly important in maintaining the levels of S-adenosylmethionine (SAM), an important biomolecule in a variety of biological processes including DNA methylation.[67] Furthermore, the methyl group transferred to homocysteine by MetH originates from methyltetrahydrofolate (CH_3–THF), involving this enzyme in the modulation of folate derivatives in the cell. Thus, MetH can be considered a methyl group reservoir, playing a central role coupling the folate and methionine cycles. The catalytic cycle in this enzyme involves the reaction of CH_3–THF with Co(I)Cbl to generate THF and MeCbl. Subsequent reaction of MeCbl with homocysteine to regenerate Co(I)Cbl yields the methionine product.[47, 52] Crystallographic studies of MetH indicated that it is a large modular enzyme with four separate domains, one of which binds

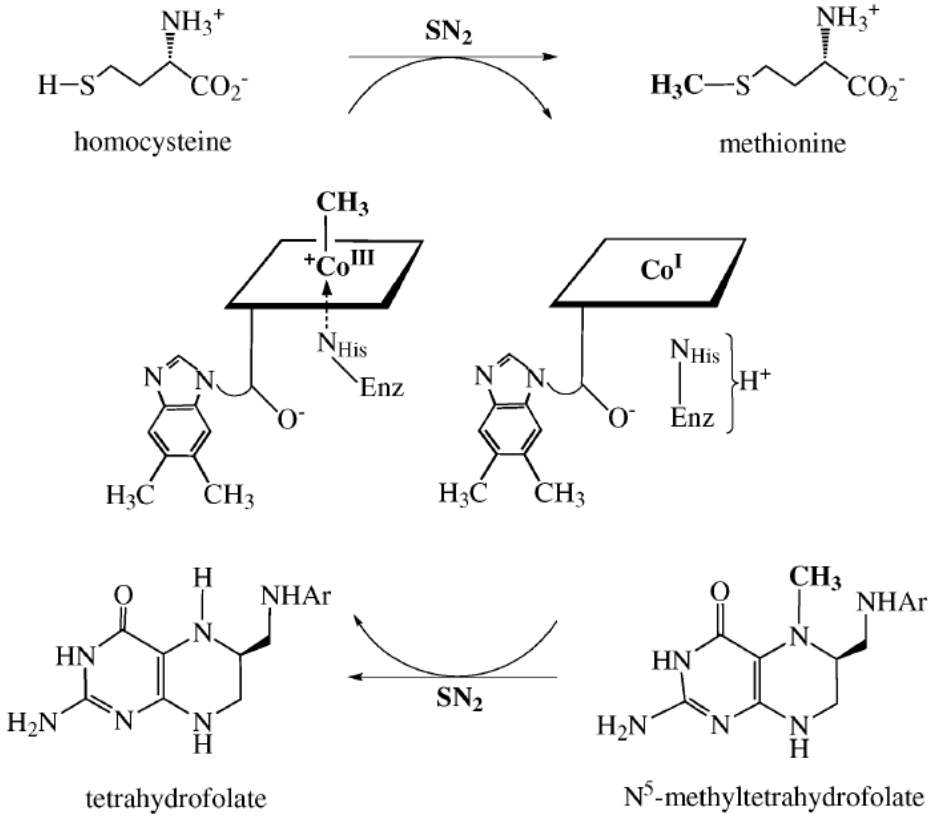

Figure 1.8: Generalized reaction cycle in methionine synthase. A similar mechanism is present in the CFeSP, however instead of homocysteine being the final methyl group acceptor, this moiety is transferred to a nickel center in the active site of ACS.[?]

the cobalamin cofactor in a base-off/his-on conformation.[68, 69, 70] The additional domains bind the various species that interact with cobalamin during the catalytic cycle, such as methyltetrahydrofolate and homocysteine, with the rate-limiting step controlled by the large conformational changes needed to swap among domains. Spectroscopic studies of a MetH variant from *Escherichia coli*, where the histidine residue that serves as the ligand to the Co ion is replaced by a glycine residue, indicated that the histidine ligand is critical for modulating controlling the equilib-

rium among the various cobalamin states encountered during turnover.[71] During turnover, it is possible that conformation of this histidine residue is modulated by the enzyme to favor the transfer of the methyl moiety of CH_3–THF to Co(I)Cbl in one half of the catalytic cycle, and the transfer of the methyl group from MeCbl to homocysteine on the subsequent half.

The Co(I)Cbl species generated in their active sites of MetH is easily oxidized in the presence of oxygen, leading to inactivation of this enzyme once every 2000 turnovers.[72] This leads to formation of Co(II)Cbl in the active site, requiring a reactivation process where a flavodoxin partner reduces the cofactor to regenerate Co(I)Cbl, allowing the catalytic cycle to resume (Figure 1.9). Reduction of Co(II)Cbl free in solution by flavodoxin however is an endergonic process, indicating that significant tuning of the reduction potential of Co(II)Cbl occurs in the presence of MetH. Spectroscopic data of a *E. coli* MetH variant locked in a conformation poised for reactivation Co(II)Cbl revealed that the Y1139 residue in the active site is critical for this tuning.[72] Spectroscopic evidence suggests that the tyrosine moiety facilities a ligand switch in Co(II)Cbl, in which the histidine bound to the lower axial site is replaced by a water moiety bound at the upper axial site. Furthermore, the Tyr residue was found to be important in orienting the bound water ligand and while also facilitating the elongation of the Co–O(H_2) bond via hydrogen bonding to this moiety in the presence of the S-adenosylmethionine substrate. The elongation of this bond is expected to stabilized the highest-occupied, primarily Co $3d_z^2$-based, "redox-active" molecular orbital, thus facilitating the reduction of the Co ion.

Bacterial metabolism employs methyltransferase enzymes for the biogenesis

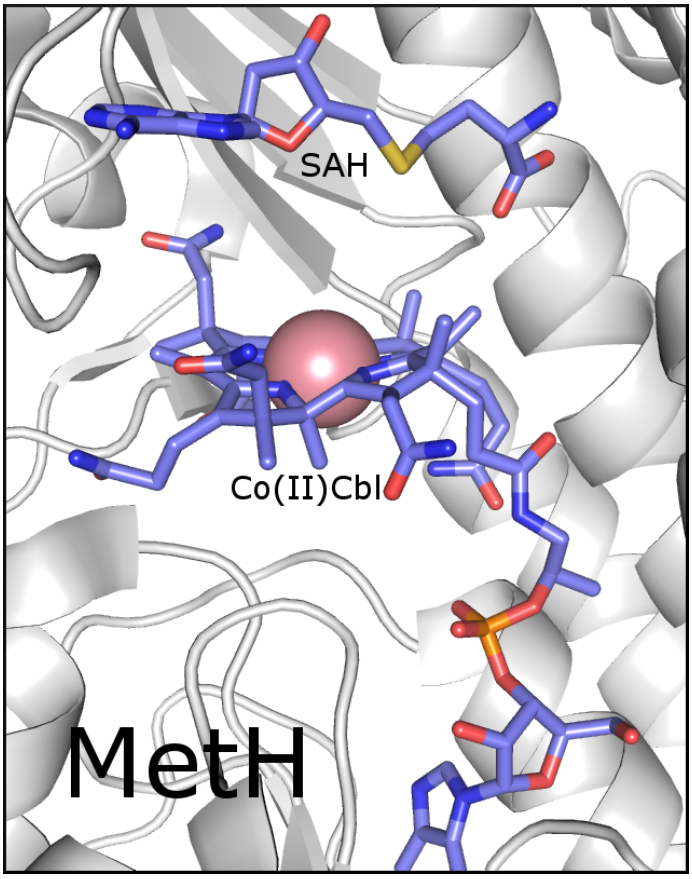

Figure 1.9: Crystallographic structure of methionine synthase (MetH) active site with Co(II)Cbl and S-adenosylhomocisteine bound trapped in a reactivation conformation. S-adenosylhomocisteine is a substrate analogue to S-adenosylmethionine lacking the migrating methyl group required in the reactivation of Co(II)Cbl. Note the absence of a histidine moiety in the lower axial ligand site. This conformation models the structure of Co(I)Cbl enforced by enzyme active site prior to methyl transfer from S-adenosylmethionine. Generated from PDB entry 1K98. Background protein structure is shown in white, Co(II)Cbl and S-adenosylhomocisteine are shown as blue sticks, and the cobalt ion of cobalamin is highlighted as a purple sphere.

of acetyl-CoA and in carbon fixation pathways. The most extensively characterized species in this group of enzymes is the corrinoid iron-sulfur protein (CFeSP), involved in the transfer of a methyl group from a variety of substrates to a nickel

center in the active site of Ni/Fe-containing acetyl-CoA synthase (ACS). CFeSP employs a cobalamin analogue where the DMB moiety is replaced by a 5′-methoxy-benzimidazolyl (MBI) moiety, referred to as Factor III_m.[73] The reaction mechanism is analogous to that observed in MetH, however crystallographic evidence indicates that no histidine ligand is available to coordinate at the lower axial site (Figure 1.10).[74] Spectroscopic studies of this enzyme instead have indicated that a water

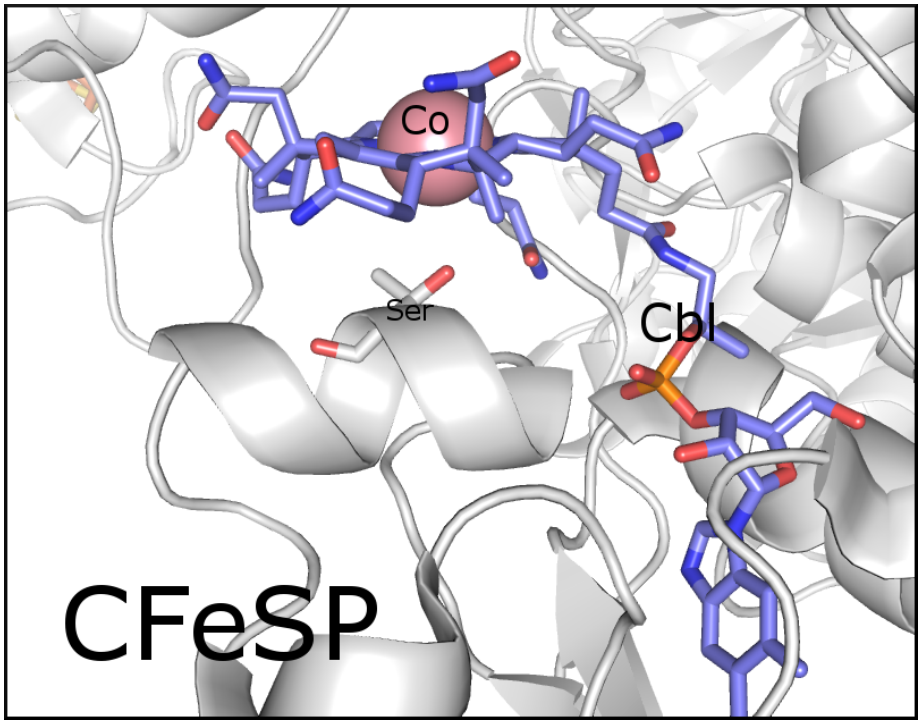

Figure 1.10: Crystallographic structure of the corrinoid iron-sulfur protein (CFeSP) active site with Co(II)Cbl bound. While not resolved in this structure, the lower axial site of the bound corrinoid is present with a water ligand based on spectroscopic evidence. Generated from PDB entry 4DJE. Background protein structure is shown in white, and the cobalt ion of cobalamin is shown as a purple sphere.

molecule is instead bound at this position. Computational assisted analysis of the spectroscopic data indicated that the Co–O(H_2) bond in the enzyme bound

methylcorrinoid is elongated by ~0.2 Å, possibly helping to promoting the transfer of the methyl moiety to the substrate by favoring the formation of Co(I) species.[73] Additional factors are thought to be necessary to fully explain the rate acceleration observed in this enzyme however. Notably, a unique reactivation mechanism has been invoked for CFeSP based on crystallography evidence.[75] In the inactivated state of CFeSP, the bound corrinoid is present in the Co(II) state. While the reduction potential of this species is estimated to be well within the range of the accompanying iron-sulfur cluster, instead of formation of a Co(I) species, a complex with the ATPase activator RACo are thought to occur when Co(II) species are generated. Particularly, in this conformation the Ser398 residue of RACo ligates to the upper axial site of Factor III_m, preventing reduction of this species by stabilization of the Co(II) state. Based on the observed conformational changes that occur upon ATP hydrolysis in the structure of RACo, it is possible to speculate that similar changes occur in the Co(II)rrinoidFeSP:RACo complex, leading to a lengthening of the Co–O(serine) bond and thus facilitating reduction to the Co(I) state.[75]

(iii) B_{12}-dependent Reductive Dehalogenases: Considerable interest has been garnered by the detoxification of halogenated organic aromatic and aliphatic compounds by anaerobic bacteria. These compounds are classified as priority pollutants by the EPA, and are generated in various agricultural and industrial processes.[76] A variety of B_{12}-dependent enzymes that facilitate this reaction have been identified in bacterial communities referred to as the reductive dehalogenases (RDases). Notably, no single organism is known to incorporate all of the RDases required for the complete dechlorination or debromination of an individual substrate, instead relying on

exchange of intermediate compounds between organisms in their ecological communities to completely detoxify these compounds. The overall reaction involved can be described as the removal of a halide ion, with subsequent addition of a hydride moiety. This reaction requires 2 electrons, and serves as a terminal electron sink for respiration in these anaerobic organisms. The catalytic mechanism of these enzymes was initially thought to involve a reaction between a Co(I)Cbl species generated in the active site and the electrophilic carbon atom of the substrate bound to the chloride moiety.[52] This mechanism was based on those observed in alkyl halide species that undergo S_{N^2} substitution reactions with Co(I)Cbl to generate various organometallic Co(III)Cbl species. Subsequent homolysis of the Co–C(subsrate) bond would yield the dehalogenated species. However, recent crystal structures of RDases from *Sulfurospirillum multivorans* (PceA) and Nitratireductorpacificus pht-3B (NprdhA) have suggested that a very different mechanism occurs.[77, 78] These structures revealed the composition of the active site, characterized by the presence of a corrinoid cofactor and two FeS clusters. While the NprdhA RDase binds cobalamin, a norpseudo-B_{12} moiety where the DMB moiety is replaced by an adenine base is observed bound to PceA (Figures 1.11 and 1.12).[79] Furthermore, one of the two FeS clusters is located within van der waals contact of one of the tetrapyrrole moieties of the corrin ring. Comparison of the primary structure of this RDase to other species indicated that the B_{12}-binding domain is highly conserved, while a large variability is observed for the substrate-binding motif, suggesting that modifications to this latter motif are present to accommodate different substrates. More intriguingly, EPR spectroscopy of NprdhA in the presence of its 3,5-dibromo-4-

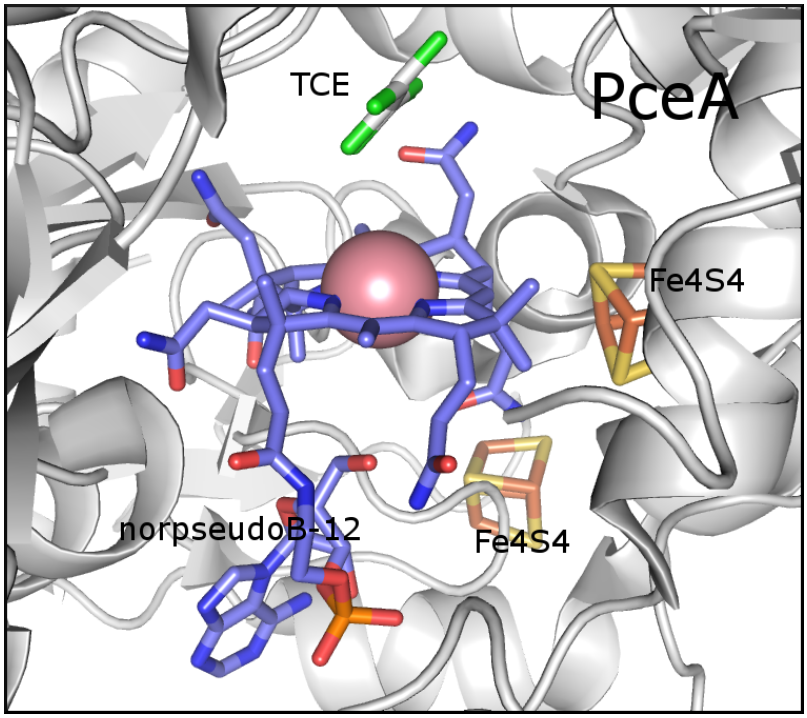

Figure 1.11: Crystallographic structure of the *Sulfurospirillum multivorans* (PceA) active site with its tricholoronethene substrate bound. The two 4Fe/4S clusters are shown as sticks. No density was observed at the lower axial site in this structure, although solvent connected channel to this position is present. Generated from PDB entry 4UQU. Background protein structure is shown in white, and the cobalt ion of cobalamin is shown as a purple sphere.

hydroxybenzoic acid (DBHA) substrate indicated a direct interaction between the Co(II) ion of the bound cobalamin cofactor and the bromide moiety. Although this conformation is not part of the catalytic cycle, it suggested that the enzyme active sites enforce a particular conformation of this substrate during turnover, possibly to facilitate transfer of the halide ion to the corrinoid. In lieu of a crystal structure of NprdhA with its substrate bound, computational docking of DBHA confirmed that the substrate binding pocket in the enzyme places significant constraints in the orientations available, likely are necessary for directing the halide moiety to the Co

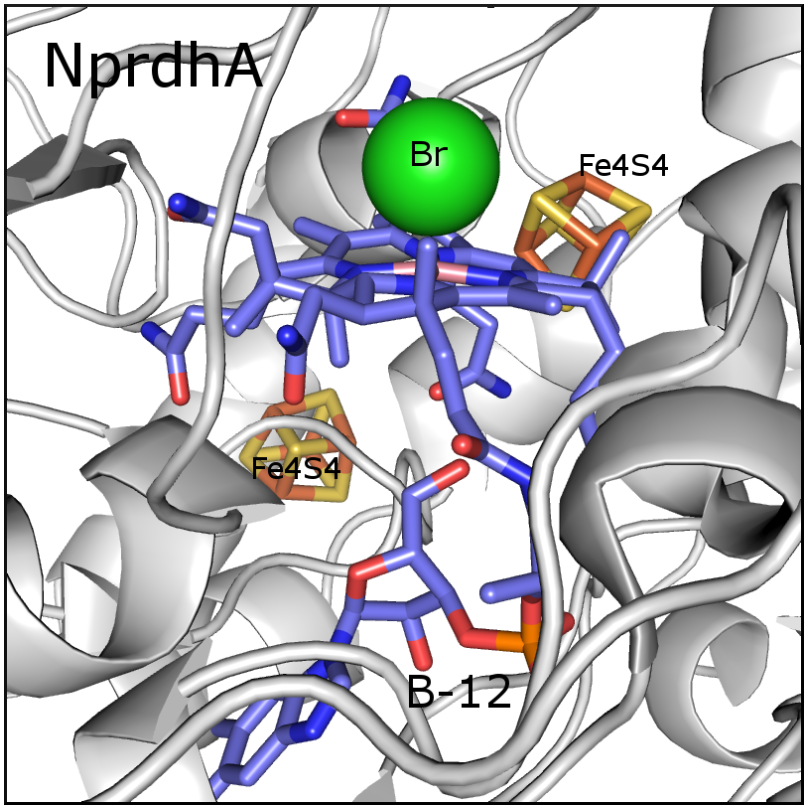

Figure 1.12: Crystallographic structure of the *Nitratireductorpacificus* pht-3B (NprdhA) reductive dehalogenase in the presence of bromide ions (green sphere). The two 4Fe/4S clusters are shown as sticks. No density was observed at the lower axial site in this structure, although solvent connected channel to this position is present. The upper axial site is present with a bromide moiety. Generated from PDB entry 4RAS. Background protein structure is shown in white.

ion.[78] The crystal structure of the PceA RDase with substrate bound discloses one of chloride atoms of the trichloroethene (TCE) moiety is present ~3.0 Å away from the Co ion, near the upper axial ligand site, with 5.8 Å distance for the putative electron transfer between Co and the proximal carbon of TCE.[77] In the absence of substrate, density consistent with a water ligand is observed at the upper axial position with a distance of 2.5 Å from Co (~0.5 Å longer than in the absence of

the enzyme). Notably, no spectroscopic data for these species is available. These seminal observations suggested a novel chemical approach employed by these enzymes, in which the cobalamin cofactor stabilizes the halide moiety during the catalytic cycle, facilitating its removal. The first step in the mechanism proposed on the basis of available crystal structures involves an electron transfer to the substrate from a Co(I)rrinoid species in the active site, generating a unique Co(II)rrinoid and substrate-based radical pair species during turnover. Subsequent electron transfer and proton group addition to the substrate, possibly mediated by the FeS clusters and nearby tyrosine residue, would yield the dehalogenated product along with a Co(II)–X(halide) species. Reduction of the halocorrinoid would regenerated the Co(I)Cbl to close the catalytic cycle. Significant questions remain in the mechanism of RDases however, particularly how the enzyme stabilizes the various redox states of the corrinoid, in particular the formation of Co(I)Cbl.[52] The role of the FeS clusters and the nature of the two electron transfers that occur is unclear, however based on the crystal structure they seem to provide a pathway for electron transfer between the buried active site and the surface of the protein, possibly facilitating redox transfers from cellular reductants. Clearly, further spectroscopic characterization of these species is warranted.

(iv) ATP:Co(I)rrinoid Adenosyltransferases: Unlike the previous B_{12}-dependent enzymes which use cobalamin cofactors in their catalytic cycles, ATP:Co(I)rrinoid adenosyltransferase (ACATs) employ corrinoids as substrates to generate AdoCbl. While methlytransferases (and purportedly reductive dehalogenases) can regenerate the active forms of their cofactors, AdoCbl-dependent enzymes are unable

to carry out an analogous reaction. These enzymes are particularly susceptible to inactivation via exposure to oxygen or nitric oxide gas, as these can oxidize the Co(II)Cbl species generated during turnover.[?] The oxidized cofactor is a dead-end in the catalytic cycle, requiring its replacement by AdoCbl. In this context, ACATs have been proposed to maintain appropriate amounts of AdoCbl available during metabolism, sustaining the activity of AdoCbl-dependent enzymes. ACATs are also involved in the biosynthesis pathway that generates AdoCbl in bacteria, as some of reactions involved require adenosylated corrinoid intermediates.[80] The general Co–C(Ado) bond formation mechanism proposed for ACATs involves a "supernucleophilic" Co(I) species generated in the active site, capable of nucleophilic attack on the 5'–carbon of ATP (Figure 1.13).[80,?,?] The reduction of Co(II)rrinoids to generate

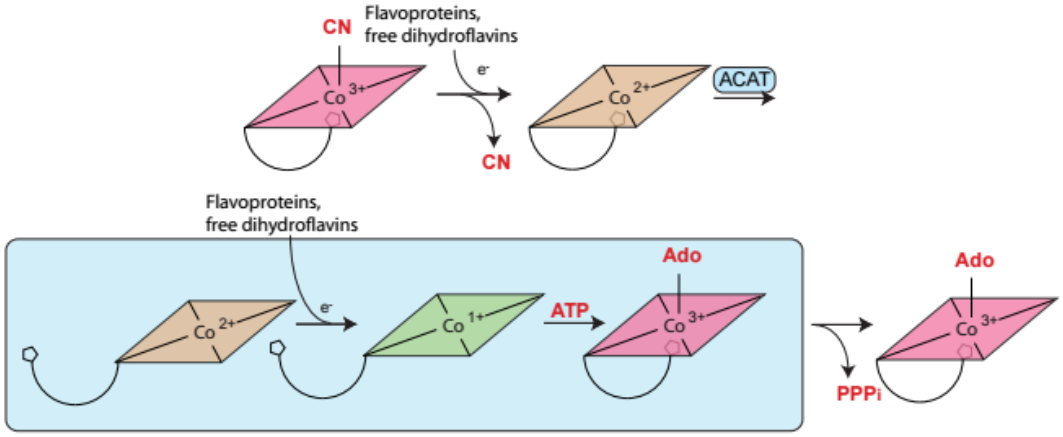

Figure 1.13: Generalized overall reaction cycle for the conversion of vitamin-B_{12} to coenzyme-B_{12}. The steps catalyzed by ATP:Co(I)rrinoid adenosyltransferase enzymes are shown inside a blue box.[?]

the key Co(I) intermediate is particularly challenging step in this mechanism, as the

reduction potential of Co(II)rrinoids free in solution is well below that of available reducing agents available in the cell. However, in the presence of ACATs, their bound Co(II)rrinoids can be reduced by free dihidroflavins readily available in the cell. Three non-homologous families of ACATs have been identified based on their quaternary structure, and classified according to their biological role on *Salmonella enterica*. Spectroscopic characterization of Co(II)Cbl in the presence of each of these ACATs types has been reported, disclosing the presence of unprecedented spectroscopic features not observed under any other conditions for their bound corrinoid substrates.[81, 82, 83] These features have been described as characteristic of Co(II)rrinoid intermediates generated by ACATs, and are described in more detail in subsequent chapters. Although ACATs share a common catalytic mechanism, there is no evolutionary relationship between the known ACAT types. Instead, these enzymes arose to satisfy AdoCbl requirements independently, serving as a classic example of convergent evolution.[84] The CobA ACAT is involved in the *de novo* synthesis of AdoCbl and in the scavenging of exogenous corrinoids. The PduO and EutT ACATs are expressed alongside elements of the *pdu* and *eut* operons, and are required for the growth of *S. enterica* on 1,2-propanediol and ethanolamine respectively. Under conditions where these metabolites are the primary source of nutrition available to the cell, expression of these operons results in the formation of polyhedral proteinaceous microcompartments. These microcompartments are postulated to house the necessary enzymatic machinery for the catabolism of 1,2-propanediol and ethanolamine, mediated by the AdoCbl-dependent enzymes propanediol dehydratase and ethanolamine ammonia lyase. The PduO-type ACATs

have been most extensive studied family, as this includes the human adenosyltransferase (hATR). Spectroscopic studies of the PduO-type ACAT from *Methylobacterium extorquens* (*Me*PduO) were the first to reveal that the generated AdoCbl product could be transferred to the methylmalonyl-CoA mutase (MMCM) enzyme, one of the two B12-dependent enzymes in humans.[49] Furthermore, mutations in the gene coding for hATR have been found in patients with methylmalonic aciduria, a disease predominantly characterized by a malfunctioning MMCM enzyme.[85] These observations suggest a critical role for the hATR ACAT in maintaining the catalytic activity of MMCM in humans.[48] Furthermore, extensive crystallographic and spectroscopic experiments on PduO-type ACATs were the first to elucidate the structure of the bound corrinoid species during the catalytic cycle.[86, 87] The crystal structure of the PduO-type ACAT from *Lactobacillus reuteri* revealed a unique coordination environment for the bound Co(II)Cbl species first deduced on the basis of spectroscopic evidence (Figure 1.14).

In the catalytic conformation, no axial ligands to the Co ion were found, as instead, the ATP substrate was observed at the position at the upper axial site, while enzyme-derived hydrophobic residues were located at the lower axial site. In this conformation, the reduction potential of Co(II)Cbl is dramatically increased, allowing for the formation of Co(I)Cbl with free dihidroflavins. Subsequent spectroscopic characterization of these species further elucidated the role of the enzyme active site in facilitating the complete removal of axial ligands to the Co(II)Cbl substrate.[88] Similar spectroscopic evidence is available for the CobA and EutT ACATs, covered in the following chapters (Figure 1.15).[89, 90]

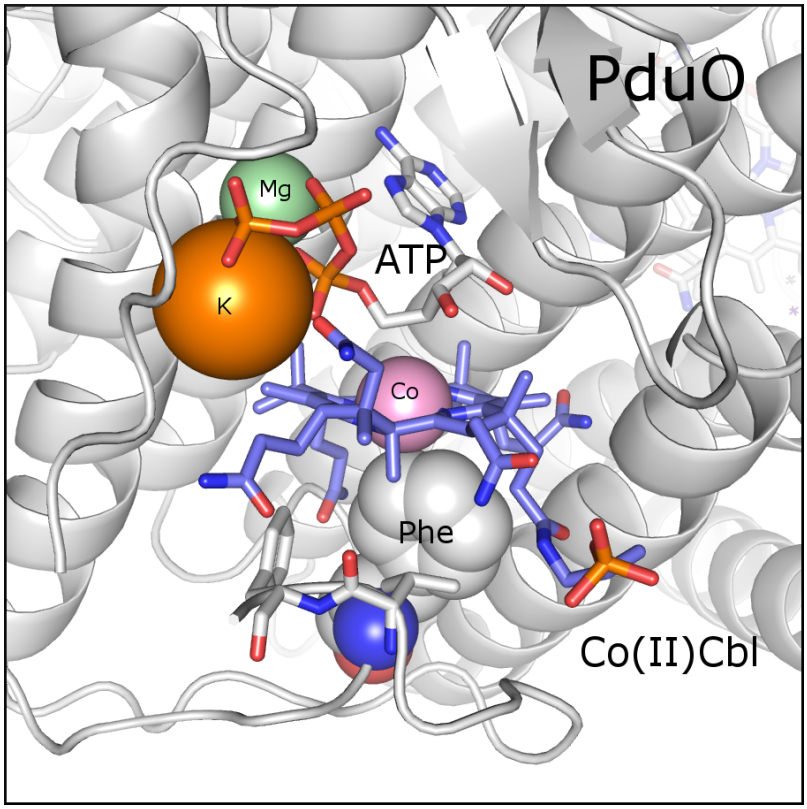

Figure 1.14: Crystallographic structure of the *Lactobacillus reuteri* PduO-type ACAT (*Lr*PudO)) active site with Co(II)Cbl and ATP cosubstrates bound. The magnesium ion (light green sphere). coordinated by the triphosphate backbone of ATP (white sticks) is shown An additional potassium ion not required for in vitro activity but present under crystallization conditions is observed (orange sphere). Background protein structure is shown in white, relevant amino acid residues are highlighted as sticks, and the cobalt ion of cobalamin is shown as a purple sphere. Van der waal surface of the Phe111 occupying the site at which the lower axial ligand is normally found is shown. Generated from PDB entry 3CI1.

1.4 Concluding Remarks

Although cobalt is a trace element in the metabolism of many organisms, the chemistry it facilities in the form of the corrinoid molecule is critical for sustaining life. In the context of B_{12}-dependent enzymes, the previous six years have produced new

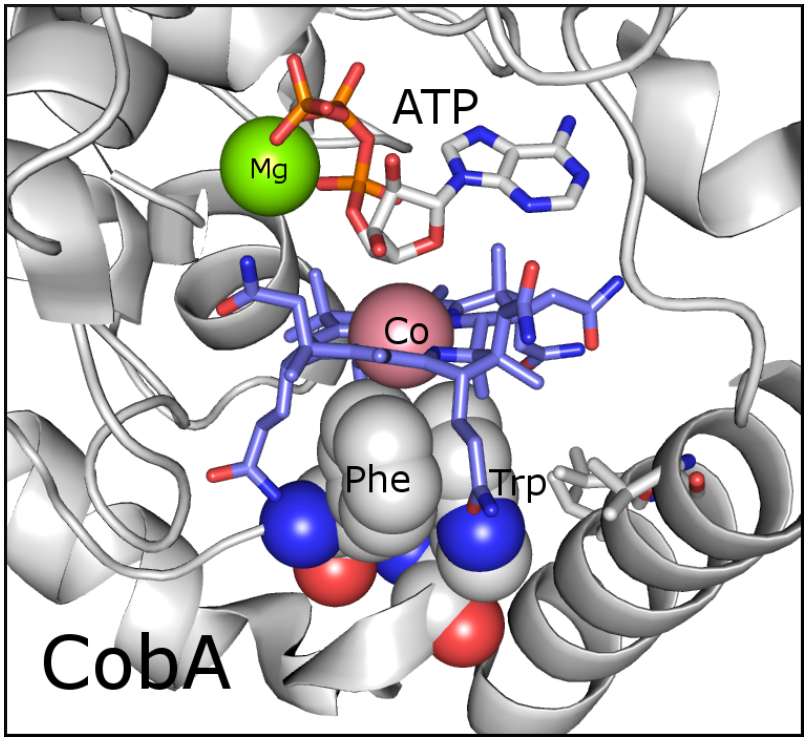

Figure 1.15: Crystallographic structure of the *Salmonella enterica* CobA ACAT (*Se*CobA) active site with Co(II)Cbl (blue sticks) and ATP (white sticks) cosubstrates bound. Generated from PDB entry 4HUT. Background protein structure is shown in white, and the cobalt ion of cobalamin is shown as a purple sphere. The van der waal surface of amino acid residues that occupy the site at which the lower axial ligand is normally found is shown (Phe91 and Trp93).

and exciting information relating to the chemistry of all the known types of enzymes that employ this unique molecule. Particularly, crystallographic evidence of many previously unavailable species has been reported, many with new implications for the mechanisms of B_{12}-dependent enzymes. This crystallographic legacy dates back to the initial crystal structure of vitamin-B_{12} in 1955 by Dorothy Hodgkin, which for the first time revealed the structure of this molecule.[91] From that time forward, cobalamin and related species has been described as complex, elegant, intricate,

and enigmatic molecules. However, beyond its apparently intractable structure, the vast chemistry facilitated by this molecule can be related to the properties of its most chemically reactive electrons.

1.5 References

[1] SB Heysfield and M Waki. Body Composition in Humans: Advances in the Development of Multicompartment Chemical Models. *NUTRITION REVIEWS*, 49(4):97–108, apr 1991.

[2] Ashley I Bush and Cyril C Curtain. Twenty years of metallo-neurobiology: where to now? *European biophysics journal : EBJ*, 37(3):241–5, mar 2008.

[3] Emily L Que, Dylan W Domaille, and Christopher J Chang. Metals in neurobiology: probing their chemistry and biology with molecular imaging. *Chemical reviews*, 108(5):1517–49, may 2008.

[4] Sónia S. Leal, Hugo M. Botelho, and Cláudio M. Gomes. Metal ions as modulators of protein conformation and misfolding in neurodegeneration. *Coordination Chemistry Reviews*, 256(19-20):2253–2270, oct 2012.

[5] Andrew J Thomson and Harry B Gray. Bio-inorganic chemistry. *Current Opinion iin Chemical Biology*, 2:155–158, 1998.

[6] Claudia Andreini, Ivano Bertini, Gabriele Cavallaro, Gemma L. Holliday, and Janet M. Thornton. Metal ions in biological catalysis: From enzyme databases to general principles. *Journal of Biological Inorganic Chemistry*, 13(8):1205–1218, 2008.

[7] Harry B Gray. Biological inorganic chemistry at the beginning of the 21st century. *Proceedings of the National Academy of Sciences of the United States of America*, 100(7):3563–3568, 2003.

[8] Clyde W. Cady, Robert H. Crabtree, and Gary W. Brudvig. Functional models for the oxygen-evolving complex of photosystem II. *Coordination Chemistry Reviews*, 252(3-4):444–455, 2008.

[9] GC Dismukes. Review Article Oxygen-Evolving Complex *. 43(1), 1986.

[10] Junko Yano, Jan Kern, Vittal K Yachandra, Håkan Nilsson, Sergey Koroidov, and Johannes Messinger. Light-dependent production of dioxygen in photosynthesis. *Metal ions in life sciences*, 15:13–43, jan 2015.

[11] Edward I. Solomon, Uma M. Sundaram, and Timothy E. Machonkin. Multicopper Oxidases and Oxygenases. *Chemical Reviews*, 96(7):2563–2606, jan 1996.

[12] Bernard Meunier, Samuël P. de Visser, and Sason Shaik. Mechanism of Oxidation Reactions Catalyzed by Cytochrome P450 Enzymes. aug 2004.

[13] Edward I. Solomon. Spectroscopic methods in bioinorganic chemistry: Blue to green to red copper sites. *Inorganic Chemistry*, 45(20):8012–8025, 2006.

[14] Jacques Meyer. Iron-sulfur protein folds, iron-sulfur chemistry, and evolution. *Journal of Biological Inorganic Chemistry*, 13(2):157–170, 2008.

[15] Paolo Ascenzi, Andrea Bellelli, Massimo Coletta, Alfredo Colosimo, Giancarlo Falcioni, Giorgio M Giacometti, Rodolfo Ippoliti, Lello Zolla, and Bruno Giardina. Multiple strategies for O2 transport: from simplicity to complexity. *IUBMB life*, 59(8-9):600–16, jan.

[16] KE van Holde. Respiratory proteins of invertebrates: Structure, function and evolution. *ZOOLOGY-ANALYSIS OF COMPLEX SYSTEMS*, 100(4):287–297, 1997.

[17] Gaochao Tian and Judith P. Klinman. Discrimination between 16O and 18O in oxygen binding to the reversible oxygen carriers hemoglobin, myoglobin, hemerythrin, and hemocyanin: a new probe for oxygen binding and reductive activation by proteins. *Journal of the American Chemical Society*, 115(20):8891–8897, oct 1993.

[18] NB Terwilliger. Functional adaptations of oxygen-transport proteins. *JOURNAL OF EXPERIMENTAL BIOLOGY*, 201(8):1085–1098, apr 1998.

[19] H C Liang, M Dahan, and K D Karlin. Dioxygen-activating bio-inorganic model complexes. *Current opinion in chemical biology*, 3(2):168–75, apr 1999.

[20] PeterM. Vitousek and RobertW. Howarth. Nitrogen limitation on land and in the sea: How can it occur? *Biogeochemistry*, 13(2), 1991.

[21] James B. Howard and Douglas C. Rees. Structural Basis of Biological Nitrogen Fixation. *Chemical Reviews*, 96(7):2965–2982, jan 1996.

[22] Juan C Fontecilla-Camps, Patricia Amara, Christine Cavazza, Yvain Nicolet, and Anne Volbeda. Structure-function relationships of anaerobic gas-processing metalloenzymes. *Nature*, 460(7257):814–22, aug 2009.

[23] JJ CHILDRESS and CR FISHER. THE BIOLOGY OF HYDROTHERMAL VENT ANIMALS - PHYSIOLOGY, BIOCHEMISTRY, AND AUTOTROPHIC SYMBIOSES. *OCEANOGRAPHY AND MARINE BIOLOGY*, 30:337–441, 1992.

[24] Stephen J Lippard. The inorganic side of chemical biology. *Nature chemical biology*, 2(10):504–507, 2006.

[25] Clarck R. Landis and Frank Weinhold. *Valency and Bonding*.

[26] S.E O'Reilly and Michael F Hochella. Lead sorption efficiencies of natural and synthetic Mn and Fe-oxides. *Geochimica et Cosmochimica Acta*, 67(23):4471–4487, dec 2003.

[27] Richard H. Holm, Pierre Kennepohl, and Edward I. Solomon. Structural and Functional Aspects of Metal Sites in Biology. *Chemical Reviews*, 96(7):2239–2314, jan 1996.

[28] R.J.P. Williams. *The Chemistry of Evolution: The Development of Our Ecosystem*. Elsevier Science, 2005.

[29] Michihiko Kobayashi and Sakayu Shimizu. Cobalt proteins. *European Journal of Biochemistry*, 261(1):1–9, mar 1999.

[30] Luciano Andres Abriata. Investigation of non-corrin cobalt(II)-containing sites in protein structures of the Protein Data Bank. *Acta Crystallographica Section B: Structural Science, Crystal Engineering and Materials*, 69(2):176–183, apr 2013.

[31] Gerhard N. Schrauzer and Erwin Deutsch. Reactions of cobalt(I) supernucleophiles. The alkylation of vitamin B12s, cobaloximes(I), and related compounds. *Journal of the American Chemical Society*, 91(12):3341–3350, jun 1969.

[32] G. N. Schrauzer, E. Deutsch, and R. J. Windgassen. The nucleophilicity of vitamin B(sub 12s). *Journal of the American Chemical Society*, 90(9):2441–2442, apr 1968.

[33] Terence S Crofts, Erica C Seth, Amrita B Hazra, and Michiko E Taga. Cobamide structure depends on both lower ligand availability and CobT substrate specificity. *Chemistry & biology*, 20(10):1265–74, oct 2013.

[34] Kenneth L. Brown. Chemistry and enzymology of vitamin B12. *Chemical Reviews*, 105(6):2075–2149, 2005.

[35] Larry A. Walker, Joseph J. Shiang, Neil A. Anderson, Stuart H. Pullen, and Roseanne J. Sension. Time-Resolved Spectroscopic Studies of B 12 Coenzymes: The Photolysis and Geminate Recombination of Adenosylcobalamin. *Journal of the American Chemical Society*, 120(29):7286–7292, jul 1998.

[36] Jian Peng, Kuo-Chun Tang, Kaitlin McLoughlin, Yang Yang, Danika Forgach, and Roseanne J Sension. Ultrafast excited-state dynamics and photolysis in base-off B12 coenzymes and analogues: absence of the trans-nitrogenous ligand opens a channel for rapid nonradiative decay. *The journal of physical chemistry. B*, 114(38):12398–405, sep 2010.

[37] Thomas A Shell and David S Lawrence. A new trick (hydroxyl radical generation) for an old vitamin (B12). *Journal of the American Chemical Society*, 133(7):2148–50, feb 2011.

[38] Bernhard Kräutler and Barbara Puffer. More radical magic with B12: B12-catalyzed, light-induced cleavage of DNA. *Angewandte Chemie - International Edition*, 50(42):9791–9792, 2011.

[39] J R Roth, J G Lawrence, and T a Bobik. Cobalamin (coenzyme B12): synthesis and biological significance., 1996.

[40] SA Sanudo-Wilhelmy, L Gomez-Consarnau, C Suffridge, and EA Webb. Role of Vitamins in Marine Biogeochemistry. *Annual Review of Marine Science*, 4(1):110301100421037, 2011.

[41] D. Gille and a. Schmid. Vitamin B12 in meat and dairy products. *Nutrition Reviews*, 73(2):106–115, 2015.

[42] Fiona O'Leary and Samir Samman. Vitamin B12 in health and disease. *Nutrients*, 2(3):299–316, mar 2010.

[43] Chung Shil Kwak, Mee Sook Lee, Se In Oh, and Sang Chul Park. Discovery of novel sources of vitamin b(12) in traditional korean foods from nutritional surveys of centenarians. *Current gerontology and geriatrics research*, 2010:374897, jan 2010.

[44] Fumio Watanabe, Yukinori Yabuta, Tomohiro Bito, and Fei Teng. Vitamin B12-containing plant food sources for vegetarians. *Nutrients*, 6(5):1861–1873, 2014.

[45] Martin T Croft, Andrew D Lawrence, Evelyne Raux-Deery, Martin J Warren, and Alison G Smith. Algae acquire vitamin B12 through a symbiotic relationship with bacteria. *Nature*, 438(7064):90–3, nov 2005.

[46] P C Dagnelie, W A van Staveren, and H van den Berg. Vitamin B-12 from algae appears not to be bioavailable. *The American journal of clinical nutrition*, 53(3):695–7, mar 1991.

[47] Karl Gruber, Barbara Puffer, and Bernhard Kräutler. Vitamin B12-derivatives-enzyme cofactors and ligands of proteins and nucleic acids. *Chemical Society reviews*, 40(8):4346–4363, 2011.

[48] Luciana Hannibal, Jihoe Kim, Nicola E Brasch, Sihe Wang, David S Rosenblatt, Ruma Banerjee, and Donald W Jacobsen. Processing of alkylcobalamins in mammalian cells: A role for the MMACHC (cblC) gene product. *Molecular genetics and metabolism*, 97(4):260–6, aug 2009.

[49] Dominique Padovani, Tetyana Labunska, Bruce A Palfey, David P Ballou, and Ruma Banerjee. Adenosyltransferase tailors and delivers coenzyme B12. *Nature chemical biology*, 4(3):194–6, mar 2008.

[50] C. M. Dobson. Identification of the gene responsible for the cblB comple-

mentation group of vitamin B12-dependent methylmalonic aciduria. *Human Molecular Genetics*, 11(26):3361–3369, dec 2002.

[51] Martin J Warren, Evelyne Raux, Heidi L Schubert, and Jorge C Escalante-Semerena. The biosynthesis of adenosylcobalamin (vitamin B12). *Natural product reports*, 19(4):390–412, aug 2002.

[52] Ruma Banerjee and Stephen W. Ragsdale. The many faces of vitamin B12: catalysis by cobalamin-dependent enzymes. *Annual review of biochemistry*, 72:209–247, nov 2003.

[53] Martha L Ludwig and Rowena G Matthews. Structure-Based Perspectives on B 12 -Dependent Enzymes. pages 269–313, 1997.

[54] *Enzyme-Catalyzed Electron and Radical Transfer*, volume 35. Kluwer Academic Publishers, New York.

[55] Karl Gruber, Riikka Reitzer, and Christoph Kratky. Radical Shuttling in a Protein: Ribose Pseudorotation Controls Alkyl-Radical Transfer in the Coenzyme B(12) Dependent Enzyme Glutamate Mutase. *Angewandte Chemie (International ed. in English)*, 40(18):3377–3380, sep 2001.

[56] D Sean Froese, Grazyna Kochan, João R C Muniz, Xuchu Wu, Carina Gileadi, Emelie Ugochukwu, Ewelina Krysztofinska, Roy A Gravel, Udo Oppermann, and Wyatt W Yue. Structures of the human GTPase MMAA and vitamin B12-dependent methylmalonyl-CoA mutase and insight into their complex formation. *The Journal of biological chemistry*, 285(49):38204–13, dec 2010.

[57] C. Drennan, S Huang, J. Drummond, R. Matthews, and M. Lidwig. How a protein binds B12: A 3.0 A X-ray structure of B12-binding domains of methionine synthase. *Science*, 266(5191):1669–1674, dec 1994.

[58] Thomas C. Brunold, Karen S. Conrad, Matthew D. Liptak, and Kiyoung Park. Spectroscopically validated density functional theory studies of the B12 cofactors and their interactions with enzyme active sites. *Coordination Chemistry Reviews*, 253(5-6):779–794, mar 2009.

[59] Shoulian Dong, Raghavakaimal Padmakumar, Ruma Banerjee, and Thomas G. Spiro. Coâˆ'C Bond Activation in B 12 -Dependent Enzymes: Cryogenic Resonance Raman Studies of Methylmalonyl-Coenzyme A Mutase. *Journal of the American Chemical Society*, 121(30):7063–7070, aug 1999.

[60] Amanda J Brooks, Monica Vlasie, Ruma Banerjee, and Thomas C Brunold. Spectroscopic and computational studies on the adenosylcobalamin-dependent methylmalonyl-CoA mutase: evaluation of enzymatic contributions to Co-C bond activation in the Co3+ ground state. *Journal of the American Chemical Society*, 126(26):8167–80, jul 2004.

[61] Amanda J Brooks, Christel C Fox, E Neil G Marsh, Monica Vlasie, Ruma Banerjee, and Thomas C Brunold. Electronic structure studies of the adenosylcobalamin cofactor in glutamate mutase. *Biochemistry*, 44(46):15167–81, nov 2005.

[62] Amanda J. Brooks, Monica Vlasie, Ruma Banerjee, and Thomas C. Brunold. Co-C bond activation in methylmalonyl-CoA mutase by stabilization of the post-

homolysis product Co2+cobalamin. *Journal of the American Chemical Society*, 127(47):16522–16528, nov 2005.

[63] Naoki Shibata, Yoshiki Higuchi, and Tetsuo Toraya. How coenzyme B12-dependent ethanolamine ammonia-lyase deals with both enantiomers of 2-amino-1-propanol as substrates: structure-based rationalization. *Biochemistry*, 50(4):591–8, feb 2011.

[64] Naoki Shibata, Hiroko Tamagaki, Naoki Hieda, Keita Akita, Hirofumi Komori, Yasuhito Shomura, Shin-Ichi Ichi Terawaki, Koichi Mori, Noritake Yasuoka, Yoshiki Higuchi, and Tetsuo Toraya. Crystal structures of ethanolamine ammonia-lyase complexed with coenzyme B12 analogs and substrates. *The Journal of biological chemistry*, 285(34):26484–93, aug 2010.

[65] Karl-Magnus Magnus Larsson, Derek T. Logan, and Pär Pár Nordlund. Structural basis for adenosylcobalamin activation in adocbl-dependent ribonucleotide reductases. *ACS Chemical Biology*, 5(10):933–942, oct 2010.

[66] Kirsten R Wolthers, Colin Levy, Nigel S Scrutton, and David Leys. Large-scale domain dynamics and adenosylcobalamin reorientation orchestrate radical catalysis in ornithine 4,5-aminomutase. *The Journal of biological chemistry*, 285(18):13942–50, apr 2010.

[67] D Voet and J Voet. Biochemstry.

[68] Vahe Bandarian, Katherine A Pattridge, Brett W Lennon, Donald P Huddler, Rowena G Matthews, and Martha L Ludwig. Domain alternation switches

B(12)-dependent methionine synthase to the activation conformation. *Nature structural biology*, 9(1):53–6, jan 2002.

[69] Supratim Datta, Markos Koutmos, Katherine A Pattridge, Martha L Ludwig, and Rowena G Matthews. A disulfide-stabilized conformer of methionine synthase reveals an unexpected role for the histidine ligand of the cobalamin cofactor. *Proceedings of the National Academy of Sciences of the United States of America*, 105(11):4115–20, mar 2008.

[70] Markos Koutmos, Supratim Datta, Katherine A Pattridge, Janet L Smith, and Rowena G Matthews. Insights into the reactivation of cobalamin-dependent methionine synthase. *Proceedings of the National Academy of Sciences of the United States of America*, 106(44):18527–32, nov 2009.

[71] Matthew D Liptak, Angela S Fleischhacker, Rowena G Matthews, and Thomas C Brunold. Probing the role of the histidine 759 ligand in cobalamin-dependent methionine synthase. *Biochemistry*, 46(27):8024–35, jul 2007.

[72] Matthew D. Liptak, Supratim Datta, Rowena G. Matthews, and Thomas C. Brunold. Spectroscopic study of the cobalamin-dependent methionine synthase in the activation conformation: Effects of the Y1139 residue and S-adenosylmethionine on the B12 cofactor. *Journal of the American Chemical Society*, 130(48):16374–16381, dec 2008.

[73] Troy A Stich, Javier Seravalli, Swarnalatha Venkateshrao, Thomas G Spiro, Stephen W Ragsdale, and Thomas C Brunold. Spectroscopic studies of the

corrinoid/iron-sulfur protein from Moorella thermoacetica. *Journal of the American Chemical Society*, 128(15):5010–20, apr 2006.

[74] Yan Kung, Nozomi Ando, Tzanko I Doukov, Leah C Blasiak, Güneş Bender, Javier Seravalli, Stephen W Ragsdale, and Catherine L Drennan. Visualizing molecular juggling within a B12-dependent methyltransferase complex. *Nature*, 484(7393):265–9, apr 2012.

[75] Sandra E. Hennig, Sebastian Goetzl, Jae-Hun Jeoung, Martin Bommer, Friedhelm Lendzian, Peter Hildebrandt, and Holger Dobbek. ATP-induced electron transfer by redox-selective partner recognition. *Nature communications*, 5:4626, jan 2014.

[76] W W Mohn and J M Tiedje. Microbial reductive dehalogenation. *Microbiological reviews*, 56(3):482–507, 1992.

[77] Martin Bommer, Cindy Kunze, Jochen Fesseler, Torsten Schubert, and Gabriele Diekert. Structural basis for organohalide respiration. *Science*, 2871(2010):2741–2745, 2014.

[78] Karl a. P. Payne, Carolina P. Quezada, Karl Fisher, Mark S. Dunstan, Fraser a. Collins, Hanno Sjuts, Colin Levy, Sam Hay, Stephen E. J. Rigby, and David Leys. Reductive dehalogenase structure suggests a mechanism for B12-dependent dehalogenation. *Nature*, 517(7535):513–516, 2014.

[79] Bernhard Kräutler, Wolfgang Fieber, Sigrid Ostermann, Mario Fasching, Karl-Hans Hans Ongania, Karl Gruber, Christoph Kratky, Christian Mikl, Anke

Siebert, and Gabriele Diekert. The Cofactor of Tetrachloroethene Reductive Dehalogenase of Dehalospirillum multivorans Is Norpseudo-B12, a New Type of a Natural Corrinoid. *Helvetica Chimica Acta*, 86(11):3698–3716, nov 2003.

[80] Paola E. Mera and Jorge C. Escalante-Semerena. Multiple roles of ATP:cob(I)alamin adenosyltransferases in the conversion of B12 to coenzyme B12. *Applied Microbiology and Biotechnology*, 88(1):41–48, 2010.

[81] Troy A Stich, Mamoru Yamanishi, Ruma Banerjee, and Thomas C Brunold. Spectroscopic evidence for the formation of a four-coordinate Co2+ cobalamin species upon binding to the human ATP:cobalamin adenosyltransferase. *Journal of the American Chemical Society*, 127(21):7660–7661, 2005.

[82] Kiyoung Park, Paola E. Mera, Jorge C. Escalante-Semerena, and Thomas C. Brunold. Kinetic and spectroscopic studies of the ATP:corrinoid adenosyltransferase PduO from Lactobacillus reuteri: Substrate specificity and insights into the mechanism of Co(II)corrinoid reduction. *Biochemistry*, 47(34):9007–9015, 2008.

[83] Kiyoung Park, Paola E. Mera, Theodore C. Moore, Jorge C. Escalante-Semerena, and Thomas C. Brunold. Unprecedented Mechanism Employed by the Salmonella enterica EutT ATP:Co ^I rrinoid Adenosyltransferase Precludes Adenosylation of Incomplete Co ^{II} rrinoids. *Angewandte Chemie International Edition*, pages n/a–n/a, 2015.

[84] Paola E. Mera and Jorge C. Escalante-Semerena. Dihydroflavin-driven adenosylation of 4-coordinate Co(II) corrinoids: Are cobalamin reductases enzymes

or electron transfer proteins? *Journal of Biological Chemistry*, 285(5):2911–2917, jan 2010.

[85] Ana Jorge-Finnigan, Cristina Aguado, Rocio Sánchez-Alcudia, David Abia, Eva Richard, Begoña Merinero, Alejandra Gámez, Ruma Banerjee, Lourdes R Desviat, Magdalena Ugarte, and Belen Pérez. Functional and structural analysis of five mutations identified in methylmalonic aciduria cblB type. *Human mutation*, 31(9):1033–42, sep 2010.

[86] Martin St Maurice, Paola Mera, Kiyoung Park, Thomas C. Brunold, Jorge C. Escalante-Semerena, Ivan Rayment, Martin St. Maurice, Paola Mera, Kiyoung Park, Thomas C. Brunold, Jorge C. Escalante-Semerena, and Ivan Rayment. Structural characterization of a human-type corrinoid adenosyltransferase confirms that coenzyme B12 is synthesized through a four-coordinate intermediate. *Biochemistry*, 47(21):5755–5766, may 2008.

[87] Paola E Mera, Martin St Maurice, Ivan Rayment, and Jorge C Escalante-Semerena. Residue Phe112 of the human-type corrinoid adenosyltransferase (PduO) enzyme of Lactobacillus reuteri is critical to the formation of the four-coordinate Co(II) corrinoid substrate and to the activity of the enzyme. *Biochemistry*, 48(14):3138–45, apr 2009.

[88] Kiyoung Park, Paola E Mera, Jorge C Escalante-semerena, and Thomas C Brunold. Spectroscopic Characterization of Active-Site Variants of the PduO-type ATP : Corrinoid Adenosyltransferase from Lactobacillus reuteri : Insights

into the Mechanism of Four-Coordinate Co (II) corrinoid Formation. (Ii), 2011.

[89] Theodore C. Moore, Sean a. Newmister, Ivan Rayment, and Jorge C. Escalante-Semerena. Structural insights into the mechanism of four-coordinate cob(II)alamin formation in the active site of the salmonella enterica ATP:Co(I)rrinoid adenosyltransferase enzyme: Critical role of residues Phe91 and Trp93. *Biochemistry*, 51(48):9647–9657, 2012.

[90] Ivan G Pallares, Theodore C Moore, Jorge C Escalante-semerena, and Thomas C Brunold. Spectroscopic Studies of the Salmonella enterica Adenosyltransferase Enzyme Se CobA: Molecular-Level Insight into the Mechanism of Substrate Cob(II)alamin Activation. *Biochemistry*, 53:7969–7982, 2014.

[91] DOROTHY CROWFOOT HODGKIN, JENNY PICKWORTH, JOHN H. ROBERTSON, KENNETH N. TRUEBLOOD, RICHARD J. PROSEN, and JOHN G. WHITE. Structure of Vitamin B12 : The Crystal Structure of the Hexacarboxylic Acid derived from B12 and the Molecular Structure of the Vitamin. *Nature*, 176(4477):325–328, aug 1955.

Chapter 2

Spectral and Electronic Properties of Nitrosylcobalamin.

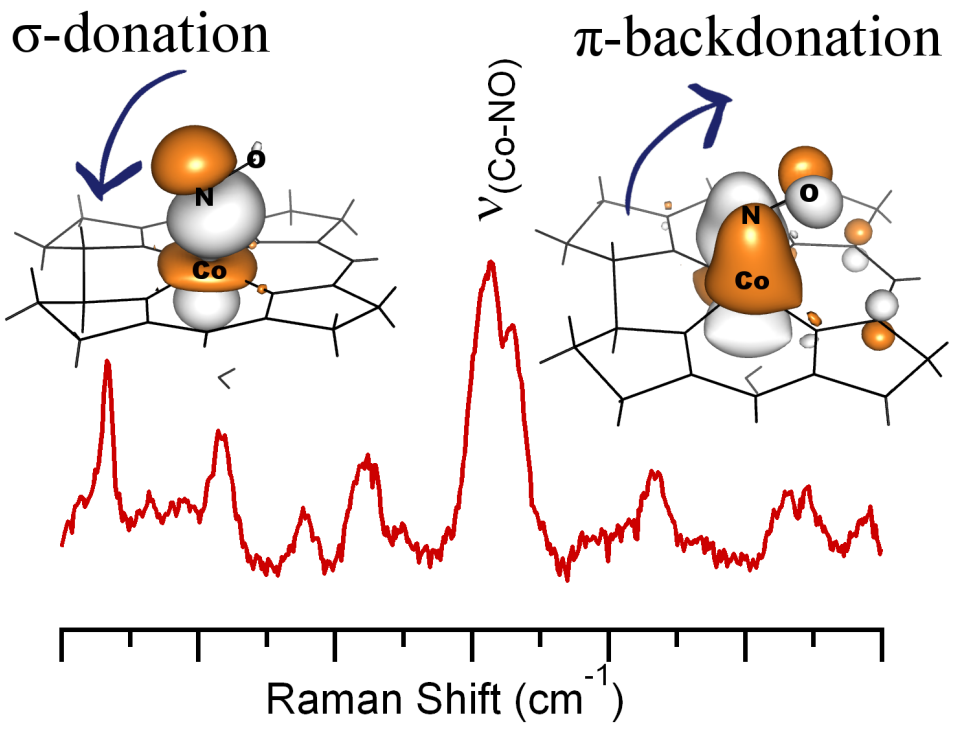

This work was published under the following: Pallares, I. G.; Brunold, T. C. "Spectral and Electronic Properties of Nitrosylcobalamin". Special thanks to Troy A. Stich for initiating the project.

2.1 Summary

Nitrosylcobalamin (NOCbl) is readily formed when Co(II)balamin reacts with nitric oxide (NO) gas. NOCbl has been implicated in the inhibition of various B_{12}-dependent enzymes, as well as in the modulation of blood pressure and of the immunological response. Previous studies revealed that among the known biologically relevant cobalamin species, NOCbl possesses the longest bond between the Co ion and the axially bound 5,6-dimethylbenzimidazole (DMB) base, which was postulated to result from a strong trans influence exerted by the NO ligand. In this study, various spectroscopic (electronic absorption, circular dichroism, magnetic circular dichroism, and resonance Raman) and computational (density functional theory (DFT) and time-dependent DFT) techniques have been used to generate experimentally validated electronic structure descriptions for the "base-on" and "base-off" forms of NOCbl. Further insights into the principal Co-ligand bonding interactions were obtained by carrying out natural bond orbital (NBO) analyses. Collectively, our results indicate that the Co $3d_{z^2}$ orbital engages in a highly covalent bonding interaction with one of the NO π^* orbitals, and that the Co–NO bond is strengthened further by sizeable π-backbonding interactions that are not present in any other Co(III)Cbl characterized to date. Due to the substantial NO^- to Co(III) charge donation, NOCbl is best described as a resonance hybrid of Co(III)-NO^- and Co(II)-NO• limiting descriptions. In contrast, our analogous computational characterization of a related species, superoxocobalamin, reveals that in this case a Co(III)-O_2^- description is adequate due to the larger oxidizing power of O_2 versus

NO. The implications of our results with respect to the unusual structural features and thermochromism of NOCbl and the proposed inhibition mechanisms of B_{12}-dependent enzymes by NOCbl are discussed.

2.2 Introduction

Cobalamins (Figure 3.1) consist of a six-coordinate low-spin Co(III) ion that is ligated equatorially by the four nitrogens of a tetrapyrrole macrocycle, known as the corrin ring.[1] The "lower" axial position is occupied by a nitrogen from the 5,6-dimethylbenzimidazole(DMB) base that is part of an intramolecular nucleotide loop bound to the corrin ring at C_{17}. At low pH, the coordinating nitrogen of the DMB group becomes protonated, which converts the cobalamins from their "base-on" state to their "base-off" form in which a solvent-derived water molecule now serves as the lower ligand.[2] An excellent model of these base-off species at neutral pH is provided by cobinamides, which are naturally occurring cobalamin precursors that lack the terminal DMB group.[3]

The biologically active forms of cobalamin differ with respect to the identity of the variable upper axial ligand, with the best characterized forms being methylcobalamin (MeCbl) and adenosylcobalamin (AdoCbl).[4] These molecules feature an organometallic bond between the Co(III) ion and either a methyl group or an ATP-derived 5'-deoxyadenosyl group. In humans, MeCbl serves as the cofactor of methionine synthase (MetH), involved in the synthesis of methionine from homocysteine,[5] while AdoCbl is required by methylmalonyl-CoA mutase (MMCM) for the isomerization of methylmalonyl-CoA to succinyl-CoA.[6] Experimental studies

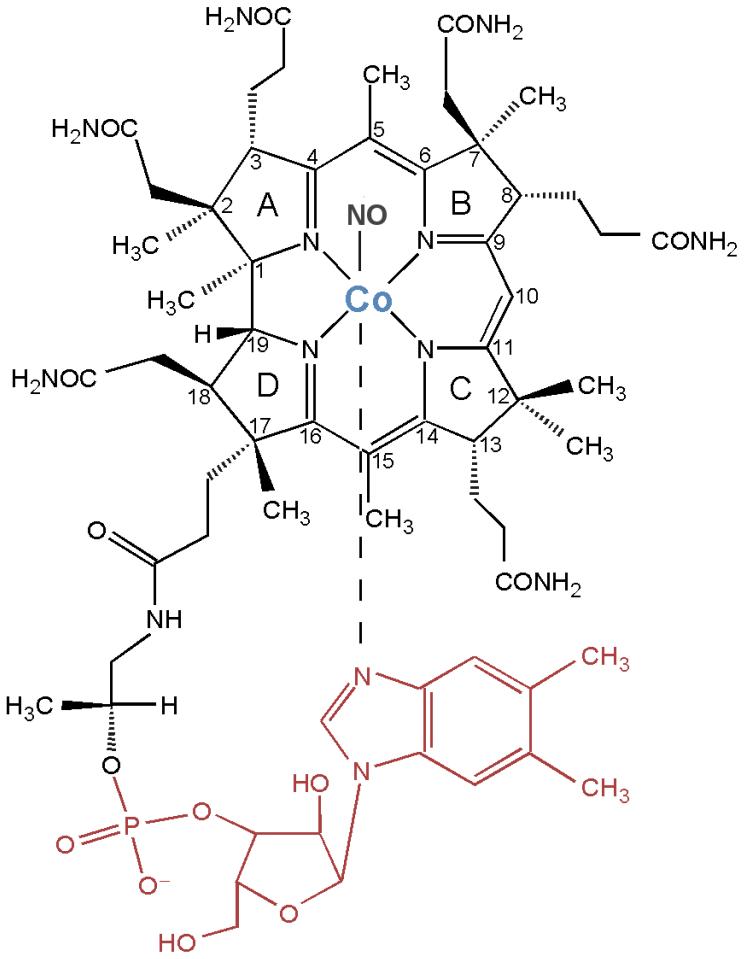

Figure 2.1: Chemical structure of nitrosylcobalamin (NOCbl), along with the numbering scheme used for the atoms in the corrin ring. Colored in red is the pendant 5,6-dimethylbenzimidazole (DMB) group, which is absent in nitrosylcobinamide $NOCbi^{+}$.

have revealed that both MetH and MMCM are inhibited by nitric oxide (NO).[7,8] While these enzymes are chemically unreactive towards NO in their resting states,[9] the Co(II)Cbl intermediates formed during catalysis (in the case of MMCM) or cofactor reactivation (MetH) are believed to be susceptible to reactions with this neutral radical species. In support of this assumption, in vitro studies have indicated that

NO reacts with Co(II)Cbl on a microsecond timescale to yield nitrosylcobalamin (NOCbl),[10, 11] while in vivo studies in animals revealed that hydroxycobalamin supplementation can inhibit the physiological response to NO,[12] due to efficient NO scavenging by the resulting Co(II)Cbl formed in the cell. Because NOCbl does not support the catalytic activities of MetH and MMCM, high cellular levels of NO are expected to result in a buildup of homocysteine and methylmalonyl-CoA, thereby causing disruption of the homocysteine metabolism and, possibly, the induction of methylmalonic aciduria.[6]

Despite the wealth of experimental evidence supporting the formation of NOCbl in vivo, the electronic structure of this species remains incompletely understood, in part because NO is a redox-active ligand, thus making an oxidation state assignment for Co ambiguous.[13] Using the Enemark-Feltham formalism for metal nitrosyls,[14] NOCbl can be described as a $\{M–NO\}^8$ type species, where the metal–NO fragment is treated as a single unit and characterized by the total number of metal d- and NO π^*- electrons. From a comparison to $\{M–NO\}^8$ metalloporphyrin species,[15] the Co–NO fragment of NOCbl is expected to adopt a bent geometry, with the NO ligand exerting a strong trans influence. Indeed, the crystal structure of NOCbl obtained at 100 K shows a very long Co–N(DMB) bond (2.32–2.35 Å), a short Co–NO bond (1.91–1.94 Å), and a Co-N-O bond angle of $120°$.[16] These axial bond distances are consistent with structures reported for Co(III)Cbl species featuring a strongly σ-donating upper ligand, thus supporting a Co(III)-NO^- description.[17] Additionally, the visible region of the electronic absorption (Abs) spectrum of NOCbl in aqueous solution at neutral pH is dominated by a broad asymmetric feature centered at 480

nm, which is characteristic of all Co(III)Cbl species.[11]

The dominant contributors to this Abs feature of Co(III)Cbl species are the so-called α/β bands that have been attributed to an electronic transition between corrin π/π^*-based molecular orbitals.[4] The energies of these bands have been shown to be sensitive to the electron-donating properties of the axial ligands.[4] Notably, in the case of NOCbl, the peak position of the α/β bands (480 nm) is similar to that of base-off alkylcobalamin species in which the lower axial DMB ligand is replaced by a water molecule (e.g. $\lambda max \approx 460$ nm for MeCbl at pH $\leqslant$ 2[18]). These observations suggest that the strongly σ-donating NO^- ligand could promote complete dissociation of the DMB group under physiological conditions. However experimental evidence exists in support of a mixture of species being present under these conditions. Detailed pH titration and NMR studies by van Eldik and coworkers led to the identification of a pKa value of 5.1 for the protonation and consequent dissociation of the DMB nitrogen, indicating that base-on NOCbl is favored at neutral pH.[11] However, this pKa value is only 0.5 pH units lower than that of the free nucleotide base (pKa of 5.56 in aqueous solution[11]), suggesting that the Co–N(DMB) bond of NOCbl is very weak. Additional NMR studies by Hassanin et al. led to the suggestion that at neutral pH, 33% of NOCbl is present in the base-off form, with the remaining 67% being in the base-on form.[2]

To improve the current understanding of the electronic structures of NOCbl in its base-on and base-off forms, we have carried out Abs, circular dichroism (CD), magnetic CD (MCD), and resonance Raman (rR) spectroscopic studies of NOCbl and nitrosylcobinamide ($NOCbi^+$). The spectroscopic data were analyzed

within the framework of density-functional theory (DFT) and time-dependent-DFT (TDDFT) calculations, employed previously with great success in computational studies of other Co(III)Cbl and Co(III)Cbi species.[19, 20, 21] To identify the principal Co-ligand bonding interactions, we have also carried out natural bond orbital (NBO) analyses. Collectively, our results provide significant new insights into the spectral and electronic properties of NOCbl and $NOCbi^+$. Additionally, by carrying out an analogous computational characterization of superoxocobalamin (O_2Cbl), intriguing electronic structure differences between this $\{Co–O_2\}^9$ species and NOCbl have been identified.

2.3 Methods

Synthesis. Aquacobalamin (H_2OCbl^+), dicyanocobinamide ($(CN)_2$Cbi), sodium borohydride ($NaBH_4$) potassium formate (HCOOK), sodium nitrite ($NaNO_2$), ascorbic acid, and copper tetrachloride ($CuCl_4$) were purchased from Sigma-Aldrich and used as obtained. Gaseous nitric oxide (NO) was generated by the reaction of $NaNO_2$ with ascorbic acid and aqueous Cu(II) chloride under an argon (Ar) atmosphere.[22] NOCbl was prepared by chemical reduction of 2 mM H_2OCbl^+ with a saturated solution of HCOOK under anaerobic conditions to yield Co(II)Cbl, which was subsequently exposed to freshly prepared NO gas for 2 hours. To halt the reaction, the solution vials were purged with Ar. $NOCbi^+$ was prepared according to the same procedure, except that in this case 2 mM diaquocobinamide ($(H_2O)_2Cbi^{2+}$) was used as a precursor. $(H_2O)_2Cbi^{2+}$ was synthesized by the addition of $NaBH_4$ to an aqueous solution of $(CN)_2$Cbi, as described in previous reports.[23, 24] The pH

of the sample solutions was 7 unless otherwise noted (See Figure A.2.4).

A comparison of the electronic Abs spectra of the resulting species to published spectra for NOCbl and $NOCbi^+$ confirmed that the reactions went to completion[25] (see Supporting information Figure A.2.1 for complete details). An electron paramagnetic resonance (EPR) characterization of these samples revealed that less than 3% of Co(II)Cbl remained in solution after NO exposure (see Figure A.2.2). Up to 60% (v/v) degassed glycerol was added under anaerobic conditions to all samples used for low-temperature Abs and MCD experiments to ensure glass formation upon freezing.

Isotopically enriched samples for rR experiments were prepared by the methods described above, except with the use of ^{15}N-labeled $NaNO_2$ (99% pure, Cambridge Isotope Laboratories, Inc). Frozen pellets were prepared by injecting small aliquots of fluid sample into a liquid N_2 bath under an argon atmosphere. Additional samples for rR studies were prepared by the addition of HCl to NOCbl to reach a final pH value of <2. The room temperature Abs spectra of this low-pH NOCbl species and $NOCbi^+$ were found to be superimposable, indicating that the former species was cleanly converted to its base-off form, as expected on the basis of the pKa value of 5.1 reported for the ligating DMB nitrogen of NOCbl.[2]

Spectroscopy. Room temperature CD and low-temperature Abs, CD, and MCD spectra were acquired using a Jasco J-715 spectropolarimeter in conjunction with an Oxford Instruments SpectroMag-4000 8T magnetocryostat. All MCD spectra were obtained by taking the difference between spectra collected with the magnetic field aligned parallel and anti-parallel to the light propagation axis to remove

contributions from the natural CD and glass strain. Room temperature Abs spectra were obtained with a Cary 5E UV/Vis spectrophotometer.

rR spectra were obtained upon excitation at 488.0 nm with a Coherent I-305 Ar^+ ion laser and 40 mW of laser power at the sample. The scattered light was collected using a 135° backscattering arrangement, dispersed by an Acton Research triple monochromator (equipped with 300, 1200, and 2400 groves/mm gratings), and analyzed with a Princeton Instrument Spec X: 100BR deep depletion, back-thinned CCD camera. Spectra were accumulated at 77 K by placing frozen pellets into a quartz finger dewar filled with liquid N_2. Spectra of fluid solution samples, contained in sealed EPR tubes under an argon atmosphere, were obtained with the same setup but by filling the finger dewar with an ice/water mixture. No spectroscopic changes attributable to photolytic or chemical degradation were observed during data collection. All rR spectra were baseline corrected using a piece-wise line function to remove the broad non-resonant fluorescence contributions, and the intensities were normalized with respect to the features in the region between 1100 and 1400 cm^{-1}. Peak positions were calibrated against the 984 cm^{-1} peak of a potassium sulfate standard, as well as the ice peak at 228 cm^{-1} for frozen samples or the water feature at 1637 cm^{-1} for fluid solution samples.

Computational Studies. Initial coordinates for the model of NOCbl were obtained from the highest resolution X-ray crystal structure reported by Hassanin et al. in 2010.[16] These coordinates were also used as the basis for generating an initial model of $NOCbi^+$, whereby the nucleotide loop was replaced by an H atom at the phosphate position and a water molecule was placed in the lower axial coordination

site originally occupied by the DMB base (see Figure 3.1). Coordinates for the O_2Cbl model were obtained from the structure reported by Hohenester et al. and used as is.[26] Due to the large number of atoms present in these species, smaller models were prepared for TDDFT excited-state and DFT frequency calculations by removal of atoms that were not expected to contribute to the spectroscopic features observed experimentally. Specifically, the corrin ring substituents were replaced by hydrogen atoms, except for the four methyl groups at the C_1, C_2, C_5, and C_{15} positions (see Figure 3.1 for the atom numbering scheme used). Additionally, the two propionamide groups at C_2 and C_{18}, along with the nucleotide loop at C_7 in the case of NOCbl, were replaced by methyl groups. This truncation scheme was adopted because the methyl groups at the C_5 and C_{15} positions were shown to be crucial for an accurate treatment of the vibrational modes of the corrin ring,[27] while the others were found to play a role in preventing excessive flattening of the corrin ring (*vide infra*). To further increase the likelihood of obtaining realistic corrin fold angles, the entire DMB base was included in all NOCbl models.

Full geometry optimizations of the complete and truncated cofactor models were performed with the Amsterdam Density Functional (ADF) 2012 suite of programs[28, 29, 30] using the Vosko-Wilk-Nusair (VWN) local-density approximation (LDA)[31] and the Perdew, Burke, and Ernzerhof (PBE) gradient corrections for exchange and correlation.[32, 33] In each case, the TZP (triple ζ with polarization) basis set[29, 30] was chosen, along with an integration constant of 5.0 and a small frozen core through 1s for C, N and O and through 2p for Co and P. The optimized models were subsequently subjected to frequency calculations to verify that a true energy

minimum was found. In each case, only positive frequencies were obtained.

For the computation of spectroscopic properties, the ORCA 2.8 software package developed by Dr. Frank Neese was employed.[34] While the optimized truncated models were used as-is, the full models were modified using the truncation scheme outlined above and subjected to partial geometry optimizations, whereby only the added H atoms were allowed to move, so as to facilitate the calculation of spectroscopic properties. Electronic transition energies and Abs intensities were computed with the TDDFT method[35, 36, 37] within the Tamm-Dancoff approximation,[38, 39] and using the PBE functional for exchange and correlation.[32, 33] The SVP (Ahlrichs polarized split valence) basis set[40] was employed for all atoms, except for cobalt, the ligating nitrogens, and the oxygen from NO, for which the TZVP basis was utilized.[41] In each case, 40 excited states were computed by including all one-electron excitations among molecular orbitals within $+/-$ 3 hartrees of the HOMO/LUMO gap. To increase computational efficiency, the resolution of the identity (RI) approximation in conjunction with the SV/J40,[42] auxiliary basis were employed in the evaluation of the Coulomb term for all calculations. The TDDFT results were used as the basis for simulating Abs and CD spectra, assuming that each electronic transition gives rise to a Gaussian-shaped band with a full width at half-max (FWHM) of $\nu_{1/2} = 1250$ cm^{-1}. All calculated spectra were uniformly red-shifted by 2200 cm^{-1} to facilitate a visual comparison with the experimental data. Finally, off-resonance Raman spectra for the fully optimized truncated models were computed with ORCA 2.8, by evaluating the numerical frequencies and electronic polarizabilities of all normal modes using DFT and the basis sets and functionals

described above. No scaling factor was applied to the computed frequencies.

The ground-state wavefunctions of the fully optimized models were analyzed further within the Natural Bond Orbital (NBO)[43] framework to assess the major bonding interactions, using the NBO5 interface as implemented in ADF via the gennbo and adfnbo programs. The VWN/LDA[31] and the PBE gradient corrections for exchange and correlation,[32, 33] along with the TZP basis set,[29] an integration constant of 5.0, and no frozen core approximation were used to compute the ground state electron density. Default parameters were used for the NBO5 interface. Isosurface plots of all orbitals and electron density difference maps were generated with Pymol using isodensity values of 0.03 a.u. and 0.003 a.u., respectively.

2.4 Results

Abs, CD, and MCD Data: The low temperature (4.5 K) Abs spectrum of NOCbl in frozen solution exhibits partially resolved bands in the lower energy region with an intensity maximum near 20,000 cm^{-1}, corresponding to the so-called α/β bands, along with a series of broad and more intense bands around 31,000 cm^{-1}, historically referred to as the γ-region (Figure 3.2, top). This spectrum is very similar to those exhibited by alkyl-Co(III)Cbl species, such as MeCbl and AdoCbl, which were previously classified as "unique" Abs spectra based primarily on the unusual appearance of the γ-region.[4] As in those latter spectra, the pair of features at 19,000 and 20,000 cm^{-1} in the Abs spectrum of NOCbl also appear to correspond to the origin and first member of a vibrational progression in a totally symmetric breathing mode of the corrin ring. In support of these assignments, the correspond-

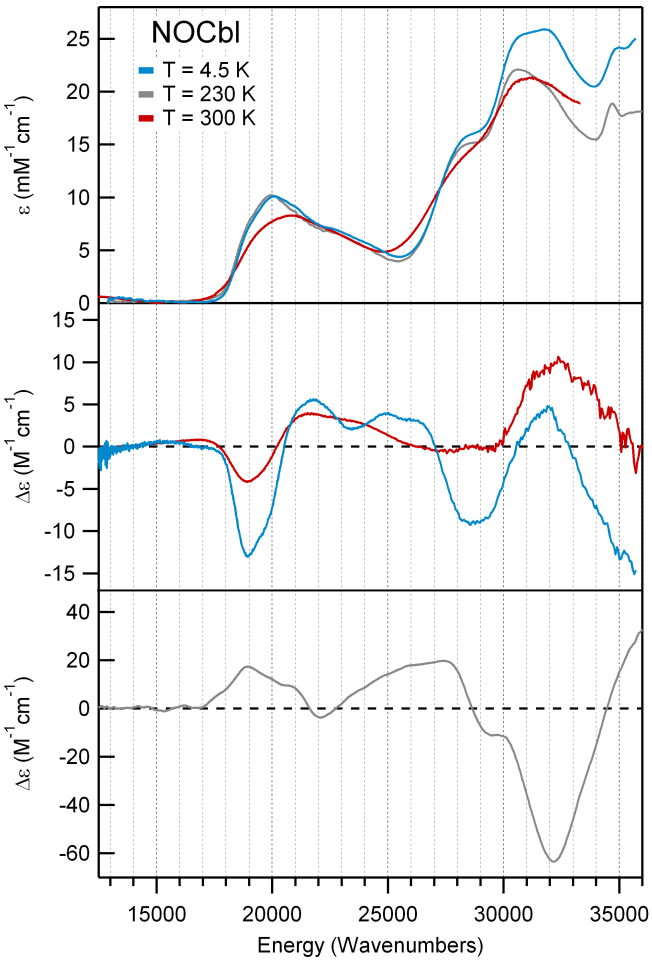

Figure 2.2: Abs (top), CD (center), and 7 T MCD (bottom) spectra at various temperatures of NOCbl.

ing features are of the same sign in both the CD and the MCD spectra of NOCbl (Figure 3.2, middle and bottom).The other bands in the visible region of the NOCbl Abs spectrum are due to at least one or more additional electronic transitions, as indicated by their opposite signs in the CD spectrum. Consistent with its classification as a "unique" Abs spectrum, several bands that arise from distinct electronic transitions can be identified in the γ-region. Specifically, two similarly intense Abs

features are present at 31,000 cm^{-1}, and a lower-energy shoulder is observed at 28,000 cm^{-1}.

Upon substitution of the DMB ligand of NOCbl with a more weakly σ-donating water molecule in $NOCbi^{+}$, a 1,000 cm^{-1} blue-shift of the α/β bands is observed (Figures 3.3, top). Additionally, a positively signed feature at 18,500 cm^{-1} appears

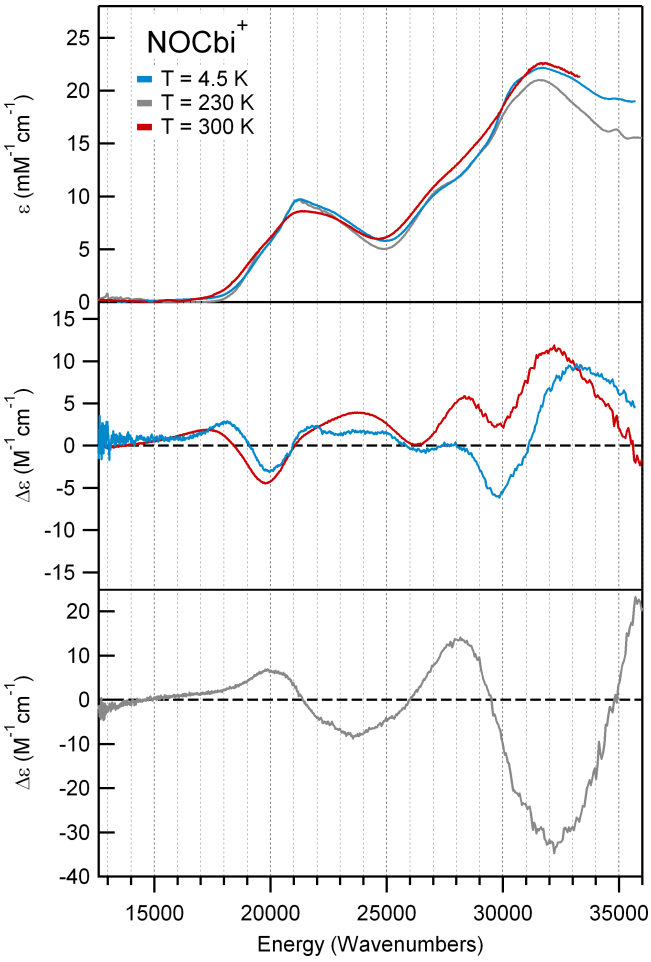

Figure 2.3: Abs (top), CD (center), and 7 T MCD (bottom) spectra at various temperatures of $NOCbi^{+}$, a spectroscopic model of base-off NOCbl.

in the CD spectrum of $NOCbi^{+}$ that has no counterpart in the NOCbl spectrum,

while the prominent negative feature at 19,000 cm^{-1} decreases in intensity and shifts to higher energy (Figure 3.3, middle). Because the MCD spectra of NOCbl and $NOCbi^{+}$ are essentially temperature-independent in the 4.5 to 50 K range (Figures S4 and S5), it can be concluded that both species possess diamagnetic ($S = 0$) ground states, consistent with a Co(III)–NO^{-} oxidation state assignment, and ruling out paramagnetic S=1 Co(II)–NO• species. Previous studies of other Co(III)corrinoids have revealed that the spectral changes in the α/β region that occur in response to a DMB→H_2O lower ligand substitution reflect a stabilization of the highest-occupied molecular orbital (HOMO) relative to the lowest-unoccupied molecular orbital (LUMO), the extent of which depends on the σ-donating strength of the upper axial ligand.[20] As the blue-shift of the α/β bands from NOCbl to $NOCbi^{+}$ (1,000 cm^{-1}) is considerably smaller than the shift observed from MeCbl to $MeCbi^{+}$ (2,500 cm^{-1}),[4] NO may appear to be a weaker σ-donating ligand than a methyl group. However, since the α/β bands of NOCbl occur at higher energies than those of MeCbl and all other alkylcobalamins,[4] their small blue-shifts from NOCbl to $NOCbi^{+}$ could also be due to the fact that the DMB moiety is only weakly interacting with the Co ion in the former species, as suggested by the unusually long Co–N(DMB) bond observed in the crystal structure of NOCbl.[16]

Intriguingly, while the Abs and CD spectra of $NOCbi^{+}$ obtained at 4.5 and 300 K exhibit insignificant differences with respect to band positions (Figure 3.3, top and middle), the Abs spectrum of NOCbl collected in fluid solution at 300 K shows the α/β bands blue-shifted by 850 cm^{-1} from their positions at 4.5 K (Figure 3.2, top). Significant temperature-dependent changes are also observed

in the CD spectrum of NOCbl, most notably a drastic decrease in the intensity of the lowest-energy, negatively-signed feature at 18,000 cm^{-1} and the appearance of a weak, positively-signed feature at even lower energy (Figure 3.2, middle). As a result, the room-temperature Abs and CD spectra of NOCbl quite closely resemble those of $NOCbi^+$. Collectively, these results suggest that by increasing the temperature from 4.5 to 300 K, the base-on to base-off equilibrium for NOCbl changes, favoring a loss of the N(DMB) ligand at high temperatures. However, consistent with published NMR results,[2] a sizeable fraction of NOCbl must remain in the base-on state even under ambient conditions, since the 300 K Abs spectra of NOCbl and $NOCbi^+$ are not superimposable (see Figure A.2.1). Notably, while the NMR data were interpreted to indicate that at room temperature 67% of the NOCbl molecules are present in the base-on state, the traces obtained by adding the 4.5 K Abs or CD spectra of NOCbl (scaled by 0.67) and $NOCbi^+$ (scaled by 0.33) differ from the 300 K Abs and CD spectra of NOCbl. This finding suggests that the Co–N(DMB) bond of the base-on fraction of NOCbl is longer at 300 K than at 4.5 K.

Resonance Raman Data. The 77 K rR spectrum of NOCbl obtained with laser excitation at 488.0 nm (20,490 cm^{-1}) shows strong enhancement of four features between 1450 and 1650 cm^{-1}. On the basis of our recent study of the vibrational properties of vitamin B_{12} and its reduced forms,[44] all of these features can be attributed to corrin-based vibrational modes. Three of them arise from totally symmetric modes (assuming an effective C_s symmetry, with the pseudo-mirror plane being oriented along the Co and C_{10} atoms and perpendicular to the corrin ring plane) and are thus particularly strongly resonance enhanced, while the fourth

is associated with an asymmetric stretching mode. Based on the vibrational analysis reported for vitamin B_{12} and our DFT-computed off-resonance Raman spectra described below, the mode associated with the most intense rR feature of NOCbl at 1496 cm^{-1}, termed ν_{S1}, involves primarily C_9–N and C_{11}–N double-bond stretching motions parallel to the Co—C_{10} vector (i.e., the corrin short axis). Alternatively, the modes at 1541 cm^{-1} and 1603 cm^{-1}, termed ν_{S2} and ν_{S3}, mainly entail in-phase stretching motions of the C_4–N and C_{16}–N bonds and of the C_5–C_6 and C_{14}–C_{15} bonds, respectively. Finally, the vibrational mode at 1572 cm^{-1} corresponds to the single asymmetric vibration of interest, ν_{as}, which primarily involves out-of-phase stretching motions of the C_4–N and C_{16}–N bonds.

A comparison of the low-energy regions of the rR spectra of NOCbl and its ^{15}NOCbl isotopomer reveals an isotope sensitive feature at 532 cm^{-1} (Figure 3.4, top traces), a region where the Co–NO stretching and Co-N-O bending modes are expected to occur.[10] Subtraction of the ^{15}NOCbl from the NOCbl trace yields a difference spectrum that shows an apparent shift of the 532 cm^{-1} feature to 496 cm^{-1} upon $^{14}NO \rightarrow {}^{15}NO$ substitution. An analogous isotope-sensitive feature is present in the rR spectrum of base-off NOCbl (our model of $NOCbi^+$, Figure 3.4, bottom traces), though in this case a much better resolved difference spectrum is obtained. Closer examination of this difference spectrum clearly discloses the presence of a shoulder on the low energy side of the positive feature, suggesting that two isotope-sensitive modes actually occur in this region. Indeed, a Gaussian deconvolution of the rR spectra in Figure 3.4 reveals that the vibrational modes of base-on and base-off NOCbl at 515 cm^{-1} and 532 cm^{-1} shift to 500 cm^{-1} and 521

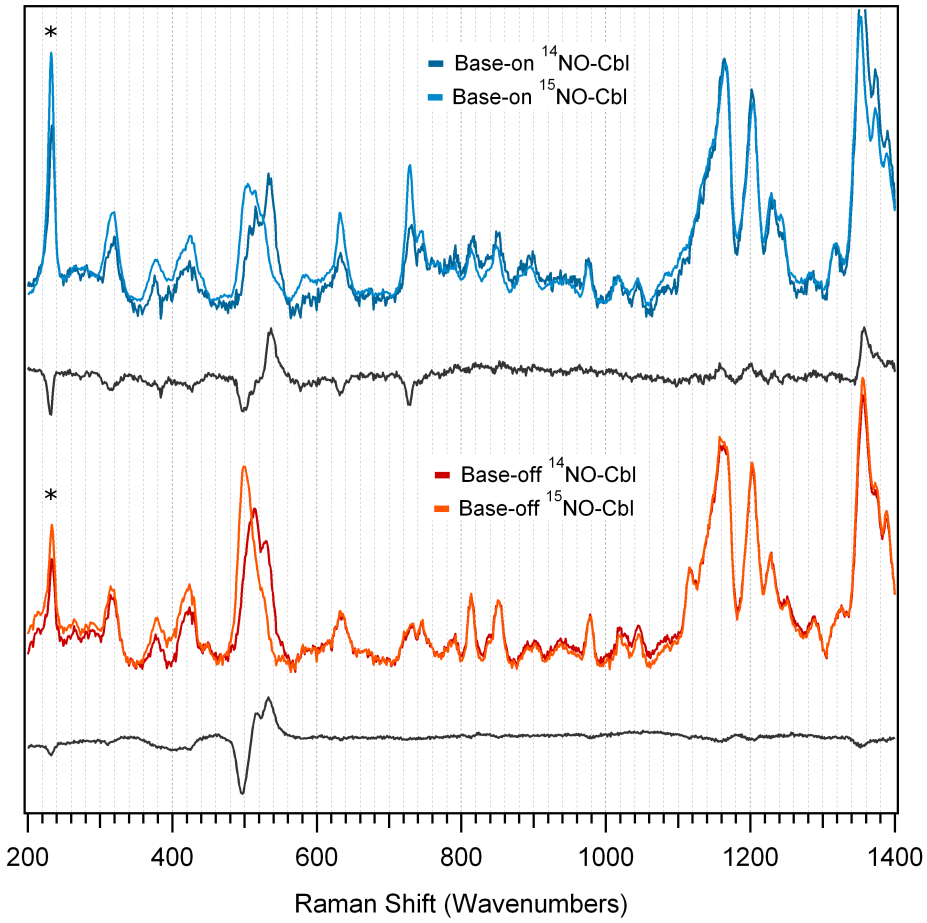

Figure 2.4: Low-energy region of rR spectra of NOCbl and its ^{15}NO enriched isotopomer in the base-on (top) and base-off (bottom) conformations, obtained at 77 K with 488 nm (20 491 cm^{-1}) laser excitation. A difference spectrum for each conformation is included below the two data sets to highlight the isotope sensitive vibrational features. Ice peaks are marked with asterisks.

cm^{-1}, respectively upon ^{14}NO $\rightarrow$^{15}NO substitution (see Figure A.2.9). In a previous rR study of NOCbl, a single isotope sensitive peak was observed at 514 cm^{-1} that shifted to 496 cm^{-1} upon ^{14}NO $\rightarrow$^{15}NO substitution. However, the spectral resolution of these published data appears to be relatively low, as only two high-energy

(>1,500 cm^{-1}) features associated with corrin-based modes could be identified,[10] compared to the four features that are readily apparent in our spectra (Figure 3.5). Additionally, considering that mode coupling typically leads to lower isotope shifts

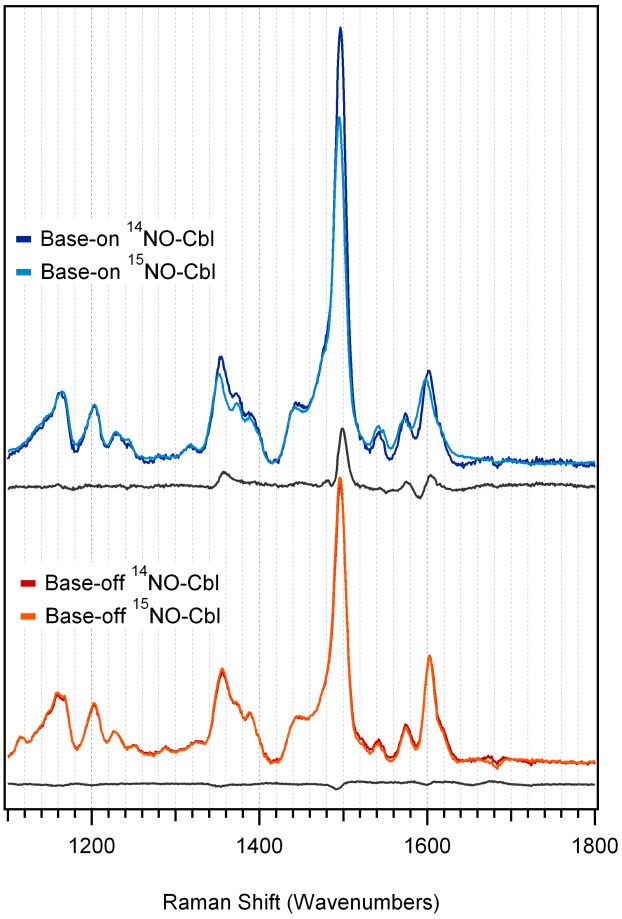

Figure 2.5: High-energy region of rR spectra of NOCbl and its ^{15}NO enriched isotopomer in the base-on and base-off conformations, obtained at 77 K with 488 nm (20 491 cm^{-1}) laser excitation. A difference spectrum for each conformation is included below the two data sets to highlight the isotope sensitive vibrational features.

than expected, the reported isotope shift of 18 cm^{-1}, which largely exceeds the 14 cm^{-1} decrease in vibrational frequency calculated using a harmonic oscillator

model for a localized Co–N stretching mode, seems unreasonably large.

The high similarity between the low-energy regions of the rR spectra of base-on and base-off NOCbl (Figure 3.4, top and bottom) indicates that the Co–NO bonding interaction is largely unperturbed by the DMB→H_2O lower ligand substitution. Consistent with this conclusion, the rR spectra of fluid solution samples of base-on and base-off NOCbl are very similar to each other as well as to the corresponding 77 K spectra (see Figures S7 and S8), despite of the thermochromism exhibited by NOCbl.

Computational Studies: Density functional theory (DFT) has been used by us with great success for the study of corrinoids in their Co(III), Co(II), and Co(I) oxidation states.[19] While different functionals have been shown to provide variable descriptions of spectroscopic properties,[45] careful evaluations of the computational results on the basis of experimental data have afforded a detailed understanding of the chemical and spectroscopic properties of a large number of different corrinoid species.[19, 4, 23, 21, 27, 46] From a recent study of MeCbl, Kozlowski and co-workers have suggested that, compared to hybrid functionals, pure GGA functionals may provide DFT results more consistent with correlated wavefunction-based methods.[47] Furthermore, work by our group[20] and others[48] has revealed that complete cofactor models should be used to obtain accurate geometric structures of cobalamins, while truncated models can be used to compute various spectroscopic parameters. In light of these findings, we have performed geometry optimizations of complete NOCbl and $NOCbi^+$ species using the pure PBE functional. The resulting structures were then suitably truncated to predict the Abs and CD spectra of these species

using TDDFT, as well as to analyze their vibrational properties (see Methods for details). For comparison, we have also carried out full geometry optimizations of these truncated models and calculated their Abs and CD spectra.

(i.) Geometries: The most significant differences between the X-ray crystal structure and our DFT optimized model of NOCbl include the Co–N(DMB) bond distance and the folding of the corrin ring. While the crystal structure of NOCbl shows an unusually long Co–N(DMB) bond of 2.35 Å, our computation predicts this bond to be elongated by an additional 0.16 Å, to 2.51 Å (see Table 4.1). A further elongation of this bond by 0.1 Å, along with a tilting of the DMB ring plane relative to the Co–N(DMB) bond vector, occurred during the geometry optimization of our truncated model lacking the propionamide side chains. Although elongation of this bond is commonly observed computationally,[20, 49] our spectroscopic results, which indicate that DMB ligation is sensitive to temperature changes, suggest instead that the elongated Co–N(DMB) bonds in our models presumably stem from the neglect of intermolecular interactions that modulate the length of this bond in solution and in the solid state. Regardless, these findings support the notion that the Co–N(DMB) bond of NOCbl is very weak and can thus be stretched, or potentially even broken, quite readily.

Distortions of the corrin ring can be assessed on the basis of the long-axis and short-axis fold angles, θ(LA) and ϕ(SA), respectively. θ(LA) is defined here as the angle between the plane containing the N_A, C_4, C_5, C_6 and N_B atoms and the plane containing the N_C, C_{14}, C_{15}, C_{16}, and N_D atoms, while ϕ(SA) corresponds to the angle between the planes containing the N_D, C_19, C_1, and N_A atoms and the

Table 2.1: Relevant structural parameters of NOCbl and NOCbi$^+$, as derived experimentally or obtained computationally. [1]From Ref 16.

Species	Model	Co–X_{upper} (Å)	Co–X_{lower} (Å)	N–O (Å)	∠Co–N–O (°)	θ-LA (°)	ϕ-SA (°)
A. NOCbl	Crystal[1]	1.91	2.35	1.14	119.4	12.4	7.5
B.	Full	1.87	2.51	1.19	119.8	9.2	8.9
C.	Truncated	1.87	2.61	1.18	119.3	3.3	5.8
D. NOCbi$^+$	Full	1.85	3.58	1.18	120.9	9.2	10.4
E.	Truncated	1.85	2.98	1.18	120.2	3.6	4.5

N_B, C_9, C_{10}, C_{11}, and N_C atoms (see Figure 3.1 for the atom numbering scheme used). As such, θ(LA) correlates with the amount of "butterfly fold" of the corrin ring and is thus particularly sensitive to the positioning or removal of the bulky DMB ligand. Alternatively, ϕ(SA) reflects the extent of "ring ruffling" due to steric constrains imposed on the propionamide and methyl groups on the A and D rings. As shown in Table 4.1, the θ(LA) values derived from the crystal structure and DFT optimized complete model of NOCbl are very similar, despite the sizable variation in the corresponding Co–N(DMB) bond distances. In contrast, considerable differences are observed for the ϕ(SA) values, suggesting that the corrin ring conformation observed experimentally may be subject to crystal-packing effects and/or intermolecular H-bonding interactions. The fact that DFT predicts both fold angles to change quite substantially upon removal of the propionamide side chains is consistent with our previous finding that distortions along the θ(LA) and ϕ(SA) coordinates require very little energy.[50]

Despite these modest discrepancies between the experimentally determined and DFT optimized NOCbl structures, the metric parameters for the Co–NO unit agree very well. Specifically, the Co–N(O) distances and Co-N-O bond angles are

identical to within 0.04 Å and <1°, respectively. Notably, the Co–N(O) bond is significantly shorter than the upper axial ligand-Co bond distances reported for all other Co(III)Cbl species,[51, 52] suggesting that this bond is exceptionally strong. Although the computation appears to overestimate the N-O bond distance by 0.05 Å, it should be noted that the value of 1.14 Å determined experimentally is surprisingly small, given that (i) the N–O bond distance in nitric oxide is 1.15 Å[53] and (ii) the NO ligand in NOCbl acquires a partial negative charge and thus increased π-antibonding electron density (*vide infra*).

Owing to the overall good agreement between the X-ray crystal structure and DFT optimized model of NOCbl, a closer examination of the energy-minimized $NOCbi^+$ model is warranted. As expected, replacing the bulky DMB base with a water molecule in the lower axial position causes sizable, though not entirely predictable, changes to both of the corrin fold angles (Table 4.1). More importantly, the optimized Co-O(H_2) distance in our complete $NOCbi^+$ model is 3.58 Å, suggesting that the Co ion resides in an effective five-coordinate ligand environment. Although this distance shortens by 0.60 Å upon removal of the propionamide side chains, the "lone pairs" on oxygen in our truncated model are not actually oriented properly to engage in a bonding interaction with the Co ion. A closer inspection of the complete $NOCbi^+$ model reveals that several of the propionamide side chains form a cage around the H_2O molecule. The fact that removing these side chains causes a large rearrangement of the water molecule suggests a role of the propionamide groups in modulating the ligation of the lower ligand by imposing steric constraints and/or providing a solvent-protected pocket for the ligand.

Finally, as expected in light of the strong Co–NO bonding interaction in NOCbl, the Co–NO unit is largely unaffected by the DMB→H_2O lower ligand substitution, with the most notable change being a small (0.02 Å) decrease in the Co–N(O) bond distance. A similar shortening was predicted previously for the Co-C(methyl) bond upon conversion of MeCbl to $MeCbi^+$.[4] Hence, despite the long Co–N(DMB) bonds in NOCbl and MeCbl, the base does play a small role in modulating the upper axial bonding interactions in these species.

(ii.) TDDFT Results: The computed Abs spectrum for the NOCbl model derived from the complete structure correctly predicts the major features observed experimentally, including the presence of two clusters of intense features near 20,000 cm^{-1} and 31,000 cm^{-1}, corresponding to the α/β-region and the γ-region, respectively (Figure 3.6, top). The computed CD spectrum is also in reasonable agreement with our experimental spectrum, with both spectra exhibiting a derivative-shaped feature associated with two oppositely-signed transitions centered at 20,000 cm^{-1} and a series of features with alternating signs in the γ-region (Figure A.2.10, top). While the computed Abs and CD spectra for the optimized truncated NOCbl model are similar to those obtained with the modified complete model, the α/β bands are blue-shifted by 900 cm^{-1} and the lowest-energy, negatively-signed feature in the CD spectrum is considerably weaker, which leads to poorer agreement with our experimental data (Figure A.2.11). Note that the blue-shift of the α/β bands for the truncated model is consistent with the expectation that a lengthening of the Co–N(DMB) bond by 0.1 Å will lead to a sizable stabilization of the HOMO.

Upon DMB→H_2O lower ligand substitution, the α/β bands in the TDDFT

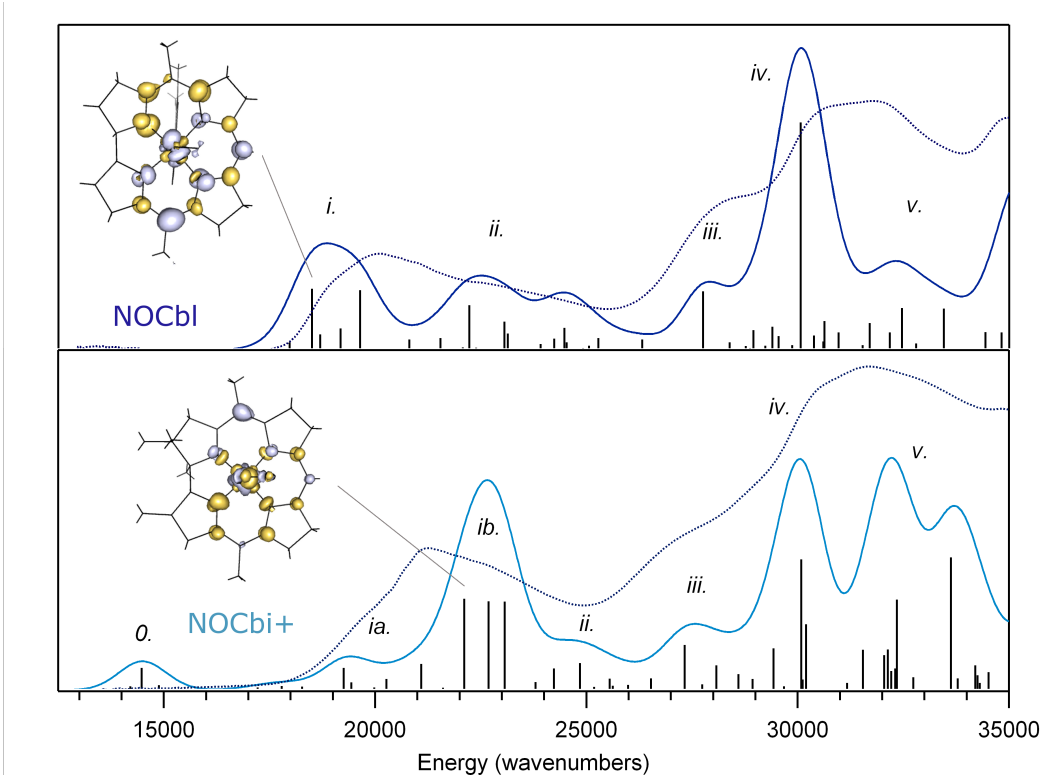

Figure 2.6: Abs spectra of NOCbl (top) and NOCbi$^+$ (bottom) collected at 4.5 K (dotted lines) superimposed on the TD-DFT results. The TD-DFT computed transitions (vertical sticks) were convoluted with Gaussian bands with a constant FWHM of 1,250 cm^{-1} to obtain the predicted spectra plotted in dark blue for NOCbl and in light blue for NOCbi$^+$. In each case, the EDDM for the α-band transition is shown on the left, where regions of loss and gain of electron density are shown in gray and gold, respectively. The calculated spectra were uniformly red-shifted by 2,200 cm^{-1} to facilitate a direct comparison with the experimental results.

computed Abs and CD spectra blue-shift by 3,500 cm^{-1} and the negative CD feature at 20,000 cm^{-1} decreases in intensity, causing an apparent blue-shift of the derivative-shaped feature to 21,000 cm^{-1} (Figure 3.6, bottom, figure S10, bottom). As expected on the basis of the negligible Co-O(H_2) bonding interaction in each of the two different NOCbi$^+$ models, the Abs and CD spectra predicted for these

species are almost identical (Figure A.2.12). Overall, the computed Abs spectra for both NOCbi$^+$ models agree quite well with the experimental spectrum across the entire spectral range investigated, except for the presence of a small feature at 15000 cm^{-1} that is not observed experimentally. In contrast, the computed CD spectra only modestly reproduce the experimental spectrum, especially in the γ-region. This discrepancy can be attributed, at least in part, to the fact that the CD spectrum is dominated by magnetic-dipole allowed transitions, which poses a significant challenge for TDDFT computations.[54]

(iii.) Vibrational Frequencies: While considerable differences are observed between the experimental Abs, CD, and MCD spectra of NOCbl and NOCbi$^+$ (cf. Figures 3.2 and 3.3), the rR spectra obtained for these species show minimal differences with respect to the frequencies of the major corrin and Co–NO based modes (*vide supra*). For this reason, and for computational practicality, the truncated NOCbl and NOCbi$^+$ models were employed in our DFT-assisted vibrational analysis. The DFT computed off-resonance Raman spectra for these models exhibit four relatively intense features in the 1450-1650 cm^{-1} region (Figure A.2.13 and A.2.14). A graphical representation of the corresponding normal modes of NOCbi$^+$ (which are very similar to those of NOCbl) in terms of atomic displacement vectors is provided in Figure 3.7. The three modes that retain the approximate C_s symmetry of NOCbi$^+$ are expected to be most strongly resonance enhanced, because only totally symmetric modes can couple to electronic transitions and thus gain rR intensity via the Frank-Condon mechanism.[55, 56] This prediction is consistent with the experimental rR spectra of NOCbl and NOCbi$^+$ obtained with laser excitation

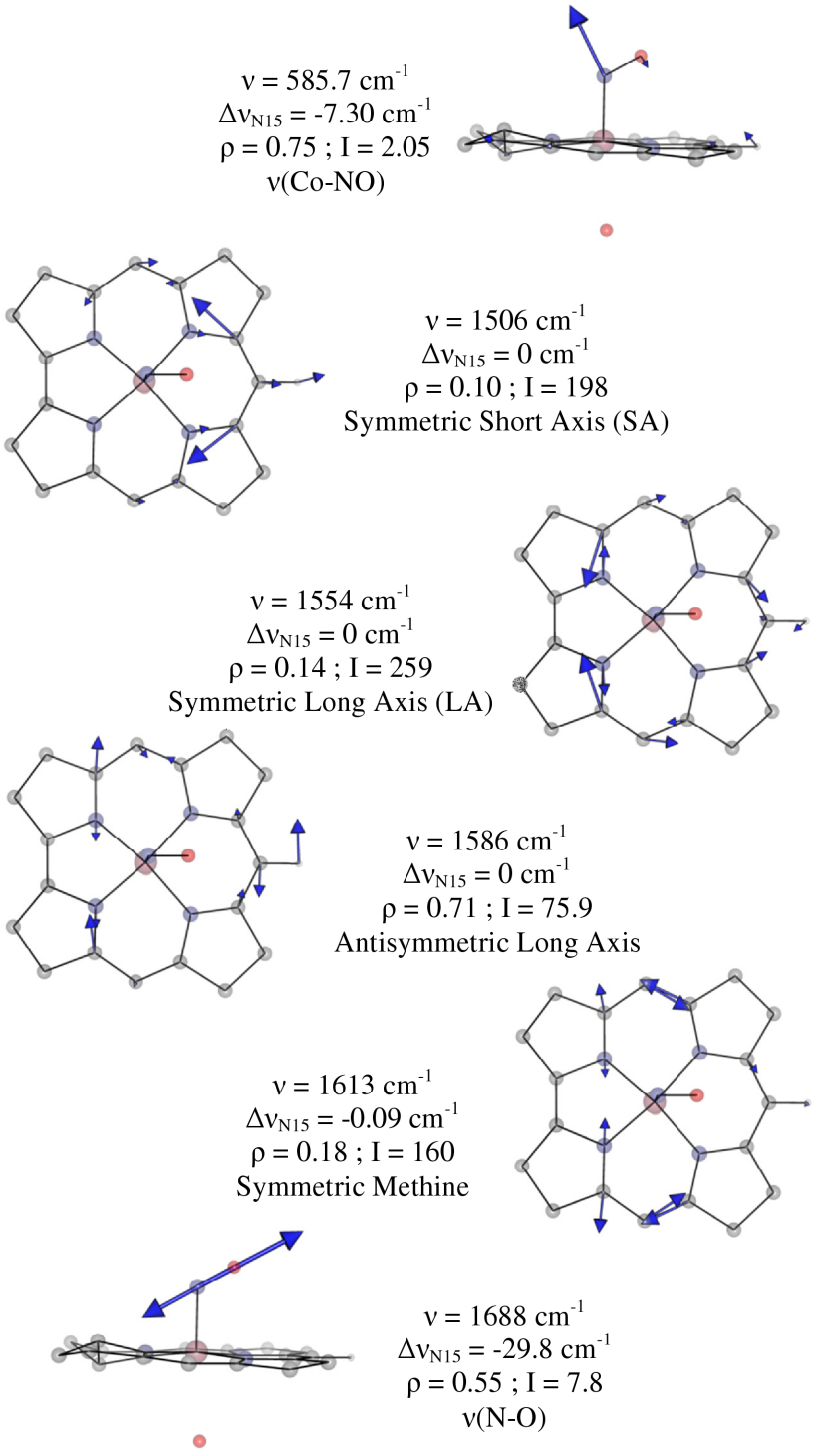

Figure 2.7: Eigenvector representations of the relevant normal modes for the truncated NOCbi^{+} model, as obtained with DFT. The computed frequency (Î½), isotope shift upon 14NOâ†'^{15}NO substitution (Δν N15), depolarization ratio (Ï'), off-resonance Raman intensity (I), and assignment are shown for each mode.

into the α/β bands (Figure 3.4). Even though DFT methods typically overestimate vibrational frequencies, the agreement between the experimental and computed frequencies for these modes is excellent, thus permitting a straightforward assignment of the relevant vibrational features. Specifically, the 1497 cm^{-1} feature observed experimentally is assigned to the formally totally symmetric ν_{S1} mode predicted at 1506 cm^{-1}, which involves nuclear motion primarily along the short axis of the corrin ring. Alternatively, the 1541 and 1603 cm^{-1} features in the experimental rR spectra are attributed to the ν_{S2} and ν_{S3} modes predicted at 1554 and 1613 cm^{-1} respectively. These modes mainly entail C–N stretching motion along the long axis of the corrin ring and symmetric methine stretching motion, respectively. The remaining feature observed at 1572 cm^{-1} is then assigned to the antisymmetric ν_{as} mode predicted at 1585 cm^{-1}. While the large depolarization ratio (0.71) computed for ν_{as} suggests that this mode should not be resonance enhanced, it is predicted to carry significant off-resonance Raman intensity and to entail large displacements of corrin ring atoms, thus facilitating intensity enhancement via Herzberg-Teller coupling.[55, 56] Overall, these assignments are consistent with the DFT-assisted vibrational analysis recently carried out for CNCbl and its reduced derivatives.[44]

Our calculations for $NOCbi^+$ also predict two modes at 569 and 585 cm^{-1} with $^{14}NO \rightarrow {}^{15}NO$ isotope shifts of $\Delta\nu N15 =$ -7.3 and -6.0 cm^{-1}, respectively. These predictions agree reasonably well with the frequencies (515 cm^{-1} and 532 cm^{-1}) and isotope shifts ($\Delta\nu N15 =$ -15 and -11 cm^{-1}) observed experimentally. Both of these modes involve large atomic displacements along the Co–N(O) stretching and Co-

N-O bending coordinates, and are coupled out of phase and in phase, respectively, with corrin ring breathing modes. As such, the distinction between bending and stretching modes becomes ambiguous in this case. Only one additional $^{14}NO \rightarrow {}^{15}NO$ isotope sensitive mode is predicted at 1688 cm^{-1}, corresponding to a relatively pure N-O stretch. While this mode is predicted to be strongly IR active, it carries negligible intensity in the computed off-resonance Raman spectrum (Figures S13 and S14, respectively). This observation, as well as the lack of mechanical coupling between the N-O and corrin ring stretches and the weak electronic coupling between the NO moiety and corrin π system (see below) predicted computationally are consistent with the absence of a feature attributable to the N-O stretch in our experimental rR spectra of NOCbl and $NOCbi^{+}$.

(iv.) DFT-Computed MO Diagrams. The good agreement between the experimental and computed Abs, CD, and vibrational data presented above indicates that DFT successfully models the salient bonding interactions present in NOCbl and $NOCbi^{+}$. For both species, the relative energies of the Co 3d-based MOs reflect the strongly σ- and weakly π -donating nature of the tetradentate corrin ligand. Among these orbitals (see Figure 3.8), the Co $3d_{x^2-y^2}$-based MO (#158 in the case of NOCbl) is essentially non-bonding and thus lowest in energy, whereas the Co 3dxy-based MO (distributed over MOs #167 and #168 due to mixing with another, energetically proximate MO) is strongly σ-antibonding with respect to the Co–N(corrin) bonds and therefore highest in energy (note that the x and y axes are rotated by 45° about z from their usual orientations due to the Co–N(corrin) π-bonding interactions). Intriguingly, the HOMO and LUMO of NOCbl derive mostly from Co 3d and NO

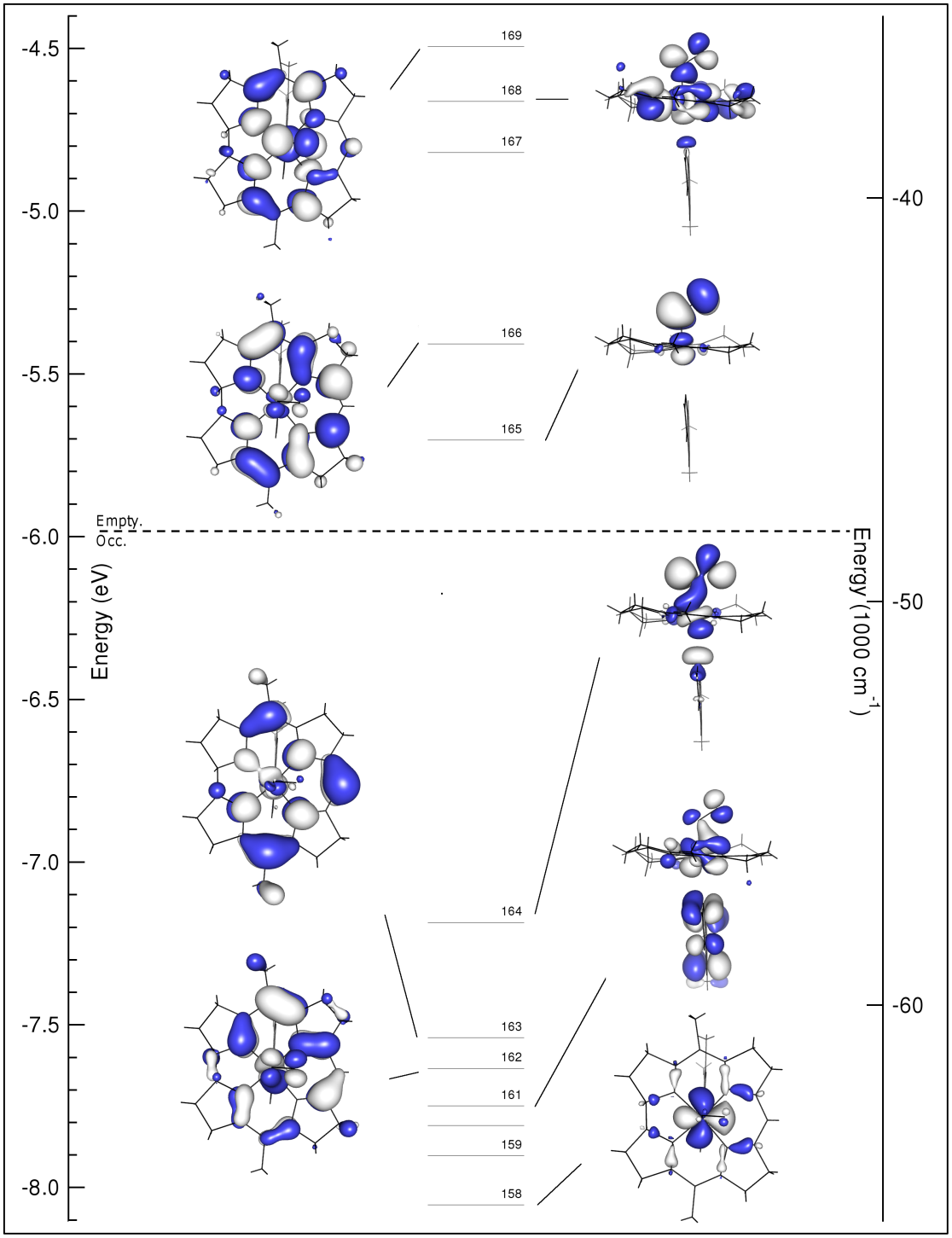

Figure 2.8: Isosurface plots of the relevant MOs of NOCbl. The dashed line separates occupied from empty orbitals.

π^*orbitals, in contrast to the case of alkylcobalamins (e.g. MeCbl) where these MOs are primarily corrin π/π^*-based.[4] Specifically, the HOMO of NOCbl contains 28% Co $3d_{z^2}$ and 40% NO $\pi^*_{\parallel}$ orbital contributions (to differentiate between the two NO π^* orbitals, the one with its lobes roughly parallel to the Co–N(O) bond axis will be denoted as $\pi^*_{\parallel}$ and the other as $\pi^*_{\perp}$), making it strongly σ bonding with respect to the Co–N(O) bond (see Figure 3.8 for MO plots and Table A.2.1 for compositions). Alternatively, the LUMO corresponds to the π antibonding combination of the Co $3d_{yz}$ and the NO $\pi^*_{\perp}$ orbitals (15% and 78%, respectively), with the bonding counterpart being considerably lower in energy (MO #162).

Upon replacement of the axial DMB ligand of NOCbl with a more weakly σ-donating water molecule in $NOCbi^+$, MOs with large Co $3d_{z^2}$ orbital contributions (MOs #163, #164, #167, and #168 of NOCbl, corresponding to MOs #128, #130, #133, and #134 of $NOCbi^+$, see Figure 3.9) are stabilized by 0.1 eV relative to the Co $3d_{x^2-y^2}$-based MO, which was chosen as the reference point because its composition remains essentially unchanged from NOCbl to $NOCbi^+$ (see Tables S1 and S2). In particular, the Co $3d_{z^2}$/NO $\pi^*_{\parallel}$-based HOMO of $NOCbi^+$ (#130) loses the σ-antibonding interaction with the lower axial ligand and gains contributions from the corrin π_7 MO. This mixing causes a large stabilization of the corrin π_7-based MO #128 of $NOCbi^+$ (corresponding to MO #163 of NOCbl) relative to the corrin π_8-based MO #132 (MO #166 of NOCbl).

(v.) TDDFT-Assisted Spectral Assignments. Given the satisfactory agreement between the experimental and computed spectroscopic data of NOCbl and $NOCbi^+$, it is reasonable to assign the key Abs features of these species within the framework

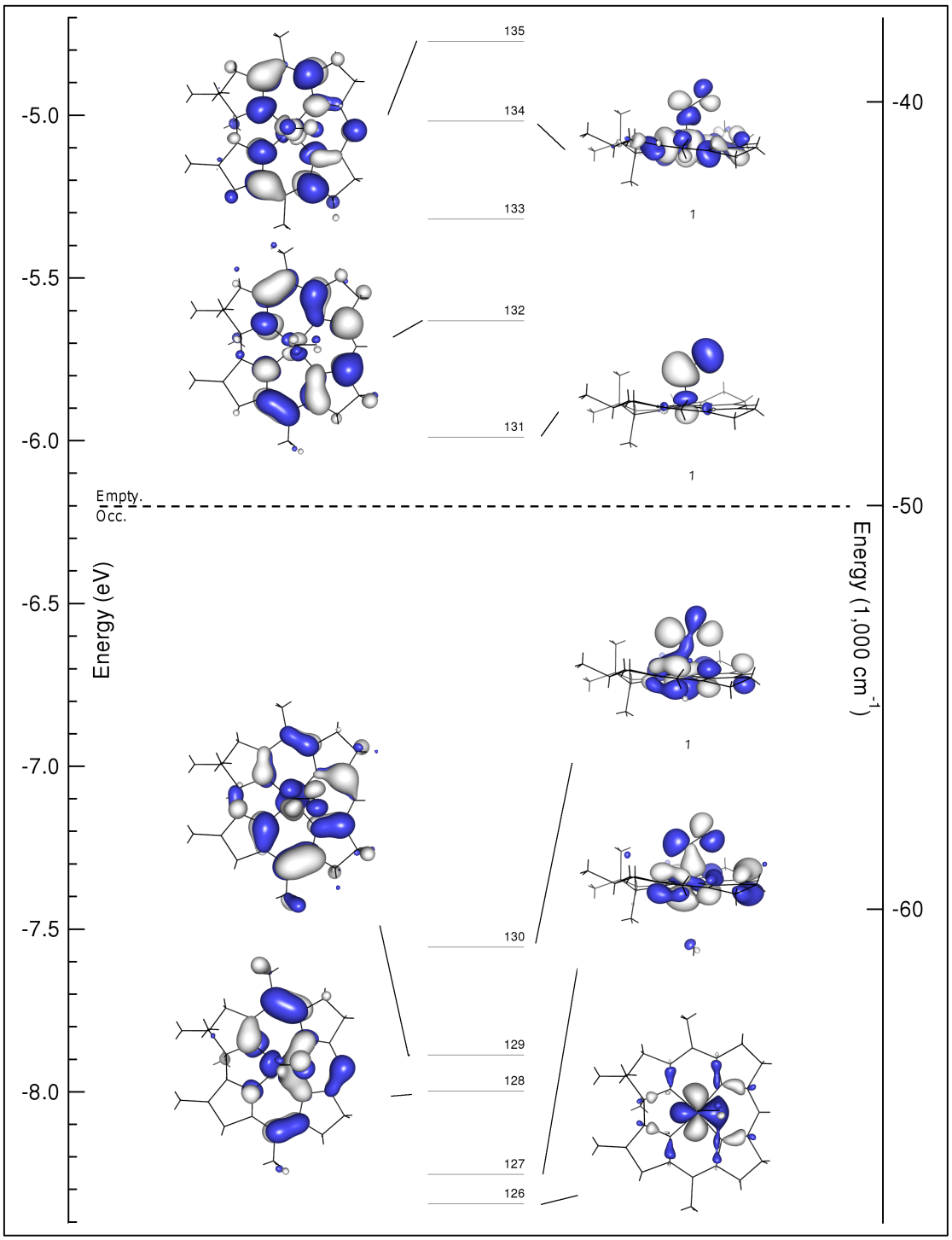

Figure 2.9: Isosurface plots of the relevant MOs of NOCbi$^+$. The dashed line separates occupied from empty orbitals.

of the DFT-based MO descriptions as provided by the TDDFT results. Because in the TDDFT formalism, electronic transitions are described as linear combinations of one-electron excitations between occupied and virtual MOs, it becomes difficult to identify the nature of a given transition in cases where multiple excitations make significant contributions. One approach to overcome this problem involves computing the corresponding electron difference density maps (EDDMs), which provide a visual representation of the changes in electron density accompanying an electronic transition. On the basis of such EDDMs (Figure 3.6), the electronic transitions producing the dominant contributions to the TDDFT-computed Abs spectra can be assigned as shown in Table A.2.3 for NOCbl and Table A.2.4 for NOCbi$^+$. In the case of NOCbl, the five lowest-energy transitions carrying significant Abs intensity give rise to one broad feature in region *i* of the computed Abs spectrum (Figure 3.6, top), with two transitions (involving excited states 12 and 15) having the largest oscillator strengths. Based on its EDDM, transition 12 primarily entails a one-electron excitation from the corrin π_7-based MO #163 to the corrin π_8-based MO #166, characteristic of the transition that is generally responsible for the α/β bands. The largest changes in electron density occur within the C9–C10–C11 fragment of the corrin ring, consistent with the strong rR enhancement of the ν_{S1} mode observed experimentally (Figure 3.5).

The EDDMs for the dominant transitions in regions *ii* (excited states 21, 23, and 26) and iii (excited state 37) display large changes in electron density around the DMB and NO ligands, due to one-electron excitations from MOs with significant orbital contributions from the DMB group. Lastly, regions *iv* and *v* are dominated by

several intense corrin $\pi \rightarrow \pi^*$ transitions that also cause a moderate electron density redistribution at the Co center as a result of the sizable Co 3d orbital character in the donor and acceptor MOs. The prediction of numerous intense features in the γ-region of the computed Abs spectrum, as opposed to a single, relatively sharp band as is usually observed for Co(III)Cbl species,[4] is consistent with the "unique" Abs spectrum obtained experimentally for NOCbl.

From NOCbl to NOCbi$^+$, TD-DFT predicts the most intense feature in the visible region of the Abs spectrum to blue-shift by 3,500 cm^{-1}, in qualitative agreement with the 1,000 cm^{-1} shift of the α/β bands shift observed experimentally (Figure 3.6). However, additional features are present in the near-IR region of the computed Abs spectrum that have no discernible counterparts in the experimental spectrum. As revealed by their EDDMs (Figure A.2.15), the transitions associated with the first two features in regions *0* and *ia* cause a large electron redistribution within the Co–NO moiety (see Table A.2.4). The fact that analogous features are not observed experimentally indicates that TDDFT incorrectly predicts the intensities and/or energies of these charge transfer (CT)-type transitions of NOCbi$^+$; similar cases where TDDFT fails to properly describe CT excited states are well documented in the literature.[57, 58] The remaining changes in the computed Abs spectra from NOCbl to NOCbi$^+$ pertain to a significant intensity redistribution among the dominant features in the γ-region, which is again in good qualitative agreement with our experimental results.

Because our TDDFT computations reproduce the key differences between the Abs spectra of NOCbl and NOCbi$^+$ observed experimentally quite well, the com-

puted MO diagrams can be used as the basis for exploring the electronic structural origin of these differences. As described above, the DMB→H_2O ligand substitution causes a stabilization of MOs with significant Co $3d_{z^2}$ orbital contributions relative to the other MOs. Of particular importance with respect to the α/β band transition is the stabilization of the corrin π_7-based donor MO relative to the corrin π_8-based acceptor MO from NOCbl (MOs #163 and #166) to $NOCbi^+$ (MOs #128 and #132), which readily explains the blue-shift of the α/β-bands observed experimentally (Figures 3.2, 3.3 and 3.6). Interestingly, in the case of alkylcobalamins that also possess a strong σ-donor ligand in the upper axial position, the blue-shift of the α/β bands in response to DMB→H_2O ligand substitution is considerably larger than in the case of NOCbl; e.g., 2,500 cm^{-1} for MeCbl4 versus 1,000 cm^{-1} for NOCbl. This difference can be understood in terms of the larger σ-donation from the upper ligand in NOCbl than in alkylcobalamins, which leads to a weaker Co–N(DMB) bond and, thus, to less pronounced changes in the electronic structure upon lower ligand substitution in the former species. In fact, our experimentally validated computed MO description for NOCbl bears some intriguing similarities to that developed previously for Co(II)Cbl, especially with regards to the energies of the Co 3d-based MOs relative to the corrin π/π^*-based MOs.[23] This observation indicates that the high degree of σ-donation from the occupied NO $\pi^*_{\|}$ orbital into the formally unoccupied Co $3d_{z^2}$ orbital leads to a significant decrease in the effective nuclear charge experienced by the Co 3d orbitals in NOCbl. However, the NO→Co charge donation is partially compensated for by the strong π-backbonding interaction involving the doubly occupied Co $3d_{yz}$ orbital and formally empty NO

$\pi^*_\perp$ orbital. A more detailed analysis of the salient Co–NO bonding interactions within the NBO formalism is presented next.

(vi.) NBO-Based Co–NO Bonding Description. While a relatively straightforward correlation can be established between the DFT/TDDFT-predicted and experimentally observed properties of NOCbl and NOCbi$^+$, a direct evaluation of the key Co–NO bonding interactions is complicated by the partial delocalization of the relevant MOs over the corrin ring. To overcome this challenge, we have resorted to the NBO formalism within which the calculated electron density is partitioned into chemically intuitive bonding MOs and electron pairs so as to generate a bonding description closely adhering to the Lewis structure formalism.[59] Because the Co–N(O) bonding interactions of NOCbl and NOCbi$^+$ are essentially identical as judged on the basis of our experimental rR data and DFT results (*vide supra*), the following analysis will focus on the electronic structure of NOCbi$^+$. The relevant NBOs, labeled by their primary orbital contributors and classified either as bonding (BD) or antibonding (BD*) with respect to the Co–NO bond, are shown in Figure 3.10 (left). As expected on the basis of the DFT results described above, the Co $3d_{z^2}$ BD-NBO is characterized by a highly covalent Co–NO σ-bonding interaction. However, shortcomings of the Lewis structure-like description for NOCbi$^+$ are evident from by the relatively large occupancies of several formally empty orbitals, most importantly the antibonding Co 3dxy BD*-NBO and Co 4s BD*-NBO, as well as the occupancies of considerably less than 2 of some of the formally doubly occupied orbitals. These observations indicate that deviations from a single Lewis structure, treated within the NBO framework as donor-acceptor hyperconjugation

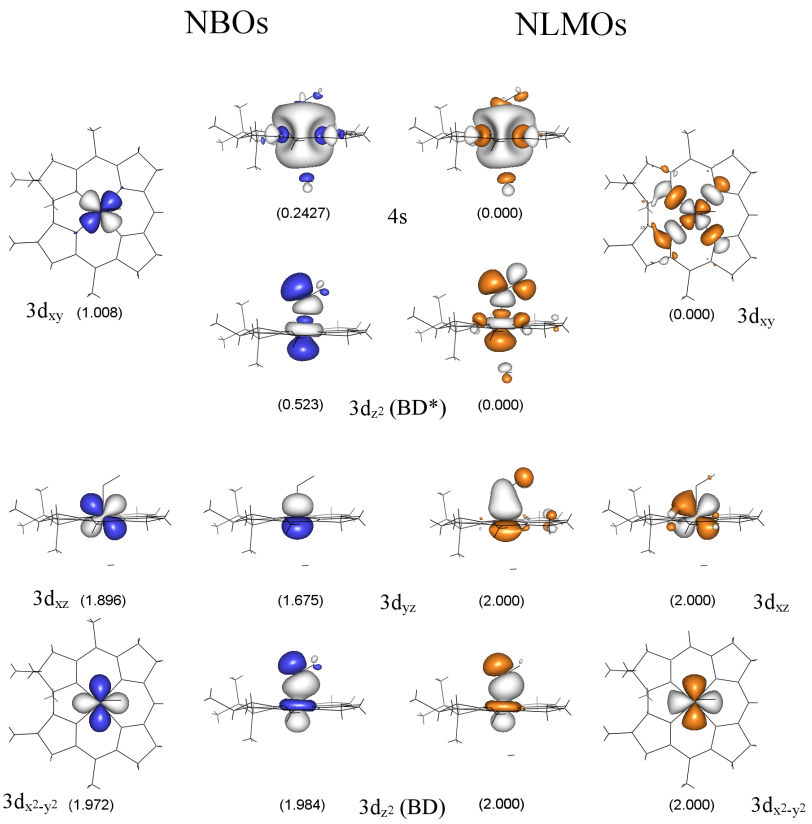

Figure 2.10: Isosurface plots of the metal-based NBOs (in blue/gray) and corresponding NLMOs (in orange/gray) of NOCbi$^+$. Occupancies are shown below each orbital. The composition of the NBOs and their percent contributions to the NLMOs are provided in Table 3.5.

interactions,[60] are important for properly describing the bonding interactions in NOCbi$^+$. These interactions can be fully accounted for by transformation of the canonical MOs to a set of natural localized MOs (NLMOs), which are constructed to retain a large amount of NBO character. These NLMOs possess integer occupancies, like the canonical MOs, and retain a high degree of the Lewis-structure description obtained with the NBO analysis, providing a useful connection between

the canonical MOs and the NBOs.[59, 61, 62]

The relevant NLMOs for NOCbi$^+$ are shown in Fig 10 (right) and their compositions are provided in Table 3.5. Inspection of the Co $3d_{z^2}$ BD-NLMO discloses a very covalent σ-bonding interaction between the Co ion and NO (58% Co $3d_{z^2}$ and 42% N(O) 2pz orbital contributions, see Table 3.5), as anticipated on the basis of the canonical MO and NBO compositions. Intriguingly, while the Co $3d_{z^2}$ BD-NLMO, as well as the nonbonding Co $3d_{x^2-y^2}$ and $3d_{xz}$ NLMOs are very similar to their corresponding NBOs, the $3d_{yz}$ BD-NLMO shows distinct differences. The composition of this NLMO reveals that it only retains 83.1% of "pure" Co $3d_{yz}$ NBO character (in comparison to >95% for the other Co-based NLMOs) due to a sizeable π-backbonding interaction between the Co $3d_{yz}$ orbital and the NO $\pi^*_\perp$ orbital (Figure 3.10, center columns). Since the Co $3d_{yz}$ orbital only mixes with the NO $\pi^*_\perp$ orbital (Figure 3.10), the amount of charge backdonation from Co to NO can be estimated to be 0.32 electrons. Due to the presence of this π-backbonding interaction, the Co ion does not retain a Co(II)-like electronic structure as might be anticipated on the basis of the large σ-donation from the NO $\pi^*_\parallel$ orbital into the Co $3d_{z^2}$ orbital. Lastly, the unoccupied Co $3d_{z^2}$ BD*-NLMO and Co 3dxy BD* NLMO are σ-antibonding with respect to the corrin ring and the axial ligand orbitals, as expected from LF theory. These NLMOs are very similar in composition to their NBO counterparts, retaining > 95% of NBO character (see Table 3.5 and Figure 3.10, outside columns).

The NBO/NLMO results can also be used to estimate the number of electrons in the Co 3d atomic orbitals (AOs), and thus an effective oxidation state of the

Table 2.2: Summary of NBO and NLMO results for NOCbi$^+$. Energies, occupancies, and percent Co/N_{NO} compositions of the Co-based NBOs are shown, in addition to the percent contributions of these NBOs to the corresponding NLMOs. Low occupancy NBOs, which correspond to formally empty orbitals, are highlighted in red.

NBO	E (eV)	Occupancy	%Co	$\%N_{NO}$	% in NLMO
Co(BD) $3d_{z^2}$	−11.572	1.984	58.1	41.9	99.1
Co $3d_{x^2-y^2}$	−8.305	1.972	100	- -	98.6
Co $3d_{xz}$	−8.106	1.896	100	- -	94.5
Co $3d_{yz}$	−8.272	1.675	100	- -	83.1
Co $3d_{xy}$	−8.682	1.008	100	- -	
Co(BD)* $3d_{z^2}$	−8.397	0.523	41.9	58.1	
Co 4s	7.116	0.243	100	- -	

Co ion. As the number of d-electrons is sensitive to the covalency of the metal-ligand bonding interactions as well as the delocalization of the 3d orbitals, the following approach was used to estimate this value (see SI for additional details). First, the %NBO composition of each NLMO (see Table 3.5) was used to calculate the fractional occupancy of the Co 3d-based NBO(s) contributing to this particular NLMO. This electron count was then partitioned into Co 3d-based and ligand-based contributions, estimated based on the %Co 3d and %N(O) contributions to each NBO. Finally, the fractional Co 3d electron counts for all NLMOs obtained using this procedure were added up to estimate the total number of Co 3d electrons. Using this approach, an effective number of Co 3d electrons of 6.27 was obtained for NOCbi$^+$, larger than a value of 6 expected for a Co(III) species. This result corroborates the conclusion drawn from the energies and compositions of the canonical MOs regarding the relatively-high Co(II) character in the electronic structures of NOCbl and NOCbi$^+$. Thus, while the large amount of electron donation from NO to Co in

the Co $3d_{z^2}$ BD-NLMO is partially offset by the strong π-backbonding interaction in the Co $3d_{yz}$ BD-NLMO, our NBO/NLMO analysis clearly shows that a Co(III)–NO^- description for $NOCbi^+$, and by analogy NOCbl, is inaccurate. Rather, these species are better described as resonance hybrids with both Co(III)–NO^- and Co(II)–NO• limiting structures being major contributors.

2.5 Discussion

Given the roles of NO as a blood pressure regulator, neurotransmitter, and second messenger,[63] as well as a cytotoxic agent in immunological response,[63] the ability of Co(II)Cbl to scavenge this molecule in vivo to form NOCbl is of considerable interest.[9, 10] Additionally, NOCbl has been shown to be potentially useful for targeted NO delivery as a chemotherapeutic or vasodilating agent,[64, 12] since its Co–NO bond can be broken under physiological conditions for controlled NO release. Thus, elucidating the nature of the bonding interaction between the NO ligand and the Co center in NOCbl represents an important step toward the development of an improved understanding of the chemical and biological properties of this molecule. Previous reports have highlighted the unique structural properties of NOCbl relative to other biologically relevant cobalamins, most notably the presence of an unprecedentedly long Co–N(DMB) bond in this species. However, because NOCbl exhibits similar spectroscopic signatures as the well characterized alkyl-Co(III)Cbls, such as MeCbl and AdoCbl,[4] it has generally been described as a Co(III)-NO^- species.

To test this assumption, we have developed experimentally validated electronic

structure descriptions for NOCbl in its base-on and base-off states. While our Abs spectrum of NOCbl in fluid solution at 300 K is similar to those reported in the literature,[2, 25] we have discovered a previously unobserved thermochromism for this species (Figures S3). From a comparison to the Abs data obtained for $NOCbi^+$, a model of base-off NOCbl, we conclude that an increase in temperature from 4.5 to 300 K causes a shift in the base-on to base-off equilibrium for NOCbl, favoring dissociation of the N(DMB) ligand at high temperatures. This change in Co coordination environment has, however, negligible effects on the Co–NO bonding interaction, as evidenced by our rR data, TDDFT results, and NBO analysis. The origin and implications of these findings is discussed below.

Co–NO Bonding: Collectively, our spectroscopic and computational data reveal that NOCbl is inadequately described as a Co(III)-NO^- species, because significant charge donation from the NO ligand notably alters the effective nuclear charge of the metal center. Compared to the methyl group of MeCbl, the NO ligand of NOCbl is an even stronger σ-donor, therefore inducing additional Co $3d_{z^2}$ orbital character into the HOMO and further enhancing the Co–N(DMB) σ antibonding interaction in this orbital. Our DFT-computed MO description indicates that the formally unoccupied Co $3d_{z^2}$ orbital contributes by as much as 29% to the HOMO of NOCbl, as compared to 7% in MeCbl.[4] This prediction is consistent with the observed lengthening of the Co–N(DMB) bond from 2.16 Å in MeCbl to 2.35 Å in NOCbl as determined by X-ray crystallography.[65, 16] The high degree of electron donation from NO is particularly evident from an analysis of the NLMOs and NBOs (Figure 3.10) derived from the canonical MOs obtained with DFT. Based on this analysis, the

doubly occupied $3d_{z^2}$ BD-NLMO contains 58% Co 3d orbital character (Table 3.5), consistent with a very covalent Co–NO bond. Another unique feature of the Co–NO bond in NOCbl and $NOCbi^+$ compared to the axial bonds in other Co(III)corrinoid species is the presence of a sizable π-backbonding interaction involving the Co $3d_{yz}$ and NO $\pi^*_\perp$ orbitals. Inspection of the Co $3d_{yz}$ BD-NLMO reveals that the NO ligand contribution to this orbital is 16%, leading to an estimate for the extent of π-donation of 0.32 electrons. This backbonding partially compensates for the large amount of σ-donation from the NO ligand into the Co $3d_{z^2}$ orbital, and represents an unprecedented mechanism by which the electronic properties of the Co(III) ion can be modulated by the axial ligands.

The high degree of NO→Co σ-donation in NOCbl weakens the Co–N(DMB) bond to the point that at high temperature, the base-on to base-off equilibrium favors a unique pentacoordinate species in aqueous solution. In the case of $NOCbi^+$, an effectively five-coordinate species is present at all temperatures, suggesting that the strong trans influence exerted by the NO ligand precludes the binding of a weakly donating water molecule even at 4.5 K. Nonetheless, during the geometry optimization of a complete $NOCbi^+$ model, the lower water ligand did not fully dissociate. A comparison of this structure and that obtained for the truncated model reveals major differences in terms of the orientation of the water molecule, indicating that the propanoamide side chains of the corrin ligand, which were absent in the truncated model, may play an important role in modulating the lower axial bonding interaction in cobalamins.

Further experimental support for our bonding description for NOCbl is provided

by published NMR data, which indicated that the ^{15}N-resonance of the NO ligand undergoes a 40 ppm upfield shift upon protonation and dissociation of the DMB ligand in the lower axial position.[11] Although the observed change in electron shielding experienced by the ^{15}N nucleus was originally attributed to an increase in the Co–N–O bond angle from base-on to base-off NOCbl, our rR and DFT results provide compelling evidence that the Co–NO core structures of these two species are in fact virtually identical. Instead, our computational data suggest that the enhanced shielding of the ^{15}N nucleus in base-off NOCbl reflects the weaker σ-antibonding interaction between Co and the lower axial ligand in that species (cf. MOs #164 of NOCbl and #130 of NOCbi$^+$ in Figures 3.8 and 3.9, respectively) and the consequent increase in N(O) natural charge by 4% (see Table 4.2).

Table 2.3: Summary of the results obtained from a natural population analysis (NPA) for the NOCbl, NOCbi$^+$, and O_2Cbl truncated models.

	Natural Charge			Natural Bond Order		
Species	Co	X_{Upper}	X_{Lower}	Co–X_{Upper}	Co–X_{Lower}	X_{Upper}–O
A. NOCbl	0.82	0.15	−0.47	0.82	0.07	1.98
B. NoCbi$^+$	0.82	0.16	−0.96	0.84	0.02	1.98
C. O_2Cbl	0.84	−0.14	−0.42	0.47	0.25	0.75

Extension to O_2Cbl: Previous crystallographic[26] and EPR studies[66] have indicated that Co(II)Cbl binds molecular oxygen reversibly to yield superoxocobalamin (O_2Cbl) as the first step in the autoxidation process that eventually yields H_2OCbl$^+$. O_2Cbl may also be of physiological importance as free cobalamin is present predominantly in the Co(II)Cbl state in vivo.[67] Given the similar frontier orbitals of

Table 2.4: EPR parameters for Co(II)Cbl in the presence of $EutT^{WT}$/Co. Percent contributions to the overall trace from individual Co(II)Cbl species are highlighted in bold. Parameters for free Co(II)rrinoids from reference 18 are also shown for comparison.

	g-values			A(^{59}Co)			A($^{17}O_\alpha$)			A($^{17}O_\beta$)		
Method	g_1	g_2	g_3	A_1	A_2	A_3	A_1	A_2	A_3	A_1	A_2	A_3
A. Experiment[1]	1.993	2.013	2.089	−30	−64.8	−18.7	−167	59	∗[2]	−201	70	∗[2]
B. DFT	1.992	1.008	2.041	−28	−50.8	−1.1	−146	77	44	−191	81	46

NO and O_2, which has been widely exploited to mimic the binding of dioxygen to metal centers in proteins by using nitric oxide, it is interesting to compare the electronic structures of NOCbl and O_2Cbl. While crystallographic data for these species have revealed that both the NO and O_2 molecules ligate to the Co center in a bent end-on fashion, the axial Co–N(DMB) bond length differs by 0.29 Å between NOCbl (2.35 Å)[16] and O_2Cbl (2.06 Å).[26] Hence, the Co–N(DMB) bond length in O_2Cbl is also considerably shorter than in MeCbl (2.16 Å)[52] but very similar to that reported for CNCbl (2.041 Å),[52] which is considered to possess a moderately strong σ-donor in the upper axial position based on computational analyses and the fact that this species exhibits a "typical" Co(III)Cbl Abs spectrum.[4]

The NLMOs for O_2Cbl are shown in Figure 2.11 and the compositions of the relevant NBOs and NLMOs are listed in Table 2.5 (note that our electronic structure description for O_2Cbl is supported by a previous single-crystal EPR characterization of this species,[66] given the good agreement between the computed and experimental g-values and hyperfine coupling constants, see Table 2.4). Due to the spin unrestricted formalism used in these calculations, the NLMOs have occupancies of 1.00 and are divided into a set of spin-up (α, majority spin. Figure 2.11, left)

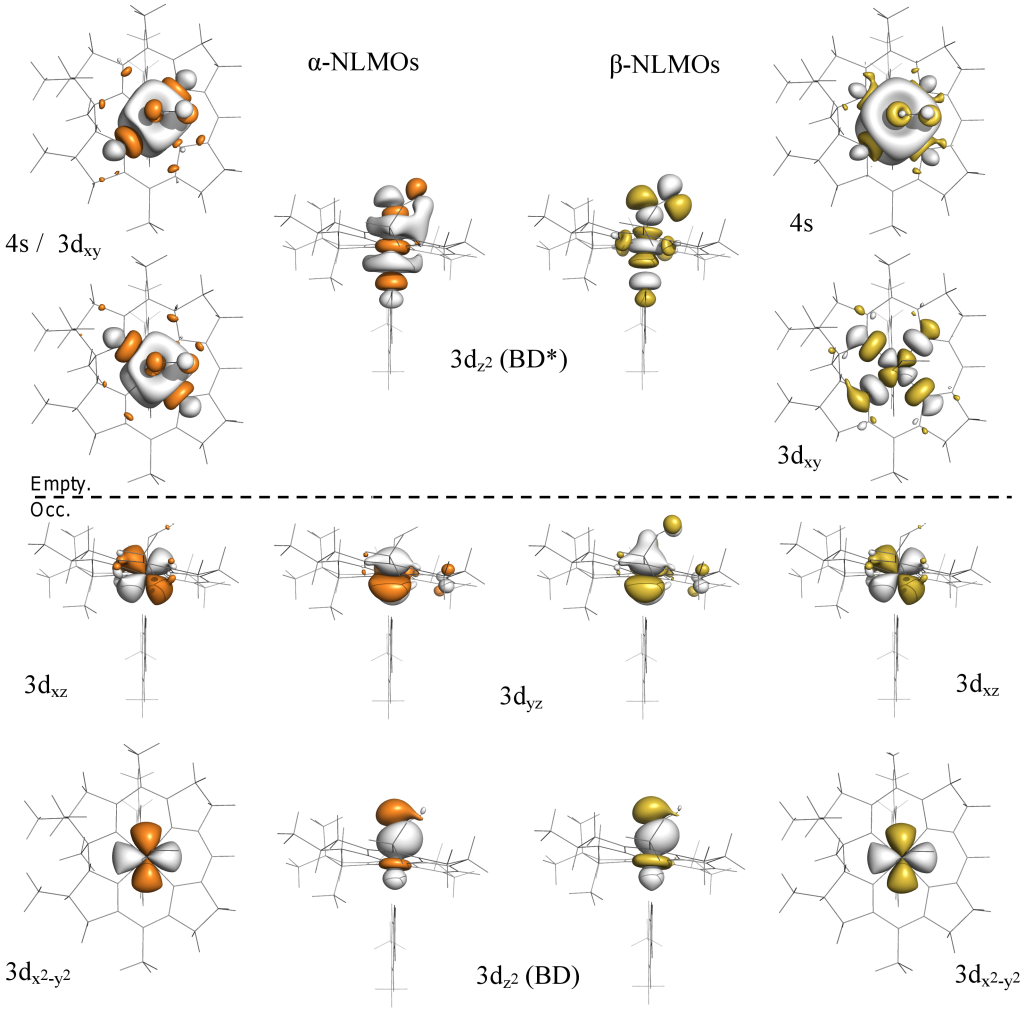

Figure 2.11: Isosurface plots of the metal-based NLMOs of O_2Cbl. Alpha orbitals (majority spin, on left) are shown in orange/gray, while beta orbitals (minority spin, on right) are shown in yellow/gray. The horizontal dashed line separates singly occupied from empty orbitals. NLMOs are labeled according to the Co-based NBO providing the largest contribution. The compositions of the NLMOs in terms of the corresponding NBOs are provided in Table 3.5.

and spin-down orbitals (β, minority spin. Figure 2.11, right). An inspection of the NLMOs of O_2Cbl reveals that these orbitals are very similar in composition to the NLMOs of NOCbl, although with some important differences. For both sets of spin-orbitals, the Co $3d_{xz}$- and Co $3d_{x^2-y^2}$- NLMOs of O_2Cbl are nonbonding with respect to the ligand framework, in an analogous manner as the NLMOs of NOCbl. Additionally, the compositions of the β-NLMOs of O_2Cbl (Table 2.5, right) reflect the presence of a relatively covalent Co–O_2 bond, with a Co 3d orbital contribution to the Co $3d_{z^2}$(BD)-β-NLMO of 41%, as compared to 58% predicted for NOCbl (see Table 3.5). However, the Co contribution to the spin-up counterpart (i.e. the Co $3d_{z^2}$(BD)-α-NLMO) is merely 24%. Thus, the net σ-donation to the Co(III) ion from O_2 in O_2Cbl is smaller than from NO in NOCbl, consistent with the greater oxidizing power of O_2 ($E^\circ = -0.16$ V vs NHE) versus NO ($E^\circ = -0.8$ V NHE).[68] Likewise, the effective number of Co 3d electrons of O_2Cbl, computed as described above for NOCbl, is 6.08, consistent with the classification of this species as a "typical" Co(III)Cbl based on its short Co–N(DMB) bond. Thus, our computational results indicate that O_2Cbl is adequately described as a Co(III)-O^- species.

Implications for Biological Systems: Biochemical studies have shown that NO can inhibit the two B_{12}-dependent enzymes found in humans, MetH and MMCM,[7,8] which could provide an additional pathway for the regulation of these enzymes. Specifically, it was shown that inhibition of MMCM in the presence of NO donors resulted in the formation of NOCbl in the active site of the enzyme.[8] For this and related enzymes, the formation of NOCbl in the active site and consequent inhibition of catalytic activity would require a repair mechanism involving NO

Table 2.5: Summary of NBO and NLMO results for O_2Cbl. Energies, occupancies, and percent Co/O_{O^2} compositions of the Co-based NBOs are shown for α (majority spin) and β (minority spin) orbitals, in addition to the percent contributions of these NBOs to the corresponding NLMOs. Low occupancy NBOs, which correspond to formally empty orbitals, are highlighted in red text.

	Alpha Orbitals				Beta Orbitals			
NBO	Occ.	%Co	%O_{O^2}	% in NLMO	Occ.	%Co	%O_{O^2}	% in NLMO
Co(BD) $3d_{z^2}$	0.962	23.6	76.4	96.1	0.992	40.8	59.2	99.1
Co $3d_{x^2-y^2}$	0.987	100	- -	98.7	0.986	100	- -	98.6
Co $3d_{xz}$	0.941	100	- -	93.9	0.943	100	- -	94.1
Co $3d_{yz}$	0.950	100	- -	94.8	0.911	100	- -	90.1
Co $3d_{xy}$	0.230	80.0	20.0		0.523	100	- -	
Co(BD)* $3d_{z^2}$	0.237	76.4	76.4		0.344	59.2	40.8	
Co 4s	0.230	20.0	80.0		0.119	100	- -	

dissociation or replacement of NOCbl by AdoCbl. Given the strong Co–NO bond in NOCbl as revealed by the present investigation, NOCbl removal from the active site of these enzymes is expected to be the main pathway for reactivation. This process could be facilitated by the strong trans influence exerted by the NO ligand. MMCM binds AdoCbl in the "base-off/His-on" conformation,[6] and based on the results obtained in this study, it can be speculated that NO coordination to the transiently formed Co(II)Cbl species in the enzyme active site will considerably weaken the Co–N(His) bond. Similarly, for B_{12}-dependent enzymes that bind AdoCbl in the base-on conformation,[69] the Co–N(DMB) bond elongation and additional geometric changes in response to NO coordination to the Co(II)Cbl intermediate may be sufficient to promote dissociation of the NOCbl product from the active site. Although more experimental evidence is needed to support these hypotheses, the results obtained

on this study offer unprecedented insights into the spectral and electronic properties of NOCbl and provide useful spectroscopic markers for probing the interaction of this species with B_{12}-dependent enzymes.

2.6 References

[1] D. C. Hodgkin, J. Kamper, M. Mackay, J. Pickworth, K. N. Trueblood, and J. G. White. Structure of vitamin B_{12}. *Nature*, 178(4524):64–6, 1956.

[2] H. A. Hassanin, L. Hannibal, D. W. Jacobsen, K. L. Brown, H. M. Marques, and N. E. Brasch. NMR spectroscopy and molecular modelling studies of nitrosylcobalamin: further evidence that the deprotonated, base-off form is important for nitrosylcobalamin in solution. *Dalton Transactions*, (3):424–433, 2009.

[3] J. D. Woodson, C. L. Zayas, and J. C. Escalante-Semerena. A new pathway for salvaging the coenzyme-B_{12} precursor cobinamide in archaea requires cobinamide-phosphate synthase (CbiB) enzyme activity. *Journal of Bacteriology*, 185(24):7193–7201, 2003.

[4] T. A. Stich, A. J. Brooks, N. R. Buan, and T. C. Brunold. Spectroscopic and computational studies of Co^{3+}-corrinoids: Spectral and electronic properties of the B_{12} cofactors and biologically relevant precursors. *Journal of the American Chemical Society*, 125(19):5897–5914, 2003.

[5] R. V. Banerjee and R. G. Matthews. Cobalamin-dependent methionine synthase. *Faseb Journal*, 4(5):1450–1459, 1990.

[6] M. L. Ludwig and R. G. Matthews. Structure-based perspectives on B_{12}-dependent enzymes. *Annual Review of Biochemistry*, 66:269–313, 1997.

[7] I. O. Danishpajooh, T. Gudi, Y. C. Chen, V. G. Kharitonov, V. S. Sharma, and G. R. Boss. Nitric oxide inhibits methionine synthase activity in vivo and disrupts carbon flow through the folate pathway. *Journal of Biological Chemistry*, 276(29):27296–27303, 2001.

[8] A. Kambo, V. S. Sharma, D. E. Casteel, V. L. Woods, R. B. Pilz, and G. R. Boss. Nitric oxide inhibits mammalian methylmalonyl-CoA mutase. *Journal of Biological Chemistry*, 280(11):10073–10082, 2005.

[9] M. Brouwer, W. Chamulitrat, G. Ferruzzi, D. L. Sauls, and J. B. Weinberg. Nitric oxide interactions with cobalamins: Biochemical and functional consequences. *Blood*, 88(5):1857–1864, 1996.

[10] D. H. Zheng and R. L. Birke. Spectroscopic evidence for nitric oxide binding with cob(II)alamin. *Journal of the American Chemical Society*, 123(19):4637–4638, 2001.

[11] M. Wolak, A. Zahl, T. Schneppensieper, G. Stochel, and R. van Eldik. Kinetics and mechanism of the reversible binding of nitric oxide to reduced cobalamin B_{12r} (cob(II)alamin). *Journal of the American Chemical Society*, 123(40):9780–9791, 2001.

[12] K. E. Broderick, L. Alvarez, M. Balasubramanian, D. D. Belke, A. Makino, A. Chan, V. L. Woods, W. H. Dillmann, V. S. Sharma, R. B. Pilz, T. D. Bigby, and G. R. Boss. Nitrosyl-cobinamide, a new and direct nitric oxide-releasing drug effective in vivo. *Experimental Biology and Medicine*, 232(11):1432–1440, 2007.

[13] L. E. Goodrich, F. Paulat, V. K. K. Praneeth, and N. Lehnert. Electronic structure of heme-nitrosyls and its significance for nitric oxide reactivity, sensing, transport, and toxicity in biological systems. *Inorganic Chemistry*, 49(14):6293–6316, 2010.

[14] J. H. Enemark and R. D. Feltham. Principles of structure, bonding, and reactivity for metal nitrosyl complexes. *Current Contents/Engineering Technology & Applied Sciences*, (47):16–16, 1988.

[15] M. Wolak and R. van Eldik. To be or not to be NO in coordination chemistry?: A mechanistic approach. *Coordination Chemistry Reviews*, 230(1-2):263–282, 2002.

[16] H. A. Hassanin, M. F. El-Shahat, S. DeBeer, C. A. Smith, and N. E. Brasch. Redetermination of the X-ray structure of nitroxylcobalamin: base-on nitroxylcobalamin exhibits a remarkably long Co-N(dimethylbenzimidazole) bond distance. *Dalton Transactions*, 39(44):10626–10630, 2010.

[17] Ed. Banerjee, Ruma. Chemistry and biochemistry of B_{12}, 1999.

[18] M. S. A. Hamza, X. Zou, K. L. Brown, and R. van Eldik. Thermodynamic and kinetic data for the base-on/base-off equilibration of alkylcobalamins. *European Journal of Inorganic Chemistry*, (2):268–276, 2003.

[19] T. C. Brunold, K. S. Conrad, M. D. Liptak, and K. Park. Spectroscopically validated density functional theory studies of the B_{12} cofactors and their interactions with enzyme active sites. *Coordination Chemistry Reviews*, 253(5-6):779–794, 2009.

[20] A. J. Reig, K. S. Conrad, and T. C. Brunold. Combined spectroscopic/computational studies of vitamin B_{12} precursors: Geometric and electronic structures of cobinamides. *Inorganic Chemistry*, 51(5):2867–2879, 2012.

[21] M. D. Liptak, A. S. Fleischhacker, R. G. Matthews, J. Telser, and T. C. Brunold. Spectroscopic and computational characterization of the base-off forms of cob(II)alamin. *Journal of Physical Chemistry B*, 113(15):5245–5254, 2009.

[22] A. T. Smith, T. Majtan, K. M. Freeman, Y. Su, J. P. Kraus, and J. N. Burstyn. Cobalt cystathionine beta-synthase: A cobalt-substituted heme protein with a unique thiolate ligation motif. *Inorganic Chemistry*, 50(10):4417–4427, 2011.

[23] T. A. Stich, N. R. Buan, and T. C. Brunold. Spectroscopic and computational studies of Co^{2+} corrinoids: Spectral and electronic properties of the biologically relevant base-on and base-off forms of Co^{2+} cobalamin. *Journal of the American Chemical Society*, 126(31):9735–9749, 2004.

[24] K. Park, P. E. Mera, J. C. Escalante-Semerena, and T. C. Brunold. Kinetic and spectroscopic studies of the ATP: Corrinoid Adenosyltransferase PduO from Lactobacillus reuteri: Substrate specificity and insights into the mechanism of co(II)corrinoid reduction. *Biochemistry*, 47(34):9007–9015, 2008.

[25] V. S. Sharma, R. B. Pilz, G. R. Boss, and D. Magde. Reactions of nitric oxide with vitamin B_{12} and its precursor, cobinamide. *Biochemistry*, 42(29):8900–8908, 2003.

[26] E. Hohenester, C. Kratky, and B. Krautler. Low-temperature crystal-structure of superoxocobalamin obtained by solid-state oxygenation of the B_{12} derivative cob(II)alamin. *Journal of the American Chemical Society*, 113(12):4523–4530, 1991.

[27] M. D. Liptak and T. C. Brunold. Spectroscopic and computational studies of Co^{1+} cobalamin: Spectral and electronic properties of the superreduced B_{12} cofactor. *Journal of the American Chemical Society*, 128(28):9144–9156, 2006.

[28] SCM ADF2012.

[29] G. T. Velde, F. M. Bickelhaupt, E. J. Baerends, C. F. Guerra, S. J. A. Van Gisbergen, J. G. Snijders, and T. Ziegler. Chemistry with ADF. *Journal of Computational Chemistry*, 22(9):931–967, 2001.

[30] C. F. Guerra, J. G. Snijders, G. te Velde, and E. J. Baerends. Towards an order-N DFT method. *Theoretical Chemistry Accounts*, 99(6):391–403, 1998.

[31] S. H. Vosko, L. Wilk, and M. Nusair. Accurate spin-dependent electron liquid correlation energies for local spin-density calculations - a critical analysis. *Canadian Journal of Physics*, 58(8):1200–1211, 1980.

[32] A. D. Becke. Density-functional exchange-energy approximation with correct asymptotic-behavior. *Physical Review A*, 38(6):3098–3100, 1988.

[33] J. P. Perdew. Density-functional approximation for the correlation-energy of the inhomogeneous electron-gas. *Physical Review B*, 33(12):8822–8824, 1986.

[34] Frank Neese. *ORCA-An Ab initio, Density Functional, and Semiempirical Program Package*, volume 4 of *10*. The name of the publisher, Universitat Bonn: Bonn, Germany, 2.9.1 edition, 2008.

[35] R. Bauernschmitt and R. Ahlrichs. Treatment of electronic excitations within the adiabatic approximation of time dependent density functional theory. *Chemical Physics Letters*, 256(4-5):454–464, 1996.

[36] M. E. Casida, C. Jamorski, K. C. Casida, and D. R. Salahub. Molecular excitation energies to high-lying bound states from time-dependent density-functional response theory: Characterization and correction of the time-dependent local density approximation ionization threshold. *Journal of Chemical Physics*, 108(11):4439–4449, 1998.

[37] R. E. Stratmann, G. E. Scuseria, and M. J. Frisch. An efficient implementation of time-dependent density-functional theory for the calculation of excitation energies of large molecules. *Journal of Chemical Physics*, 109(19):8218–8224, 1998.

[38] S. Hirata and M. Head-Gordon. Time-dependent density functional theory for radicals - an improved description of excited states with substantial double excitation character. *Chemical Physics Letters*, 302(5-6):375–382, 1999.

[39] S. Hirata and M. Head-Gordon. Time-dependent density functional theory within the Tamm-Dancoff approximation. *Chemical Physics Letters*, 314(3-4):291–299, 1999.

[40] K. Eichkorn, O. Treutler, H. Ohm, M. Haser, and R. Ahlrichs. Auxiliary basis-sets to approximate coulomb potentials. *Chemical Physics Letters*, 240(4):283–289, 1995.

[41] A. Schafer, H. Horn, and R. Ahlrichs. Fully optimized contracted gaussian-basis sets for atoms Li to Kr. *Journal of Chemical Physics*, 97(4):2571–2577, 1992.

[42] F. Neese and G. Olbrich. Efficient use of the resolution of the identity approximation in time-dependent density functional calculations with hybrid density functionals. *Chemical Physics Letters*, 362(1-2):170–178, 2002.

[43] A. E. Reed J. E. Carpenter J. A. Bohmann C. M. Morales E. D. Glendening, J. K. Badenhoop and F. Weinhold. Nbo 5.0.

[44] K. Park and T. C. Brunold. Combined spectroscopic and computational analysis of the vibrational properties of vitamin B_{12} in its Co^{3+}, Co^{2+}, and Co^{1+} oxidation states. *Journal of Physical Chemistry B*, 117(18):5397–5410, 2013.

[45] T. Andruniow, P. M. Kozlowski, and M. Z. Zgierski. Theoretical analysis of electronic absorption spectra of vitamin B_{12} models. *Journal of Chemical Physics*, 115(16):7522–7533, 2001.

[46] K. S. Conrad and T. C. Brunold. Spectroscopic and computational studies of glutathionylcobalamin: Nature of Co-S bonding and comparison to Co-C bonding in coenzyme-B_{12}. *Inorganic Chemistry*, 50(18):8755–8766, 2011.

[47] K. Kornobis, N. Kumar, P. Lodowski, M. Jaworska, P. Piecuch, J. J. Lutz, B. M. Wong, and P. M. Kozlowski. Electronic structure of the S1 state in methyl-

cobalamin: Insight from CASSCF/MC-XQDPT2, EOM-CCSD, and TD-DFT calculations. *Journal of Computational Chemistry*, 34(12):987–1004, 2013.

[48] Carme Rovira and Pawel M. Kozlowski. First principles study of coenzyme-B_{12}. crystal packing forces effect on axial bond lengths. *Journal of Physical Chemistry B*, 111(12):3251–3257, 2007.

[49] D. A. Pratt and W. A. van der Donk. Theoretical investigations into the intermediacy of chlorinated vinylcobalamins in the reductive dehalogenation of chlorinated ethylenes. *Journal of the American Chemical Society*, 127(1):384–396, 2005.

[50] A. J. Brooks, M. Vlasie, R. Banerjee, and T. C. Brunold. Spectroscopic and computational studies on the adenosylcobalamin-dependent methylmalonyl-CoA mutase: Evaluation of enzymatic contributions to Co-C bond activation in the Co^{3+} ground state. *Journal of the American Chemical Society*, 126(26):8167–8180, 2004.

[51] L. Randaccio, S. Geremia, G. Nardin, and J. Wuerges. X-ray structural chemistry of cobalamins. *Coordination Chemistry Reviews*, 250(11-12):1332–1350, 2006.

[52] L. Randaccio, S. Geremia, N. Demitri, and J. Wuerges. Vitamin B_{12}: Unique metalorganic compounds and the most complex vitamins. *Molecules*, 15(5):3228–3259, 2010.

[53] *Tables of Interatomic Distances and Configuration in Molecules and Ions*. The Chemical Society, London, 1958.

[54] A. D. Becke. Perspective: Fifty years of density-functional theory in chemical physics. *Journal of Chemical Physics*, 140(18):18A301 (18 pp.)–18A301 (18 pp.), 2014.

[55] D. Lee and A.C. Albrecht. *A Unified View of Raman, Resonance Raman, and Fluorescence Spectroscopy*, volume 12 of *Advances in Infrared and Raman Spectroscopy*. Wiley, Great Britain, 1985.

[56] A.B.P Lever. *Inorganic Electronic Spectroscopy*. Elsevier Publishing Company, New York, NY, 1st edition, 1968.

[57] A. Vlcek and S. Zalis. Modeling of charge-transfer transitions and excited states in d^6 transition metal complexes by DFT techniques. *Coordination Chemistry Reviews*, 251(3-4):258–287, 2007.

[58] A. Dreuw and M. Head-Gordon. Failure of time-dependent density functional theory for long-range charge-transfer excited states: The zincbacteriochlorin-bacterlochlorin and bacteriochlorophyll-spheroidene complexes. *Journal of the American Chemical Society*, 126(12):4007–4016, 2004.

[59] F. Weinhold and C.L. Landis. *Valency and Bonding*. Cambridge University Press, 2005.

[60] E. D. Glendening, C. R. Landis, and F. Weinhold. Nbo 6.0: Natural bond orbital analysis program (vol 34, pg 1429, 2013). *Journal of Computational Chemistry*, 34(24):2134–2134, 2013.

[61] A. E. Reed, L. A. Curtiss, and F. Weinhold. Intermolecular interactions from a natural bond orbital, donor-acceptor viewpoint. *Chemical Reviews*, 88(6):899–926, 1988.

[62] A. E. Reed and F. Weinhold. Natural localized molecular-orbitals. *Journal of Chemical Physics*, 83(4):1736–1740, 1985.

[63] D. E. Koshland. The molecule of the year. *Science*, 258(5090):1861–1861, 1992.

[64] J. A. Bauer. Synthesis, characterization and nitric oxide release profile of nitrosylcobalamin: a potential chemotherapeutic agent. *Anti-Cancer Drugs*, 9(3):239–244, 1998.

[65] C. B. Perry and H. M. Marques. Fifty years of X-ray crystallography of vitamin B_{12} and its derivatives. *South African Journal of Science*, 100(7-8):368–380, 2004.

[66] J. H. Bayston, N. K. King, F. D. Looney, and M. E. Winfield. Superoxocobalamin first intermediate in autoxidation of vitamin B_{12r}. *Journal of the American Chemical Society*, 91(10):2775–&, 1969.

[67] T. A. Stich, N. R. Buan, J. C. Escalante-Semerena, and T. C. Brunold. Spectroscopic and computational studies of the ATP : Corrinoid Adenosyltransferase (CobA) from Salmonella enterica: Insights into the mechanism of adenosylcobalamin biosynthesis. *Journal of the American Chemical Society*, 127(24):8710–8719, 2005.

[68] Elizabeth J. Blaesi, Jessica D. Gardner, Brian G. Fox, and Thomas C. Brunold. Spectroscopic and computational characterization of the NO adduct of

substrate-bound Fe(II) cysteine dioxygenase: Insights into the mechanism of O_2 activation. *Biochemistry*, 52(35):6040–6051, 2013.

[69] *Enzyme-Catalyzed Electron and Radical Transfer*, volume 35. Kluwer Academic Publishers, New York.

Chapter 3

Spectroscopic studies of the *Salmonella enterica* adenosyltransferase enzyme *Se*CobA

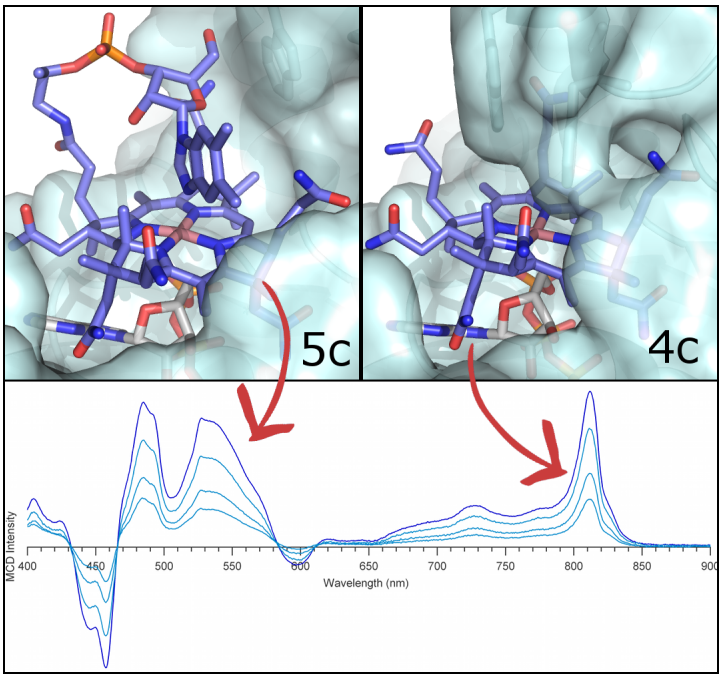

This work was published under the following: I. G. Pallares, T. C. Moore, J. C. Escalante-Semerena, and T. C. Brunold "Spectroscopic studies of the *Salmonella enterica* adenosyltransferase enzyme *Se*CobA: Molecular-level insight into the mechanism of substrate cob(II)alamin activation".

3.1 Summary

CobA from *Salmonella enterica* (*Se*CobA) is a member of the family of ATP:co(I)rrinoid adenosyltransferase (ACAT) enzymes that participate in the biosynthesis of adenosylcobalamin (AdoCbl) by catalyzing the transfer of the adenosyl group from an ATP molecule to a reactive co(I)rrinoid species transiently generated in the enzyme active site. This reaction is thermodynamically challenging, as the reduction potential of the co(II)rrinoid precursor in solution is far more negative than that of available reducing agents in the cell (e.g. flavodoxin), precluding nonenzymic reduction to the Co(I) oxidation state. However, in the active sites of ACATs, the Co(II)/Co(I) redox potential is raised by >250 mV via the formation of a unique four coordinate co(II)rrinoid species. In the case of the *Se*CobA ACAT, crystallographic and kinetic studies have revealed that the phenylalanine-91 (F91) and tryptophan-93 (W93) residues are critical for in vivo activity, presumably by blocking access to the lower axial ligand site of the co(II)rrinoid substrate. To assess further the importance of the F91 and W93 residues with respect to enzymatic function, we have characterized various *Se*CobA active site variants using electronic absorption, magnetic circular dichroism, and electron paramagnetic resonance spectroscopies. Our data provide unprecedented insight into the mechanism by which *Se*CobA converts the co(II)rrinoid substrate to four-coordinate (4c) species, with the hydrophobicity, size, and ability to participate in off-set π-stacking interactions of key active-site residues all being critical for activity. The structural changes that occur upon co(II)rrinoid binding also appear to be crucial for properly orienting the

transiently generated Co(I) "supernucleophile" for rapid reaction with co-substrate ATP.

3.2 Introduction

Adenosylcobalamin (AdoCbl) is one of Nature‘s most complex cofactors, employed by biological systems as a controlled source of radical species.[1,2] It is composed of a redox-active cobalt ion coordinated equatorially by the four nitrogen atoms of a tetrapyrrole macrocycle known as the corrin ring. A pendant 5,6-dimethylbenzimidazole (DMB) base attached to the corrin macrocycle by an intramolecular loop occupies the "lower" (Coα) axial position, while an ATP-derived 5‘-deoxyadenosyl moiety is bound to the Co ion in the upper (Coβ) position via a unique organometallic bond (Figure 3.1).[3] AdoCbl serves as the cofactor for a class of enzymes that catalyze various 1,2-rearrangement reactions.[4] These AdoCbl-dependent enzymes can be grouped into three families: (i) enzymes that form aldehydes via dehydration or deamination of substrates, which include diol dehydratase, glycerol dehydratase, and ethanolamine ammonia lyase;[5,6] (ii) aminomutases, such as D-ornithine 4,5-aminomutase and L-leucine 2,3-aminomutase, which facilitate the migration of primary amine groups;[7] and(iii) mutases, such as methylmalonyl-CoA mutase and glutamate mutase, which catalyze carbon skeleton rearrangements.[8,9] A common feature shared by all of these enzymes is the controlled homolytic cleavage of the Co–C(Ado) bond of AdoCbl in response to substrate binding, to yield a reactive Ado based radical capable of abstracting a hydrogen atom from the substrate.[4]

While only some bacteria and archaea possess the complete enzymatic machin-

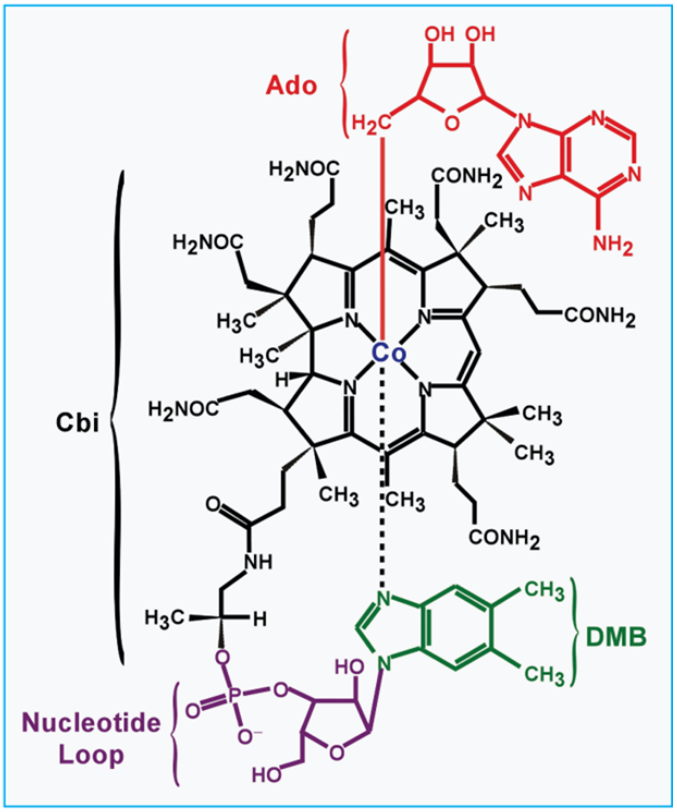

Figure 3.1: Chemical structure of adenosylcobalamin (AdoCbl), the final product of the reaction catalyzed by ATP:co(I)rrinoid adenosyltransferases (ACATs). In the case of adenosylcobinamide (AdoCbi^{+}) and related species, the DMB moiety and nucleotide loop are absent.

ery to synthesize AdoCbl from small molecule precursors, all organisms that require AdoCbl in their metabolism must produce ATP:co(I)rrinoid adenosyltranferase (ACAT) enzymes.[10] ACATs catalyze the formation of the Co–C(Ado) bond via the transfer of the 5'-deoxyadenosyl moiety of ATP to a cobalamin substrate.[11] To date, three non-homologous, structurally distinct classes of ACATs have been identified and classified according to their role in *Salmonella enterica* sv Typhimurium LT2 (hereafter *S. enterica*), which contains a member of each class in its genome.[12, 13, 14]

The *S. enterica* CobA (*Se*CobA) enzyme is involved in the de novo synthetic pathway of AdoCbl and in scavenging incomplete corrinoids, as its gene is constitutively expressed by the cell to maintain basal levels of AdoCbl.[12] Alternatively, the gene encoding the PduO ACAT is only expressed when 1,2-propanediol is present, whereas expression of the gene encoding EutT requires the presence of ethanolamine and AdoCbl.[15, 14, 16] Note that in humans, the single ACAT employed (generally referred to as hATR) is homologous to the PduO enzyme, and malfunctioning of hATR has been linked to diseases related to cobalamin-deficiency, such as methylmalonic aciduria.[17, 18, 19, 20]

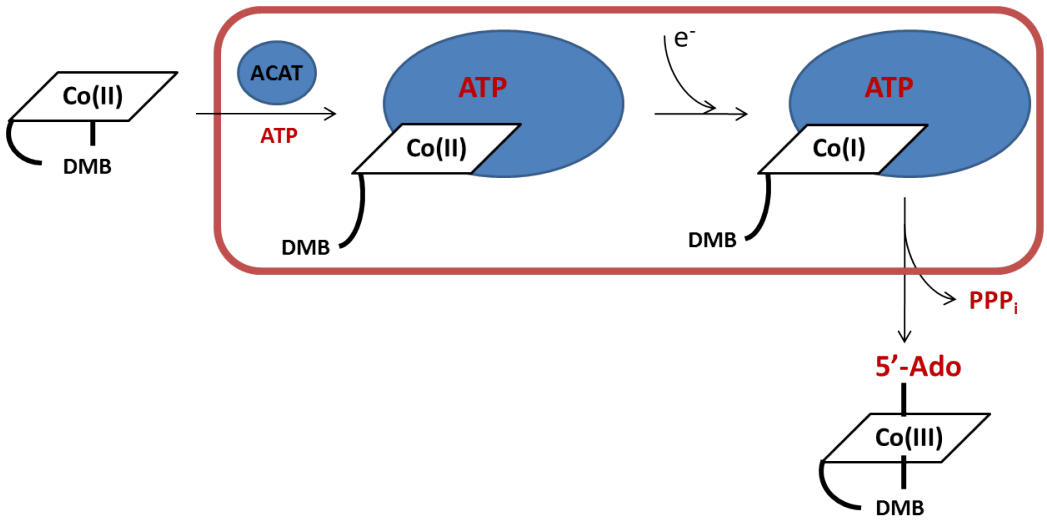

Figure 3.2: Proposed mechanism for the reaction catalyzed by ACATs, adapted from references 24 and 67. Complexation of the enzyme active site with co-substrate ATP promotes the binding of Co(II)Cbl and its conversion to a 4c species via removal of the axial ligand. One-electron reduction of this species produces a Co(I)Cbl intermediate that is properly oriented for nucleophilic attack on the 5' carbon of ATP to form AdoCbl.

Previous studies of ACATs have led to the proposal that these enzymes employ a common mechanism for the biosynthesis of AdoCbl.[21] This mechanism involves the

one-electron reduction of a co(II)rrinoid precursor to form a "supernuclephilic" Co(I) species,[22] which performs a nucleophilic attack on the 5‘ carbon of ATP to yield the adenosylated product (Figure 3.2).[23, 11] The reduction of co(II)rrinoid to produce the key Co(I) intermediate is thermodynamically challenging, as the Co(II)/Co(I) reduction potential for the naturally encountered substrates ($E^\circ = -610$ mV vs. NHE for cob(II)alamin (Co(II)Cbl), and $E^\circ = -490$ mV vs. NHE for cob(II)inamide ($Co(II)Cbi^+$), a Co(II)Cbl precursor missing the nucleotide loop and DMB base)[24] is too negative for the reducing agents available in the cell (the semiquinone/reduced flavin couple in FldA, the purported physiological partner to at least one ACAT, CobA, is $E^\circ = -440$ mV vs. NHE).[25, 26, 27] Early spectroscopic studies of *Se*CobA, as well as of the *Lactobacillus reuteri* PduO-type ACAT (*Lr*PduO) have provided strong evidence for the formation of a structurally unique co(II)rrinoid species in the active sites of these enzymes.[23, 28, 29, 30] In particular, electron paramagnetic resonance (EPR) characterization of co(II)rrinoids bound to these enzymes complexed with ATP revealed unusually large g-shifts and A(Co) hyperfine coupling constants, consistent with the Co(II) ion residing in an effectively square planar, four-coordinate (4c) ligand environment.[23, 28] Formation of a 4c intermediate was shown to stabilize the singly-occupied redox-active Co $3d_{z^2}$-based molecular orbital, and thus to raise the reduction potential by an estimated $\geqslant 250$ mV, to within the range of biologically available reductants.[22, 23] Further evidence for enzymatic tuning of the Co(II)/Co(I) redox potential was obtained from magnetic circular dichroism (MCD) studies, which revealed the appearance of a series of sharp, positively-signed features between ~10 000 and 20 000 cm^{-1} when $Co(II)Cbi^+$ binds to *Se*CobA/ATP or

*Lr*PduO/ATP that are unique among co(II)rrinoid species.[31]

Subsequent crystallographic studies confirmed the presence of 4c Co(II)Cbl species bound to the active sites of *Se*CobA and *Lr*PduO in the presence of ATP, and provided insights into the mechanism by which ACATs generate 4c co(II)rrinoids. Specifically, it was found that a non-coordinating Phe residue occupies the lower axial position of the Co(II)Cbl cofactor where the DMB ligand would normally be found (F112 in LrPduO,33 F91 in *Se*CobA34). A subsequent combined kinetics and spectroscopic study of *Lr*PduO revealed that F112, along with the adjacent F187 and V186 residues form a hydrophobic "wall" in response to co(II)rrinoid binding, blocking ligand access to the Coα face of the corrin ring,[32] while a salt-bridge interaction between residues D35 and R128 near the corrin ring was found to be important for properly positioning the co(II)rrinoid substrate.[29] Although the detailed mechanism of 4c co(II)rrinoid formation employed by *Se*CobA is less well understood, the most recently published X-ray crystal structure of this enzyme provided similar information about the conformation of the active site during catalysis. Notably, this structure revealed the active site geometry at the catalytic site containing 4c Co(II)Cbl species (the "closed" conformation), as well as the binding geometry of pentacoordinate (5c) Co(II)Cbl prior to enzyme activation (the "open" conformation).[31] It also confirmed the unique binding motif of ATP,[33] oriented towards the corrin ring for nucleophilic attack by the Co ion, and disclosed additional amino acid residues responsible for displacing the lower axial ligand of the bound corrinoid in the "closed" conformation of the enzyme. In analogy to the previously characterized *Lr*PduO ACAT, a set of hydrophobic residues, namely F91,

W93, V13, and V17 in *Se*CobA, are positioned near the lower face of the cofactor, thus providing a wall of hydrophobic residues between the Co(II) ion and the solvent. Unlike in *Lr*PduO, however, where a single aromatic residue is present at the location were the DMB coordinates to the Co(II) ion in solution,[34, 35] two bulky, aromatic amino acids in an off-set π-stacking conformation are positioned at this location in *Se*CobA (Figure 3.3). This pair of residues is adjacent only to the V13 and V17 residues of the N-terminal helix that caps the active site, while the remaining interactions are with solvent molecules and pendant groups from the corrin ring. Preliminary studies on the *Methanosarcina mazei* (Mma) CobA/ATP complex, a *Se*CobA homologue lacking the N-terminal helix, revealed that these Val residues are important for increasing the yield of 4c co(II)rrinoid species, but are not essential for activity.[17] Alternatively, amino acid substitutions at the F91 and W93 positions were shown to have a drastic effect in the catalytic efficiency of *Se*CobA.[31]

Previously we have employed MCD and EPR spectroscopies to probe the coordination environment of the Co center in co(II)rrinoids[36, 37] and to monitor the structural changes that occur in the catalytic cycles of various cobalamin-dependent enzymes and ACATs.[31, 30, 28, 29] MCD spectroscopy offers a particularly sensitive probe of co(II)rrinoid species formed during enzymatic turnover, as with this technique ligand field (LF) and charge transfer (CT) transitions can be observed that are masked by intense corrin $\pi \rightarrow \pi^*$ transitions in the corresponding Abs spectra. In the present study, we have used Abs, MCD, and EPR spectroscopies to characterize several *Se*CobA variants with substitutions of residues F91 or W93. These variants

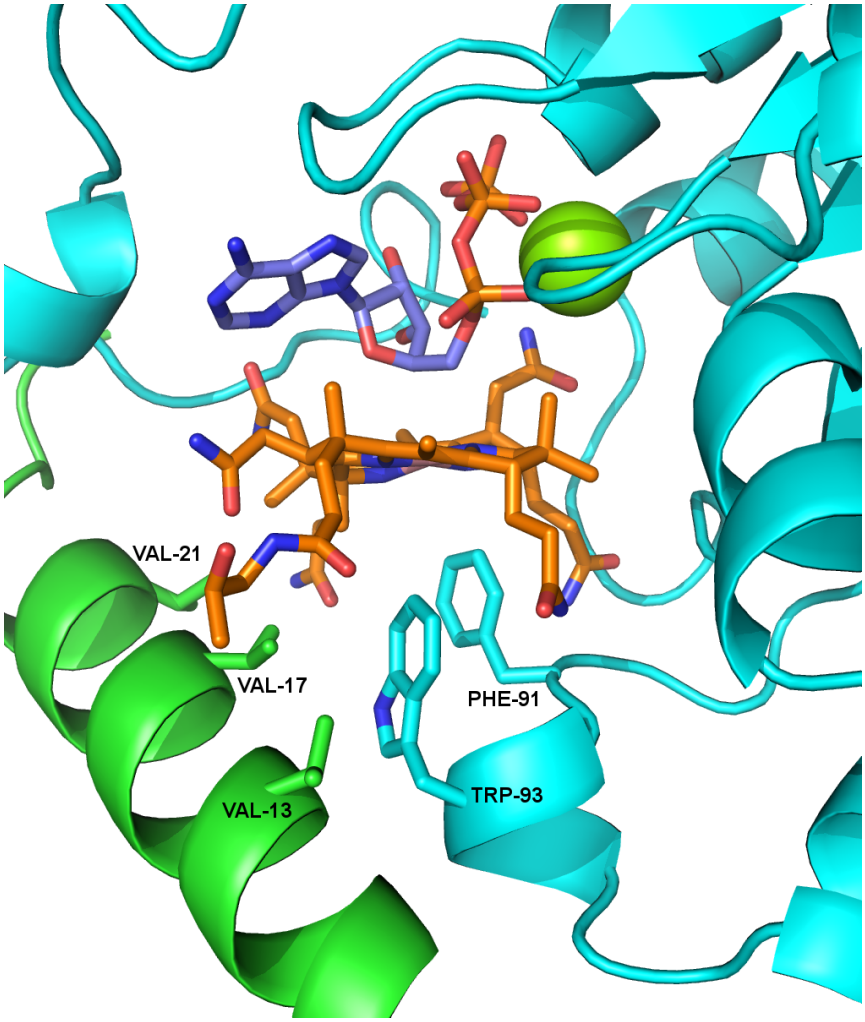

Figure 3.3: X-ray crystal structure of *Se*CobA in the region of the active site featuring 4c Co(II)Cbl (orange), co-substrate ATP (purple), and Mg^{2+} ion (green), based on PDB entry 4HUT. The subunit containing the F91 and W93 residues (shown as sticks) is colored in cyan. The N-terminal helix of the adjacent subunit, which caps the active site and contains the V13, V17, and V21 residues in this "closed" conformation, is highlighted in green.

were chosen to assess the importance of specific intermolecular interactions with respect to the formation of 4c co(II)rrinoids by varying the size of residues 91 and 93 (F91Y, W93F, F91W, W93A), their relative positioning (F91W–W93F), and polarity

(F91Y, W93H). By carrying out studies with Co(II)Cbl and Co(II)Cbi^+, both of which are substrates of the enzyme in vivo,[38, 39, 40] significant insights have been obtained into how the strength of the axial ligand–Co bonding interaction modulates the yield of formation of 4c co(II)rrinoid species in *Se*CobA.

3.3 Methods

Cofactors and Chemicals. The chloride salt of aquacobalamin ($[H_2OCbl]Cl$), dicyanocobinamide ($(CN)_2Cbi$), and potassium formate (HCOOK) were purchased from Sigma and used as obtained. Diaquacobinamide ($[(H_2O)_2Cbi]^{2+}$) was prepared by adding $NaBH_4$ to an aqueous solution of $(CN)_2Cbi$, loading the reaction mixture on a C_{18} SepPack column, washing with doubled distilled H_2O, and eluting the product with methanol, as described in previous reports.[29, 23] Co(II)Cbl and Co(II)Cbi^+ were prepared by adding a small volume of saturated HCOOK to degassed solutions of H_2OCbl^+ and $(H_2O)_2Cbi^{2+}$, respectively, and the progress of the reduction was monitored spectrophotometrically.

Protein Preparation and Purification. Wild-type and variant CobA from *Salmonella enterica* sv. Typhimurium LT2 was purified as described elsewhere.[38] Briefly, the wild-type cobA gene was cloned into the pTEV5 overexpression plasmid42, which includes a cleavable, N-terminal hexahistidine tag. *Se*CobA variants were generated using the QuikChange II site-directed mutagenesis kit (Stratagene). All proteins were overexpressed in *Escherichia coli* BL21 and purified on a HisTrap nickel-affinity column (GE Life Sciences). The N-terminal hexahistidine tag was cleaved using recombinant tobacco etch virus (rTEV) protease.[41] Proteins were

purified to homogeneity as determined by SDS-polyacrylamide gel electrophoresis (PAGE).[42]

Sample Preparation. Purified ~300 to ~500 μM *Se*CobA in 50 mM Tris buffer (pH 8) containing 0.5 mM DTT was complexed with Co(II)Cbl or Co(II)Cbi^+ under anoxic conditions in a ~0.8:1 cofactor:protein ratio (see SI for details). If appropriate, MgATP was added in a tenfold molar excess over protein as the source of ATP. Solutions were then injected into the appropriate sample cells in an oxygen-free glovebox, after which they were immediately frozen and stored in liquid nitrogen.

Spectroscopy. Magnetic circular dichroism (MCD) spectra were collected on a Jasco J-715 spectropolarimeter in conjunction with an Oxford Instruments SM-4000 8T magnetocryostat. All MCD spectra were obtained by taking the difference between spectra collected with the magnetic field oriented parallel and antiparallel to the light propagation axis to remove contributions from the natural CD and glass strain. X-band EPR spectra were obtained by using a Bruker ESP 300E spectrometer in conjunction with an Oxford ESR 900 continuous-flow liquid helium cryostat and an Oxford ITC4 temperature controller. The microwave frequency was measured with a Varian EIP model 625A CW frequency counter. All spectra were collected using a modulation amplitude of 10 G and a modulation frequency of 100 kHz. EPR spectral simulations were performed using the WEPR program developed by Dr. Frank Neese.

Computations. Initial atomic coordinates for the structure of *Se*$CobA^{WT}$ in complex with ATP and Co(II)Cbl were obtained from the most recently published crystal structure (PDB code: 4HUT).[38] The Pymol software was used to introduce

in silico amino acid substitutions into the *Se*CobA subunit containing 4c Co(II)Cbl and ATP. The newly introduced residues were positioned so as to minimize steric clashes, while preserving the orientation of the original residue as closely as possible. Molecular mechanics as implemented in GROMACS 4.5 was then employed to minimize the energy of the protein model in the presence of water solvent (using the simple point charge (SPC) model for water molecules)[43] with a box size of 5 nm. The Amber98 force field was used for the protein residues, and supplemented with parameters for ATP by Carson et al.[44] and for cobalamin by Marques et al.[45, 46] To speed up calculations, the other subunit of the *Se*CobA dimer containing 5c Co(II)Cbl was removed, except for the N-terminal helix that interacts with the subunit of interest. No significant differences in the secondary structure were observed among the energy-minimized models of the variants, and computed Ramachandran plots for the optimized structures indicated that no misoriented amino acids or unreasonable conformations were present. From these optimized structures, the residues at positions 91 and 93 were excised and used in subsequent DFT single-point calculations with Orca 3.0. To evaluate the magnitude of dispersion interactions, all DFT computations were performed with the B3LYP functional and TZVP basis set for all atoms and by choosing the dispersion correction developed by Grimme and coworkers.[47, 48, 49, 35]

3.4 Results

Corrinoid binding to wild-type *Se*CobA (*Se*CobA^{WT}): The low-temperature absorption (LT-Abs) spectrum of Co(II)Cbi^{+} (Figure 3.4 A, gray trace) is characterized

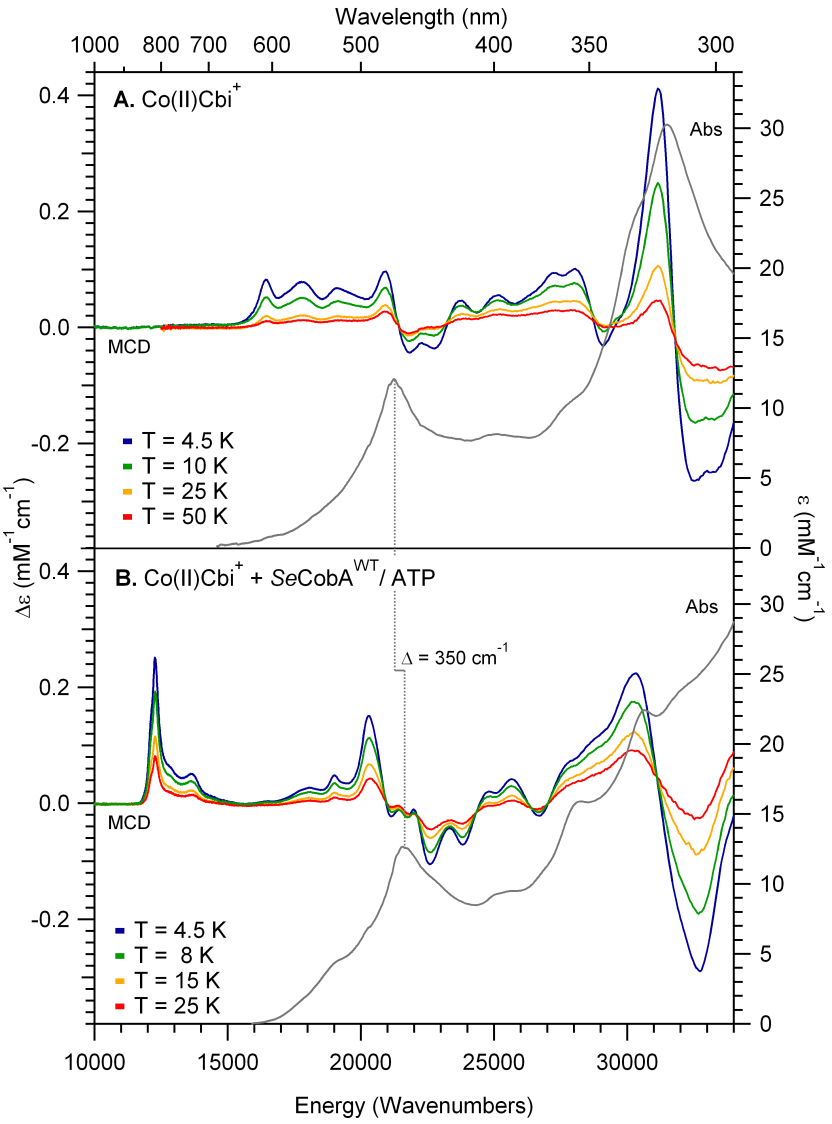

Figure 3.4: LT-Abs spectra collected at 4.5 K (gray traces) and 7 T VT-MCD spectra of (A) free Co(II)Cbi^{+} and (B) Co(II)Cbi^{+} in the presence of *Se*CobA^{WT} and ATP.

by an intense feature centered at ~21 000 cm^{-1}, the so-called α-band that has previously been assigned to a corrin-based $\pi \rightarrow \pi^{*}$ transition on the basis of its high extinction coefficient and TD-DFT results.[50, 51] This feature is blue-shifted by ~150

cm^{-1} from its position in the Abs spectrum of Co(II)Cbl (Figure 3.5 A, gray trace), as reported previously.[36] In the presence of the *Se*CobA^{WT}/ATP complex (Figure 3.4 B, gray trace) the α-band undergoes a further (~350 cm^{-1}) shift to higher energy. As the strength of the metal-ligand interaction in co(II)rrinoids was previously found to modulate the relative energies of the corrin π/π^* frontier molecular orbitals (MOs),[37] the observed blue-shift of the α-band is consistent with large perturbations to the axial ligand environment of Co(II)Cbi$^+$ in the presence of *Se*CobA. Further insight into the nature of these perturbations is obtained by MCD spectroscopy. Most importantly, a series of sharp, positively-signed intense bands appear in the low energy region (~10 000 to 20 000 cm^{-1}) of the MCD spectrum upon Co(II)Cbi$^+$ binding to the *Se*CobA^{WT}/ATP complex (Figure 3.4 B, color traces) that are characteristic of co(II)rrinoid species bound to ACATs.[36, 28, 30] From their large MCD-to-Abs intensity ratios (alternatively, C/D ratios; see Figure A.3.5) and relatively narrow bandwidths, the features at 12,300 (δ-band), and 13,600 (β-band) have been assigned to the electronic origin and vibrational sideband of a single LF transition.[23] These features are red-shifted from their counterparts in the free Co(II)Cbi$^+$ MCD spectrum by ~4 000 cm^{-1} (Figure 3.4 A, color traces), consistent with the formation of an essentially 4c co(II)rrinoid species.[23, 52, 28] As no spectroscopic features from five-coordinate (5c) co(II)rrinoid species are observed in this region of the spectrum, the intensity of the δ-band can been used to estimate the relative yield of 4c co(II)rrinoid species generated by ACATs.[29] In the case of Co(II)Cbi$^+$ bound to *Se*CobA^{WT}, the intensity of the δ-band relative to that of the 16 400 cm^{-1} feature of 5c Co(II)Cbi$^+$ indicates that the 4c yield is ~50% (Table

3.3). Additionally, a sharp positive feature is observed at 19 000 cm^{-1} (λ-band), alongside an intense positive band at 20 300 cm^{-1} (σ-band). Since these features are found at lower energies than the α-band, the lowest energy corrin-based $\pi \rightarrow \pi^*$ transition observed for co(II)rrinoids,[30, 53] and given their large C/D ratios and high MCD intensities, they can be attributed to electronic transitions with significant CT character. The bands observed at higher energies have been assigned primarily to corrin $\pi \rightarrow \pi^*$ transitions on the basis of their small C/D ratios and low MCD intensities.[36, 29] Although the relative intensities of these features vary significantly among co(II)rrinoids species (Figure A.3.6), establishing specific bands assignments becomes difficult due to the presence of multiple electronic transitions of varied LF, CT, and $\pi \rightarrow \pi^*$ character expected in this region of the spectrum.

As in the case of Co(II)Cbi^+, the Abs spectrum of Co(II)Cbl also changes in the presence of *Se*CobA/ATP, with the α-band undergoing a ~450 cm^{-1} blue-shift (Figure 3.5, gray traces). Intriguingly, in the MCD spectrum of Co(II)Cbl and *Se*$CobA^{WT}$/ATP, the intensity of the δ-band is considerably weaker than in the analogous Co(II)Cbi^+ spectrum (Figure 3.5 B), indicating a large (~5-fold) decrease in the relative yield of 4c species when Co(II)Cbl serves as the substrate of *Se*$CobA^{WT}$. Thus, the magnitude of the blue-shift of the α-band observed in the Abs spectrum alone does not correlate directly with the yield of 4c species formed in the *Se*$CobA^{WT}$ active site. A further analysis of the MCD spectrum of Co(II)Cbl and *Se*$CobA^{WT}$/ATP indicates that the remaining spectral contributions are consistent with the presence of a 5c Co(II)Cbl species with N(DMB) bound to the Co(II) ion. However the MCD features of this 5c species are significantly

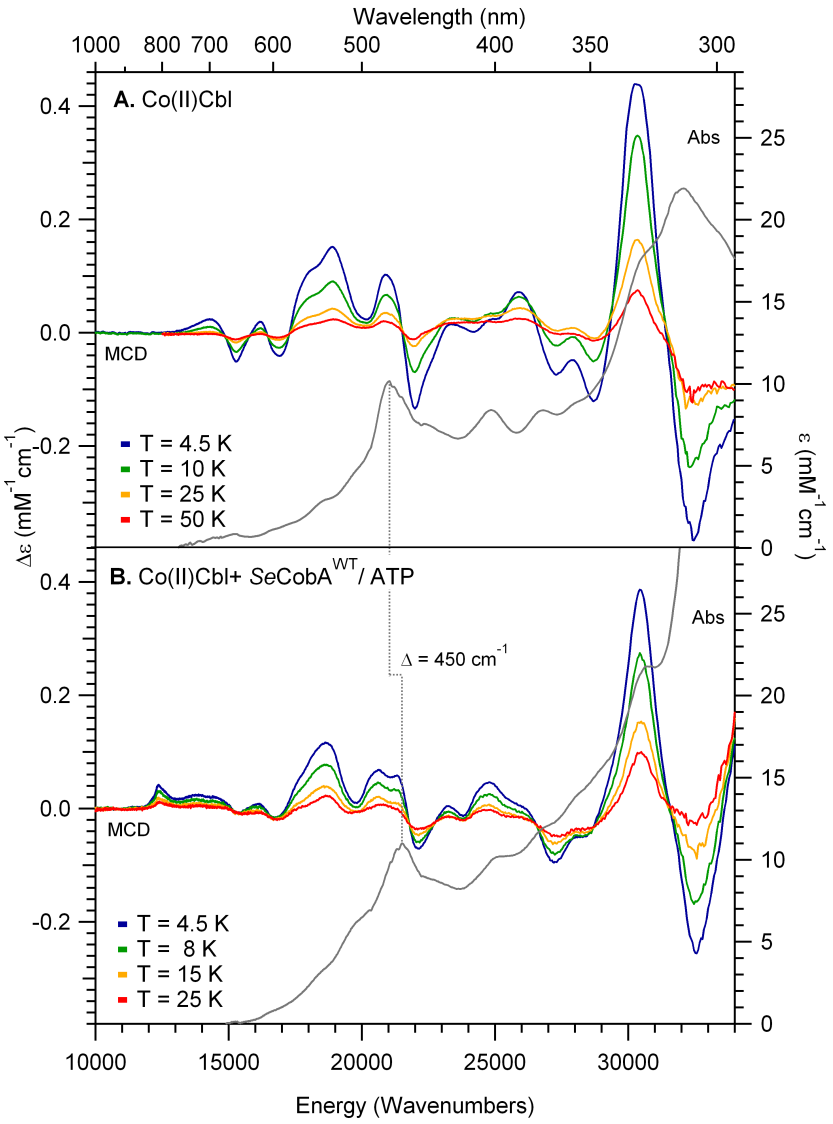

Figure 3.5: LT-Abs spectra collected at 4.5K (gray traces) and 7 T VT-MCD spectra of (A) free Co(II)Cbl and (B) Co(II)Cbl in the presence of *Se*CobA^{WT} and ATP.

different from those observed for free Co(II)Cbl. Specifically, the positive feature at ~19 000 cm^{-1} in the MCD spectrum of Co(II)Cbl red-shifts by ~200 cm^{-1} in the presence of *Se*CobA^{WT} / ATP, while the positive feature at 21 000 cm^{-1} blue-shifts

by ~400 cm^{-1} (Figure 3.7, top). Since features in this region of the MCD spectrum of Co(II)Cbl have previously been assigned to LF and CT transitions that are sensitive to changes in the axial ligand environment,[54] the band shifts induced by the addition *Se*CobA^{WT}/ATP are consistent with perturbations to the DMB base via interactions with the protein scaffold. Lastly, the high energy region (> 22 000 cm^{-1}) of the MCD spectrum of Co(II)Cbl in the presence of *Se*CobA^{WT}/ATP is reminiscent of that of free Co(II)Cbl, in particular with regards to the intense derivative-shaped feature at 31 000 cm^{-1} (also see Figure A.3.7). Inspection of the remaining bands in this region, however, reveals sizable differences in terms of their positions and relative intensities, suggesting that the conformation of the corrin ring in the 5c Co(II)Cbl fraction is significantly altered from that of free Co(II)Cbl. These results are in agreement with the bond distances and angles of the enzyme-bound 5c and 4c Co(II)Cbl species derived from the most recent crystal structure of *Se*CobA^{WT} (Table 4.1). A comparison of the relevant structural parameters of free Co(II)Cbl[55] and the 5c Co(II)Cbl fraction bound to *Se*CobA^{WT}/ATP indicates that the Co–N(DMB) bond length increases by ~0.2 Å upon enzyme binding, concurrent with a ~6° increase in the long-axis, butterfly fold angle, θ(LA).[1] Upon removal of the DMB ligand, θ(LA) decreases by ~6°, ϕ(SA) increases by ~3°, and the Co–5'C(ATP) distance shortens by ~0.4 Å, highlighting the effect of the rearrangement of the F91 and W93 active-site residues on the relative positioning and conformation of the co(II)rrinoid substrate.

[1] θ(LA) is the angle between the plane containing the NA, C4, C5, C6, and NB atoms and the plane containing the NC, C14, C15, C16, and ND atoms, while ϕ(SA) corresponds to the angle between the planes containing the ND, C19, C1, and NA atoms and the NB, C9, C10, C11, and NC atoms (see Figure A.3.8 for the atom numbering scheme used)

Table 3.1: Relevant structural parameters of free and *Se*CobA bound Co(II)rrinoid species as determined by X-ray crystallography.[a] From Ref 57. [b] From PDB structure 4HUT.[38] *(n/a)*, not applicable

Co(II)Cbl Species	Co–C(ATP) / Å	Co–N(DMB) / Å	θ-LA / °	ϕ-SA / °
No Protein[a]	*n/a*	2.13	19.6	6.3
5c *Se*CobA site ("open")[b]	3.42	2.32	26.2	7.7
4c *Se*CobA site ("closed")[b]	3.06	*n/a*	19.5	10.7

Point Substitutions at the W93 position: *(i) W93A.* Previous studies have indicated that the tryptophan residue at position 93 (W93) is critical for retaining enzyme activity;[17] thus, it was originally postulated that this residue played a similar role to that of F112 in the *Lr*PduO ACAT. However, the most recent crystal structure of *Se*CobA^{WT} with Co(II)Cbl and MgATP bound shows instead that a nearby phenylalanine (F91) residue is positioned on the face of the corrin ring where the DMB group is usually found. It is possible that the aromatic side chain of the W93 residue is associated with this F91 residue in an off-set π-stacking fashion during catalysis. Since replacement of W93 by alanine completely abolishes the catalytic activity of the enzyme with Co(II)Cbl, while modest activity is retained with Co(I)Cbl,[38] the W93A substitution likely affects the Co(II)/Co(I) reduction step. Indeed, the MCD spectra of Co(II)Cbi$^+$ and Co(II)Cbl in the presence of *Se*CobA^{W93A}/ATP are almost identical to the corresponding MCD spectra in the absence of ATP (Figure 3.6 and 3.7, trace G) and the MCD spectra of the free cofactors (Figures 3.6 and 3.7, trace H), indicating that the variant is unable to generate 4c co(II)rrinoids.

(ii) W93F. Substitution of Trp-93 by Phe, a smaller planar and non-polar amino

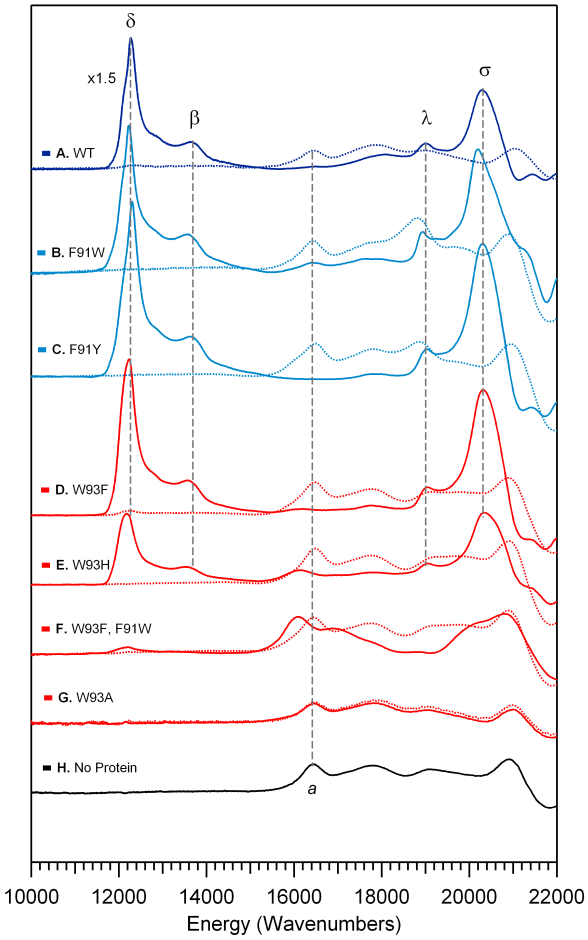

Figure 3.6: MCD spectra of Co(II)Cbi$^+$ obtained in the presence of *Se*CobA^{WT} and various variants. Solid lines show the spectra in the presence of ATP, while dotted lines are the corresponding traces in the absence of ATP. Panels A-to-G are labeled according the amino acid substitution(s) introduced in *Se*CobA. The primary spectroscopic features due to 4c Co(II)Cbi$^+$ species are labeled for the *Se*CobA^{WT} spectrum and are highlighted by vertical lines. Additional spectroscopic changes in reference to the MCD spectrum of free Co(II)Cbi$^+$ (panel H, band a) are also highlighted.

acid, results in a *Se*CobA variant with similar behavior as the WT enzyme in Co(II) and Co(I) in vitro assays.[38] Accordingly, the MCD spectrum of Co(II)Cbi$^+$ in the presence of *Se*CobA^{W93F}/ATP is very similar to that obtained with *Se*CobA^{WT},

Table 3.2: Kinetic parameters for the adenosylation of Co(II)Cbl and Co(II)Cbi$^+$ by *Se*CobA^{WT}.[a]From Ref 34.

	Co(II)rrinoid		
Species	K_M (μM)	k_{cat} (s^{-1})	k_{cat}/K_M ($M^{-1}s^{-1}$)
Co(II)Cbi$^+$	16.3 ± 3.5	$(7.7 \pm 0.4) \times 10^{-3}$	$(4.7 \pm 0.6) \times 10^2$
Co(II)Cbl[a]	25 ± 5	$(6.0 \pm 0.9) \times 10^{-3}$	$(2.0 \pm 0.4) \times 10^2$
	ATP		
Co(II)Cbi$^+$	25.4 ± 9.0	$(6.7 \pm 0.7) \times 10^{-3}$	$(2.6 \pm 0.4) \times 10^2$
Co(II)Cbl[a]	66 ± 18	$(5.0 \pm 0.7) \times 10^{-3}$	$(0.8 \pm 0.2) \times 10^2$

though the prominent low-energy δ-band at ~12 300 cm^{-1} is marginally broadened, suggesting that the Phe residue provides more conformational freedom to the bound corrinoid (Figure 3.6, traces A and D). A quantitative analysis of this spectrum reveals that a larger fraction of 4c Co(II)Cbi$^+$ species is generated in the variant than in *Se*CobA^{WT}/ATP (Table 3.3, D). In contrast, in the MCD spectrum of Co(II)Cbl with *Se*CobA^{W93F}/ATP, the intensity of the δ-band is decreased four-fold from that obtained in the presence of *Se*CobA^{WT}. The MCD features at 15 000 and 20 000 cm^{-1} associated with the remaining 5c Co(II)Cbl species are very similar to those observed for the analogous species in *Se*CobA^{WT} and distinct from those displayed by free Co(II)Cbl (Figure 3.7, traces A and D, bands a and b). This result indicates that the 5c fraction of Co(II)Cbl is also bound to the *Se*CobA^{W93F}/ATP complex, and adopts a similar conformation as the 5c Co(II)Cbl species in *Se*CobA^{WT}. Thus, the decreased yield of 4c Co(II)Cbl species in *Se*CobA^{W93F} can be attributed to the smaller size of the introduced Phe residue relative to the native Trp, which leads

to decreased steric crowding when Co(II)Cbl binds to the enzyme active site in the DMB-on form.[29] Due to the weaker interaction of the H2O ligand with the Co(II) ion in Co(II)Cbi$^+$, the decreased steric crowding in the active site of *Se*CobA^{W93F} has a smaller effect on the 4c→5c equilibrium when this species is used as the substrate.

(iii) W93H. Compared to the results obtained with *Se*CobA^{W93F}, the MCD spectrum of Co(II)Cbi$^+$ in the presence of *Se*CobA^{W93H}/ATP displays a broadening and intensity weakening of the δ- and σ-bands. These changes signify a two-fold decrease in the yield of 4c Co(II)Cbi$^+$, consistent with a less constrained active site upon introduction of the smaller imidazole side chain (Figure 3.6 and Table 3.3, E). As expected from the lower 4c Co(II)Cbi$^+$ yield in *Se*CobA^{W93H}, increased contributions from 5c (i.e. water bound) Co(II)Cbi$^+$ are observed in the 16 000 – 20 000 cm^{-1} region of the MCD spectrum; however, these features are not identical to those seen in the corresponding MCD spectrum in the absence of ATP. Specifically, the feature corresponding to the lowest-energy LF transition of Co(II)Cbi$^+$ is red-shifted by ~300 cm^{-1} in the spectrum of the sample containing *Se*CobA^{W93H}/ATP (Figure 3.6 E, band a), indicating that the 5c Co(II)Cbi$^+$ fraction features an elongated Co–O(H_2) bond.[23, 56] Thus, while a smaller fraction of 4c Co(II)Cbi$^+$ species is generated in *Se*CobA^{W93H} than in the wild-type enzyme, the remaining 5c Co(II)Cbi$^+$ fraction is significantly perturbed upon binding to *Se*CobA^{W93H}. The absence of features in the 14 000 – 16 000 cm^{-1} region of the MCD spectrum of Co(II)Cbi$^+$ in the presence of *Se*CobA^{W93H} indicates that the side imidazole chain of H93 does not serve as ligand to the Co(II) ion, ruling out the possibility that His-binding precludes the

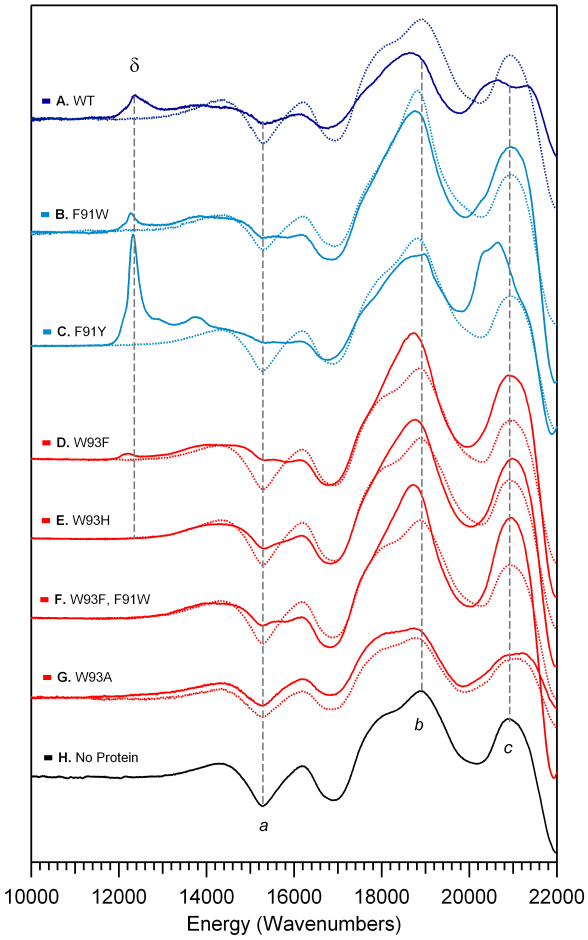

Figure 3.7: MCD spectra of Co(II)Cbl obtained in the presence of *Se*CobA^{WT} and various variants. Solid lines show the spectra in the presence of ATP, while dotted lines are the corresponding traces in the absence of ATP. Panels A-to-G are labeled according to the amino acid substitution(s) introduced in *Se*CobA. The feature due to 4c Co(II)Cbl species (band δ) is highlighted by a vertical line. Additional spectroscopic changes in reference to the MCD spectrum of free Co(II)Cbl (panel H, bands a, b and c) are also highlighted.

formation of a 4c species (Figure 3.6 D; see Figure 3.9 for a comparison to a His-on species). Similar to the results obtained for *Se*CobA^{W93F}, the W93H substitution has a more dramatic effect on the 4c→5c equilibrium when Co(II)Cbl instead of

Co(II)Cbi$^+$ is used as the substrate. In fact, the MCD spectrum of Co(II)Cbl in the presence of *Se*CobA^{W93H}/ATP (Figure 3.7 E), does not contain any discernible contributions from the δ-band transition, while the features at higher energies are analogous to those observed in the presence of *Se*CobA^{WT} and *Se*CobA^{W93F}. These findings indicate that the side chain of residue W93 is particularly important for promoting the dissociation of the DMB moiety from the Co(II) ion, as replacement of the native heterocyclic 9-membered indole ring by smaller phenyl and imidazole groups progressively shifts the equilibrium towards 5c co(II)rrinoid species, inhibiting the formation of 4c Co(II)Cbl in *Se*CobA^{W93H}.

Substitutions of residue F91: *(i) F91W.* In the MCD spectrum of Co(II)Cbi$^+$ in the presence of *Se*CobA^{F91W} and ATP, the δ- and β-bands are similarly intense as in the spectrum obtained with *Se*CobA^{WT}/ATP (Figure 3.6 B). Interestingly, the λ- and σ-bands are red-shifted by ~100 cm^{-1} from their positions in the spectra of other *Se*CobA variants capable of generating 4c Co(II)Cbi$^+$. As both of these bands arise from mixed CT / LF transitions of 4c Co(II)Cbi$^+$ that are sensitive to perturbations of the frontier MOs of the corrin ring, these shifts indicate that the conformation of the corrin ring is uniquely perturbed in the active site of *Se*CobA^{F91W}/ATP. As in the case of Co(II)Cbi$^+$, the intensity of the δ-band in the MCD spectrum of Co(II)Cbl in the presence of *Se*CobA^{F91W}/ATP is comparable to that observed in the spectrum with *Se*CobA^{WT}/ATP (Figure 3.7 B). These results conclusively demonstrate that *Se*CobA^{F91W} is capable of generating 4c Co(II)Cbi$^+$ and Co(II)Cbl species with yields approaching those achieved by *Se*CobA^{WT}. However, kinetic studies of *Se*CobA^{F91W} with Co(II)Cbl showed diminished catalytic activity relative

Table 3.3: Positions of the δ-band in the MCD spectra of 4c Co(II)Cbi$^+$ and Co(II)Cbl generated in the active sites of *Se*CobA^{WT} and several variants. Shifts in the δ-band are shown in relation to the position of this feature in the spectrum Co(II)Cbi$^+$ in the presence of *Se*CobA^{WT}/ATP. Also shown are the relative yields of 4c species estimated from the δ-band band intensities (see SI for details). The expected yields based on kinetic results obtained with Co(II)Cbl are also shown in parenthesis.[38]

	Co(II)Cbi$^+$		
*Se*CobA	$\nu(\delta)$ / cm^{-1}	$\Delta\nu(\delta)$ / cm^{-1})	4c Yield / %
A. none (WT)	12 270	0	50
B. F91W	12 230	−40	85
C. F91Y	12 300	30	> 95
D. W93F	12 240	−30	89
E. F91H	12 180	−90	41
F. W93F/F91W	12 210	−60	5
G. W93A	*n/a*	*n/a*	*n/d*
	Co(II)Cbl		
A. none (WT)	12 350	80	8 (25)
B. F91W	12 260	−10	7 (4)
C. F91Y	12 320	50	40 (45)
D. W93F	12 220	−50	2 (68)
E. F91H	*n/a*	*n/a*	(19)
F. W93F/F91W	*n/a*	*n/a*	(20)
G. W93A	*n/a*	*n/a*	*n/d*

to *Se*CobA^{WT}, while the activity with Co(I)Cbl was largely retained, suggesting that the Co(II)/Co(I) reduction step is detrimentally affected by the F91W substitution. These seemingly conflicting results can be reconciled by recognizing that the larger size of the indole group of residue 91 in *Se*CobA^{F91W} relative to the phenyl group

in *Se*CobA^{WT} introduces new steric constraints in the active site that affect the orientation of the bound 4c co(II)rrinoid as evidenced by the shift in the λ- and σ-bands observed spectroscopically. These structural changes could suppress the rate of electron transfer to the Co(II) ion and/or lead to uncontrolled side reactions of the transiently generated Co(I)Cbl "supernucleophile". While our spectroscopic results suggest that this improper orientation of the co(II)rrinoid substrate only occurs in the *Se*CobA^{F91W}/ATP complex, thus favoring the latter scenario, further experiments are needed to further clarify the origins of the decreased activity observed for this variant.

(ii) W93F,F91W. The MCD spectrum of Co(II)Cbi$^+$ in the presence of *Se*CobA^{W93F,F91W}/ATP exhibits a very weak and broad δ-band, from which we can estimate that the yield of 4c Co(II)Cbi$^+$ species is reduced more than tenfold from that achieved by *Se*CobA^{WT} and twenty-fold from that of *Se*CobA^{F91W} (Figure 3.6 F). The remaining 5c Co(II)Cbi$^+$ fraction is also bound to the active site of the double-variant, but with a perturbed Co–O(H_2) interaction, as indicated by the ~300 cm^{-1} red-shift of the lowest energy LF transition near ~16 000 cm^{-1} from its position observed for free Co(II)Cbi$^+$ (Figure 3.6 H).[56] As expected from the low yield of 4c Co(II)Cbi$^+$ in *Se*CobA^{W93F,F91W}/ATP, the MCD spectrum of Co(II)Cbl in the presence of this variant lacks the δ-band, indicating that no 4c Co(II)Cbl is generated under the experimental conditions used (Figure 3.7 F). Further inspection of this spectrum indicates that the 5c Co(II)Cbl species is significantly perturbed by the enzyme (Figure 3.7 F, bands a and b), as observed for other *Se*CobA variants capable of generating 4c Co(II)Cbi$^+$.

While our results indicate that the introduction of the F91W and W93F substitutions in *Se*CobA^{W93F,F91W} drastically lowers the yield of 4c co(II)rrinoid species, this variant was shown to exhibit similar k_{cat} and K_M values as *Se*CobA^{WT}. Although these observations are difficult to rationalize based on spectroscopic and kinetic data alone, inspection of the *Se*CobA^{WT} crystal structure reveals that residues F91 and W93 are positioned so as to participate in and off-set π-stacking interaction, with the larger W93 side chain occupying the more remote position relative to the corrin ring. Switching the relative positioning of these residues in *Se*CobA^{W93F,F91W} likely causes the co(II)rrinoid substrates to adopt a different orientation within the enzyme active site, especially at the low temperatures used in our spectroscopic experiments. Under the conditions used to characterize the *Se*CobA^{F91W,W93F} variant kinetically (i.e. in the absence of glycerol and at 298 K), the enhanced thermal motion of residues 91 and 93 may cause the active site to adopt a more wildtype-like conformation, resulting in k_{cat} and K_M values similar to those of *Se*CobA^{WT}.

(iii) F91H. The MCD spectrum of Co(II)Cbi$^+$ in the presence of ATP-free *Se*CobA^{F91H} lacks any contributions from 4c co(II)rrinoid species, and instead is very similar to the MCD spectrum of free Co(II)Cbl (Figure 3.9 B). As the nucleotide loop and terminal DMB group are absent in Co(II)Cbi$^+$, the characteristic spectroscopic features of nitrogen ligation observed in the MCD spectrum of Co(II)Cbi$^+$ in the presence of *Se*CobA^{F91H} indicates that the newly introduced H91 residue can coordinate to the Co(II) ion. The corresponding EPR spectrum reveals that 50% of the Co(II)Cbi$^+$ substrate is present in the His-on state (Figure 3.8, B), while the remaining fraction retains the water ligand (Table 3.4, B).

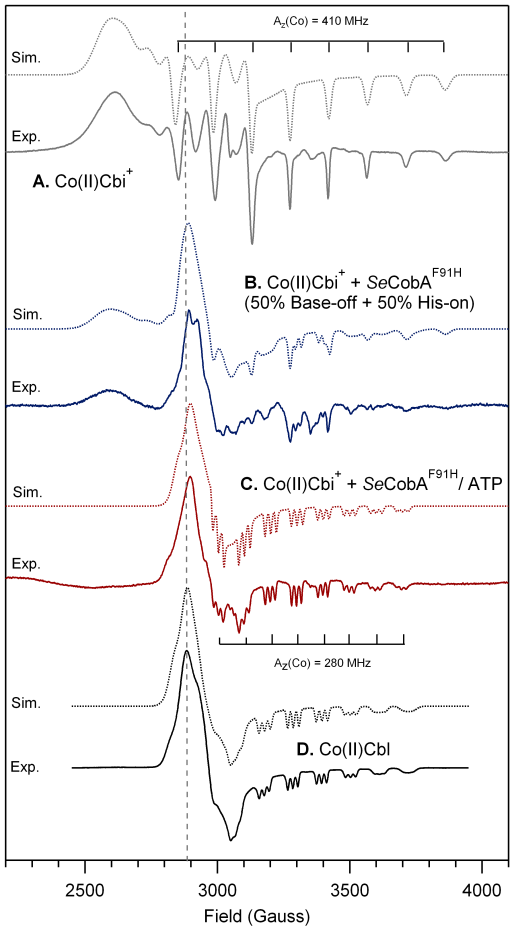

Figure 3.8: X-band EPR spectra collected at 40 K of (A) free Co(II)Cbi$^+$, (B) Co(II)Cbi$^+$ in the presence of *Se*CobA^{F91H}, and (C) Co(II)Cbi$^+$ in the presence of *Se*CobA^{F91H} and ATP. For reference, the spectrum of free Co(II)Cbl is shown in panel (D), with the most intense feature highlighted by a dashed line. EPR spectra were collected using a 9.36 GHz microwave source, 2 mW microwave power, 5 G modulation amplitude, 100 kHz modulation frequency and a 328 ms time constant. Spectra were simulated using the parameters provided in Table 3.4.

Upon addition of ATP to this complex, the positively-signed MCD features at 17 500 and 18 700 cm^{-1} red-shift by ~500 cm^{-1}, while the lower-energy derivative-shaped features are replaced by an unprecedented set of weak positive bands above

Table 3.4: EPR parameters for Co(II)Cbi$^+$ in the presence and absence of the *Se*CobA^{F91H} / ATP complex. Values for free Co(II)Cbl are also shown for comparison.

		g-values			A(^{59}Co)			A(^{14}N)		
Species		g_z	g_y	g_x	A_z	A_y	A_x	A_z	A_y	A_x
A. Free Co(II)Cbi$^+$	base-off	2.002	2.345	2.335	410	240	240	*n/a*	*n/a*	*n/a*
B. Co(II)Cbi$^+$ +*Se*CobA^{F91H}	base-off	2.002	2.365	2.335	410	240	240	*n/a*	*n/a*	*n/a*
	his-on	2.001	2.235	2.275	305	30	30	60	10	10
C. Co(II)Cbi$^+$ +*Se*CobA^{F91H} +ATP	his-on	2.002	2.235	2.280	280	30	30	52	10	10
D. Co(II)Cbl	base-on	2.001	2.235	2.275	305	30	30	60	10	10

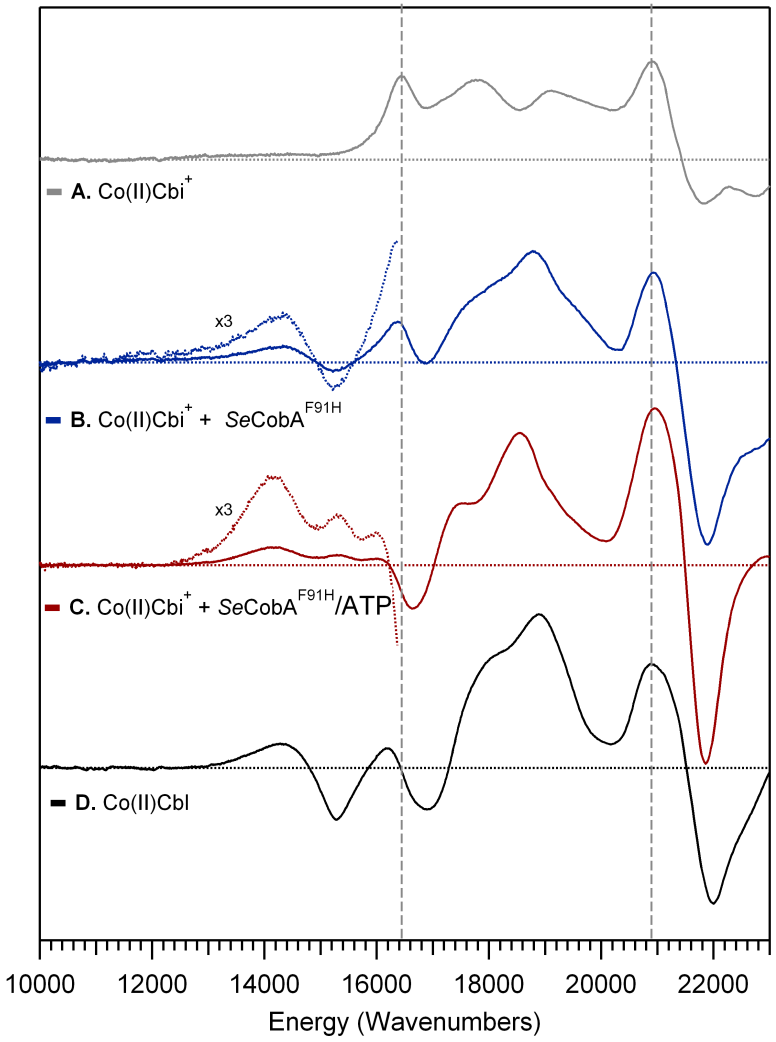

Figure 3.9: MCD spectra collected at 7 T and 4.5K of (A) free Co(II)Cbi$^+$, (B) Co(II)Cbi$^+$ in the presence of *Se*CobA, and (C) Co(II)Cbi$^+$ in the presence of *Se*CobA and ATP. For reference, the spectrum of free Co(II)Cbl is shown in panel (D). The most intense features of free Co(II)Cbi$^+$ are highlighted by dashed vertical lines. The lower energy region the spectra of protein-bound species is scaled by a factor of 3 to highlight unique features in this region.

with nearby amino acids.

(iv) F91Y. The MCD spectrum of Co(II)Cbi$^+$ in the presence of *Se*CobA^{F91Y}/ATP is strikingly similar to that obtained with *Se*CobA^{WT}/ATP, though the δ-, β-, λ-, and σ-bands associated with the 4c Co(II)Cbi$^+$ fraction are considerably more intense. Additionally, the features at ~15 000 cm^{-1} due to 5c Co(II)Cbi$^+$ are notably absent in the variant spectrum, indicating that introduction of a Tyr residue at position 91 results in a near complete conversion of the enzyme-bound Co(II)Cbi$^+$ to a 4c species (Table 3.3, C). Similarly, the MCD spectrum of Co(II)Cbl in the presence of *Se*CobA^{F91Y}/ATP reveals a fivefold increase in the yield of 4c species relative to that achieved by the *Se*CobA^{WT} enzyme (Table 3.3 and Figure 3.7, C). Thus, even though the relative yield of 4c co(II)rrinoid species generated by *Se*CobA^{F91Y} remains ~50% lower when Co(II)Cbl instead of Co(II)Cbi$^+$ is used as the substrate, this variant is much more effective at generating 4c co(II)rrinoid species than *Se*CobA^{WT}. Consistent with these results, *Se*CobA^{F91Y} was found to have a threefold larger k_{cat} and six-fold lower K_M than *Se*CobA^{WT} when Co(II)Cbl was used as the substrate.[38]

3.5 Discussion

Over 25 enzymes are required for the complete biosynthesis of AdoCbl by prokaryotes. A critical step in this de novo pathway involves the attachment of a 5'-deoxyadenosyl (Ado) group to the cobalt ion on the Coβ face, carried out by the *Se*CobA ACAT in *S. enterica*.[23] While no eukaryotes are known to synthesize AdoCbl *de novo*, they retain genes encoding ACAT enzymes in their genomes. For exam-

ple, the human ACAT, hATR, converts Co(II)Cbl to AdoCbl and delivers it to the methylmalonyl-CoA mutase (MMCM) enzyme in order to restore catalytic activity following cofactor deactivation.[20, 31, 57] Intriguingly, the three distinct families of known ACATs seem to employ the same general catalytic mechanism, even though they share little primary sequence homology and differ with respect to the morphology of the corrinoid binding site.[11, 23, 28] While a recent report has highlighted the molecular interactions that are critical for catalytic activity of the *Lr*PduO ACA,[29] a homologue of hATR, the roles of individual active site residues in the remaining ACAT families have not yet been elucidated. To enhance our current understanding of the mechanism by which *Se*CobA and related ACATs catalyze the Ado group transfer from ATP to co(II)rrinoid substrates, we have employed MCD spectroscopy to monitor the effects of active-site amino-acid substitutions on the co(II)rrinoid/*Se*CobA interaction. As this enzyme is tasked with (i) binding the ATP and co(II)rrinoid co-substrates, (ii) co(II)rrinoid reduction, and (iii) directing nucleophilic attack of the highly reactive Co(I) intermediate toward the 5′-carbon of ATP, the particular step that is affected by a given substitution is unclear from kinetic studies alone.

Effects of amino acid substitutions on the 5c $\rightarrow$ 4c Co(II)rrinoid conversion yield and Co–C(Ado) bond formation: The K_M values established from recent kinetic studies of *Se*CobA^{WT} can be compared to the relative yields of formation of 4c Co(II)Cbl established by our MCD experiments (see SI for details)[29] to determine whether a given amino acid substitution at the active site of *Se*CobA^{WT} mainly affects the Co(II)/Co(I) reduction step or the subsequent nucleophilic attack of the

transiently generated Co(I) species on co-substrate ATP. Because 4c co(II)rrinoid formation is a prerequisite for generating the Co(I) "supernucleophile", changes to the 5c→4c co(II)rrinoid equilibrium should correlate directly with enzymatic activity. As summarized in Table 3.3 (right columns), a correlation indeed exists between changes in enzymatic activity caused by amino acid substitutions and the relative yield of 4c co(II)rrinoid, indicating that the reduced activity of the variants is largely due to perturbations to the Co(II)/Co(I) reduction step. While the 8% relative yield of 4c Co(II)Cbl determined by our MCD studies of *Se*CobA^{WT} is smaller than the value of 25% estimated from the corresponding K_M value (see SI for details), the dramatic increase in the relative yield of formation of 4c Co(II)Cbl observed spectroscopically with *Se*CobA^{F91Y} correlates well with kinetic data. Similarly, the lower 4c Co(II)Cbl yields achieved by the *Se*CobA^{W93H} and *Se*CobA^{W93F,F91W} variants relative to *Se*CobA^{WT}, are consistent with the K_M values determined for these variants.

The most recently reported crystal structure of *Se*CobA in the presence of Co(II)-Cbl and MgATP indicates that residues W93 and F91, which are critical for 4c co(II)rrinoid formation in the active site of *Se*CobA^{WT}, remain partially solvent exposed in the "closed" conformation (Figure 3.10). Our spectroscopic results do not preclude the possibility that subtle changes in the solvation environment could affect the organization of the active site of *Se*CobA, in particular with respect to the burial of the F91 and W93 side chains, and thus the activity of the enzyme.[58, 59] However, given the general agreement between our spectroscopic data and published kinetic results, it appears that these changes, if present, have relatively minor effects on

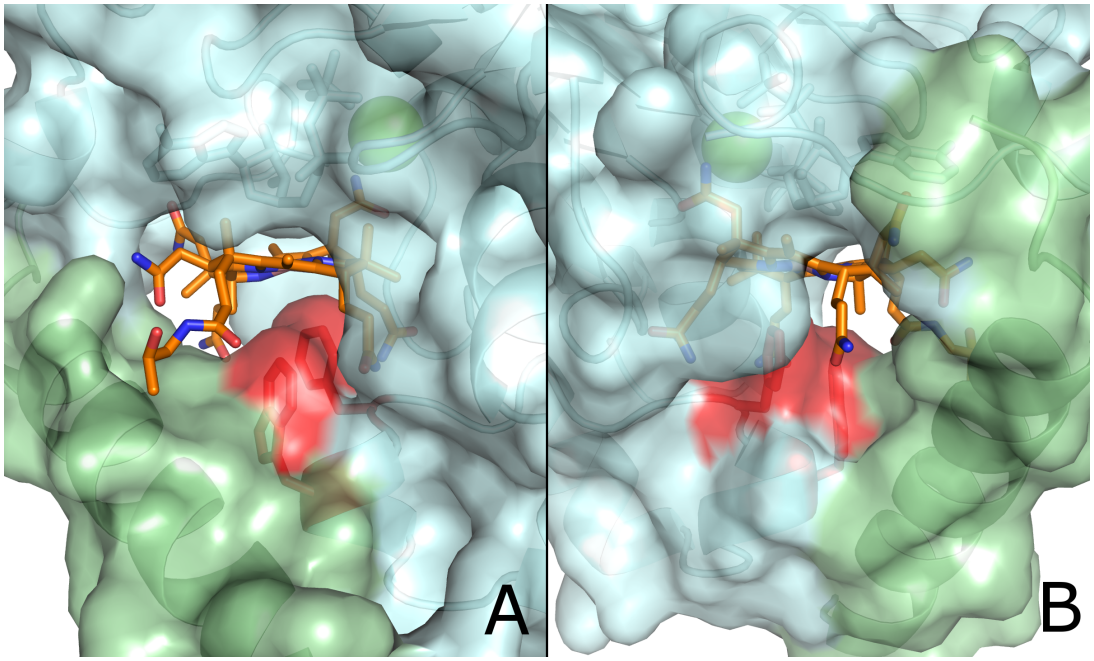

Figure 3.10: Surface representation of the cobalamin-binding site in the "closed" conformation of *Se*CobA based on PDB entry 4HUT. In panel (A) the protein is oriented as in Figure 3.3, while in panel (B) the backside of the active site is shown. Contributions from the F91 and W93 residues are shown in red to highlight the exposure of these residues to solvent.

the activity of *Se*CobA variants under physiological conditions.

Differences between the relative yields of 4c co(II)rrinoids estimated on the basis of KM values and observed by MCD spectroscopy could also arise from perturbations to the Co–C(Ado) bond formation step; e.g., via alterations in the relative positioning of the co(I)rrinoid intermediate and the adenosyl moiety of ATP. While changes to both the 5c $\rightarrow$ 4c co(II)rrinoid conversion yield and the Co–C(Ado) bond formation step likely contribute to the altered catalytic rates of the *Se*CobA variants investigated, our spectroscopic data suggest that the latter is the predominant contributor when F91 is replaced by a Trp residue. The F91W

substitution significantly increases the bulk of the protein scaffold below the Coβ face of the corrin ring (Table 3.5), and thus is expected to introduce steric crowding in the "closed" conformation. Consistent with this prediction, the MCD spectra of Co(II)Cbi^{+} in the presence of *Se*CobA^{F91W} and *Se*CobA^{WT} show considerable differences (Figure 3.6). Hence, even though the relative yield of 4c co(II)rrinoid achieved by *Se*CobA^{F91W} is high, this variant displays little catalytic activity. When the F91W substitution is paired with the W93F substitution to mitigate this steric clash, the catalytic activity increases substantially, despite the fact that the fraction of 4c co(II)rrinoid in the *Se*CobA^{W93F,F91W} variant is much smaller than in *Se*CobA^{F91W}. Thus, while maximizing the yield of 4c co(II)rrinoid species is critical for high catalytic activity, careful control of the positioning of the corrinoid substrate in the active site of *Se*CobA is also important for catalysis.

Our MCD spectra also provide insight into the geometry adopted by the Co(II)-Cbl substrate in the "open" conformation of *Se*CobA, prior to removal of the DMB moiety. A comparison of the MCD features exhibited by free Co(II)Cbl and of the 5c Co(II)Cbl species in the presence of the different *Se*CobA/ATP complexes investigated reveals small but noticeable differences. In particular, the decrease in the intensity of the negatively signed band at ~15 000 cm^{-1}, along with the minor red-shift of the positive feature at ~17 000 cm^{-1} observed for *Se*CobA^{WT} and all variants except for *Se*CobA^{W93A} (Figure 3.7) indicates that the 5c Co(II)Cbl fraction is enzyme bound, with a perturbed Co–N(DMB) bonding interaction. This finding is consistent with the crystal structure of *Se*CobA^{WT}, which indicates that in the "open" conformation, residue W93 is in very close proximity to the ribose

Table 3.5: DFT-computed dispersion energies (E_D) for different pairs of amino acid residues in the active site of *Se*CobA^{WT} and several variants in the "closed" conformations, and estimated free energy changes for the equilibrium between the 4c and 5c states of the Co(II)Cbl and Co(II)Cbi$^+$ substrates ($\Delta\Delta G_{4c}$) based on the 5c→4c co(II)rrinoid conversion yield from Table 3.3. The change in solvent accessible surface area (ΔSA) for each pair of residues in the absence of the protein is provided as a measure of the bulkiness of each pair. All values are shown in relation to Co(II)Cbi$^+$ bound to the *Se*CobA^{WT}/ATP complex (in gray). Cases where the ΔSA values are > 27 Å^2 are highlighted in red.

*Se*CobA	Active Site	$\Delta\Delta G_{4c}$ / kJ·mol^{-1}			
Substitution	Model	ΔE_{D3} / kJ·mol^{-1}	ΔSA / Å^2	Co(II)Cbi$^+$	Co(II)Cbl
A. W93A	Phe,Ala	115	−56.7	»9	»9
B. W93H	Phe,His	64	−34.7	0.74	8.98
C. W93F	Phe,Phe	40	−17.9	−4.2	7.7
D. W93F,F91W	Trp,Phe	17	27.2	5.7	>9
E. none(WT)	Phe,Trp	0	0.0	0.00	4.60
F. F91Y	Tyr,Trp	−13	8.5	−5.79	0.82
F. F91W	Trp,Trp	−39	48.5	−3.37	5.09

moiety that makes up part of the nucleotide loop of Co(II)Cbl. This steric clash may contribute to the elongated Co–N(DMB) bond of the 5c Co(II)Cbl species observed in the X-ray crystal structure of *Se*CobA^{WT} (see Table 4.1). As the nearby F91 side chain is properly positioned to participate in a π-stacking interaction with residue W93 in the "open" conformation, substitution of F91 would be expected to introduce further perturbations to the Co–N(DMB) bond of enzyme-bound Co(II)Cbl, consistent with our MCD data. Thus, we conclude that in the "open" conformation of *Se*CobA^{WT}, the F91 and W93 residues are positioned so as to weaken the Co–N(DMB) bond via steric interactions with the bulky DMB moiety.

Mechanism of 4c Co(II)rrinoid formation: Because MCD spectroscopy pro-

vides a uniquely sensitive tool for discriminating between 4c and 5c co(II)rrinoids, it is possible to use our data as the basis for estimating the change in free energy for the formation of 4c species in response to active site amino acid substitutions, $\Delta\Delta G_{4c}$ (see SI for details). Using Co(II)Cbi^{+} bound to the *Se*CobA^{WT}/ATP complex as the reference point, our analysis yields a range of $\Delta\Delta G_{4c}$ values between -6 and $+9$ kJ/mol based on the detection limit of 4c co(II)rrinoid species by our MCD instrument (~1% relative to the entire population of co(II)rrinoids). On average, $\Delta\Delta G_{4c}$ increases by ~8 kJ/mol when Co(II)Cbl instead of Co(II)Cbi^{+} is used as the substrate (Table 3.3, right columns), which can be attributed to the increased strength of the Co–N(DMB) bond relative to the Co–O(H_2) bond. The increase in Co–N(DMB) bond strength estimated from our results is consistent with the 40-fold decrease in K_M values previously observed for the binding of AdoCbl to MMCM (which binds AdoCbl in a base-off/His-on fashion)3 relative to hATR (which excludes the binding of axial ligands to the Coα face of the corrin ring where the DMB group would usually be found).[20, 34, 60] However, this difference is not constant across the entire series of *Se*CobA variants investigated, since specific, species-dependent intermolecular interactions between the protein side chains and the DMB moiety are likely important for promoting Co–N(DMB) bond dissociation (vide supra). The fact that *Se*CobA^{WT} achieves a higher 5c $\rightarrow$ 4c conversion yield with Co(II)Cbi^{+} as the substrate is consistent with its main role in the adenosylation of incomplete corrinoids that generally lack the nucleotide loop and terminal DMB base.

A comparison of the "open" and "closed" conformations observed in the crystal

structure of *Se*CobA^{WT} complexed with Co(II)Cbl and MgATP reveals only minor differences in the vicinity of the Coβ face of the corrin ring that is oriented toward co-substrate ATP. In contrast, large conformational differences exist near the Coα face of the corrin ring, in particular with regards to residues F91 and W93 that move by ~12.1 and ~7.5 Å, respectively, relative to their solvent-exposed positions in the "open" conformation, to fill the space originally occupied by the DMB moiety. Given the size and hydrophobicity of these residues, as well as their positioning in an off-set π-stacking configuration in the "closed" conformation, it is likely that dispersion interactions play a role in stabilizing the "closed" over the "open" conformation of *Se*CobA.[61, 62] To evaluate this possibility, the magnitude of dispersion interactions involving residues 91 and 93 was estimated by DFT computations (see Experimental section for details). Inspection of the computed dispersion energies, E_D, for various combinations of residues reveals a correlation between these values and the relative population of 4c Co(II)Cbi$^+$ generated in the different *Se*CobA variants investigated (Table 3.3). While the computed E_D values are generally much larger than the dispersion energies reported for related model systems,[61, 63] they properly reproduce the experimental trends and correlate well with the size of the interacting π-systems.[64] Consistent with the inability of *Se*CobA^{W93A} to convert Co(II)Cbl and Co(II)Cbi$^+$ to 4c species and the lack of catalytic activity displayed by this variant, the computed E_D value for the Phe-Ala fragment is 115 kJ/mol smaller than that obtained for the Phe-Trp fragment present in *Se*CobA^{WT}, highlighting the importance of the F91 residue in stabilizing the "closed" conformation of the protein. A largely reduced ED value (by ~64 kJ/mol) is also predicted for the Phe-His pair,

consistent with our spectroscopic data for *Se*CobA^{W93H}, which indicate that this variant is relatively ineffective at converting Co(II)Cbi^{+} to a 4c species and fails to promote dissociation of the DMB group from Co(II)Cbl. Finally, replacement of Phe by Tyr, a polar aromatic residue, results in a modest (~13 kJ/mol) increase in the computed ED value, in qualitative agreement with the higher relative 4c co(II)rrinoid yields observed experimentally for the *Se*CobA^{F91Y} variant.

The E_D values obtained for the remaining active site models agree less well with the experimental trends, supporting our hypothesis that additional factors affect the 5c→4c co(II)rrinoid conversion yield (vide supra). As our spectroscopic results reveal a uniquely perturbed conformation of the co(II)rrinoid substrate in the *Se*CobA variants possessing the F91W substitution (*Se*CobA^{F91W} and *Se*-CobA^{F91W,W93F}), it is worth noting that the introduction of the larger indole moiety dramatically increases the bulkiness of the active site, as indicated by the >27 Å^2 increase in the solvent-accessible surface area (ΔSA) of the paired 91 and 93 residues in these variants (Table 3.5). Thus, it is likely that our simple models do not properly account for all of the changes in protein conformation that are needed to accommodate the larger residues. Similar factors may contribute to the poor agreement between the computed E_D value and the relative yield of 4c co(II)rrinoid formation in the case of *Se*CobA^{W93F}.

Despite certain exceptions to the general trend in the E_D values, our computational results provide strong evidence that favorable enthalpic contributions from off-set π-stacking interactions between residues 91 and 93 in the "closed" conformation of *Se*CobA contribute to 4c co(II)rrinoid formation. In addition, our results

indicate that in the absence of a bulky, planar residue, as in the case of *Se*CobA^{W93A}, steric interactions needed for lower ligand exclusion no longer exist, possibly allowing solvent molecules to interact with the corrin ring, as shown by the essentially unperturbed conformation of co(II)rrinoids in the presence of this variant. Similarly, introduction of smaller aromatic residues (as in *Se*CobA^{W93F} and *Se*CobA^{W93H}) likely diminishes the conformational rigidity of the active site, consistent with the broadening of the δ-band in the corresponding MCD spectra (Figure 3.6, traces D and E), while introduction of larger residues results in significant steric strain that may cause distortions of the corrin ring, as observed for *Se*CobA^{F91W}. Furthermore, our experimental and computational results indicate that the replacement of a hydrogen atom in the F91 side chain by a hydroxyl group does not result in large changes in the conformation of the active site. However, it does increase dispersion interactions with the nearby W93 residue, thus stabilizing the "closed" conformation. The calculated ~13 kJ/mol increase in E_D is on the order of our experimentally estimated difference in $\Delta\Delta G_{4c}$ of ~8 kJ/mol for the dissociation of the DMB moiety from Co(II)Cbl vs H_2O dissociation from Co(II)Cbi$^+$ (vide supra), indicating that this contribution alone may be sufficient to account for the dramatic increase in the 4c Co(II)Cbl yield achieved by *Se*CobA^{F91Y}.

Implications for the mechanism of co(II)rrinoid reduction and adenosylation in vivo: Crystallographic studies revealed that ATP binding to *Se*CobA^{WT} causes the active site to adopt a conformation in which it can engage in dipolar interactions with the acetamide and propionamide side chains on the corrin ring and thus facilitate the binding of the co(II)rrinoid substrate.[33, 38] In this "open" conformation

of *Se*CobA^{WT}, the lower axial ligand (either DMB or H_2O) remains associated with the Co(II) ion, but likely interacts with the nearby W93 residue. Further structural changes to the active site structure occur upon formation of the "closed" conformation, in particular to the N-terminal region of the adjacent subunit as well as the segment between residues M87 and C105, which adopt helical structures. As a result, the co(II)rrinoid substrate shifts ~0.3 Å closer to the 5'-C of ATP while the F91 and W93 residues move below the Coα face of the corrin ring to generate a unique 4c co(II)rrinoid species. While the "open" and "closed" conformations of the enzyme exist in an equilibrium, it is only in the "closed" conformation where the required tuning of the Co(II)/Co(I) reduction potential occurs via elimination of any axial ligand interactions. As evidenced by the spectroscopic data obtained in this study, the equilibrium between these conformations depends on the nature of the axial ligand of the bound co(II)rrinoid and is sensitive to amino acid substitutions in the active site of *Se*CobA. Collectively, our data indicate that the "closed" conformation is stabilized over the "open" conformation by hydrophobic effects, as observed for the related *Lr*PudO ACAT, and by π-stacking interactions between residues F91 and W93.

In the X-ray crystal structure of *Se*CobA^{WT}, the distance between the Co(II) ion of the 4c fraction of Co(II)Cbl and the 5'C of co-substrate ATP is ~3.0 Å, which is only ~1.0 Å larger than the Co–C(Ado) bond distance in AdoCbl.[3] As this 4c fraction of Co(II)Cbl is activated for one-electron reduction by flavins to produce a "supernucleophilic" co(I)rrinoid species, the close proximity between the two substrates is critical for avoiding undesired side reactions. The positioning of the

corrinoid relative to the co-substrate ATP is likely controlled, at least in part, by the conformation of the M87–C105 loop. In support of this hypothesis, *Se*CobA^{F91W} displays a drastically diminished catalytic activity due to misalignment of the corrinoid substrate, even though it achieves wildtype-like relative yields of formation of 4c Co(II)Cbl and Co(II)Cbi^{+}. These findings highlight the delicate balance of interactions that must be present in the active site of *Se*CobA for the formation of 4c co(II)rrinoids. Our findings also provide clues as to why *Ralstonia* species express CobA with Tyr at position 91 in lieu of the Phe present in *Se*CobA.[38] While in vivo *Se*CobA is responsible for the adenosylation of a variety of corrinoid substrates,[10] our results indicate that Co(II)Cbl provides a significant challenge for this enzyme, as only ~8% of Co(II)Cbl is converted to a 4c species. Substitution of F91 by a Tyr residue increases the amount of 4c species generated from Co(II)Cbl fivefold. It is possible that these homologous CobAs with active-site tyrosines have been selected for in vivo conditions that demand a very high turnover of AdoCbl, or perhaps these organisms are "fed" cobalamin by mutualistic strains and no longer need to process cobinamide. Another possibility is that the active site tyrosine is more effective at generating 4c species of cobamides that possess Coβ-ligands other than DMB, which could include one of several types of purines, phenolics, or DMB-derivatives.[39] The in vitro effectiveness of *Se*CobA^{WT} to adenosylate alternative cobamides has yet to be determined.

3.6 References

[1] T. Toraya. Cobalamin-dependent dehydratases and a deaminase: Radical catalysis and reactivating chaperones. *Archives of Biochemistry and Biophysics*, 544:40–57, 2014.

[2] E. N. G. Marsh, D. P. Patterson, and L. Li. Adenosyl radical: Reagent and catalyst in enzyme reactions. *Chembiochem*, 11(5):604–621, 2010.

[3] L. Randaccio, S. Geremia, N. Demitri, and J. Wuerges. Vitamin b-12: Unique metalorganic compounds and the most complex vitamins. *Molecules*, 15(5):3228–3259, 2010.

[4] *Enzyme-Catalyzed Electron and Radical Transfer*, volume 35. Kluwer Academic Publishers, New York.

[5] N. Shibata, J. Masuda, T. Tobimatsu, T. Toraya, K. Suto, Y. Morimoto, and N. Yasuoka. A new mode of b-12 binding and the direct participation of a potassium ion in enzyme catalysis: X-ray structure of diol dehydratase. *Structure with Folding & Design*, 7(8):997–1008, 1999.

[6] A. Abend, V. Bandarian, R. Nitsche, E. Stupperich, J. Retey, and G. H. Reed. Ethanolamine ammonia-lyase has a "base-on" binding mode for coenzyme b-12. *Archives of Biochemistry and Biophysics*, 370(1):138–141, 1999.

[7] *Aminomutases*. John Wiley & Sons, Inc., 1999.

[8] M. L. Ludwig and R. G. Matthews. Structure-based perspectives on b-12-dependent enzymes. *Annual Review of Biochemistry*, 66:269–313, 1997.

[9] E. N. G. Marsh and D. P. Ballou. Coupling of cobalt-carbon bond homolysis and hydrogen atom abstraction in adenosylcobalamin-dependent glutamate mutase. *Biochemistry*, 37(34):11864–11872, 1998.

[10] M. J. Warren, E. Raux, H. L. Schubert, and J. C. Escalante-Semerena. The biosynthesis of adenosylcobalamin (vitamin b-12). *Natural Product Reports*, 19(4):390–412, 2002.

[11] P. E. Mera and J. C. Escalante-Semerena. Multiple roles of atp:cob(i) alamin adenosyltransferases in the conversion of b-12 to coenzyme b-12. *Applied Microbiology and Biotechnology*, 88(1):41–48, 2010.

[12] J. C. Escalantesemerena, S. J. Suh, and J. R. Roth. Coba function is required for both the denovo cobalamin biosynthesis and assimilation of exogenous corrinoids in salmonella typhimurium. *Journal of Bacteriology*, 172(1):273–280, 1990.

[13] C. L. V. Johnson, M. L. Buszko, and T. A. Bobik. Purification and initial characterization of the salmonella enterica pduo atp : cob(i)alamin adenosyltransferase. *Journal of Bacteriology*, 186(23):7881–7887, 2004.

[14] N. R. Buan, S. J. Suh, and J. C. Escalante-Semerena. The eutt gene of salmonella enterica encodes an oxygen-labile, metal-containing atp : Corrinoid adenosyltransferase enzyme. *Journal of Bacteriology*, 186(17):5708–5714, 2004.

[15] P. E. Mera, M. S. Maurice, I. Rayment, and J. C. Escalante-Semerena. Structural and functional analyses of the human-type corrinoid adenosyltransferase (pduo) from lactobacillus reuteri. *Biochemistry*, 46(48):13829–13836, 2007.

[16] N. R. Buan and J. C. Escalante-Semerena. Purification and initial biochemical characterization of atp : Cob(i)alamin adenosyltransferase (eutt) enzyme of salmonella enterica. *Journal of Biological Chemistry*, 281(25):16971–16977, 2006.

[17] *Spectroscopic and Computational Insights into the Mechanism Employed by Adenosyltrasferases for Coenzyme-B12 Biosynthesis.* Thesis, 2010.

[18] R. Banerjee. Radical peregrinations catalyzed by b-12 enzymes. *Biochemistry*, 40(29):8634–8634, 2001.

[19] A. Jorge-Finnigan, C. Aguado, R. Sanchez-Alcudia, D. Abia, E. Richard, B. Merinero, A. Gamez, R. Banerjee, L. R. Desviat, M. Ugarte, and B. Perez. Functional and structural analysis of five mutations identified in methylmalonic aciduria cblb type. *Human Mutation*, 31(9):1033–1042, 2010.

[20] D. Padovani, T. Labunska, B. A. Palfey, D. P. Ballou, and R. Banerjee. Adenosyltransferase tailors and delivers coenzyme b-12. *Nature Chemical Biology*, 4(3):194–196, 2008.

[21] M. V. Fonseca and J. C. Escalante-Semerena. Reduction of cob(iii)alamin to cob(ii)alamin in salmonella enterica serovar typhimurium lt2. *Journal of Bacteriology*, 182(15):4304–4309, 2000.

[22] M. D. Liptak and T. C. Brunold. Spectroscopic and computational studies of co1+ cobalamin: Spectral and electronic properties of the "superreduced" b-12 cofactor. *Journal of the American Chemical Society*, 128(28):9144–9156, 2006.

[23] T. A. Stich, N. R. Buan, J. C. Escalante-Semerena, and T. C. Brunold. Spectroscopic and computational studies of the atp : Corrinoid adenosyltransferase (coba) from salmonella enterica: Insights into the mechanism of adenosylcobalamin biosynthesis. *Journal of the American Chemical Society*, 127(24):8710–8719, 2005.

[24] D. Lexa and J. M. Saveant. The electrochemistry of vitamin-b12. *Accounts of Chemical Research*, 16(7):235–243, 1983.

[25] N. R. Buan and J. C. Escalante-Semerena. Computer-assisted docking of flavodoxin with the atp: Co(i)rrinoid adenosyltransferase (coba) enzyme reveals residues critical for protein-protein interactions but not for catalysis. *Journal of Biological Chemistry*, 280(49):40948–40956, 2005.

[26] D. M. Hoover, J. T. Jarrett, R. H. Sands, W. R. Dunham, M. L. Ludwig, and R. G. Matthews. Interaction of escherichia coli cobalamin-dependent methionine synthase and its physiological partner flavodoxin: Binding of flavodoxin leads to axial ligand dissociation from the cobalamin cofactor. *Biochemistry*, 36(1):127–138, 1997.

[27] H. Olteanu, K. R. Wolthers, A. W. Munro, N. S. Scrutton, and R. Banerjee. Kinetic and thermodynamic characterization of the common polymorphic

variants of human methionine synthase reductase. *Biochemistry*, 43(7):1988–1997, 2004.

[28] K. Park, P. E. Mera, J. C. Escalante-Semerena, and T. C. Brunold. Kinetic and spectroscopic studies of the atp: Corrinoid adenosyltransferase pduo from lactobacillus reuteri: Substrate specificity and insights into the mechanism of co(ii)corrinoid reduction. *Biochemistry*, 47(34):9007–9015, 2008.

[29] K. Park, P. E. Mera, J. C. Escalante-Semerena, and T. C. Brunold. Spectroscopic characterization of active-site variants of the pduo-type atp:corrinoid adenosyltransferase from lactobacillus reuteri: Insights into the mechanism of four-coordinate co(ii)corrinoid formation. *Inorganic Chemistry*, 51(8):4482–4494, 2012.

[30] T. A. Stich, M. Yamanishi, R. Banerjee, and T. C. Brunold. Spectroscopic evidence for the formation of a four-coordinate co2+ cobalamin species upon binding to the human atp: Cobalamin adenosyltransferase. *Journal of the American Chemical Society*, 127(21):7660–7661, 2005.

[31] T. C. Brunold, K. S. Conrad, M. D. Liptak, and K. Park. Spectroscopically validated density functional theory studies of the b-12 cofactors and their interactions with enzyme active sites. *Coordination Chemistry Reviews*, 253(5-6):779–794, 2009.

[32] P. E. Mera, M. St Maurice, I. Rayment, and J. C. Escalante-Semerena. Residue phe112 of the human-type corrinoid adenosyltransferase (pduo) enzyme of

lactobacillus reuteri is critical to the formation of the four-coordinate co(ii) corrinoid substrate and to the activity of the enzyme. *Biochemistry*, 48(14):3138–3145, 2009.

[33] C. B. Bauer, M. V. Fonseca, H. M. Holden, J. B. Thoden, T. B. Thompson, J. C. Escalante-Semerena, and I. Rayment. Three-dimensional structure of atp : corrinoid adenosyltransferase from salmonella typhimurium in its free state, complexed with mgatp, or complexed with hydroxycobalamin and mgatp. *Biochemistry*, 40(2):361–374, 2001.

[34] Martin St Maurice, Paola Mera, Kiyoung Park, Thomas C. Brunold, Jorge C. Escalante-Semerena, and Ivan Rayment. Structural characterization of a human-type corrinoid adenosyltransferase confirms that coenzyme b12 is synthesized through a four-coordinate intermediate. *Biochemistry*, 47(21):5755–66, 2008.

[35] F Neese. Orca. an ab initio, density functional and semiempirical program package, 2008.

[36] T. A. Stich, N. R. Buan, and T. C. Brunold. Spectroscopic and computational studies of co2+ corrinoids: Spectral and electronic properties of the biologically relevant base-on and base-off forms of co2+ cobalamin. *Journal of the American Chemical Society*, 126(31):9735–9749, 2004.

[37] M. D. Liptak, A. S. Fleischhacker, R. G. Matthews, J. Telser, and T. C. Brunold. Spectroscopic and computational characterization of the base-off forms of cob(ii)alamin. *Journal of Physical Chemistry B*, 113(15):5245–5254, 2009.

[38] T. C. Moore, S. A. Newmister, I. Rayment, and J. C. Escalante-Semerena. Structural insights into the mechanism of four-coordinate cob(ii)alamin formation in the active site of the salmonella enterica atp:co(i)rrinoid adenosyltransferase enzyme: Critical role of residues phe91 and trp93. *Biochemistry*, 51(48):9647–9657, 2012.

[39] Nomenclature of corrinoids (1973 recommendations) - iupac-iub commission on biochemical nomenclature. *Biochemistry*, 13(7):1555–1560, 1974.

[40] M. G. Johnson and J. C. Escalantesemerena. Identification of 5,6-dimethylbenzimidazole as the co-alpha ligand of the cobamide synthesized by salmonella-typhimurium - nutritional characterization of mutants defective in biosynthesis of the imidazole ring. *Journal of Biological Chemistry*, 267(19):13302–13305, 1992.

[41] P. G. Blommel and B. G. Fox. A combined approach to improving large-scale production of tobacco etch virus protease. *Protein Expression and Purification*, 55(1):53–68, 2007.

[42] U. K. Laemmli. Cleavage of structural proteins during assembly of head of bacteriophage-t4. *Nature*, 227(5259):680, 1970.

[43] *Intermolecular Forces*. Reidel Publishing Company, 1981.

[44] K. L. Meagher, L. T. Redman, and H. A. Carlson. Development of polyphosphate parameters for use with the amber force field. *Journal of Computational Chemistry*, 24(9):1016–1025, 2003.

[45] H. M. Marques, B. Ngoma, T. J. Egan, and K. L. Brown. Parameters for the amber force field for the molecular mechanics modeling of the cobalt corrinoids. *Journal of Molecular Structure*, 561(1-3):71–91, 2001.

[46] E. N. G. Marsh and G. D. R. Melendez. Adenosylcobalamin enzymes: Theory and experiment begin to converge. *Biochimica Et Biophysica Acta-Proteins and Proteomics*, 1824(11):1154–1164, 2012.

[47] J. G. Brandenburg and S. Grimme. A dispersion-corrected density functional theory case study on ethyl acetate conformers, dimer, and molecular crystal. *Theoretical Chemistry Accounts*, 132(11), 2013.

[48] S. Grimme, J. Antony, T. Schwabe, and C. Muck-Lichtenfeld. Density functional theory with dispersion corrections for supramolecular structures, aggregates, and complexes of (bio)organic molecules. *Organic & Biomolecular Chemistry*, 5(5):741–758, 2007.

[49] S. Grimme, J. Antony, S. Ehrlich, and H. Krieg. A consistent and accurate ab initio parametrization of density functional dispersion correction (dft-d) for the 94 elements h-pu. *Journal of Chemical Physics*, 132(15), 2010.

[50] J.M. Pratt. *Inorganic Chemistry of Vitamin B12*. Adademic Press Inc, London, 1972.

[51] K. Park and T. C. Brunold. Combined spectroscopic and computational analysis of the vibrational properties of vitamin b-12 in its co3+, co2+, and co1+ oxidation states. *Journal of Physical Chemistry B*, 117(18):5397–5410, 2013.

[52] M. St Maurice, P. E. Mera, M. P. Taranto, F. Sesma, J. C. Escalante-Semerena, and I. Rayment. Structural characterization of the active site of the pduo-type atp : Co(i)rrinoid adenosyltransferase from lactobacillus reuteri. *Journal of Biological Chemistry*, 282(4):2596–2605, 2007.

[53] T. A. Stich, A. J. Brooks, N. R. Buan, and T. C. Brunold. Spectroscopic and computational studies of co3+-corrinoids: Spectral and electronic properties of the b-12 cofactors and biologically relevant precursors. *Journal of the American Chemical Society*, 125(19):5897–5914, 2003.

[54] A. J. Brooks, M. Vlasie, R. Banerjee, and T. C. Brunold. Co-c bond activation in methylmalonyl-coa mutase by stabilization of the post-homolysis product co2+ cobalamin. *Journal of the American Chemical Society*, 127(47):16522–16528, 2005.

[55] B. Krautler, W. Keller, and C. Kratky. Coenzyme-b12 chemistry - the crystal and molecular-structure of cob(ii)alamin. *Journal of the American Chemical Society*, 111(24):8936–8938, 1989.

[56] M. D. Liptak, S. Datta, R. G. Matthews, and T. C. Brunold. Spectroscopic study of the cobalamin-dependent methionine synthase in the activation conformation: Effects of the y1139 residue and s-adenosylmethionine on the b-12 cofactor. *Journal of the American Chemical Society*, 130(48):16374–16381, 2008.

[57] D. Padovani and R. Banerjee. A rotary mechanism for coenzyme b-12 synthesis by adenosyltransferase. *Biochemistry*, 48(23):5350–5357, 2009.

[58] C. L. Dias, T. Ala-Nissila, M. Karttunen, I. Vattulainen, and M. Grant. Microscopic mechanism for cold denaturation. *Physical Review Letters*, 100(11):4, 2008.

[59] C. L. Dias, T. Ala-Nissila, J. Wong-ekkabut, I. Vattulainen, M. Grant, and M. Karttunen. The hydrophobic effect and its role in cold denaturation. *Cryobiology*, 60(1):91–99, 2010.

[60] R. Banerjee, C. Gherasim, and D. Padovani. The tinker, tailor, soldier in intracellular b-12 trafficking. *Current Opinion in Chemical Biology*, 13(4):484–491, 2009.

[61] S. M. Butterfield, P. R. Patel, and M. L. Waters. Contribution of aromatic interactions to alpha-helix stability. *Journal of the American Chemical Society*, 124(33):9751–9755, 2002.

[62] A. Radzicka and R. Wolfenden. Comparing the polarities of the amino-acids - side-chain distribution coefficients between the vapor-phase, cyclohexane, 1-octanol, and neutral aqueous-solution. *Biochemistry*, 27(5):1664–1670, 1988.

[63] B. W. Gung, X. W. Xue, and H. J. Reich. Off-center oxygen-arene interactions in solution: A quantitative study. *Journal of Organic Chemistry*, 70(18):7232–7237, 2005.

[64] S. Grimme. Do special noncovalent pi-pi stacking interactions really exist? *Angewandte Chemie-International Edition*, 47(18):3430–3434, 2008.

Chapter 4

Spectroscopic studies of the EutT adenosyltransferase from *Salmonella enterica:*

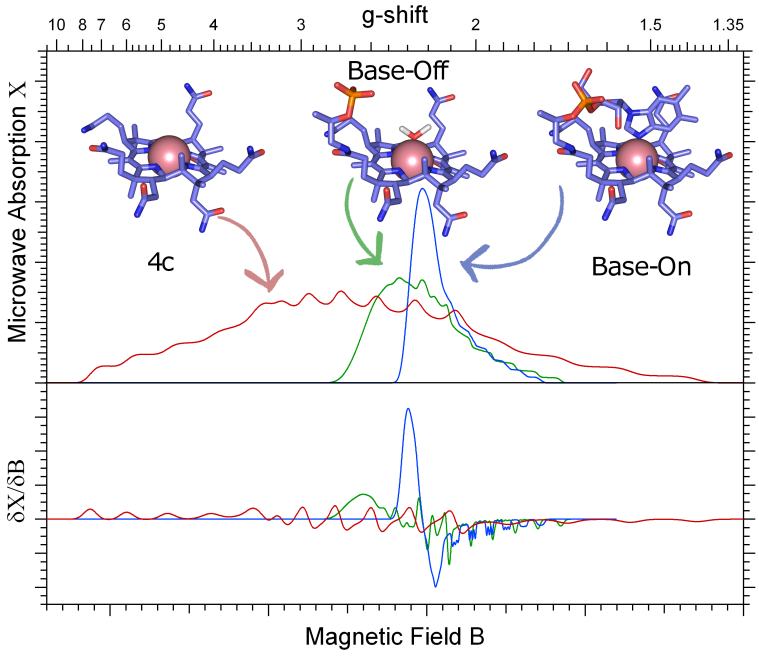

This work is under review as: I. G. Pallares, T. C. Moore, J. C. Escalante-Semerena, and T. C. Brunold "Spectroscopic studies of the EutT adenosyltransferase from Salmonella enterica: Evidence for the presence of base-off Cob(II)alamin prior to four coordinate Co(II)Cbl formation.".

4.1 Summary

EutT from Salmonella enterica is a member of a class of enzymes termed ATP:-Co(I)rrinoid adenosyltransferases (ACATs), implicated in the biosynthesis of adenosylcobalamin (AdoCbl). In the presence of co-substrate ATP, ACATs raise the Co(II)/Co(I) reduction potential of their cob(II)alamin [Co(II)Cbl] substrate by > 250 mV via the formation of a unique four-coordinate (4c) Co(II)Cbl species, thereby facilitating the formation of a "supernucleophilic" cob(I)alamin intermediate required for the formation of the AdoCbl product. While the three-dimensional structures and mechanisms of the other two ACAT families (CobA and PduO) have largely been elucidated, little information is currently available about the interaction between the Co(II)Cbl substrate and the EutT active site. Previous kinetic studies of EutT revealed the importance of a $HX_{11}CCX_2C(83)$ motif for catalytic activity and have led to the proposal that residues in this motif serve as the binding site for a divalent transition metal cofactor [e.g. Fe(II) or Zn(II)]. This motif is absent in other ACAT families, suggesting that EutT employs a distinct mechanism for AdoCbl formation. To assess how metal ion binding to the $HX_{11}CCX_2C(83)$ motif affects the relative yield of 4c Co(II)Cbl generated in the EutT active site, we have characterized several enzyme variants possessing a single alanine substitution at either the H67, H75, C79, C80, or C83 position by using electronic absorption, magnetic circular dichroism, and electron paramagnetic resonance spectroscopies. Our results indicate that Fe(II) or Zn(II) binding to the $HX_{11}CCX_2C(83)$ motif of EutT is required for promoting the formation of 4c Co(II)Cbl. Intriguingly, our spectroscopic data

also reveal the presence of an equilibrium between five-coordinate "base-on" and "base-off" Co(II)Cbl species bound to the EutT active site at low ATP concentrations, which shifts in favor of "base-off" Co(II)Cbl in the presence of excess ATP, suggesting that the base-off species serves as a precursor to 4c Co(II)Cbl.

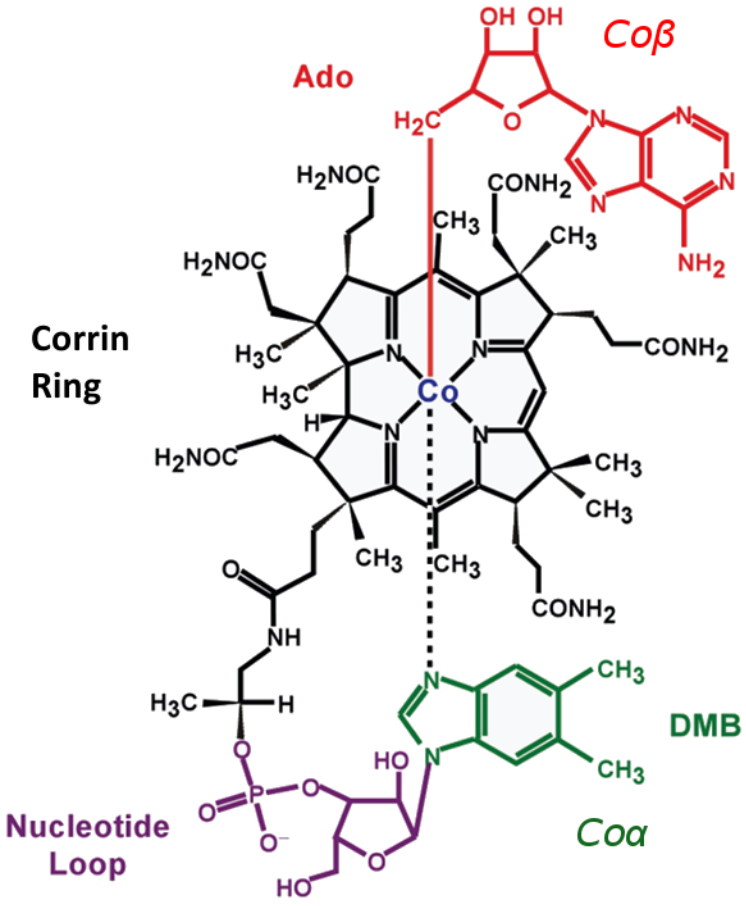

Figure 4.1: Chemical structure of adenosylcobalamin (AdoCbl), the final product of the reaction catalyzed by ATP:Co(I)rrinoid adenosyltransferases (ACATs).

4.2 Introduction

EutT is the most recently identified ATP:Co(I)rrinoid adenosyltransferase (ACAT) enzyme,[1, 2] involved in maintaining the supply of adenosylcobalamin (AdoCbl) in *Salmonella enterica*.[3] AdoCbl and related corrinoid species are characterized by the presence of a redox-active Co(III) ion that is ligated equatorially by the four nitrogen atoms of a tetrapyrrole macrocycle, termed the corrin ring, and by the 5,6-dimethylbenzimidazole (DMB) base at the end of an intramolecular nucleotide loop in the "lower" axial (Coα) position (Figure 5.1). Various ligands can occupy the "upper" axial (Coβ) position, with biologically relevant forms containing an adenosyl (AdoCbl), methyl (MeCbl), glutathionyl (GSCbl), or nitrosyl (NOCbl) moiety.[4, 5, 6] For the case of AdoCbl, homolytic cleavage of the Co–C(Ado) bond to generate an adenosyl radical and a five-coordinate Co(II)Cbl species with a vacant Coβ position is the first step in reactions catalyzed by AdoCbl-dependent eliminases/mutases.[7] Loss or inactivation of AdoCbl during turnover leads to deactivation of these enzymes, requiring replacement of their cofactor.[8] ACATs are thus implicated in the reactivation of AdoCbl-dependent enzymes, as these adenosyltransferases generate AdoCbl (or coenzyme-B_{12}) from ATP and Co(II)Cbl substrates.[3, 9]

In *Salmonella enterica*, the EutT gene is part of a 16-gene operon, whose expression is triggered by the presence of ethanolamine and adenosylcobalamin (AdoCbl),[10, 11] leading to the formation of proteinaceous polyhedron-shaped bodies. These so-called *eut* metabolosomes are postulated to encapsulate the metabolic

machinery employed by the cell for the catabolism of ethanolamine.[12, 13] The ability of *S. enterica* to the use ethanolamine as a source of nutrition was suggested to provide this bacterium with a growth advantage over other intestinal flora under inflammatory conditions,[14] as ethanolamine is readily available in the mammalian gut.[11, 15] In this metabolic pathway, the AdoCbl-dependent ethanolamine ammonia lyase (EAL) enzyme (the product of the eutB and eutC genes) catalyzes the conversion of ethanolamine to acetaldehyde and ammonia.[16] EutT has been postulated to supply the levels of AdoCbl required for EAL to perform this function.[2, 17] Notably, the presence of eutT genes was observed to correlate with higher incidence of gastroenteritis.[18]

In addition to EutT, two non-homologous ACATs are present in *S. enterica*.[3] The *Se*CobA ACAT is continuously produced to maintain basal concentrations of AdoCbl and is involved in the de novo synthesis of AdoCbl and in the scavenging of incomplete corrinoids.[19, 20] The gene encoding for *Se*PduO is part of the *pdu* operon that allows *S. enterica* to utilize 1,2-propanediol as a source of carbon and energy. PduO-type enzymes are homologous to the human adenosyltransferase (hATR), which has been shown to deliver its AdoCbl product directly to the B_{12}-dependent methylmalonyl CoA-mutase (MMCM) enzyme.[21, 22] Despite the lack of sequence and structural homologies among the known families of ACATs, a common Co–C(Ado) bond formation mechanism has previously been proposed for these enzymes involving the reduction of a Co(II)rrinoid precursor in their active sites to generate a "supernucleophilic" Co(I) species capable of attacking the 5′-carbon of ATP.[3, 23, 24] A particularly challenging step in this mechanism in-

volves the reduction of Co(II)rrinoids to generate the key Co(I) intermediate, as the reduction potentials of Co(II)rrinoids free in solution are well below those of available reducing agents in the cell (e.g. E°(NHE) = âŁ“610 mV for Co(II)Cbl and âŁ“490 mV for cob(II)inamide [Co(II)Cbi^{+}], a Co(II)Cbl precursor that lacks the nucleotide loop and DMB moiety).[25] However, Co(II)Cbl species bound to the active sites of EutT and the PduO-type ACAT from *Lactobacillus reuteri* (*Lr*PduO) are readily reduced by free dihydroflavins to generate Co(I)Cbl, (e.g. E°(NHE) = $-$228 mV for FMN at pH 7.5)[26, 27] or by reduced flavoproteins in the case of *Se*CobA (E°(NHE) = $-$440 mV for the semiquinone/reduced flavin couple of FldA, the purported physiological partner of *Se*CobA).[28, 29, 30] Extensive biochemical,[31, 32] crystallographic,[32, 33, 34, 35] and spectroscopic studies[36, 37, 38] of *Se*CobA and different PduO-type ACATs have revealed that a structurally unique four-coordinate (4c) Co(II)Cbl species is generated by these enzymes in the presence of ATP. The most recent X-ray crystal structures reported for *Se*CobA and *Lr*PduO complexed with Co(II)Cbl and MgATP have provided visual evidence that the DMB moiety that occupies the Coα position of Co(II)Cbl in solution is displaced by a non-coordinating phenylalanine residue (F112 in *Lr*PduO and F91 in *Se*CobA). Subsequent electron paramagnetic resonance (EPR) and magnetic circular dichroism (MCD) characterization of Co(II)Cbl in the presence of *Se*CobA and *Lr*PduO identified the roles specific amino acid residues play with regard to the formation of 4c Co(II)Cbl.[38, 39] These studies were facilitated by the fact that a sharp feature centered at ~12 000 cm^{-1} appears in the MCD spectra of Co(II)Cbl bound to *Se*CobA/MgATP and *Lr*PduO/MgATP, whose intensity correlates directly with the relative amount of 4c

Co(II)Cbl generated in these enzymes. The appearance of this feature was shown to reflect a sizable stabilization of the singly-occupied, redox-active Co $3d_{z^2}$-based molecular orbital in 4c Co(II)Cbl, which was predicted to lead to an increase in the Co(II)/Co(I) reduction potential by $\geqslant$250 mV.[24, 36, 40]

Spectroscopic evidence exists that also supports the formation of a 4c Co(II)Cbl species in the active site of EutT in the presence of MgATP.[41] However, in contrast to the *Se*CobA and PduO-type ACATs, EutT is unable to generate 4c Co(II)Cbi^+ and thus cannot adenosylate this Co(II)Cbl precursor. Because EutT has thus far eluded characterization by X-ray crystallography, the approach by which it binds its cob(II)alamin substrate and generates 4c Co(II)Cbl remains unknown. Initial biochemical characterization of EutT provided evidence that this enzyme requires a divalent transition metal cofactor for catalytic activity, in striking contrast to the other known families of ACATs.[2] The activity of EutT was found to be highest in the presence of Fe(II) ions under anaerobic conditions, followed by Zn(II) and Co(II) ions, with only the latter two also supporting catalytic activity in the presence of oxygen.[27] Inspection of the primary sequence of EutT led to the proposal that that $HX_{11}CCX_2C$(83) motif may be involved in divalent metal ion binding, as similar motifs are found in *B. subtilis* CbiX, a 4Fe/4S-containing enzyme, as well as some Zn-finger proteins. Elemental analyses of wild-type EutT ($EutT^{WT}$) and variants with a single alanine substitution at either the H67, C79, C80, or C83 position confirmed that $EutT^{WT}$ incorporates Fe(II) and Zn(II) ions in a ~2:1 complex-to-metal ratio, with the $EutT^{C80A}$ and $EutT^{C83A}$ variants exhibiting a dramatically reduced metal ion affinity. Futhermore, the level of metal incorporation into $EutT^{WT}$ and the

alanine variants was found to correlate directly with enzymatic activity.[41]

To obtain further insight into the roles played by the divalent metal cofactor of EutT with respect to the formation of 4c Co(II)Cbl, we have employed MCD and EPR spectroscopies to probe the interaction of Co(II)Cbl with $EutT^{WT}$ containing either Fe(II) [$EutT^{WT}$/Fe] or Zn(II) [$EutT^{WT}$/Zn] well as variants possessing a single alanine substitution at the H67, H75, C79, C80, or C83 position. These techniques offer a uniquely sensitive probe of changes in the coordination environment of the cobalt ion as Co(II)Cbl binds to the EutT active site. While MCD spectroscopy allows for the identification of ligand field (LF) and charge transfer (CT) transitions whose energies are substantially different for 4c and five-coordinate (5c) Co(II)Cbl, EPR spectroscopy provides a complementary probe of the 5c "base-on" (DMB bound) and "base-off" (water bound) fractions of Co(II)Cbl generated in the EutT active site. Collectively, these techniques have enabled us to determine how the relative populations of 4c and 5c Co(II)Cbl species generated in the $EutT^{WT}$ active site are affected by divalent metal ion incorporation and amino acid substitutions in the $HX_{11}CCX_2C(83)$ motif. We discuss the implications of our results with respect to the mechanism employed by EutT to generate AdoCbl.

4.3 Methods

Cofactors and Chemicals. The chloride salt of aquacobalamin ([H_2OCbl]Cl) and potassium formate (HCOOK) were purchased from Sigma and used as obtained. Co(II)Cbl was generated by addition of a small amount (~40 mL) of saturated HCOO-K solution to reduce a degassed sample (0.5 mL) of aqueous H_2OCbl^+ (~5 mM) in

a sealed vial. The progress of the reduction was monitored spectrophotometrically. The magnesium salt of ATP was used throughout all experiments.

Protein Preparation and Purification. EutT production and purification was performed as described elsewhere.[27] Briefly, EutT from *Salmonella enterica* sv. Typhimurium LT2 was overexpressed from a pTEV6 vector in *Escherichia coli* BL21, which generated a fusion protein with cleavable N-terminal hexahistidine (H_6) and maltose binding protein (MBP) tags. EutT variants were generated using the QuikChange II site-directed mutagenesis kit (Stratagene). All proteins were purified on a HisTrap nickel-affinity column (GE Healthcare). The H_6-MBP tag was cleaved using recombinant tobacco-etch protease (rTEV).[42] The tag was separated from the protein using a HisTrap nickel-affinity column and an amylose column (New England Biolabs).

To prepare samples of metallated EutT for spectroscopic studies, the protein was concentrated to a least 25 mg/mL (Amicon Ultra, 10,000 MWCO). EutT was placed into dialysis units (D-tube mini, Novagen) and moved into an anoxic chamber. The EutT solution was then dialyzed three times for 30 min against degassed buffer (1L, HEPES buffer (50 mM, pH 7) constaining NaCl (300 mM), TCEP (0.25 mM), EDTA (2 mM), and low (10 μM) or high (1 mM) concentrations of MgATP). To generate EutT/Fe, ApoEutT samples were dialyzed against chelex-treated buffer containing $FeSO_4$ (1 mM) and low or high MgATP (3×1L, 30 min each). Since recombinant EutT co-purifies with zinc,[27] EutT/Zn was instead prepared by dialysis against chelex-treated buffer devoid of EDTA, but containing low or high MgATP (3×1L, 30 min each). Metallated EutT samples were gently resuspended with 100% glycerol

to a final concentration of 10 mg/mL and 60% glycerol. Samples were stored in airtight serum vials (Wheaton) and flash-frozen in liquid nitrogen until use.

Sample Preparation. Purified EutT ~300-600 μM) in HEPES buffer (50 mM, pH 7) containing NaCl (300 mM) and TCEP (0.25 mM) was incubated with Co(II)Cbl under anoxic conditions. To generate EutT samples in the presence of excess Mg-ATP, ~10 μL of a concentrated MgATP solution were added to yield a final MgATP concentration of > 5 mM. Details of sample compostions are further described in Table A.4.1. Protein solutions were injected into the appropriate sample cells in an oxygen-free chamber. Following removal from the anoxic chamber, the samples were frozen and stored in liquid nitrogen. For the MCD samples, room temperature absorption (Abs) spectra were collected under an N_2 atmosphere before they were frozen. No changes in the Abs spectrum of Co(II)Cbl due to oxidation or sample degradation were observed after freezing the samples.

Spectroscopy. MCD and low-temperature Abs spectra were collected on a Jasco J-715 spectropolarimeter in conjunction with an Oxford Instruments SM-4000 8T magnetocryostat. All MCD spectra presented herein were obtained by taking the difference between spectra collected with the magnetic field oriented parallel and antiparallel to the light propagation axis to remove contributions from the natural CD and glass strain. X-band EPR spectra were obtained by using a Bruker ESP 300E spectrometer in conjunction with an Oxford ESR 900 continuous-flow liquid helium cryostat and an Oxford ITC4 temperature controller. The microwave frequency was measured with a Varian EIP model 625A CW frequency counter. All spectra were collected using a modulation amplitude of 10 G and a modulation frequency of 100

kHz. EPR spectral simulations were performed using Dr. Mark Nilges's SIMPOW program.[43]

4.4 Results

Effect of metal substitution on 4c Co(II)Cbl formation: To determine how the identity of the divalent metal ion cofactor affects the binding of Co(II)Cbl to EutT, we collected low-temperature Abs and MCD data of Co(II)Cbl in the absence and presence of enzyme and cosubstrate ATP. In the Abs spectrum of Co(II)Cbl obtained in the absence of EutT (Figure 5.2, C), an intense feature is observed at 21 000 cm^{-1} (the so-called α-band) that has previously been attributed to the lowest-energy corrin $\pi \rightarrow \pi^*$ transition on the basis its high intensity and TDDFT calculations.7,45 The prominent shoulder on the low energy side of the α-band was assigned to metal-to-ligand charge transfer (MLCT) transitions,[7, 44] while the intense, sharp feature peaking at 32 000 cm^{-1} was attributed to another corrin $\pi \rightarrow \pi^*$ transition. Upon the addition of wild-type EutT metallated with Fe(II) ions ($EutT^{WT}$/Fe) and substochiometric amounts (<10 μM) of MgATP to a solution of Co(II)Cbl, the intensity of this near-UV Abs band decreases by ~30% (Figure A.4.7), consistent with substrate Co(II)Cbl binding to the enzyme active site (vide infra). In the presence of $EutT^{WT}$/Fe and a ~10-fold molar excess of MgATP ($EutT^{WT}$/Fe + MgATP), a similar decrease in the intensity of this Abs feature is observed, along with a ~550 cm^{-1} blue-shift of the α-band (Figure 5.2, A). In previous studies of Co(II)Cbl in the presence of *Se*CobA or *Lr*PduO, a sizeable blue-shift of the α-band was shown to reflect the formation of a 4c Co(II)Cbl species in the enzyme active site.[36, 37] Intriguingly, the

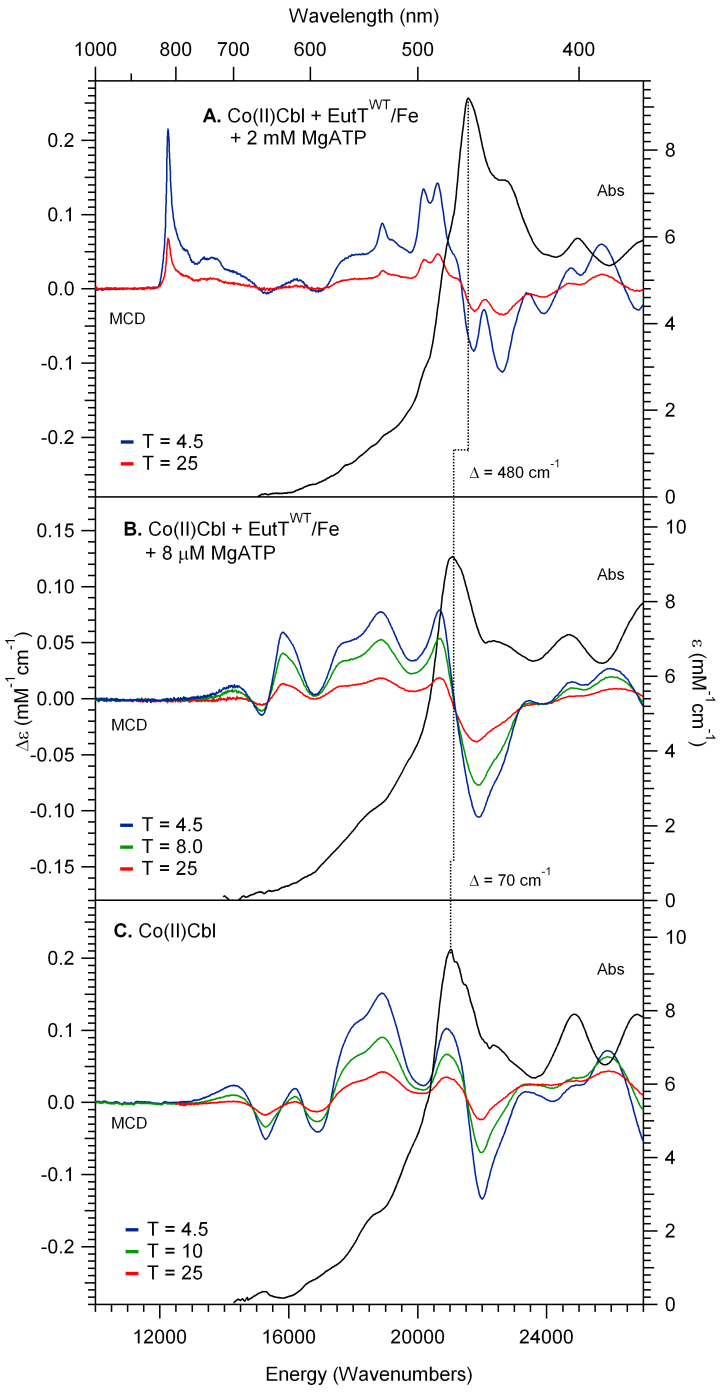

Figure 4.2: Abs spectra collected at 4.5 K (black traces) and 7 T VT-MCD spectra of (A) Co(II)Cbl in the presence of $EutT^{WT}$/Fe and a large molar excess (2 mM) of MgATP, (B) Co(II)Cbl in the presence of $EutT^{WT}$/Fe and substoichiometric (8 μL) MgATP, and (C) free Co(II)Cbl. In the Abs spectra, a dashed vertical line marks shifts in the position of the α-band.

shift of the α-band of Co(II)Cbl caused by the addition of EutT^{WT}/Fe + MgATP is ~150 cm^{-1} larger than that induced by the addition of *Se*CobA or *Lr*PduO and MgATP (Table 4.1).

Table 4.1: Positions of the δ-band (MCD) and the α-band (Abs) of 4c Co(II)Cbl Species Generated in the Active Site of EutT^{WT} and Several Variants. Shifts in the δ-band are shown relative to the position of this feature in the MCD spectrum of Co(II)Cbl in the presence of EutT^{WT}/Fe and excess MgATP. Also shown are the relative yields of 4c Co(II)Cbl species estimated from the δ-band intensities. Shifts in the α-band are shown relative to the position of this feature in the Abs spectrum of Co(II)Cbl in the absence of ACATs (λmax = 475 nm).

Metal Present	*Se*EutT Substitution	ν(δ) / cm^{-1}	Δν(δ) / cm^{-1}	ν(α) / cm^{-1}	Δν(α) / cm^{-1}	4c-Co(II)Cbl yield / %
A. Zn(II)	none (WT), >10x ATP	12 277	−22	21 645	615	> 95
B.	none (WT)	12 217	−38	21 552	522	81
C.	none (WT), no TCEP	12 225	−30	21 551	521	71
D. Fe(II)	none (WT)	12 255	0	21 575	545	> 95
E.	C79A	12 232	−23	21 505	475	46
F.	H75A	12 195	−60	21 164	134	26
G.	H67A	12 195	−60	21 030	0	12
H.	C80A	*n/a*	*n/a*	21 142	112	*n/d*
I.	C83A	*n/a*	*n/a*	21 053	23	*n/d*

The MCD spectrum of Co(II)Cbl in the absence of EutT is characterized by a series of derivative-shaped features that give rise to the appearance of four oppositely-signed bands centered at ~16 000 cm^{-1}, as well as additional, positively-signed bands around 19 000 cm^{-1} (Figure 5.2, C).[7] The two lowest-energy features in this spectrum have previously been assigned to LF transitions primarily involving electronic excitations from the doubly-occupied Co $3d_{xz}$- and $3d_{yz}$-based molecular

orbitals (MOs) to the singly occupied Co $3d_{z^2}$-based MO.[45] Additional features between 16 000 and 22 000 cm^{-1} have generally been attributed to metal-to-ligand charge transfer (MLCT) or additional LF transitions, with specific assignments made difficult by the presence of multiple transitions with similar energies in this region.

The MCD spectrum of Co(II)Cbl in the presence of $EutT^{WT}$/Fe exposed to oxygen is superimposable on that of Co(II)Cbl free in solution (Figure A.4.1, bottom). This observation suggests that Co(II)Cbl does not bind to $EutT^{WT}$/Fe under aerobic conditions, consistent with the minor spectroscopic changes observed in the corresponding Abs spectrum (Figure A.4.1, top). In contrast, the MCD spectrum of Co(II)Cbl in the presence of anaerobic $EutT^{WT}$/Fe and substoichiometric (~10 μM) MgATP exhibits unique features in the 14 000 – 22 000 cm^{-1} region (Figure 5.2, B). Most notably, the positive features at ~16 000 and ~21 000 cm^{-1} in the MCD spectrum of free Co(II)Cbl (Figure 5.2, C) red-shift by ~500 and ~400 cm^{-1}, respectively, in the presence of $EutT^{WT}$/Fe (Figure 5.2, B), which could potentially reflect the formation of base-off Co(II)Cbl (vide infra). The corresponding Abs spectrum reveals that the α-band does not actually red-shift in the presence of $EutT^{WT}$, suggesting that the MCD feature at 21 000 cm^{-1} arises from one of the many CT transitions of Co(II)Cbl whose energies are expected to be particularly sensitive to changes in the local environment of Co(II)Cbl. Further changes in the relative intensities and bandwidths of features that occur in this region of the MCD spectrum provide additional evidence that a significant fraction of Co(II)Cbl binds to the $EutT^{WT}$/Fe active site in the absence of co-substrate MgATP.

The low-energy region of the MCD spectrum of Co(II)Cbl in the presence of EutT^{WT}/Fe and a large (> 10-fold) molar excess of MgATP is characterized by an intense, positively-signed sharp feature at ~12 300 cm^{-1} (δ-band) and a broad band at ~13 600 cm^{-1} (β-band) (Figure 5.2, A). These features, which have previously been assigned to the electronic origin and a vibrational sideband of the Co $3d_{x^2-z^2} \rightarrow 3d_{z^2}$ LF transition, are characteristic of 4c Co(II)rrinoids generated in the active sites of ACATs via elimination of any axial ligand interactions.[36, 38, 39, 40] The relative MCD intensities of the δ-band associated with 4c Co(II)Cbl and features originating from 5c Co(II)Cbl indicate that >90% of the Co(II)Cbl substrate was converted to a 4c species in this sample (Table 4.1, D). Consistent with this high 5c→4c conversion yield, additional spectroscopic features from 4c Co(II)Cbl are clearly observed at ~20 000 cm^{-1}, termed the λ- and σ-bands (Figure A.4.2), which are usually masked by more intense contributions from the remaining 5c Co(II)Cbl species. The high 5c→4c Co(II)Cbl conversion yield obtained by EutT^{WT}/Fe in the presence of excess MgATP largely exceeds the conversion yields reported for *Se*CobA and *Lr*PduO under similar conditions (~8% and 40% respectively).[38, 39]

The Abs and MCD spectra of Co(II)Cbl in the presence of EutT^{WT}/Fe and its metal-substituted EutT^{WT}/Zn derivative are nearly indistinguishable from each other under both minimal and excess MgATP conditions (Figure A.4.2), indicating that the Fe(II)- and Zn(II)-bound forms of EutT^{WT} possess very similar Co(II)Cbl binding sites. The 5c→4c Co(II)Cbl conversion yield in the presence of EutT^{WT}/Zn and a threefold excess of MgATP is ~81%, which is somewhat lower than that obtained with EutT^{WT}/Fe under similar conditions (Table 4.1, B). However in the

presence of ~5 mM MgATP (a >10-fold molar excess of MgATP over EutT), the 5c→4c Co(II)Cbl conversion of EutT^{WT}/Zn becomes analogous to that of EutT^{WT}/Fe (Table 4.1, A). Even though EutT^{WT}/Zn remains stable under aerobic conditions (in contrast to EutT^{WT}/Fe), a small (~10%) decrease in the 5c→4c Co(II)Cbl conversion yield is noted in the absence of TCEP, possibly due to partial oxidation of the Cys residues (Table 4.1, C). Because the identity of the divalent metal ion that is present in EutT^{WT} in vivo is currently unknown, these findings clearly warrant further spectroscopic studies of both EutT^{WT}/Fe and EutT^{WT}/Zn. Given that EutT^{WT} is active with Fe(II) and Zn(II), it is obvious that the divalent metal ion primarily plays a structural role. Circular dichroism (CD) studies of EutT in the absence and presence of divalent metal ions did not reveal any significant conformational differences between the two enzyme forms, suggesting that the metal binding site encompasses a relatively small portion of the protein fold.[27]

Effect of co-substrate MgATP concentration on the 5c→4c Co(II)Cbl conversion yield: Because the single unpaired electron of Co(II)Cbl resides in the Co $3d_{z^2}$-based MO, electron paramagnetic resonance (EPR) spectroscopy provides an extremely sensitive probe of perturbations to the axial ligand of Co(II)Cbl by the protein environment. At low MgATP concentration (~10 μM), a broad positive feature around 2620 G can be clearly discerned in the EPR spectrum of Co(II)Cbl in the presence of EutT^{WT}/Fe (Figure 5.3, B). This feature is notably absent in the EPR spectrum of base-on Co(II)Cbl (Figure 5.3, A), which lacks any visible features below 2800 G; rather, it is characteristic of a base-off species in which the DMB ligand has been replaced by a solvent-derived water molecule (Figure 5.3,

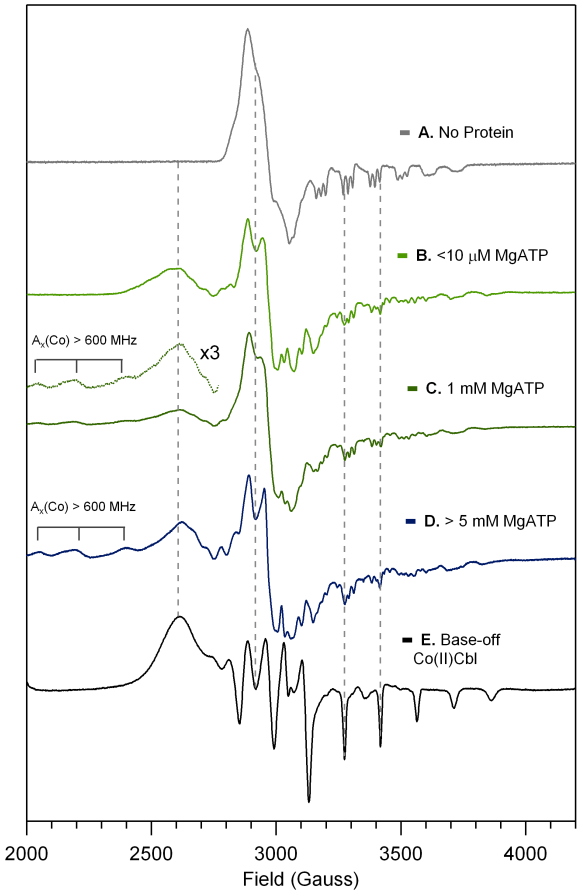

Figure 4.3: Experimental X-band EPR spectra collected at 20 K of (A) free Co(II)Cbl, (B) Co(II)Cbl in the presence of EutT^{WT}/Fe and minimal (< 10 μM) MgATP, and (C) Co(II)Cbl in the presence of EutT^{WT}/Fe with 3-fold molar excess of MgATP and (D) a >10-fold excess of MgATP. The spectrum of Co(II)Cbi^{+} (E), a base-off Co(II)Cbl analogue is shown for comparison. EPR spectra were collected using a 9.36 GHz microwave source, 2 mW microwave power, 5 G modulation amplitude, 100 kHz modulation frequency and a 328 ms time constant. Features from base-off Co(II)Cbl are highlighted with vertical dashed lines. Features from 4c Co(II)Cbl species at low magnetic fields are noted.

E). The presence of partially resolved hyperfine structure on the 2620 G feature suggests that the enzyme active site imposes conformational constraints on the Co(II)Cbl substrate even in the absence of MgATP. While both base-off and base-on Co(II)Cbl contribute to the region of the EPR spectrum above 2800 G, the presence

of an intense derivative-shaped feature centered at 2950 G and peak splittings near ~3350 G due to ^{14}N (I=1) superhyperfine coupling are a clear indication of DMB coordination to the Co(II) ion. From the relative intensities of these features, we estimate that ~60% of the Co(II)Cbl substrate is present in the base-off conformation, while the remaining ~40% is in the base-on conformation. The presence of sharp features in the 3000 G region of the EPR spectrum suggests that the DMB moiety of base-on Co(II)Cbl is conformationally constrained and thus bound to the active site $EutT^{WT}$/Fe, as these features are absent in the EPR spectrum of free Co(II)Cbl and cannot be attributed to the presence of base-off Co(II)Cbl (vide infra). Upon the addition of at least a threefold molar excess (~1 mM) of MgATP, a series of weak, derivative-shaped features appear in the 1900 to 2450 G region of the EPR spectrum of Co(II)Cbl in the presence of $EutT^{WT}$/Fe (Figure 5.3, C). These broad features are characteristic of square planar, low-spin Co(II) species, consistent with the formation of 4c Co(II)Cbl in the active site of $EutT^{WT}$/Fe, as observed previously for other ACATs.[36, 37, 46] In the presence of a >10-fold molar excess of MgATP, the features from 4c Co(II)Cbl gain intensity at the expense of those associated with 5c base-on and base-off Co(II)Cbl, indicating an increase in the 5c→4c Co(II)Cbl conversion yield (Figure 5.3, D). Thus, excess MgATP appears to facilitate the formation of 4c Co(II)Cbl by promoting DMB dissociation to generate 5c base-off Co(II)Cbl and/or by stabilizing the 4c Co(II)Cbl species formed in the active site. While additional features below 1900 G should be observed in the EPR spectrum of 4c Co(II)Cbl in the presence of $EutT^{WT}$/Fe, these features are masked by intense signals from a ferric minority species in the sample (characteristic derivatives-shaped feature at

Table 4.2: Spin-Hamiltonian parameters for Co(II)Cbl in the absence and presence of EutT^{WT}/Zn(II) and MgATP. Parameters for 4c Co(II)rrinoids generated by *Se*CobA and *Lr*PduO from references 36 and 37 are shown for comparison (G and H). *n/a*, not applicable.

A. Co(II)Cbl	base-on	100	2.004	2.232	2.269	303	30	40	49
B. Co(II)Cbl / EutT^{WT}(Zn) / minimal MgATP									
	base-on	38	2.004	2.232	2.269	303	30	40	49
	base-off	62	1.991	2.315	2.459	387	222	227	*n/a*
C. Co(II)Cbl / EutT^{WT}(Zn) / 0.5-fold MgATP									
	base-off	100	1.991	2.315	2.459	387	222	227	*n/a*
D. Co(II)Cbl / EutT^{WT}(Zn) / equimolar MgATP									
	base-off	100	1.993	2.313	2.459	389	217	224	*n/a*
E. Co(II)Cbl / EutT^{WT}(Zn) / > 10-fold excess MgATP									
	base-on	19	2.004	2.232	2.269	303	30	40	49
	base-off	23	1.991	2.315	2.459	387	222	227	*n/a*
	4c	58	1.800	2.553	3.610	760	625	1362	*n/a*
F. Co(II)Cbi^{+}	base-off	*n/a*	2.060	2.670	2.730	805	590	635	*n/a*
G. Co(II)Cbl / *Lr*CobA+ATP	4c	*n/a*	1.900	2.700	2.720	770	755	595	*n/a*
H. Co(II)Cbi^{+} / *Se*CobA+ATP	4c	*n/a*	2.060	2.670	2.730	805	590	635	*n/a*

~1600 G, Figure A.4.3).

As in the case of EutT^{WT}/Fe, the EPR spectrum of Co(II)Cbl in the presence of EutT^{WT}/Zn and substoiochiometric (~10 μM) MgATP exhibits features consistent with the presence of both base-on and base-off Co(II)Cbl (Figures 5.4 and 5.6, B). Although this spectrum is qualitatively similar to that obtained in the presence of EutT^{WT}/Fe under similar conditions (Figure A.4.3), it is better resolved and

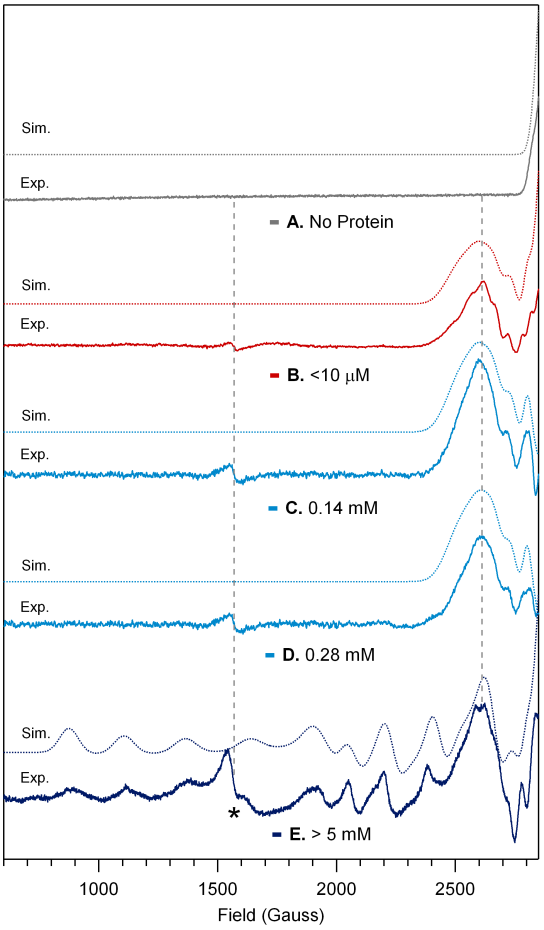

Figure 4.4: Low-field region of X-band EPR spectra collected at 20 K of (A) free Co(II)Cbl, (B) Co(II)Cbl in the presence of EutT^{WT}/Zn and < 10 μM MgATP, and (C) Co(II)Cbl in the presence of EutT^{WT}/Zn and a substoichiometric amount of MgATP, (D) a equimolar amount of MgATP, and (E) a tenfold molar excess of MgATP. The prominent feature from base-off Co(II)Cbl is highlighted by a vertical line, and the feature arising from ferric impurities is marked by an asterisk. EPR spectra were collected using a 9.36 GHz microwave source, 2 mW microwave power, 5 G modulation amplitude, 100 kHz modulation frequency and a 328 ms time constant. Spectra were simulated using the parameters provided in Table 4.2.

thus provides more compelling evidence for the presence of a unique base-off Co(II)Cbl species and of perturbed base-on Co(II)Cbl. Intriguingly, in the presence of EutT^{WT}/Zn and half molar to equimolar amounts of MgATP, the EPR spectra

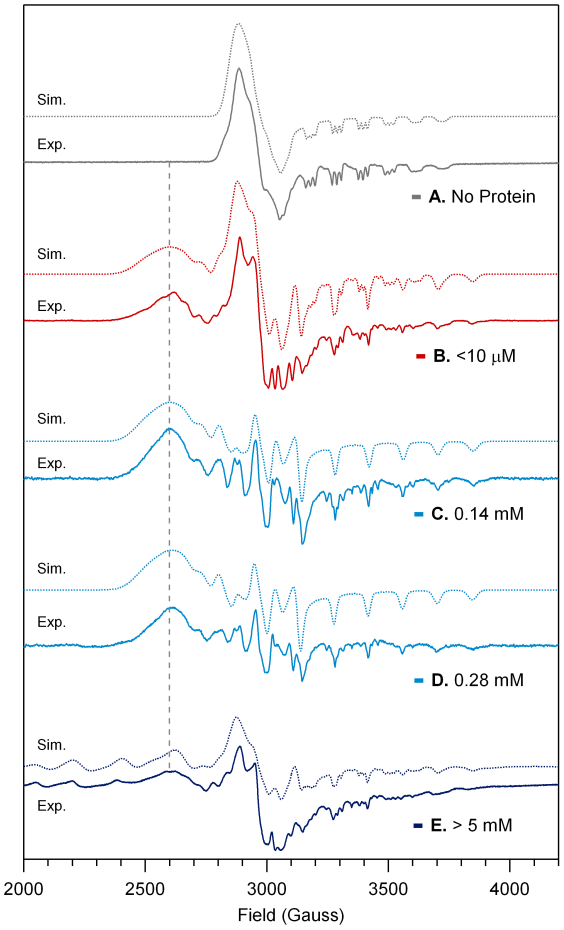

Figure 4.5: High-field region of X-band EPR spectra collected at 20 K of (A) free Co(II)Cbl, (B) Co(II)Cbl in the presence of $EutT^{WT}$/Zn and < 10 μM MgATP, and (C) in the presence of $EutT^{WT}$/Zn a substoichiometric amount of MgATP, (D) a equimolar amount of MgATP, and (E) a tenfold molar excess of MgATP. The prominent feature from base-off Co(II)Cbl is highlighted by a vertical line. See Figure 5.4 caption for instrument settings. Spectra were simulated using the parameters provided in Table 4.2.

lack any features from base-on Co(II)Cbl (Figures 5.4 and 5.6, C and D). These spectra are, however, very similar to those obtained for $Co(II)Cbi^{+}$ free in solution (Figure 5.3, E), indicating that under these conditions the Co(II)Cbl substrate is bound to $EutT^{WT}$/Zn in a base-off conformation. Note that no spectroscopic

features from base-on or 4c Co(II)Cbl are discernible in these spectra. A fit of these spectra yields spin-Hamiltonian parameters essentially identical to those obtained for free Co(II)Cbi$^+$ (Table 4.2), with the exception of a 15âĽ“20 MHz smaller A_z(Co) hyperfine coupling parameter.

Since this parameter correlates with the covalency of the Co–O(H_2) bond (i.e. it decreases as covalency increases), this observation indicates that the water molecule coordinated to the base-off Co(II)Cbl species in EutT^{WT}/Zn forms a more covalent bond with the Co(II) ion than does the axially bound water molecule in Co(II)Cbi$^+$. This finding suggests that the Co–O(H_2) bond is slightly compressed in the EutT^{WT}/Zn active site, thus implying that the α-face of the corrin ring does not become completely exposed to solvent upon DMB dissociation. In the presence of a tenfold molar excess of MgATP, the EPR spectrum of Co(II)Cbl with EutT^{WT}/Zn exhibits sharp features between 800 and 1900 G (Figures 5.4 and 5.6, E). These features are identical to those displayed by 4c Co(II)Cbl bound to EutT^{WT}/Fe + MgATP, though the absence of Fe(III) in our EutT^{WT}/Zn samples allows for the observation of additional peaks at lower fields. A fit of this spectrum yields g-shifts and A(Co) hyperfine splitting parameters that are significantly larger than those reported for the 4c Co(II)rrinoids generated in the active site of the other ACATs (Table 4.2, E). The increased rhombicity of the g-tensor (resulting in $g_x > g_y > g_z$) is noteworthy, as the magnitudes of the g-shifts are very sensitive to the conformation of 4c Co(II)rrinoids. Particularly intriguing are the very large values obtained for g_x and A_x(Co) (3.61 and 1362 MHz, respectively). These values suggest that the conformation of the 4c Co(II)Cbl species in EutT is substantially different from that

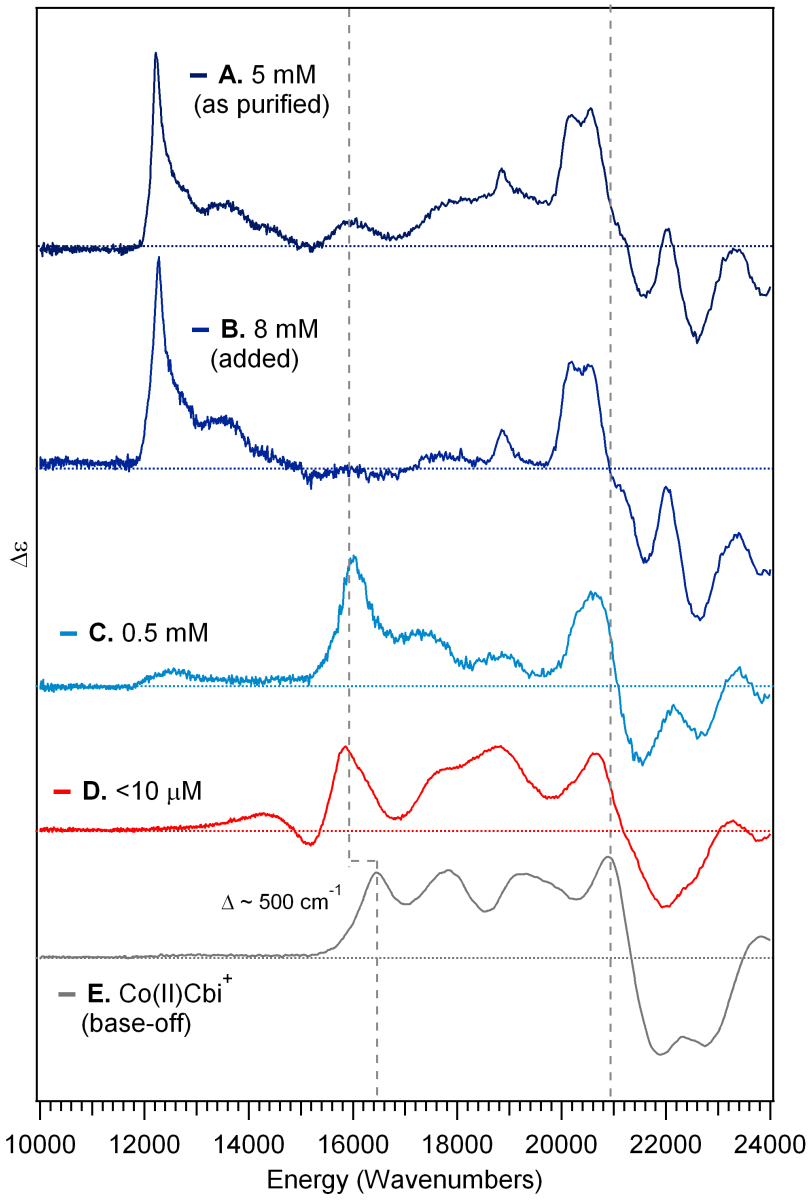

Figure 4.6: MCD spectra of Co(II)Cbl obtained in the presence of $EutT^{WT}$/Zn and various MgATP concentrations. (A) ~10 mM MgATP (~10-fold molar excess), (C) equimolar amounts of MgATP and EutT, and (D) substoichiometric (< 10 μM) MgATP. Trace (B) was obtained after the addition of MgATP to the sample used in (C) to increase the concentration to > 5 mM (»10-fold excess). The MCD spectrum of $Co(II)Cbi^{+}$ (E), a base-off Co(II)Cbl analogue, is shown for comparison. Primary spectroscopic features of this species are highlighted by dashed vertical lines.

adopted in the other ACATs.[33, 34]

Based on the findings summarized above, the MCD spectrum of Co(II)Cbl in the presence of EutT^{WT}/Zn and an approximately equimolar amount of MgATP is dominated by a base-off Co(II)Cbl species that is generated in the enzyme active site (Figure 5.7, C). Intriguingly, this spectrum is not superimposable on that of Co(II)Cbi^{+}, as the features near 16 000 and 21 000 cm^{-1} are red-shifted by ~500 and ~300 cm^{-1}, respectively, in the spectrum of the enzyme-bound base-off Co(II)Cbl species (Figure 5.7, E). These shifts are very similar to those observed for Co(II)Cbl in the presence of EutT^{WT}/Zn and substoichiometric MgATP (Figure 5.7, D). Based on our EPR results, these changes can be attributed to the formation of a slightly perturbed base-off Co(II)Cbl species in the active site of EutT^{WT}/Zn. Addition of a tenfold molar excess of MgATP to a sample of Co(II)Cbl in the presence of EutT^{WT}/Zn and equimolar MgATP leads to the appearance of an MCD spectrum that is dominated by contributions from a 4c Co(II)Cbl species (Figure 5.7, B) and indistinguishable from that obtained with EutT^{WT}/Zn purified in the presence of a large (~10-fold) molar excess MgATP (Figure 5.7, A). This observation suggests that the base-off Co(II)Cbl generated in EutT^{WT} is a possible intermediate in the formation of 4c Co(II)Cbl. This unique base-off Co(II)Cbl species is present in the active site of EutT^{WT}/Zn even under low MgATP conditions (i.e. >30-fold Co(II)Cbl:MgATP molar excess), indicating that MgATP does not have to be present in the active site before the enzyme can bind Co(II)Cbl and displace its DMB moiety. This is in stark contrast to the ordered binding scheme observed for *Se*CobA and *Lr*PduO, where ATP must bind first for the enzyme to adopt a conformation suitable

for binding of Co(II)rrinoids.[3, 33, 34]

Effect of amino acid substitutions on 4c Co(II)Cbl formation: The activity of EutT^{WT} and selected variants has previously been shown to correlate with the degree of Fe(II) or Zn(II) incorporation into the enzyme. The C79, C80, C83, and H67 residues that are part of the conserved $HX_{11}CCX_2C(83)$ motif of EutT^{WT} were found to be particularly important for the binding of divalent transition metal ions, as variants containing alanine substitutions at these positions displayed significantly lower metallation levels than the wild-type enzyme.[27] Because the three-dimensional structure of EutT^{WT} has yet to be determined, the nature of the divalent metal ion binding site and the mechanism by which metal incorporation into the $HX_{11}CCX_2C(83)$ motif modulates the catalytic activity of EutT^{WT} are currently unknown. In order to address this issue, we studied the effects of alanine substitutions within this motif on the binding of Co(II)Cbl to EutT/Fe and the yield of 4c Co(II)Cbl species.

The MCD spectra of Co(II)Cbl in the presence of EutT/Fe variants possessing a single alanine substitution at either the H67, H75, C79, C80, or C83 position are show in Figure 4.7. While the spectra of Co(II)Cbl in the presence of EutT^{C80A}/Fe and EutT^{C83A}/Fe only contain features from 5c Co(II)Cbl, those obtained with EutT^{C79A}/Fe, EutT^{H67A}/Fe, and EutT^{H75A}/Fe additionally contain contributions from 4c Co(II)Cbl. However, as judged on the basis of the relative intensities of the MCD features associated with the 4c fraction of Co(II)Cbl, the 5c$\rightarrow$4c Co(II)Cbl conversion yields achieved by these latter variants are lower than that observed for EutT^{WT}/Fe. Overall, the 5c$\rightarrow$4c Co(II)Cbl conversion yields correlate well with

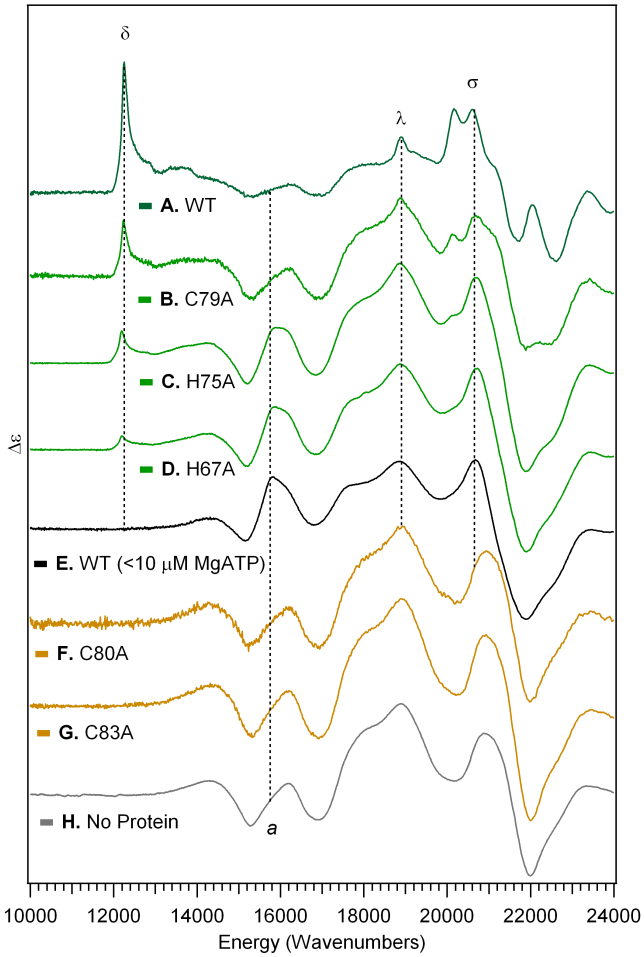

Figure 4.7: MCD spectra of Co(II)Cbl obtained in the presence of EutT^{WT}/Fe and selected variants (with > 5 mM MgATP unless otherwise noted). The primary spectroscopic features due to 4c Co(II)Cbl species in the presence of EutT^{WT}/Fe (A) are highlighted by dashed vertical lines. Additional spectroscopic changes in reference to Co(II)Cbl in the absence of protein (H) are also highlighted.

the degree of Fe(II) incorporation into these variants as determined previously by elemental analysis, which revealed that EutT^{C80A} and EutT^{C83A} bind negligible amounts of Fe(II), while EutT^{C79A} and EutT^{H67A} incorporate ~50% less Fe(II) than the wild-type enzyme. It was unclear from these data alone if the alanine substitu-

tions of residues within the $HX_{11}CCX_2C(83)$ motif cause a decrease in the 5c→4c Co(II)Cbl conversion yield by suppressing Co(II)Cbl binding to the enzyme active site or by impeding the removal of the DMB moiety from the Co(II) ion. Based on our spectroscopic data, it is likely that these two effects are correlated (vide supra).

The MCD spectra of Co(II)Cbl in the presence of $EutT^{C80A}$/Fe and $EutT^{C83A}$/Fe are virtually superimposable on that of free Co(II)Cbl (Figure 4.7), lacking any features attributable to base-off Co(II)Cbl. This observation indicates that both the $EutT^{C80A}$/Fe and the $EutT^{C83A}$/Fe variants do not bind Co(II)Cbl. In contrast, the MCD spectrum of Co(II)Cbl in the presence of $EutT^{C79A}$/Fe contains qualitatively similar, though considerably smaller contributions from 4c Co(II)Cbl as the spectrum obtained with $EutT^{WT}$/Fe. Despite the modest fraction of 4c Co(II)Cbl generated by this variant (about 50% of $EutT^{WT}$/Fe), the characteristic features from 4c Co(II)Cbl can be readily distinguished from those associated with 5c Co(II)Cbl species. Removal of the 4c Co(II)Cbl contributions to this MCD spectrum (via subtraction of the properly scaled spectrum of 4c Co(II)Cbl in the presence of $EutT^{WT}$/Fe) results in a spectrum that is essentially superimposable on that of free Co(II)Cbl (Figure A.4.8), indicating that the remaining Co(II)Cbl fraction is not bound to the enzyme. Thus, the 50% decrease in the 5c→4c Co(II)Cbl conversion yield in response to the C79A substitution likely stems from the ~50% decrease in Fe(II) incorporation, as the Fe(II)-bound fraction of the protein appears capable of generating a similar 4c Co(II)Cbl species as $EutT^{WT}$/Fe. These findings indicate that C79 is not critical for maintaining the structure of the active site to the same degree as the C80 and C83 residues, in particular with regards to the binding

of Co(II)Cbl and the removal of the DMB moiety. In support of this conclusion, EutT^{C79A}/Fe has been found to be nearly as active as EutT^{WT}/Fe. It is therefore not surprising that residue C79 is not conserved amongst the known EutT ACATs.

A detailed analysis of the MCD spectra of Co(II)Cbl in the presence of EutT^{H67A}/Fe and EutT^{H75A}/Fe (Figure A.4.9 and A.4.10) reveals that these variants produce a significant fraction of base-off Co(II)Cbl, which is responsible for the features at ~16 000 and ~20 600 cm^{-1}. Moreover, the presence of base-off Co(II)Cbl in these variants is discernible in by the apparent red-shift of the features observed at ~16 000 cm^{-1} (Figure 4.7, see a). The absence of a feature at 21 000 cm^{-1} shows that no base-on Co(II)Cbl remains unbound in solution, while the low intensity of the δ band at ~12 000 cm^{-1} indicates that only a small fraction of 4c Co(II)Cbl is formed in the active sites of these variants. EPR data obtained for samples prepared under the same conditions confirm the presence of base-off and 4c Co(II)Cbl species, but also contain sizeable contributions from base-on Co(II)Cbl (Figure A.4.4). Because these spectra are very similar to that obtained with EutT^{WT}/Fe (except for differences in relative intensities due to variations in the different Co(II)Cbl populations) and the corresponding MCD spectra indicate that all species are enzyme-bound, we conclude that the Co(II)Cbl binding motif of the enzyme is not disrupted by the H75A and H67A substitutions. However, since these substitutions cause an increase in the relative populations of enzyme-bound base-off and base-on Co(II)Cbl species at the expense of the 4c Co(II)Cbl fraction, residues H75 and H67 appear to play a role in the process of 4c Co(II)Cbl formation by promoting axial ligand dissociation from 5c Co(II)Cbl either directly or indirectly by enhancing the degree of Fe(II) and

Zn(II) incorporation into EutT.

4.5 Discussion

The EutT^{WT} active site promotes DMB dissociation to generate base-off Co(II)Cbl: As show in this study, the combined use of MCD and EPR spectroscopies is well suited to characterize the base-off, base-on, and 4c Co(II)Cbl species generated in the EutT^{WT} active site and to determine their relative populations. Our EPR data indicate that in the presence of EutT^{WT} and substoichiometric MgATP, as much as 60% of Co(II)Cbl is present in the base-off conformation. Nevertheless, it has recently been shown that EutT^{WT} is unable to bind Co(II)Cbi^{+}, a naturally occurring base-off Co(II)Cbl analogue, and small but significant differences are observed between the MCD spectra of free Co(II)Cbi^{+} and the EutT-bound base-off Co(II)Cbl species.[41] These findings suggest that specific interactions between certain amino acid residues and the nucleotide loop are required to produce base-off Co(II)Cbl in the enzyme active site. These interactions could introduce changes to the conformation of the corrin ring, especially in the region of C(17) that serves as the anchor of the nucleotide loop (Figure 5.1), as well as alter the environment around the H_2O ligand in base-off Co(II)Cbl, both of which could contribute to the small MCD and EPR spectral differences that exist between free and enzyme-bound base-off Co(II)Cbl. A more constrained conformation of the corrin ring of the base-off Co(II)Cbl species generated in the EutT^{WT} active site would also explain the observation of resolved hyperfine structure in the g_x region of the corresponding EPR spectrum (Figure 5.4). Similarly, the slight differences between the MCD and

EPR spectra of the base-on Co(II)Cbl species bound to EutT^{WT} and free Co(II)Cbl could arise from enzyme-induced structural perturbations to the corrin ring prior to DMB dissociation. A constrained corrin ring conformation may be a critical prerequisite for the removal of the DMB ligand from the Co(II) ion, as otherwise the Co(II)Cbl substrate could simply reorient in response to external forces acting on the nucleotide loop.

Nature of the 4c Co(II)Cbl species generated in the EutT active site: The 4c Co(II)Cbl species generated in the active sites of other ACATs such as *Lr*PduO and *Se*CobA exhibit large (~600 to ~800 MHz) cobalt hyperfine coupling parameters, A(Co), consistent with a high degree of localization of the unpaired spin density on the Co(II) ion in the absence of axial ligands. The unusually large g-shifts from the free-electron value of 2.0023 displayed by these species ($g_x \approx g_y \gg g_z \sim 2.0$) have been shown to reflect an increase in the extent of spin-orbit mixing between the ground state and LF excited states due to a large stabilization of the Co $3d_{z^2}$-based MO in this conformation.[36, 37] To this end, it is interesting to note that the 4c Co(II)Cbl species generated in the active site of EutT^{WT} displays a rhombic g-tensor ($g_x > g_y > g_z$) with the largest g_x, g_z, and A(Co) values observed for any Co(II)rrinoid characterized to date (Table 4.2). While these results provide compelling evidence that the 4c Co(II)Cbl species generated in the EutT^{WT} active site adopts a unique conformation, it is difficult to interpret the corresponding g- and A-values in terms of specific perturbations to the 4c Co(II)Cbl structure because a proper description of the electronic structure of this species requires the use of wavefunction-based multireference techniques and a non-perturbative approach for the calculation

of spin-orbit coupling effects.[40] The available crystal structures for *Lr*PduO and *Se*CobA in the presence of Co(II)Cbl and MgATP show that the corrin ring of the 4c Co(II)Cbl species generated in these enzymes adopts a planar conformation in which the corrin nitrogen atoms have become nearly symmetry-equivalent.[33, 34] A computational analysis of 4c Co(II)Cbl indicated that in this species the unpaired spin density is localized in an MO that also has sizable contributions from orbitals other than the Co $3d_{z^2}$ orbital. In the case of 4c Co(II)Cbl generated in the EutT^{WT} active site, the large difference between the g_x and g_y values indicates that the Co $3d_{xz}$ - and Co $3d_{yz}$-based MOs have substantially different energies, consistent with a non-planar conformation of the corrin ring. A perturbed conformation of the corrin ring in the 4c Co(II)Cbl species generated by EutT^{WT} could also explain the largely red-shifted α-band observed in the Abs spectrum of this species, as the corrin π^*-based HOMO that serves as the donor orbital for this transition contains small contributions from the Co $3d_{xz}$ and Co $3d_{yz}$ orbitals.[36]

Another intriguing difference between the 4c Co(II)Cbl species formed in the EutT^{WT} active site and those observed in the presence of other ACATs is the large difference in intensity of the δ-band at ~12 000 cm^{-1} in the corresponding MCD spectra (Figure 5.2, A). Even in the presence of a >50-fold molar excess of MgATP, conditions under which complete conversion to 4c Co(II)Cbl should occur, the MCD intensity of the δ-band remains less than 0.22 mM^{-1} cm^{-1} for all EutT samples studied (Table 4.1). For the 4c Co(II)Cbl species formed in the active sites of *Se*CobA and *Lr*PduO, the intensity of this feature was previously estimated to be 0.505 mM^{-1} cm^{-1} (by accounting for the relative populations of 4c and 5c Co(II)Cbl). The lower

MCD intensity of the δ-band in the spectrum of 4c Co(II)Cbl generated in the active site of EutT species remains puzzling,[41] but likely reflects the uniquely perturbed conformation of the 4c Co(II)Cbl substrate bound to this enzyme.

Comparison of the Co(II)→Co(I)Cbl conversion mechanisms of ACATs: In all ACATs studied to date, the redox tuning of the Co(II)Cbl substrate required for the formation of the essential Co(I)Cbl intermediate is achieved by inducing a complete dissociation of the axially bound DMB ligand to generate a square planar 4c Co(II)rrinoid species that can be readily reduced by intracellular reducing agents.[26] In the case of *Lr*PduO, the side chains of residues F112, F187, and V186 were found to form a hydrophobic "wall" upon binding of Co(II)Cbl and MgATP, serving to block solvent access to the Coα face of the corrin ring, and a salt bridge interaction between D35 and R128 near the corrin ring binding site was found to be critical for promoting the dissociation of the DMB moiety.[35, 38] A similar overall mechanism was proposed for *Se*CobA, where residues F91 and W93 were found to be important for generating 4c Co(II)rrinoids and for properly positioning the Co(I) intermediate that is subsequently formed during turnover.[33, 39] However, the differences in the specific architectures of these active sites have an effect on the relative populations of 4c Co(II)rrinoids that are being formed. While *Se*CobA and *Lr*PduO achieve very similar relative yields of 4c Co(II)Cbi$^+$ species (~50%), *Lr*PduO is able to generate ~40% of 4c Co(II)Cbl while for *Se*CobA this yield is decreased to ~8%.[36, 37, 39] The higher 5c→4c conversion yields for Co(II)Cbi$^+$ compared to Co(II)Cbl have generally been attributed to the weaker axial bond in Co(II)Cbi$^+$ and the fact that a higher level of coordination among different active site residues

is required to remove the DMB moiety from the Co(II) ion of Co(II)Cbl.[38] From this perspective, it is rather unusual that EutT^{WT} can only adenoslylate Co(II)Cbl, and not Co(II)Cbi^{+}. Although previous studies revealed that Co(II)Cbi^{+} does bind to the EutT^{WT} active site, albeit weakly, the axially bound water ligand is retained in this process.[41]

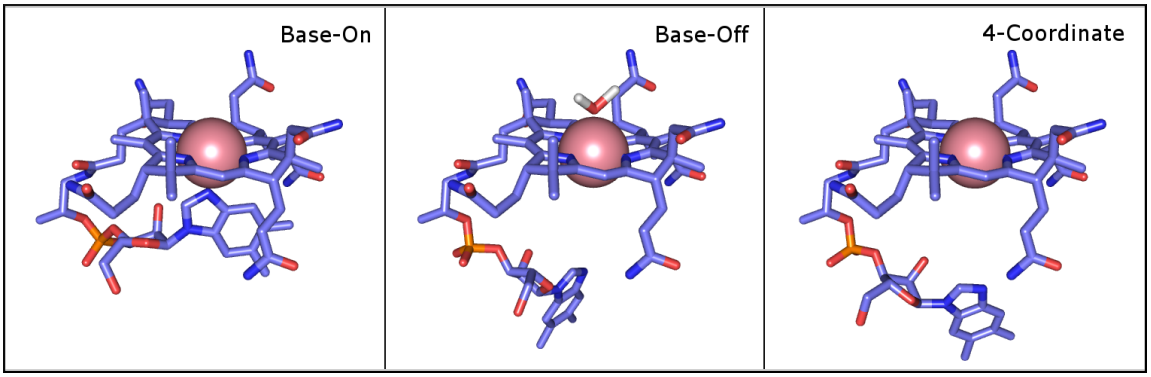

Figure 4.8: Proposed structures of the Co(II)Cbl species formed in the presence of EutT. Note that the base-on and base-off Co(II)Cbl species remain 5-coordinate (5c), and differ primarily in the nature of the axial ligand and the orientation of the nucleotide loop. While the water ligand in the case of base-off Co(II)Cbl can occupy either axial position, only the case where it occupies the Coβ position (as favored by our data) is shown. In the case of 4c Co(II)Cbl, specific interactions with protein residues that are required to exclude any axial ligands are not shown.

The results obtained in the present study indicate that binding of Co(II)Cbl to the EutT^{WT} active site and the formation of a large population of a 5c base-off species occur even in the absence of MgATP. However, 4c Co(II)Cbl is generated only in the presence of an excess of co-susbtrate MgATP, with higher concentrations promoting higher yields. These observations suggest a mechanism for EutT^{WT} in which the active site forms a unique base-off Co(II)Cbl species prior to MgATP incorporation that serves as a precursor to 4c Co(II)Cbl. As removal of the H_2O ligand is more facile than removal of the DMB moiety, the presence of a base-

off species would facilitate the formation of 4c Co(II)Cbl and would explain the high 5c→4c yield observed for EutT^{WT} (>95 % for EutT^{WT}/Fe + MgATP). In this proposed mechanism, specific residues in the enzyme active site serve to constrain the corrin ring in place, giving rise to the unique spectroscopic features observed experimentally, with additional protein motifs sequestering the DMB moiety away from the Co(II) ion. In the case of Co(II)Cbi$^+$, the absence of the nucleotide loop and terminal DMB moiety prevent the active site from adopting the proper conformation needed for the formation of a 4c Co(II)Cbi$^+$ species in response to MgATP binding near the Coβ face of the corrin ring. Given that Co(II)Cbi$^+$ has been found to bind to EutT much less tightly than Co(II)Cbl, it is plausible that the former can respond to MgATP binding to the active site simply by repositioning itself without loss of the axial ligand. In the case of enzyme-bound 5c base-off Co(II)Cbl, MgATP binding to the active site in a position suitable to react with the subsequently formed Co(I)Cbl intermediate could trigger the dissociation of an axially bound water molecule on the Coβ face of the corrin ring, thereby permitting the enzyme to control the timing of Co(I)Cbl formation and suppress the likelihood of undesired side-reactions by this "supernucleophile". While the specific amino acid residues used to stabilize enzyme-bound 5c base-off and 4c Co(II)Cbl species remain unknown in the absence of a crystal structure of EutT, it is tempting to speculate that the divalent metal site and $HX_{11}CCX_2C$(83) motifs are involved in the removal of the DMB moiety, and thus are important for 4c Co(II)Cbl formation. Studies of Co(II)-substituted EutT, aimed at elucidating the structure of this metal site and evaluating its role in the catalytic cycle of EutT, will be presented in the following chapter.

4.6 References

[1] David E Sheppard, Joseph T Penrod, Thomas Bobik, John R Roth, and Eric Kofoid. Evidence that a B12-Adenosyl Transferase Is Encoded within the Ethanolamine Operon of Salmonella enterica. *Journal of bacteriology*, 186(22):7635 – 7644, 2004.

[2] Nicole R Buan, Sang-jin Suh, and Jorge C Escalante-semerena. The eutT Gene of Salmonella enterica Encodes an Oxygen-Labile, Metal-Containing ATP:Corrinoid Adenosyltransferase Enzyme. *Journal of Bacteriology*, 186(17):5708–5714, 2004.

[3] Paola E. Mera and Jorge C. Escalante-Semerena. Multiple roles of ATP:cob(I)alamin adenosyltransferases in the conversion of B12 to coenzyme B12. *Applied Microbiology and Biotechnology*, 88(1):41–48, 2010.

[4] Troy A Stich, Amanda J Brooks, Nicole R Buan, and Thomas C Brunold. Spectroscopic and computational studies of Co3+-corrinoids: spectral and electronic properties of the B12 cofactors and biologically relevant precursors. *Journal of the American Chemical Society*, 125(19):5897–914, may 2003.

[5] Karen S Conrad and Thomas C Brunold. Spectroscopic and computational studies of glutathionylcobalamin: nature of Co-S bonding and comparison to Co-C bonding in coenzyme B12. *Inorganic chemistry*, 50(18):8755–66, sep 2011.

[6] Ivan G Pallares and Thomas C Brunold. Spectral and electronic properties of nitrosylcobalamin. *Inorganic chemistry*, 53(14):7676–91, jul 2014.

[7] Troy a. Stich, Nicole R. Buan, and Thomas C. Brunold. Spectroscopic and computational studies of Co2+corrinoids: Spectral and electronic properties of the biologically relevant base-on and base-off forms of Co2+cobalamin. *Journal of the American Chemical Society*, 126(31):9735–9749, 2004.

[8] K. Mori, R. Bando, N. Hieda, and T. Toraya. Identification of a Reactivating Factor for Adenosylcobalamin-Dependent Ethanolamine Ammonia Lyase. *Journal of Bacteriology*, 186(20):6845–6854, oct 2004.

[9] Ruma Banerjee and Stephen W. Ragsdale. The many faces of vitamin B12: catalysis by cobalamin-dependent enzymes. *Annual review of biochemistry*, 72:209–247, nov 2003.

[10] Todd O Yeates, Christopher S Crowley, and Shiho Tanaka. Bacterial microcompartment organelles: protein shell structure and evolution. *Annual review of biophysics*, 39:185–205, 2010.

[11] C. Chowdhury, S. Sinha, S. Chun, T. O. Yeates, and T. a. Bobik. Diverse Bacterial Microcompartment Organelles. *Microbiology and Molecular Biology Reviews*, 78(3):438–468, 2014.

[12] Cheryl a Kerfeld, Sabine Heinhorst, and Gordon C Cannon. Bacterial microcompartments. *Annual review of microbiology*, 64:391–408, 2010.

[13] Edith M. Sampson and Thomas a. Bobik. Microcompartments for B12-dependent 1,2-propanediol degradation provide protection from DNA and

cellular damage by a reactive metabolic intermediate. *Journal of Bacteriology*, 190(8):2966–2971, 2008.

[14] P. Thiennimitr, S. E. Winter, M. G. Winter, M. N. Xavier, V. Tolstikov, D. L. Huseby, T. Sterzenbach, R. M. Tsolis, J. R. Roth, and a. J. Baumler. Intestinal inflammation allows Salmonella to use ethanolamine to compete with the microbiota. *Proceedings of the National Academy of Sciences*, 108(42):17480–17485, 2011.

[15] Danielle a Garsin. Ethanolamine utilization in bacterial pathogens: roles and regulation. *Nature reviews. Microbiology*, 8(4):290–295, 2010.

[16] Naoki Shibata, Hiroko Tamagaki, Naoki Hieda, Keita Akita, Hirofumi Komori, Yasuhito Shomura, Shin-Ichi Ichi Terawaki, Koichi Mori, Noritake Yasuoka, Yoshiki Higuchi, and Tetsuo Toraya. Crystal structures of ethanolamine ammonia-lyase complexed with coenzyme B12 analogs and substrates. *The Journal of biological chemistry*, 285(34):26484–93, aug 2010.

[17] Nicole R. Buan and Jorge C. Escalante-Semerena. Purification and initial biochemical characterization of ATP:Cob(I)alamin adenosyltransferase (EutT) enzyme of Salmonella enterica. *Journal of Biological Chemistry*, 281(25):16971–16977, 2006.

[18] Olga Tsoy, Dmitry Ravcheev, and Arcady Mushegian. Comparative genomics of ethanolamine utilization. *Journal of Bacteriology*, 191(23):7157–7164, 2009.

[19] Martin J Warren, Evelyne Raux, Heidi L Schubert, and Jorge C Escalante-Semerena. The biosynthesis of adenosylcobalamin (vitamin B12). *Natural product reports*, 19(4):390–412, aug 2002.

[20] J. C. Escalante-Semerena, S. J. Suh, and J. R. Roth. cobA Function is required for both de novo cobalamin biosynthesis and assimilation of exogenous corrinoids in Salmonella typhimurium. *Journal of Bacteriology*, 172(1):273–280, 1990.

[21] Ana Jorge-Finnigan, Cristina Aguado, Rocio Sánchez-Alcudia, David Abia, Eva Richard, Begoña Merinero, Alejandra Gámez, Ruma Banerjee, Lourdes R Desviat, Magdalena Ugarte, and Belen Pérez. Functional and structural analysis of five mutations identified in methylmalonic aciduria cblB type. *Human mutation*, 31(9):1033–42, sep 2010.

[22] Dominique Padovani, Tetyana Labunska, Bruce A Palfey, David P Ballou, and Ruma Banerjee. Adenosyltransferase tailors and delivers coenzyme B12. *Nature chemical biology*, 4(3):194–6, mar 2008.

[23] M V Fonseca and J C Escalante-Semerena. Reduction of Cob(III)alamin to Cob(II)alamin in Salmonella enterica serovar typhimurium LT2. *Journal of bacteriology*, 182(15):4304–9, aug 2000.

[24] Mathew D Liptak and Thomas C Brunold. Spectroscopic and computational studies of Co1+cobalamin: spectral and electronic properties of the "superreduced" B12 cofactor. *Journal of the American Chemical Society*, 128(28):9144–56, jul 2006.

[25] Dominique Faure, Doris Lexa, and Jean-Michel Savéant. Electrochemistry of vitamin B12. *Journal of Electroanalytical Chemistry and Interfacial Electrochemistry*, 140(2):297–309, 1982.

[26] Paola E. Mera and Jorge C. Escalante-Semerena. Dihydroflavin-driven adenosylation of 4-coordinate Co(II) corrinoids: Are cobalamin reductases enzymes or electron transfer proteins? *Journal of Biological Chemistry*, 285(5):2911–2917, jan 2010.

[27] T. C. Moore, P. E. Mera, and J. C. Escalante-Semerena. The EutT Enzyme of Salmonella enterica Is a Unique ATP:Cob(I)alamin Adenosyltransferase Metalloprotein That Requires Ferrous Ions for Maximal Activity. *Journal of Bacteriology*, 196(4):903–910, 2014.

[28] Nicole R. Buan and Jorge C. Escalante-Semerena. Computer-assisted docking of flavodoxin with the ATP:Co(I)rrinoid adenosyltransferase (CobA) enzyme reveals residues critical for protein-protein interactions but not for catalysis. *Journal of Biological Chemistry*, 280(49):40948–40956, 2005.

[29] Vincent Massey Stephen G. Mayhe, Gordon P. Foust. Oxidation-Reduction Properties of Flavodoxin from Peptostreptococcus elsdenii. *Journal of Biological Chemistry*, (4), 1969.

[30] David M. Hoover, Joseph T. Jarrett, Richard H. Sands, William R. Dunham, Martha L. Ludwig, and Rowena G. Matthews. Interaction of Escherichia coli cobalamin-dependent methionine synthase and its physiological partner

flavodoxin: Binding of flavodoxin leads to axial ligand dissociation from the cobalamin cofactor. *Biochemistry*, 36(1):127–138, 1997.

[31] Paola E. Mera, M. St Maurice, Ivan Rayment, and Jorge C. Escalante-Semerena. Structural and functional analyses of the human-type corrinoid adenosyltransferase (PduO) from Lactobacillus reuteri. *Biochemistry*, 46(48):13829–13836, 2007.

[32] Maris V. Fonseca, Nicole R. Buan, Alexander R. Horswill, Ivan Rayment, and Jorge C. Escalante-Semerena. The ATP:Co(I)rrinoid adenosyltransferase (CobA) enzyme of Salmonella enterica requires the 2âŁ²-OH group of ATP for function and yields inorganic triphosphate as its reaction byproduct. *Journal of Biological Chemistry*, 277(36):33127–33131, 2002.

[33] Theodore C. Moore, Sean a. Newmister, Ivan Rayment, and Jorge C. Escalante-Semerena. Structural insights into the mechanism of four-coordinate cob(II)alamin formation in the active site of the salmonella enterica ATP:Co(I)rrinoid adenosyltransferase enzyme: Critical role of residues Phe91 and Trp93. *Biochemistry*, 51(48):9647–9657, 2012.

[34] Martin St Maurice, Paola Mera, Kiyoung Park, Thomas C. Brunold, Jorge C. Escalante-Semerena, and Ivan Rayment. Structural characterization of a human-type corrinoid adenosyltransferase confirms that coenzyme B12 is synthesized through a four-coordinate intermediate. *Biochemistry*, 47(21):5755–5766, may 2008.

[35] Paola E Mera, Martin St Maurice, Ivan Rayment, and Jorge C Escalante-Semerena. Residue Phe112 of the human-type corrinoid adenosyltransferase (PduO) enzyme of Lactobacillus reuteri is critical to the formation of the four-coordinate Co(II) corrinoid substrate and to the activity of the enzyme. *Biochemistry*, 48(14):3138–45, apr 2009.

[36] Troy A. Stich, Nicole R. Buan, Jorge C. Escalante-Semerena, and Thomas C. Brunold. Spectroscopic and computational studies of the ATP:corrinoid adenosyltransferase (CobA) from Salmonella enterica: Insights into the mechanism of adenosylcobalamin biosynthesis. *Journal of the American Chemical Society*, 127(24):8710–8719, 2005.

[37] Kiyoung Park, Paola E. Mera, Jorge C. Escalante-Semerena, and Thomas C. Brunold. Kinetic and spectroscopic studies of the ATP:corrinoid adenosyltransferase PduO from Lactobacillus reuteri: Substrate specificity and insights into the mechanism of Co(II)corrinoid reduction. *Biochemistry*, 47(34):9007–9015, 2008.

[38] Kiyoung Park, Paola E Mera, Jorge C Escalante-semerena, and Thomas C Brunold. Spectroscopic Characterization of Active-Site Variants of the PduO-type ATP : Corrinoid Adenosyltransferase from Lactobacillus reuteri : Insights into the Mechanism of Four-Coordinate Co (II) corrinoid Formation. (Ii), 2011.

[39] Ivan G Pallares, Theodore C Moore, Jorge C Escalante-semerena, and Thomas C Brunold. Spectroscopic Studies of the Salmonella enterica Adenosyltransferase

Enzyme Se CobA: Molecular-Level Insight into the Mechanism of Substrate Cob(II)alamin Activation. *Biochemistry*, 53:7969–7982, 2014.

[40] Matthew D. Liptak, Angela S. Fleischhacker, Rowena G. Matthews, Joshua Telser, and Thomas C. Brunold. Spectroscopic and computational characterization of the base-off forms of cob(II)alamin. *Journal of Physical Chemistry B*, 113(15):5245–5254, 2009.

[41] Kiyoung Park, Paola E. Mera, Theodore C. Moore, Jorge C. Escalante-Semerena, and Thomas C. Brunold. Unprecedented Mechanism Employed by the Salmonella enterica EutT ATP:Co ^I rrinoid Adenosyltransferase Precludes Adenosylation of Incomplete Co ^{II} rrinoids. *Angewandte Chemie International Edition*, pages n/a–n/a, 2015.

[42] Paul G. Blommel and Brian G. Fox. A combined approach to improving large-scale production of tobacco etch virus protease. *Protein Expression and Purification*, 55(1):53–68, 2007.

[43] Mark J. Nilges. *No Title*. PhD thesis, University of Illinois, Urbana-Champaign, IL, 1979.

[44] Pratt. *Inorganic Chemistry of Vitamin B-12*.

[45] Amanda J. Brooks, Monica Vlasie, Ruma Banerjee, and Thomas C. Brunold. Co-C bond activation in methylmalonyl-CoA mutase by stabilization of the post-homolysis product Co2+cobalamin. *Journal of the American Chemical Society*, 127(47):16522–16528, nov 2005.

[46] Troy A Stich, Mamoru Yamanishi, Ruma Banerjee, and Thomas C Brunold. Spectroscopic evidence for the formation of a four-coordinate Co2+ cobalamin species upon binding to the human ATP:cobalamin adenosyltransferase. *Journal of the American Chemical Society*, 127(21):7660–7661, 2005.

Chapter 5

Evidence for the requirement of a tetrahedrally coordinated divalent metal cofactor with cysteine ligation by the *Salmonella enterica* EutT adenosyltransferase.

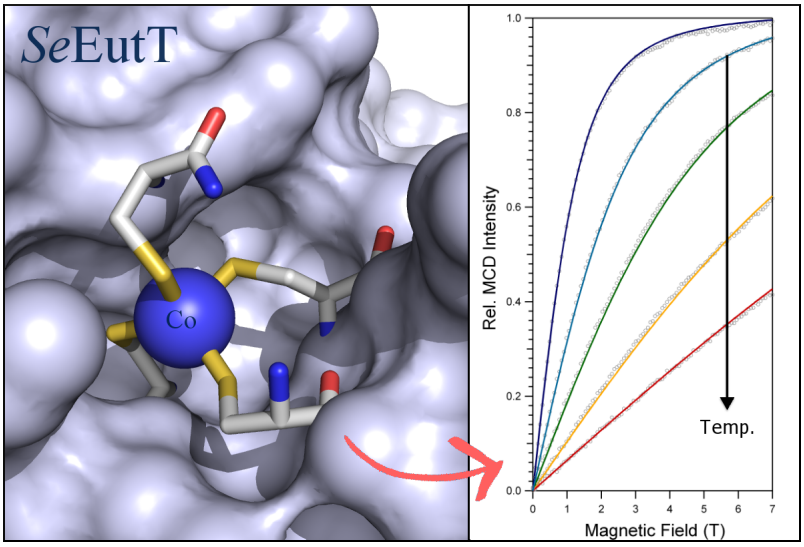

This work is under preparation as: I. G. Pallares, T. C. Moore, J. C. Escalante-Semerena, and T. C. Brunold "Evidence for the requirement of a tetrahedrally coordinated divalent metal cofactor with cysteine ligation by the *Salmonella enterica* EutT adenosyltransferase."

5.1 Summary

The EutT enzyme from *Salmonella enterica*, a member of a family of ATP:Co(I)rrinoid adenosyltransferase (ACAT) enzymes, requires a divalent transition metal ion for catalysis with Fe(II) yielding the highest activity. EutT also contains a unique cysteine-rich $HX_{11}CCX_2C(83)$ motif not found in other ACATs, and employs an unprecedented mechanism for the formation of adenosylcobalamin (AdoCbl). Recent kinetic and spectroscopic studies of this enzyme revealed that residues in the $HX_{11}CCX_2C(83)$ motif are required for the tight binding of a divalent metal ion and are critical for the formation of a four-coordinate (4c) Co(II)Cbl intermediate in the catalytic cycle. However, the nature of the divalent metal binding site of EutT remains ill-defined, and it has yet to be shown if residues in the $HX_{11}CCX_2C(83)$ motif directly serve as ligands. To address these questions, we have characterized a EutT derivative in which Co(II) was substituted for the native metal ion by using electronic absorption, electron paramagnetic resonance, and magnetic circular dichroism (MCD) spectroscopies. Our results indicate that the reduced catalytic activity of Co(II)-substituted EutTWT ($EutT^{WT}$/Co) relative to the native Fe(II)-containing enzyme arises from the incomplete incorporation of Co(II) ions and, thus, a decrease in the 4c Co(II)Cbl yield. Our MCD data of $EutT^{WT}$/Co reveal further that the Co(II) ions reside in a distorted tetrahedral coordination environment with direct cysteine sulfur ligation. Additional spectroscopic studies of EutT/Co variants possessing a single alanine substitutions at either the His67, His75, Cys79, Cys80, or Cys83 position indicate that Cys80 coordinates to the Co(II) ion, while the

additional residues are important for maintaining the structural integrity and/or high affinity of the metal binding site. The role of this unique metal binding motif in the adenosylation of Co(I)Cbl is discussed.

5.2 Introduction

ATP:Co(I)rrinoid adenosyltransferase (ACAT) enzymes serve a critical role in the biosynthesis of adenosylcobalamin (AdoCbl, also known as coenzyme B_{12}).[1, 2] While notably absent in higher eukaryotes such as plants and fungi, these enzymes are found in several domains of life where they catalyze the transfer of the adenosyl (Ado) moiety of an ATP molecule to a Co(I)rrinoid "supernucleophile" transiently generated in their active sites.[3] ACATs are thus responsible for maintaining the supply of AdoCbl required during metabolism, using corrinoid precursors salvaged from external sources (such as vitamin B_{12}) or, in the case of certain bacteria, synthesized de novo. To date, three evolutionary unrelated families of ACATs have been identified and classified according to their in vivo roles in *Salmonella enterica* sv Typhimuriurm LT2 as CobA, PduO, and EutT.[4, 5, 6] For CobA[7, 8, 9] and PduO, the latter of which is homologous to the human ACAT,[10, 11, 12, 13] extensive spectroscopic, kinetic, and structural studies have provided insights into how these enzymes accomplish the thermodynamically challenging reduction of the Co(II)rrinoid substrate that precedes the adenosylation step. Initial spectroscopic evidence indicated ACATs generate an essentially square-planar four-coordinate (4c) species via the removal of the axial ligand from the Co(II)rrinoid substrate, which has been estimated to increase the reduction midpoint potential of the Co(II)/Co(I)rrinoid

couple by as much as $\geqslant$250 mV.[10, 14] X-ray crystal structures of CobA from *Salmonella enterica* (*Se*CobA) and PduO from *Lactobacillus reuteri* (*Lr*PduO) complexed with Co(II)Cbl and MgATP confirmed the formation of a 4c Co(II)Cbl intermediate and revealed that a phenylalanine residue, which is part of a "wall" of hydrophobic of residues, occupies the position where the dimethylbenzimidazole (DMB) ligand of Co(II)Cbl is present in the free cofactor. Though electron density due to the DMB was not observed in these crystal structures, the intermolecular loop that connects this moiety to the corrin ring was found to be oriented away from the active site.[11, 15] Spectroscopic characterization of enzyme variants revealed that the driving force for the displacement of the DMB ligand is provided by the formation of favorable interactions among active site residues when 4c Co(II)Cbl is generated.[16, 17] Although in the case of EutT structural information is not currently available, the primary sequence of this class of enzymes contains a partially conserved $HX_{11}CCX_2C(83)$ motif that has no counterpart in the other known ACAT families. Spectroscopic and kinetic characterization of EutT variants with a single alanine substitution within this motif indicated that these residues are critical for the uptake of divalent metal ions [M(II)] and the formation of 4c Co(II)Cbl.[18, 19] For example, $EutT^{C80A}$ was found to be unable to convert Co(II)Cbl to AdoCbl both in vivo and in vitro, which has been shown in a subsequent spectroscopic study to reflect the inability of Co(II)Cbl to bind to the active site of this variant. Similarly, $EutT^{C83A}$ and $EutT^{H67A}$ displayed no in vivo activity, though low in vitro activity was observed. Alternatively, the $EutT^{C79A}$ variant retained most of the activity displayed by the wild-type enzyme. While $EutT^{C79A}$ and $EutT^{H67A}$ bind Zn(II) and Fe(II), albeit at lower levels

relative to EutT^{WT}, both EutT^{C80A} and EutTC83A only incorporate trace amounts of Zn(II) and fail to bind Fe(II).[19] Thus, the $HX_{11}CCX_2C(83)$ motif the clearly plays a significant role in modulating the activity of EutT; however, it remains unknown how residues in this motif interact with the Co(II)Cbl and ATP substrates, or how they assist in the binding of divalent transition metal ions. Molecular oxygen and bathophenantroline inhibit the formation of AdoCbl by EutT, suggesting that an Fe(II) cofactor is required for enzyme activity.[4] The similarity of the $X_{11}CCX_2C(83)$ primary sequence motif of EutT to that of the 4Fe/4S cluster motif found in the CbiX cobaltochelatase from *B. subtillis* initially led to the proposal that EutT is capable of cobalamin reductase activity.[4] However, a recent study of EutT reconstituted with Fe(II) (EutT/Fe) by magnetic circular dichroism (MCD) spectroscopy indicated the lack of features in the 10,000 to 35,000 cm^{-1} energy window where contributions from 4Fe/4S clusters and related species are usually found.[18, 20, 21] Further evidence against the presence of an 4Fe/4S cluster in EutT is provided by the fact that the Zn(II)-bound enzyme is equally active as EutT/Fe. While Fe(II)- and Zn(II)-containing enzymes are difficult to characterize spectroscopically, information about the ligand environment of the native metal ion can often be obtained by conducting spectroscopic studies of their Co(II)-substituted derivatives. The optical spectra of these Co(II) species are dominated by ligand field transitions that vary substantially as a function of coordination number and geometry.[22, 23, 24, 25, 26] For this reason and the fact that Co(II)-binding to the $X_{11}CCX_2C(83)$ motif of EutT has been shown to promote the binding of substrate Co(II)Cbl as well as its conversion to the catalytically relevant 4c species, we have characterized EutT reconstituted

with Co(II) (EutT/Co) in the absence and presence of Co(II)Cbl substrate by using MCD and EPR spectroscopies. By collecting variable-temperature variable-field MCD data of substrate-free EutT/Co, significant new insight has been obtained into the nature of the divalent metal ion binding site of EutT. To determine which specific residues in the $X_{11}CCX_2C(83)$ motif might serve as ligands to the Co(II) ion, we have also characterized EutT/Co variants with a single alanine substitution at either the His67 (H67), His75(H75), Cys79 (C79), Cys80 (C80), or Cys83 (C83) position. The results obtained in this study provide significant new insight into the unique mechanism employed by EutT to generate 4c Co(II)Cbl species.

5.3 Methods

Cofactors and Chemicals. Aquacobalamin ([H_2OCbl]Cl) and potassium formate (HCOOK) were obtained from Sigma and used as is. Co(II)Cbl was generated anoxically by the addition of a ~30 μL of saturated HCOOK solution to a degassed sample (500 μL) of aqueous H_2OCbl^+ (5 mM) in a sealed vial. Formation of Co(II)-Cbl was monitored spectrophotometrically by monitoring the absorbance at 474 nm, and the reaction was deemed complete when spectroscopic features from H_2OCbl^+ were no longer visible. The magnesium salt of ATP was used throughout all experiments.

Protein Preparation and Purification. EutT was obtained and purified as described elsewhere.[19] Briefly, the eutT gene of *Salmonella enterica* sv. Typhimurium LT2 was overexpressed from a pTEV6 vector in *Escherichia coli* BL21, which generated a fusion protein with cleavable N-terminal hexahistidine (H_6) and maltose

binding protein (MBP) tags. EutT variants were generated using the QuikChange II site-directed mutagenesis kit (Stratagene). All proteins were purified on a His-Trap nickel-affinity column (GE Healthcare). The H_6-MBP tag was cleaved using recombinant tobacco-etch protease (rTEV).[27] The tag was removed from the protein solution using a HisTrap nickel-affinity column and an amylose column (New England Biolabs). EutT to be remetallated for spectroscopic samples was prepared freshly. The protein was concentrated to a least 25 mg/mL (Amicon Ultra, 10,000 MW cut off), placed into dialysis units (D-tube mini, Novagen), and moved into an anoxic chamber. ApoEutT was then prepared by repeated (three times 30 minutes) dialysis against degassed buffer (50 mM HEPES, pH 7, 300 mM NaCl, 0.25 mM TCEP) containing EDTA (2 mM) and low (10 μM) or high (1 mM) concentrations of MgATP. Next, apoEutT was remetallated with Co(II) via dialysis (three times 30 minutes) against chelex-treated buffer with 1 mM $CoCl_2$ salt and either 10 μM or 1 mM MgATP, as appropriate. The EutT/Co samples were mixed with 100% glycerol to a final concentration of ~10 mg/mL in 60% (v/v) glycerol. Samples were stored in airtight serum vials (Wheaton) and flash-frozen in liquid nitrogen until use.

Sample Preparation. For samples containing Co(II)Cbl, purified ~300 to ~600 μM EutT/Co in 50 mM Hepes buffer (pH 7), 300 mM NaCl, 0.25 mM TCEP was complexed with Co(II)Cbl under anoxic conditions. The samples were injected into the appropriate sample holders (MCD cells or quartz EPR tubes) in an oxygen-free glovebox. After removing from the glovebox, room temperature Abs spectra of samples in MCD cells were collected under an N_2 atmosphere and all samples were then frozen and stored in liquid nitrogen.

Spectroscopy. Low-temperature Abs and MCD spectra were collected on a Jasco J-715 spectropolarimeter in conjunction with an Oxford Instruments SM-4000 8T magnetocryostat. All reported MCD spectra were obtained by taking the difference between spectra collected with the magnetic field oriented parallel and antiparallel to the light propagation axis to remove contributions from the natural CD and glass strain. To remove temperature-independent contributions to the MCD spectra, δMCD spectra are reported. These were obtained by subtraction of a corresponding MCD spectrum obtained at 25 K. VTVH-MCD data was obtained at three different wavelengths corresponding to the most intense features in the MCD spectrum of EutT/Co. The resulting saturation curves were fit using the software developed by Dr. Frank Neese.[28] X-band EPR spectra were obtained by using a Bruker ESP 300E spectrometer in conjunction with an Oxford ESR 900 continuous-flow liquid helium cryostat and an Oxford ITC4 temperature controller. The microwave frequency was measured with a Varian EIP model 625A CW frequency counter. All spectra were collected using a modulation amplitude of 10 G and a modulation frequency of 100 kHz. EPR spectral simulations were performed using Dr. Mark Nilges's SIMPOW6 program.[29]

5.4 Results

Wild-type EutT/Co enzyme: Previous studies of EutT have focused on the Zn(II)- and Fe(II)-bound forms of the enzyme (EutT/Zn and EutT/Fe respectively). Wild-type EutT/Fe ($EutT^{WT}$/Fe) was deemed to be the most physiologically relevant species, as under anoxic conditions the specific activity of this enzyme was twice

as large as that of EutT^{WT}/Zn.[19] However, besides a small difference in their relative populations, the four-coordinate (4c) Co(II)Cbl species generated in the active sites of EutT^{WT}/Zn and EutT^{WT}/Fe in the presence of excess MgATP are spectroscopically indistinguishable, suggesting that Zn(II) substitution does not affect the Co(II)/Co(I)Cbl reduction step.[18] The MCD spectrum of Co(II)Cbl in the presence of EutT^{WT}/Co and excess MgATP is similar to, but not identical with, that obtained with EutT^{WT}/Fe. In the former spectrum (Figure 5.1, A), a sharp positive peak is observed at 12 200 cm^{-1} along with additional features at 19 000 and 20 400 cm^{-1} that are not present in the MCD spectrum of free Co(II)Cbl (Figure 5.1, B). These features, which have previously been labeled as the δ- λ- and σ-bands respectively, are characteristic of 4c Co(II)Cbl.[17] However, several additional weak MCD features are observed on the high-energy side of δ-band that have no counterparts in the MCD spectra of other 4c Co(II)rrinoid species. These features are attributed to the high spin Co(II) center that is present in EutT/Co (vide infra).

While the spectroscopic signatures of the 4c Co(II)Cbl species generated in the EutT/Co active site indicate that this species is present in a very similar conformation as that formed in EutT/Fe, a decrease in the relative intensity of the δ-band is observed for EutT^{WT}/Co that can be attributed to a ~44% lower 5c→4c Co(II)Cbl conversion yield in the Co(II)-bound form of the enzyme. Consistent with this hypothesis, the remaining spectroscopic features in the 14 000 to 21 000 cm^{-1}, which arise from the fraction of base-on Co(II)Cbl free in solution, are more intense in the presence of EutT/Co than EutT^{WT}/Fe (Figure A.5.1). These findings indicate that a significant fraction of Co(II)Cbl does not bind to EutT/Co, suggesting that the

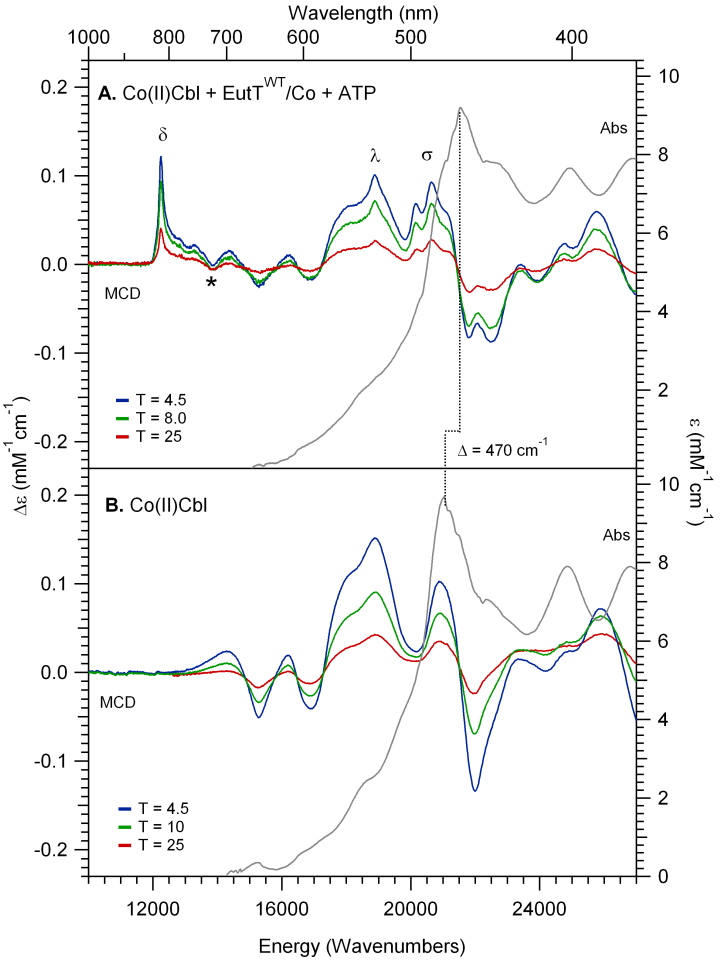

Figure 5.1: LT-Abs spectra collected at 4.5K (gray traces) and 7 T VT-MCD spectra of (A) Co(II)Cbl in the presence of EutT^{WT}/Co(II) and ATP and (B) free Co(II)Cbl. MCD features arising from 4c Co(II)Cbl are labeled with greek letters. The feature in the MCD spectrum at ~14 000 cm^{-1} due to the presence of Co(II) bound to EutT is noted by an asterisk.

substitution of Co(II) for Fe(II) leads to a decreased Co(II)Cbl binding affinity of EutT. As the degree of metal incorporation has previously been shown to correlate with the relative population of Co(II)Cbl bound to EutT/Fe,[18] it is reasonable to assume that the larger fraction of unbound Co(II)Cbl in the presence of EutT/Co stems from incomplete Co(II) incorporation.

While the MCD spectrum of Co(II)Cbl in the presence of EutT^{WT}/Co and excess MgATP appears to lack any contributions from base-off Co(II)Cbl, features associated with this species are difficult to discern because they are readily obscured by contributions from base-on Co(II)Cbl. Therefore, we used EPR spectroscopy as complementary probe of the axial ligand environment of the different Co(II)Cbl species that are present in samples of EutT^{WT}/Co and excess MgATP. The EPR spectrum of Co(II)Cbl in the presence of EutT/Co and <10 μM MgATP concentration is dominated by features from base-on Co(II)Cbl species (Figure A.5.3, A), though the weak positive feature observed at 2 600 G is characteristic of base-off Co(II)Cbl. The low intensity of this feature is consistent with ~21% of the cofactor being present in this conformation. In the presence of threefold molar excess of MgATP (Figure A.5.3, B), EPR features associated with base-off Co(II)Cbl display a significant increase in relative intensity (indicating that the relative population of this species has increased to ~50%). While contributions from 4c Co(II)Cbl are not readily discernible, weak features centered at 2 000 G are consistent with the presence of such a species. Due to the broad nature of the features from 4c Co(II)Cbl, the relative population of this species would have to exceed 25% to produce detectable contributions to our EPR spectra. The remaining features in the EPR spectrum of Co(II)Cbl in the presence of EutT/Co and a 3-fold molar excess of MgATP arise from "base-on" Co(II)Cbl species. Although these features are very similar to those displayed by Co(II)Cbl free in solution, the sharpening of the features at 3 000 G is consistent with the presence an enzyme-bound base-on species, as the conformational freedom of Co(II)Cbl is expected to be reduced in the enzyme active site.

Notably, no features arising from dipolar interactions between the 3/2 spins of the Co(II) ion and the 1/2 spin of the bound base-off and 4c Co(II)Cbl species are observed.

In summary, our spectroscopic data indicate that EutT^{WT}/Co interacts with Co(II)Cbl in a similar manner as the native EutT^{WT}/Fe enzyme, though the yield of Co(II)Cbl bound to the active site is lower. This difference most likely arises from non-stoichiometric Co(II) incorporation into EutT^{WT}, since the presence of a divalent metal cofactor appears to be critical for Co(II)Cbl binding to EutT. Although the relative binding affinity of EutT for Co(II) is unknown, a comparison of the observed 5c→4c Co(II)Cbl conversion yields of EutT^{WT} complexed with Co(II), Zn(II), and Fe(II) suggests that Co(II) occupies only ~56% of the active sites (vide supra). This estimate is consistent with the results obtained in a previous biochemical characterization of EutT^{WT}/Co, which revealed that the specific activity of this form of the enzyme is ~60% of that displayed by EutT^{WT}/Fe.

Nature of the M(II) binding site in EutT^{WT}: As noted above, a subset of weak features in the MCD spectrum of Co(II)Cbl in the presence of EutT/Co and excess MgATP are unlikely to arise from any Co(II)Cbl species. Consistent with this hypothesis, these same features dominate the MCD spectrum of EutT/Co obtained in the absence of Co(II)Cbl substrate (Figure 5.2, A). Evidence that these features arise from Co(II) bound to the functionally relevant, divalent metal-ion binding site of EutT is provided by the fact that in the MCD spectrum of EutT^{WT}/Zn in the presence of CoCl2, the intensities of these are reduced ~50-fold (Figure 5.2, B). This results indicates that ~2% of Co(II) is able to bind to the divalent metal site of

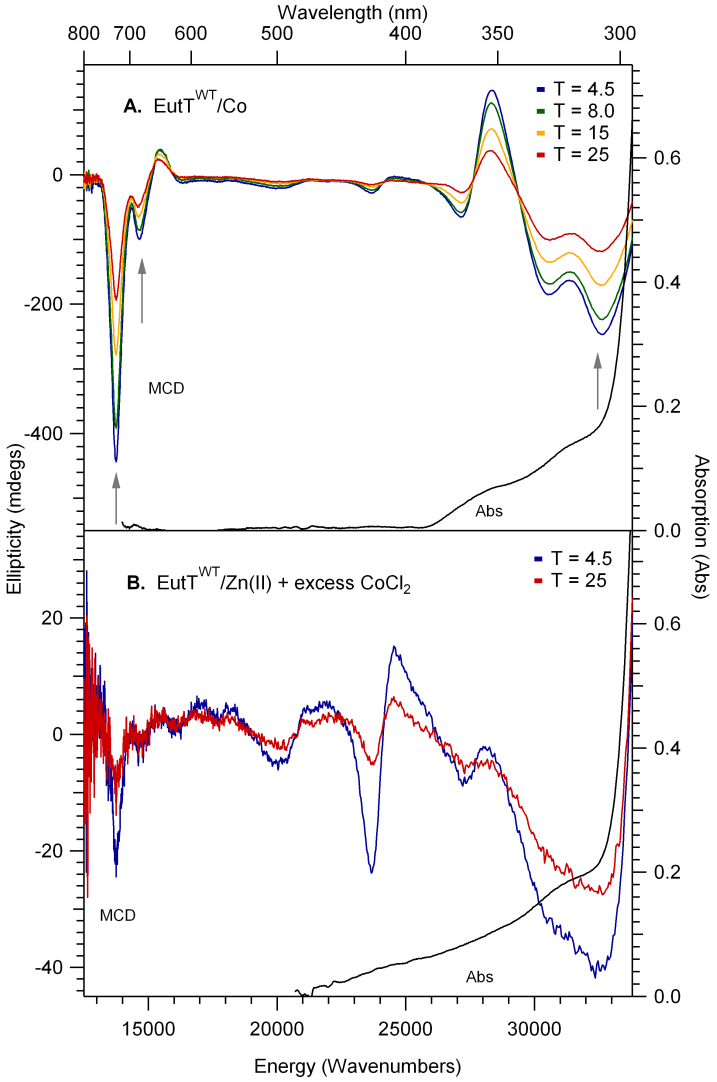

Figure 5.2: LT-Abs spectra collected at 4.5K (black traces) and 7 T VT-MCD spectra of (A) reconstituted EutT^{WT}/Co and (B) as purified EutT^{WT}/Zn with $CoCl_2$. Gray arrows in (A) indicate the bands at which VTVH-MCD data was collected.

EutT^{WT}/Zn, presumably due to slightly substoichiometric incorporation of Zn(II) into this site. Notably, the intensity of the remaining MCD features between 17 000 and 26 000 cm^{-1} does not vary significantly between EutT/Co and EutT/Zn in the

presence of $CoCl_2$. Thus, they must arise from non-specifically bound Co(II) (vide supra).

The features observed at 15 000 and 30 000 cm^{-1} in the MCD spectrum of EutT/Co are reminiscent of those previously observed for metalloenzymes featuring a Co(II) ion in a tetrahedral coordination environment with at least one cysteine ligand. The MCD spectra of these species are characterized by a set low-energy features assigned to the spin-allowed $^4A_2 \rightarrow {}^4T_1(P)$ ligand field (LF) transition in the parent T_d point group and additional features at higher energies attributed transitions containing predominantly S→Co(II) ligand-to-metal charge-transfer (LMCT) character.[30, 31] By analogy, the prominent negative feature at 13 800 cm^{-1} with a shoulder at 14 600 cm^{-1} and positively signed band at 15 500 cm^{-1}, in the MCD spectrum of EutT/Co can be assigned to components of the $^4A_2 \rightarrow {}^4T_1(P)$ LF transition. Notably, the intensity profile and splitting pattern of these features is very similar to that observed for Co(II) bound to the active site of alcohol dehydrogenase (ADH/Co), a Zn(II)-containing enzyme in vivo, as well as Co(II)-substituted stellacyanin, a type-1 blue copper protein.[30, 31] However, the intense negatively-signed feature at 13 800 cm^{-1} in the MCD spectrum of EutT/Co is significantly red-shifted from its counterparts in the ADH/Co and Co(II)-substituted stellcyanin spectra (observed 16 000 to 15 000 cm^{-1}, respectively). A shift of this feature to lower energy has previously been correlated with an increase in the number of thiolate-based ligands of tetrahedral Co(II) complexes, suggesting that multiple cysteine residues may be present at the divalent metal site of EutT.

At higher energies, the MCD spectrum of EutT/Co exhibits a series of intense

bands, including a positive feature at 28 400 cm^{-1} and two negative features at 30 500 and 32 700 cm^{-1} (Figure 5.2, A). The intensities of these features are comparable to those of the lower-energy bands associated with LF transitions, but their widths are significantly larger. Based on their energies and bandwidths, these near-UV features are assigned to S→Co(II) MLCT transitions. Analogous features are observed in the MCD spectra of ADH/Co and Co(II)-bound stellacyanin, as well as Co(II)-substituted rubredoxin proteins known to contain multiple sulfur-based ligands at their active sites.[32] In the case of ADH/Co, MCD features due to S→Co(II) MLCT transitions are observed between 26 000 and 35 000 cm^{-1} for Co(II) bound to the catalytic site (consisting of two cysteine residues, one histidine, and a solvent-derived water molecule) or the structural site (consisting of four cysteine residues), with the intensities of the features arising from the former, less symmetric site being significantly larger. In the case of Co(II)-substituted stellacyanin (which coordinates the metal via a single cysteine residue, two histidines, and the oxygen moiety from a glutamine residue), the S→Co(II) MLCT transitions are centered at 28 000 cm^{-1} with the lowest-energy, positively signed feature located at 25 500 cm^{-1}, considerably lower in energy than its counterpart in the MCD spectrum of EutT/Co. This feature occurs at even lower energies for the Co(II)-substituted forms of the related type-1 copper protein azurin and plastocyanin (24 500 and 22 500 cm^{-1} respectively). Thus, the relatively high energies of the S→Co(II) MLCT transitions observed for EutT/Co are consistent with the presence of at least two cysteine residues at the Co(II)-binding site (which will decrease the Lewis acidity of the metal ion), but the identity of the additional ligand(s) remains unknown.

Additionally, because the MCD spectrum of EutT/Co is very similar to that of Co(II) bound to either the catalytic or structural site of ADH, both of which are known via X-ray crystallography to adopt a fairly regular tetrahedral geometry, it can be concluded that the Co(II) ion of EutT/Co also resides in a weakly distorted tetrahedral coordination environment.[33]

Table 5.1: EPR parameters for Co(II)Cbl in the presence of $EutT^{WT}$/Co. Percent contributions to the overall trace from individual Co(II)Cbl species are highlighted in bold. Parameters for free Co(II)rrinoids from reference 18 are also shown for comparison.

			g-values			A(^{59}Co)			A(^{14}N)		
		%Cont.	g_z	g_y	g_x	A_z	A_y	A_x	A_z	A_y	A_x
A. Free Co(II)Cbl	base-on	**100**	2.004	2.232	2.269	303	30	40	49	49	49
B. Free Co(II)Cbi$^+$	base-off	**100**	1.994	2.314	2.423	402	210	226	*n/a*	*n/a*	*n/a*
C. $EutT^{WT}$/Co + Co(II)Cbl	base-on	**81**	2.004	2.232	2.269	303	30	40	49	49	49
	base-off	**19**	1.991	2.315	2.459	387	222	227	*n/a*	*n/a*	*n/a*
D. $EutT^{WT}$/Co + Co(II)Cbl	base-on	**41**	2.004	2.232	2.269	303	30	40	49	49	49
+ xcs ATP	base-off	**38**	1.991	2.315	2.459	387	222	227	*n/a*	*n/a*	*n/a*
	4c	**21**	1.800	2.573	3.610	760	615	1362	*n/a*	*n/a*	*n/a*

To further clarify the geometry of the metal binding site of EutT/Co, variable-temperature variable-field (VTVH) MCD data were collected at the peak positions of the three most intense bands arising from the $^4A_2 \rightarrow {}^4T_1(P)$ LF and S→Co(II) MLCT transitions (Figure 5.2). Using the MCD theory for S > 1/2 systems derived by Neese and Solomon, the observed MCD saturation behavior was used to obtain spin-Hamiltonian parameters for the Co(II) ion bound to EutT/Co, in particular the sign and magnitude of the zero-field splitting parameter, D.[28] As the VTVH-MCD saturation behavior depends on a total of eight different parameters, the approach

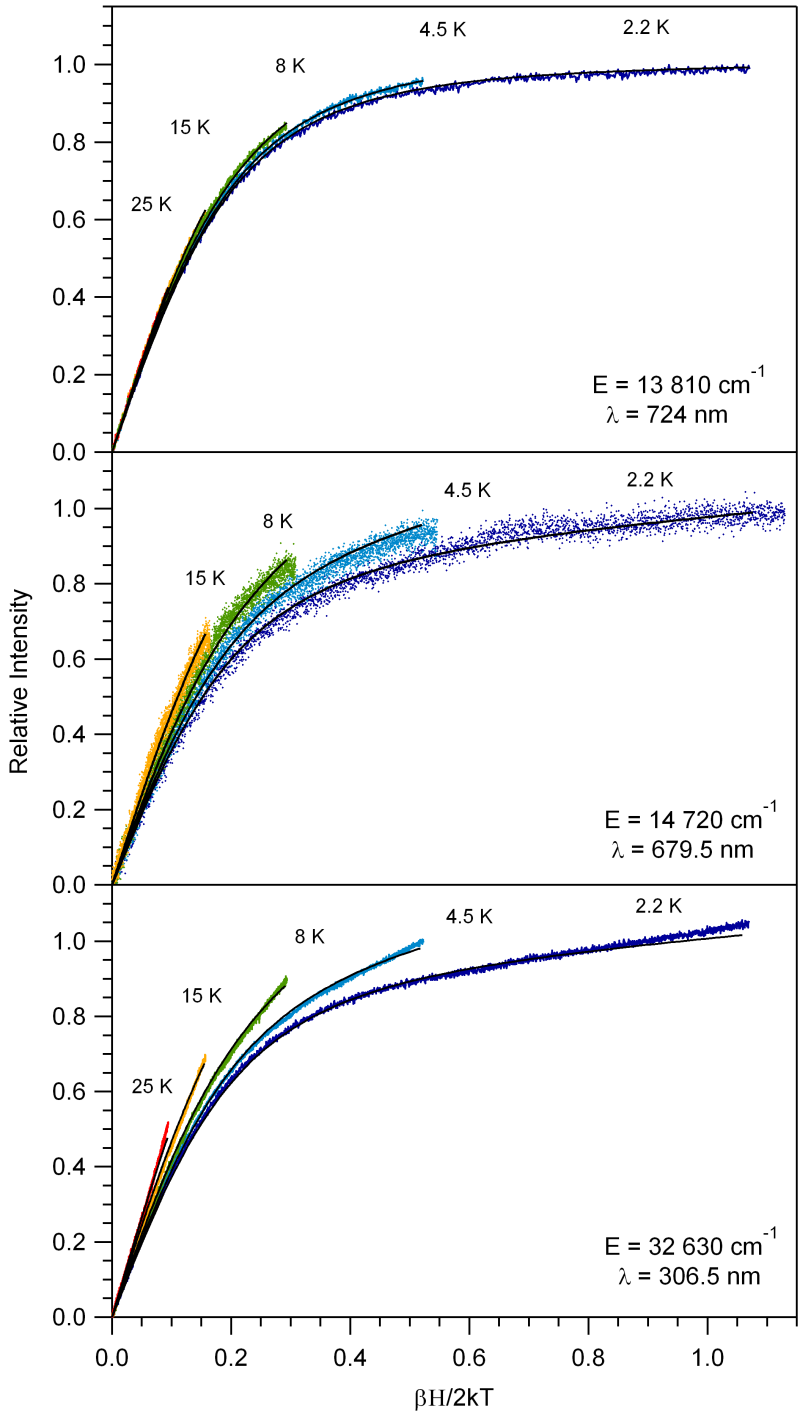

Figure 5.3: Experimental VTVH-MCD data collected at 724, 679.5, and 306.5 nm for $EutT^{WT}$/Co shown as colored dots. Traces were obtained at temperatures of 2.2, 4.5, 8, 15, and 25 K for magnetic fields ranging from 0 to 7 T. Theoretical fits are shown as solid lines.

employed by Fiedler emphet al was used to fit the spin-Hamiltonian parameters.[34] To reduce the number of fit parameters, an isotropic g = 2.20 value was assumed for the Co(II) ion bound to EutT/Co based on the g-values reported for other high-spin, tetra-coordinate Co(II) complexes (note that the fitted values for the remaining spin-Hamiltonian parameters are expected to depend only weakly on the g-values chosen). The sign and value for D were then obtained by systematically varying this parameter and fitting the three transition moment products to achieve the best agreement between the experimental and calculated VTVH-MCD data while keeping the remaining spin-Hamiltonian parameters constant. For each value of D, the goodness of the fit was evaluated by computing the χ^2 value. A similar approach was used to estimate the E/D ratio, which was varied from 0.00 to 0.33 for each value of D considered.

The saturation behaviors of the most intense features in the MCD spectrum of EutT/Co, located at 13 810 and 32 630 cm^{-1} (724 and 306.5 nm respectively), both strongly favor negative values for D. The VTVH MCD data set for the feature at 13 810 cm^{-1}, which exhibits the least amount of nesting, is relatively insensitive to the magnitude of D although a shallow minimum in our fits is observed for D = -10 cm^{-1} and E/D = 0.08. In contrast, the VTVH MCD data obtained at 32 630 cm^{-1} show significant nesting, which requires an E/D ratio close to zero and large negative values for D. An improved estimate of D and E/D was obtained by summation of the χ^2 values for the three individual VTVH MCD data sets to calculate the global χ^2 value, which reached a distinct minimum for values of D = $-$ 13.0(5) cm^{-1} and E/D = 0.08(2). These spin-Hamiltonian values are comparable

to those previously determined for tetra-coordinate Co(II) sites with minor low-symmetry distortions from an ideal tetrahedral geometry, consistent with our MCD results described above.[23, 25, 26]

Effect of amino-acid substitutions on the Co(II)-binding to EutT: Previous studies of EutT/Fe indicated that substitutions of residues in the $HX_{11}CCX_2C(83)$ motif cause large variations in catalytic activity. A spectroscopic characterization of these variants revealed that the 4c Co(II)Cbl yield as well as the degree of Fe(II) incorporation were diminished. Substitution of residues in this motif also results in a dramatic decrease in Co(II) incorporation into EutT (Figure 5.4). Specifically, the ΔMCD spectra of $EutT^{C80A}$/Co and $EutT^{C83A}$/Co exhibit spectroscopic features that are due solely to non-specifically bound Co(II) (Figure 5.4, E and F). This result indicates that residues C80 and C83 are critical for the binding of Co(II) to the enzyme. Previously, both the C80A and C83A substitutions have been shown to strongly suppress Fe(II)-binding to EutT, thereby largely precluding the binding of Co(II)Cbl to the enzyme active site, and kinetic assays indicated that as-isolated $EutT^{C80A}$ is completely inactive, while $EutT^{C83A}$ is capable of very slow turnover. Thus, the available data suggest that both C80 and C83 serve as ligands at the divalent metal site of EutT, with C80 playing a particularly critical role.

The ΔMCD spectrum of $EutT^{C79A}$/Co is nearly identical to that of $EutT^{WT}$/Co, except for a minor (~50 cm^{-1}) blue-shift of the prominent negative feature at 14 000 cm^{-1} (Figure 5.4, B). However, the intensity of this feature is reduced by ~45% from that displayed by the wild-type enzyme, indicating that the C79A substitution results in a large decrease in Co(II) incorporation, mirroring the results obtained

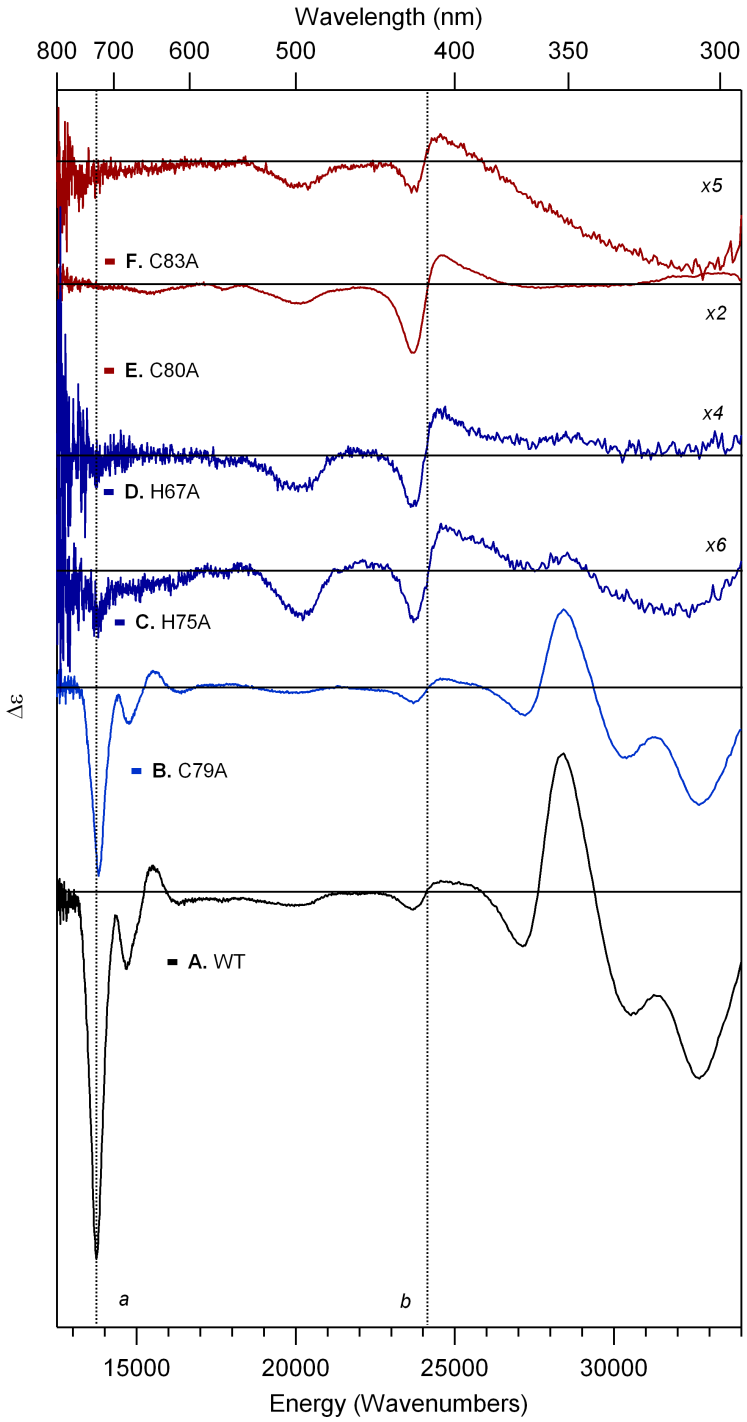

Figure 5.4: ΔMCD spectra of EutTWT/Co(II) and selected variants (colored lines) obtained by subtracting the corresponding MCD spectra collected at 25 K. Panels A-to-G are labeled according to the amino acid substitution(s) introduced in EutT. The main features from the primary metal binding site are highlighted by a dashed vertical line (a). The derivative feature from non-specific Co(II) binding is also noted (b).

previously for Zn(II)- and Fe(II)-binding to this variant. Based on these results, we conclude that the side chain of C79 does not coordinate to the divalent metal ion, but does play an important role in increasing the degree of metal incorporation into EutT. Intriguingly, the ΔMCD spectra of EutT^{H67A}/Co and EutT^{H75A}/Co appear to lack the characteristic features of Co(II) bound to the divalent metal site (Figure 5.4, C and D), even though EutT^{H67A} and EutT^{C79A} have been shown to bind Fe(II) almost stoichiometrically. While weak features are observed in the region where the $^4A_2 \rightarrow {}^4T_1(P)$ LF and S→Co(II) MLCT transitions are expected to occur, the intensities of these features indicate that at most 1% of the divalent metal sites of these variants are occupied by Co(II). Because EutT^{H67A} and EutT^{H75A} remain catalytically active when reconstituted with Fe(II) or Zn(II), our results indicate that the structural changes induced by these substitutions primarily affect the ability of EutT to incorporate Co(II) ions.

Interaction between EutT^{WT}/Co and AdoCbl: The low-temperature Abs, CD, and MCD spectra of AdoCbl in the presence of EutT^{WT}/Co are shown in Figure 5.5. The lowest-energy features observed at ~20 000 cm^{-1} in these spectra are essentially identical to those displayed by free AdoCbl. Because the energies of these features, the so-called α/β-bands, are highly sensitive to changes in the axial ligation, our spectra are consistent with an unperturbed ligand environment of AdoCbl in the presence of EutT^{WT}/Co. The MCD spectrum collected at 4.5 K, which is dominated by temperature-dependent contributions from the paramagnetic Co(II) ions bound to the divalent metal site of EutT, reveals a minute blue-shift of the intense negatively-signed feature due to the $^4A_2 \rightarrow {}^4T_1(P)$ transition along with

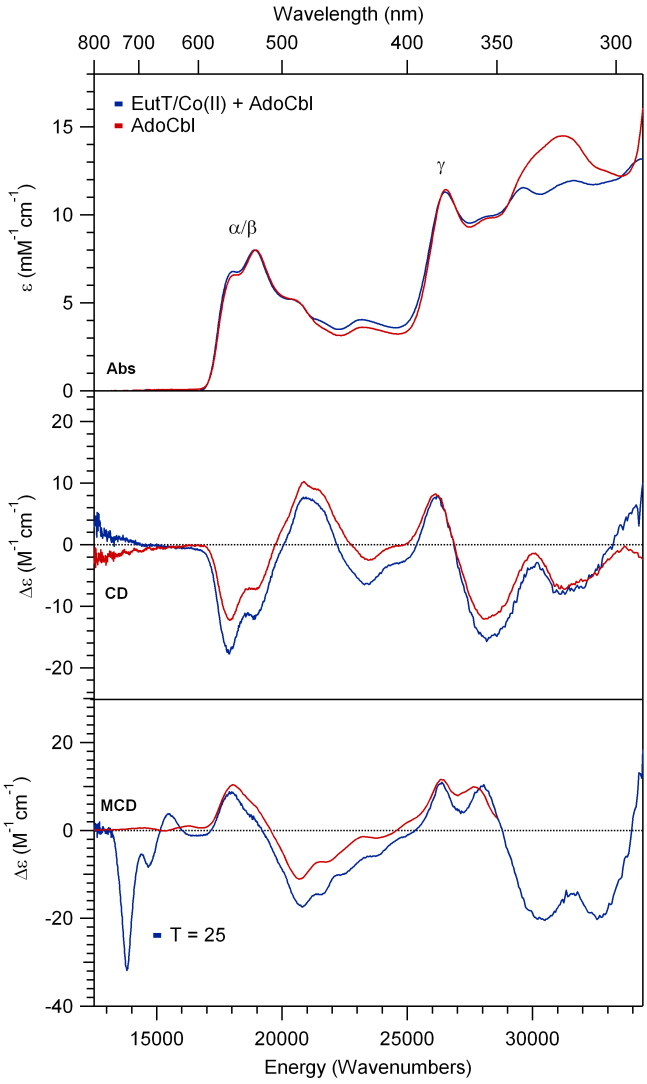

Figure 5.5: CD (Top), MCD (middle), and Abs (bottom) spectra of AdoCbl in the presence of EutTWT/Co (blue), and free in solution (red). Spectra were collected at 4.5K unless otherwise noted.

minor changes in the intensities and positions of the S→Co(II) MLCT features. In contrast, the spectroscopic features associated with non-specifically bound Co(II) ions appear to be dramatically perturbed by the presence of AdoCbl. To remove the

temperature-independent contributions from AdoCbl to this spectrum, the trace obtained at 25 K was subtracted to obtain the ΔMCD spectra shown in Figures 5.6 and 5.7. These difference spectra indicate that all of the spectroscopic features arising from non-specifically bound Co(II) ions are replaced by a new set of bands that have no counterparts in the ΔMCD spectrum of EutT/Co in the absence of AdoCbl (Figure 5.7). This finding indicates that a large fraction of AdoCbl is bound to EutT, despite the lack of changes observed in our spectra of AdoCbl upon the addition of EutT/Co. Thus, our data suggest that once AdoCbl is formed, it remains bound to the EutT active site, albeit in a minimally perturbed, DMB-on conformation.

It is tempting to speculate that in samples of AdoCbl in the presence of Eut-T^{WT}/Co, the non-specific Co(II) binding site of EutT actually corresponds to the Mg^{2+} binding site of MgATP. In the X-ray crystal structures of *Se*CobA and *Lr*PduO, the Mg^{2+} ion is present in an octahedral ligand environment consisting of 3 oxygen atoms from the triphosphate moiety and 2 ordered water molecules in addition the carbonyl oxygen of a nearby asparagine residue. Incorporation of AdoCbl into the EutT active site would necessarily preclude the binding of MgATP, leaving the site where the Mg^{2+} would be located following the transfer of the adenosyl moiety from MgATP to Co(I)Cbl available for Co(II) to bind.

5.5 Discussion

Since its initial identification as an ACAT, the EutT enzyme from Salmonella enterica has been postulated to employ a novel mechanism for generating AdoCbl.[4, 35]

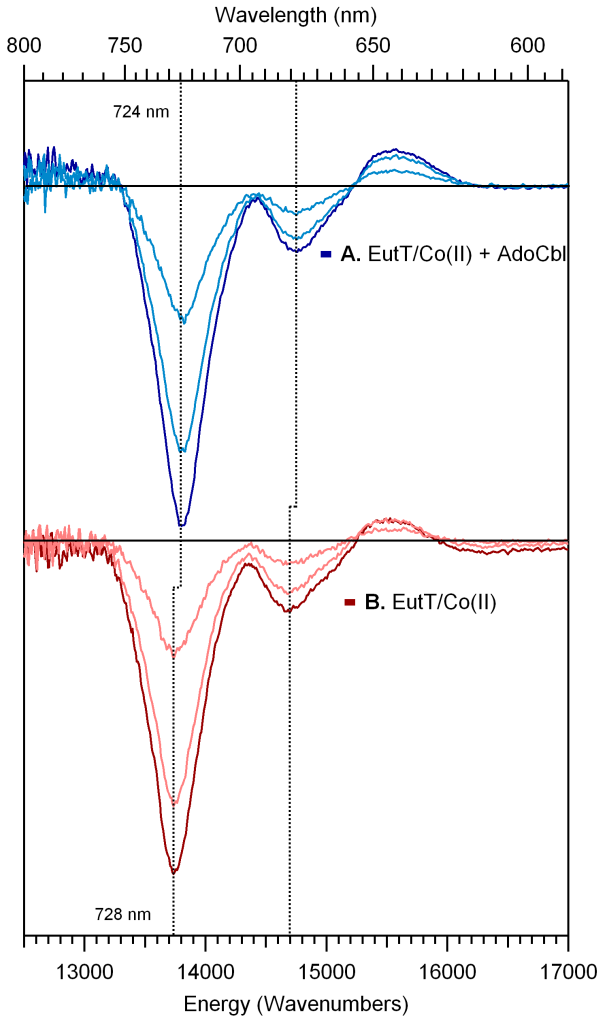

Figure 5.6: ΔMCD spectra of (A) EutT^{WT}/Co with AdoCbl and (B) EutT^{WT}/Co at 4.5, 8 and 15 K obtained by subtracting the corresponding MCD spectra collected at 25 K. Positions of the main features from the primary metal binding are highlighted by dashed vertical lines.

Notably, a divalent transition metal ion was found to be critical for supporting catalytic activity of this enzyme (with Fe(II) or Zn(II) incorporation yielding the highest specific activities). However, while recent experimental studies have provided insight into the unique mechanism employed by EutT for the activation of

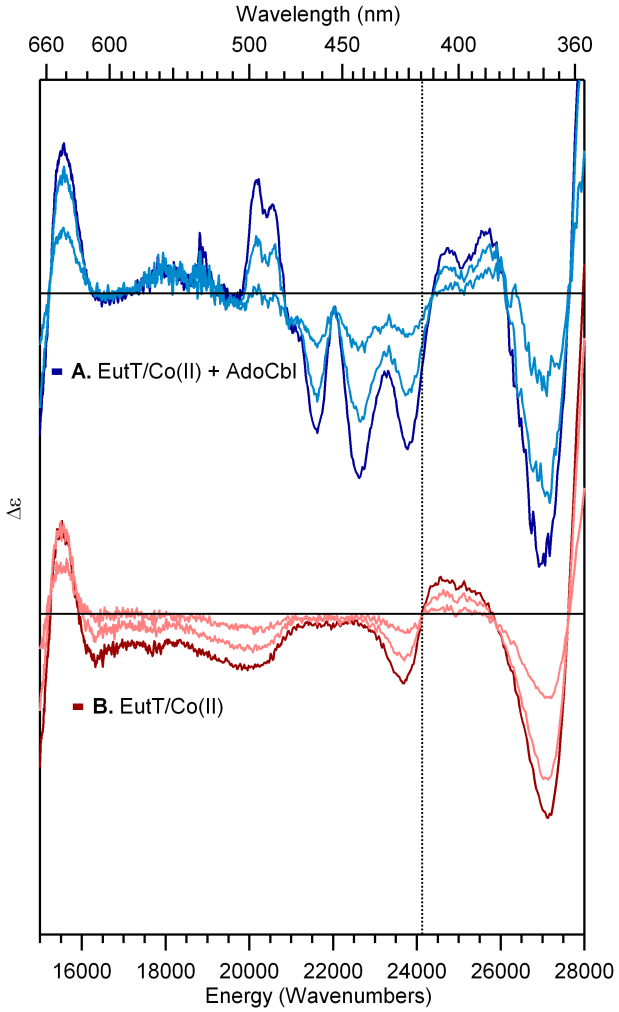

Figure 5.7: ΔMCD spectra of (A) EutT^{WT}/Co(with AdoCbl and (B) EutT^{WT}/Co at 4.5, 8 and 15 K obtained by subtracting the corresponding MCD spectra collected at 25 K. The center position of the main derivative feature from the secondary, non-specific, Co^{2+} binding is highlighted by a dashed vertical line.

the Co(II)Cbl substrate for reduction, the nature of the putative Fe(II)-binding site remained elusive. In this study, we have used Co(II) as a spectroscopic probe of Fe(II) to obtain unprecedented insights into the structure of the divalent metal binding site of EutT and its role in the catalytic cycle of this enzyme.

Nature of the divalent metal binding site of EutT: Based on our spectroscopic data obtained for EutT/Co, the catalytically-relevant divalent metal-binding site where Fe(II) [and possibly Zn(II)] are expected to bind in vivo is tetrahedral with small distortions from ideal symmetry. While fits of our VTVH-MCD studies yielded D and E/D values that are also consistent a five-coordinate site,[25, 26] the energies and intensities of the LF transitions are more consistent with the presence of a four-coordinate Co(II) species.[24, 36] A comparison of the MCD spectra of $EutT^{WT}$/Co and other Co-substituted metalloproteins indicates that two or more cysteine residues are likely ligated to the Co(II) ion in the former. Our findings thus provide compelling evidence for the presence of a M(II)–S(Cys) bond in EutT, as has been inferred previously.[19] LF transitions of tetrahedral, high-spin Fe(II) complexes occur in the near-infrared (<10,000 cm^{-1}) while CT transitions for Fe(II) complexes with thiolate ligation are expected to occur at energies > 33 000 cm^{-1}, which makes it virtually impossible to observe these transitions with our MCD instrument.[37, 38] Introducing single-point alanine substitutions into the $HX_{11}CCX_2C(83)$ motif was found in the present study to cause a drastic reduction in Co(II) binding to EutT, consistent with previous observations linking this motif to Zn(II) and Fe(II) incorporation. The MCD spectra of EutT/Co variants suggest that residues C80 and C83 are critical ligands for this site, in agreement with previous biochemical characterizations of the $EutT^{C80A}$ and $EutT^{C83A}$ variants. Despite the close proximity of residues C79 and C80, our data indicate that $EutT^{C79A}$ binds ~55% as much Co(II) as $EutT^{WT}$, and no differences in the corresponding MCD spectra are observed, ruling out the possibility that C79 also serves as a ligand to the Co(II) ion.

The Co(II) binding site of EutT also appears to be sensitive to removal of the H67 and H75 residues, as the EutT^{H67A} and EutT^{H75A} variants do not show any detectable amounts of Co(II) incorporation. In contrast, both of these variants are capable of binding Fe(II) or Zn(II) and of generating significant amounts of 4c Co(II)Cbl species (~12% and ~26% relative to EutT^{WT}/Fe for EutT^{H67A} and EutT^{H75A} respectively), which provides clear evidence against residues H67 and H75 serving as ligands to the metal center. The fact that the H67A and H75A substitutions have a particularly large effect on Co(II)-incorporation into EutT indicates that this metal ion binds more weakly to the divalent metal site of EutT than Fe(II) or Zn(II), consistent with our observation that Co(II) is unable to displace Zn(II) from EutT^{WT}/Zn.

In summary, our results, along with previous spectroscopic and biochemical studies of EutT, provide strong evidence that C80 and C83 serve as ligands to divalent metal ion, while H67, H75 and C79 play more subtle structural roles. Although our spectroscopic data are most consistent with a tetrahedral geometry and the presence of multiple cysteine sulfur ligands, it is not possible to propose a specific structure for this site. However, as EutT is known to be a dimer in solution and to incorporate one Zn(II) or Fe(II) ion per complex,[19] it is reasonable to assume that both EutT subunits contribute ligands to a single metal site. In this scenario, the C80 and C83 residues from each of the EutT monomers would be involved in Zn(II)-, Fe(II)-, or Co(II)-binding, consistent with the dramatic decrease in metal ion incorporation by EutT in response to the removal of the C80 or C83 side chains.

Examples of tetrahedral cysteine coordination of Zn(II) are provided by Zn-

finger motifs, and in many cases, Co(II) has been used as a spectroscopic probe of these sites.[39, 40] Similar to EutT, the Zn-finger motifs have a higher affinity for Zn(II) than Co(II).[41, 42] Tetrahedral coordination of Fe(II) with 4 cysteine residues is observed for rubredoxins, electron-transfer proteins commonly found in sulfur-metabolizing anaerobic organisms that cycle between the Fe(II) and Fe(III) oxidation states.[43, 44] While we propose that a similar Fe(II) binding site may be present in EutT, it appears to play primarily a structural role critical for the binding of Co(II)Cbl, rather than a role as a redox cofactor. In fact, exposure of $EutT^{WT}$/Fe to molecular oxygen results in the deactivation of the enzyme by preventing it from binding Co(II)Cbl, possibly due to loss of the nascent Fe(III) from the divalent metal site. The stability of rubredoxins has been shown previously to be related to the ability of the protein environment to retain the native fold even in the absence of Fe ions,[45, 46] while strength of the Fe(III)–S(thiolate) bonds and redox properties of this motif have been shown to be modulated by hydrogen-bonding interactions between the enzyme scaffold and the ligating cysteine residues.[47, 48] In contrast, EutT does not retain the proper conformation for Co(II)Cbl binding in the absence of transition metal ions, so the loss of Fe(III) from the divalent metal site upon air-exposure of EutT/Fe is not necessarily unexpected. Also, a role for Fe(II) ions as a structural motif in EutT is not particularly unusual, given the similarities between the divalent metal site of this enzyme and the Zn-finger motifs.[49]

Precedent for divalent metal sites in cobalamin-dependent enzymes: While our spectroscopic data provide compelling evidence for the presence of a tetrahedral divalent metal binding site in EutT, they do not allow for a clear distinction between

2-cysteine and 4-cysteine ligand environments. Besides C80 and C83, no other highly conserved residues of EutT are known to have large deleterious effects on metal incorporation or Co(II)Cbl binding. Thus, the $M(S_{Cys})_4$ model proposed above is the simplest one that accounts for all of the experimental data currently available for EutT. While no other ACATs possess this motif, there are known examples of enzymes that bind corrinoid cofactors and incorporate FeS species in their enzyme folds. The CbiX cobaltochetalase from *B. subtillis*, which participates in the biosynthesis of AdoCbl via insertion of cobalt into a sirohydrochlorin precursor, was shown to contain a 4Fe/4S cluster, although the physiolocal role of this motif remains unknown.[50] Alternatively, corrinoid iron-sulfur proteins (CoFeSPs), which catalyze methyl-transfer reactions, are known to employ a 4Fe/4S cluster for the reactivation of their bound cobalamin cofactor following its accidental oxidation to the Co(II)Cbl state.[51, 52] Finally, recent crystal structures of the AdoCbl-dependent reductive dehalogases PceA from *Sulforospirillum multivorans* and NprdhA from *Nitratireductor pacificus* revealed two 4Fe/4S motifs, approximately ~8 Å and ~12 Å away from the Co center of the corrinoid cofactor. These clusters have been postulated to facilitate the shuttling of electrons from the donors at the protein's surface to the active site containing Co(II)Cbl, which lies buried in the enzyme core.[53, 54] Thus, the presence of a FeS motif in EutT is not unique; however, a single $Fe(S_{cys})_4$ site serving primarily a structural role is a novel feature among corrinoid-binding enzymes.

Effect of metal substitution on EutT activity: Consistent with previous biochemical studies, our spectroscopic data indicate that the substitution of Co(II) for Fe(II)

in EutT^{WT} results in a decrease in the relative yield of 4c Co(II)Cbl by 55%. This is expected to cause a similar drop in the amount of Co(I)Cbl species that can be generated by EutT^{WT}/Co, suggesting that the reduction in the specific activity of EutT observed upon Co(II) substitution is caused by a decrease in the rate of Co(II)→Co(I)Cbl reduction. The MCD features associated with the 4c fraction of Co(II)Cbl in the presence EutT^{WT}/Co are analogous to those observed with EutT^{WT}/Zn and EutT^{WT}/Fe, while the overall shape of the MCD spectrum is nearly identical with that of EutT^{C79A}/Fe. This variant is known to exhibit a ~40% decrease in Fe(II) binding relative to EutT^{WT}/Fe, and a ~60% decrease in the relative yield of 4c Co(II)Cbl. As metal incorporation is known to be critical for the formation of 4c Co(II)Cbl species, the decrease in the specific activity of EutT^{WT}/Co must stem from incomplete Co(II) binding to the divalent metal site, rather than the formation of a perturbed, non-competent active site geometry in the presence of Co(II).

Substitution of Zn(II) for Fe(II) has previously been shown to have no effect on the relative yield of 4c Co(II)Cbl species generated by EutT^{WT}. However, the specific activity of EutT^{WT}/Zn is significantly lower than that of EutT^{WT}/Fe, indicating that the metal substation must affect later steps in the reaction. To this end, it is interesting to note that a structural comparison of the Zn(S_{cys})$_4$ and native Fe(S_{cys})$_4$ motifs in the *Clostridium pasteurianum* rubredoxin revealed that the M(II)–S(Cys) bonds were on average ~0.1 Å longer in the Zn-bound structure [2.345 vs. 2.262 Å].[49] While these differences did not result in drastic perturbations to the enzyme fold of the *C. pasteurianum* rubredoxin, similar structural changes in EutT accompanying Zn(II) substitutions for Fe(II) would affect the Co–C bond formation step by altering

the relative positions of the transiently generated Co(I)Cbl supernucleophile and co-substrate ATP. In support of this proposal, amino acid substations in the active sites of the CobA- and PduO-type ACATs have previously been shown to induce perturbations in the relative positioning of the two substrates and thus to cause a decrease in catalytic activity, despite the fact that the variants retained the ability to generate sizable amounts of 4c Co(II)Cbl.[16, 17]

Role of putative M(S_{cys})$_4$ motif in the catalytic mechanism of EutT: Extensive kinetic and spectroscopic investigations of EutT have provided significant insights into the catalytic mechanism employed by this enzyme. In vivo bioassay studies revealed that EutT is not capable of adenosylating cob(II)inamide (Co(II)Cbi$^+$), a naturally occurring Co(II)Cbl analogue lacking the terminal DMB moiety and nucleotide loop.[6] MCD data indicated that in the presence of EutT and excess ATP, no 4c Co(II)Cbi$^+$ species is being formed, precluding reduction of this alternative substrate to the Co(I) "superreduced" state in the absence of non-physiological reducing agents. When provided with Co(I)Cbi, however, EutT was found to catalyze the adeonsylation step as effectively as with Co(I)Cbl$^-$.[35] Because dissociation of the axially bound water molecule from Co(II)Cbi$^+$ is thermodynamically more facile than the removal of the DMB ligand from Co(II)Cbl, this finding indicated that EutT has a unique requirement of either the nucleotide loop or the terminal DMB moiety for the formation of 4c Co(II)Cbl. A spectroscopic characterization of Co(II)Cbl in the presence of EutT and substoichiometric amounts of ATP disclosed the formation of sizeable amounts of a base-off Co(II)Cbl species, in which the DMB moiety is replaced by a solvent-derived water molecule.[18] This finding suggested

that EutT employs a unique strategy for generating 4c Co(II)Cbl; namely, that it binds the Co(II)Cbl substrate prior to ATP and that in this process, it promotes the dissociation of the DMB moiety to generate a base-off Co(II)Cbl intermediate. In the absence of divalent metal ions (or upon oxygen exposure in the case of EutT^{WT}/Fe), no base-off Co(II)Cbl was observed, and the base-on Co(II)Cbl species did not appear to bind to the EutT active site. Thus, it appears that the M(S_{cys})$_4$ site of EutT/Co serves the role of promoting the dissociation of the DMB ligand upon Co(II)Cbl binding to the enzyme active site. Molecular interactions between the nucleotide loop or terminal DMB moiety and specific residues of EutT in close proximity to the M(S_{cys})$_4$ site could assist in anchoring the cobalamin cofactor in the enzyme, and possibly help maintain the structure of the active site upon formation of 4c Co(II)Cbl. The requirement of these interactions would explain why Co(II)Cbi$^+$ is not adenosylated by EutT. Interestingly, for the previously characterized CobA- and PduO-type ACATs, both of which can adenosylate Co(II)Cbl as well as Co(II)Cbi$^+$, crystallographic evidence exists that rules out any interaction between the protein and the DMB moiety.[11, 15, 23]

The ability of Co(II)Cbl to bind to the active site of EutT in the absence of cosusbtrate MgATP is also unusual. For the other known ACATs, an ordered binding with ATP incorporation occurring before Co(II)Cbl binding was established, which affords an additional level of regulation as to when the Co(I)Cbl supernucleophile is generated. In the case of EutT with Co(II)Cbl bound, the presence of equimolar amounts of ATP results in an increase in the relative amount of base-off Co(II)Cbl species. As a molar excess of ATP co-substrate relative to EutT is needed to promote

4c Co(II)Cbl formation, ATP likely facilitates dissociation of the remaining water ligand from the Co(II) ion. Although the specific mechanism for this step is unclear from the available experimental data, it is tempting to speculate that the H_2O moiety in the base-off Co(II)Cbl generated by EutT is bound on the "upper" (i.e., Coβ) face of the corrin ring, as observed previously for B_{12}-dependent enzymes that bind Co(II)Cbl in the base-off conformation, such as CoFeSPs and methionine synthase (MetH).[55, 56] In this scenario, the binding of MgATP near the Coβ face of Co(II)Cbl, a prerequisite for the adenosyl transfer to Co(I)Cbl, could drive the dissociation of the H_2O ligand from base-off Co(II)Cbl to generate 4c Co(II)Cbl.

Though the exact role of the putative $M(S_{cys})_4$ site of EutT remains unclear, it is interesting to note that FeS clusters have been shown to be used as redox sensors for transcription enzymes to regulate expression under oxidative stress.[57, 58] Given the known deactivation of $EutT^{WT}$/Fe in the presence of molecular oxygen, a possible role of the $M(S_{cys})_4$ motif as s redox sensor seems plausible. In the context of the Eut metabolosome, the $M(S_{cys})_4$ motif of EutT could serve an additional regulatory role to control the levels of AdoCbl generated under aerobic and anaerobic conditions.

5.6 References

[1] Paola E. Mera and Jorge C. Escalante-Semerena. Multiple roles of ATP:cob(I)alamin adenosyltransferases in the conversion of B12 to coenzyme B12. *Applied Microbiology and Biotechnology*, 88(1):41–48, 2010.

[2] Martin J Warren, Evelyne Raux, Heidi L Schubert, and Jorge C Escalante-Semerena. The biosynthesis of adenosylcobalamin (vitamin B12). *Natural product reports*, 19(4):390–412, aug 2002.

[3] J R Roth, J G Lawrence, and T a Bobik. Cobalamin (coenzyme B12): synthesis and biological significance., 1996.

[4] Nicole R Buan, Sang-jin Suh, and Jorge C Escalante-semerena. The eutT Gene of Salmonella enterica Encodes an Oxygen-Labile, Metal-Containing ATP:Corrinoid Adenosyltransferase Enzyme. *Journal of Bacteriology*, 186(17):5708–5714, 2004.

[5] Thomas a. Bobik Celeste L. V. Johnson, Edith Pechonick, Sanghee D. Park, Gregory D. Havemann, Nicole A. Leal. Functional genomics, biochemical, and genetic characterisation of the Salmonella pduO gene, and ATP_Cob(I)alamin adenosyltranseferase gene. *Journal of Bacteriology*, 183(5):1577–1584, 2011.

[6] Nicole R. Buan and Jorge C. Escalante-Semerena. Purification and initial biochemical characterization of ATP:Cob(I)alamin adenosyltransferase (EutT) enzyme of Salmonella enterica. *Journal of Biological Chemistry*, 281(25):16971–16977, 2006.

[7] C. B. Bauer, M. V. Fonseca, H. M. Holden, J. B. Thoden, T. B. Thompson, J. C. Escalante-Semerena, and I. Rayment. Three-dimensional structure of ATP: Corrinoid adenosyltransferase from Salmonella typhimurium in its free state, complexed with MgATP, or complexed with hydroxycobalamin and MgATP. *Biochemistry*, 40(2):361–374, 2001.

[8] J. C. Escalante-Semerena, S. J. Suh, and J. R. Roth. cobA Function is required for both de novo cobalamin biosynthesis and assimilation of exogenous corrinoids in Salmonella typhimurium. *Journal of Bacteriology*, 172(1):273–280, 1990.

[9] Maris V. Fonseca and Jorge C. Escalante-Semerena. An in Vitro Reducing System for the Enzymic Conversion of Cobalamin to Adenosylcobalamin. *Journal of Biological Chemistry*, 276(34):32101–32108, 2001.

[10] Kiyoung Park, Paola E. Mera, Jorge C. Escalante-Semerena, and Thomas C. Brunold. Kinetic and spectroscopic studies of the ATP:corrinoid adenosyltransferase PduO from Lactobacillus reuteri: Substrate specificity and insights into the mechanism of Co(II)corrinoid reduction. *Biochemistry*, 47(34):9007–9015, 2008.

[11] Martin St Maurice, Paola Mera, Kiyoung Park, Thomas C. Brunold, Jorge C. Escalante-Semerena, and Ivan Rayment. Structural characterization of a human-type corrinoid adenosyltransferase confirms that coenzyme B12 is synthesized through a four-coordinate intermediate. *Biochemistry*, 47(21):5755–5766, may 2008.

[12] Martin St. Maurice, Paola E. Mera, María P. Taranto, Fernando Sesma, Jorge C. Escalante-Semerena, and Ivan Rayment. Structural characterization of the active site of the PduO-Type ATP:Co(I)rrinoid adenosyltransferase from Lactobacillus reuteri. *Journal of Biological Chemistry*, 282(4):2596–2605, 2007.

[13] Troy A Stich, Mamoru Yamanishi, Ruma Banerjee, and Thomas C Brunold. Spectroscopic evidence for the formation of a four-coordinate Co2+ cobalamin species upon binding to the human ATP:cobalamin adenosyltransferase. *Journal of the American Chemical Society*, 127(21):7660–7661, 2005.

[14] Troy A. Stich, Nicole R. Buan, Jorge C. Escalante-Semerena, and Thomas C. Brunold. Spectroscopic and computational studies of the ATP:corrinoid adenosyltransferase (CobA) from Salmonella enterica: Insights into the mechanism of adenosylcobalamin biosynthesis. *Journal of the American Chemical Society*, 127(24):8710–8719, 2005.

[15] Theodore C. Moore, Sean a. Newmister, Ivan Rayment, and Jorge C. Escalante-Semerena. Structural insights into the mechanism of four-coordinate cob(II)alamin formation in the active site of the salmonella enterica ATP:Co(I)rrinoid adenosyltransferase enzyme: Critical role of residues Phe91 and Trp93. *Biochemistry*, 51(48):9647–9657, 2012.

[16] Kiyoung Park, Paola E Mera, Jorge C Escalante-semerena, and Thomas C Brunold. Spectroscopic Characterization of Active-Site Variants of the PduO-type ATP : Corrinoid Adenosyltransferase from Lactobacillus reuteri : Insights

into the Mechanism of Four-Coordinate Co (II) corrinoid Formation. *Inorganic Chemistry*, (Ii), 2011.

[17] Ivan G Pallares, Theodore C Moore, Jorge C Escalante-semerena, and Thomas C Brunold. Spectroscopic Studies of the Salmonella enterica Adenosyltransferase Enzyme Se CobA: Molecular-Level Insight into the Mechanism of Substrate Cob(II)alamin Activation. *Biochemistry*, 53:7969–7982, 2014.

[18] Ivan G Pallares, Theodore C Moore, Jorge C Escalante-semerena, and Thomas C Brunold. Spectroscopic studies of the EutT ACAT. *Journal of the American Chemical Society*, (In Review), 2015.

[19] T. C. Moore, P. E. Mera, and J. C. Escalante-Semerena. The EutT Enzyme of Salmonella enterica Is a Unique ATP:Cob(I)alamin Adenosyltransferase Metalloprotein That Requires Ferrous Ions for Maximal Activity. *Journal of Bacteriology*, 196(4):903–910, 2014.

[20] a J Thomson, M R Cheesman, and S J George. Variable-temperature magnetic circular dichroism. *Methods in enzymology*, 226(1966):199–232, 1993.

[21] E I Solomon, T C Brunold, M I Davis, J N Kemsley, S K Lee, N Lehnert, F Neese, a J Skulan, Y S Yang, and J Zhou. Geometric and electronic structure/function correlations in non-heme iron enzymes. *Chemical reviews*, 100(1):235–350, 2000.

[22] Lucia Banci, Alessandro Bencini, Cristiano Benelli, and Dante Gatteschi. Spectral-Structural Correlations in High-Spin Cobalt (II) Complexes. *Structure and Bonding*, (Ii):37–86, 1982.

[23] Mahesh Sundararajan, Dmitry Ganyushin, Shengfa Ye, and Frank Neese. Multireference ab initio studies of zero-field splitting and magnetic circular dichroism spectra of tetrahedral Co(II) complexes. *Dalton transactions (Cambridge, England : 2003)*, (30):6021–6036, 2009.

[24] James F. Riordan and Bert L. Vallee, editors. *Methods in Enzymology*. Academic Press, INC., 1993.

[25] James a Larrabee, Christopher M Alessi, Esi T Asiedu, Justin O Cook, Keith R Hoerning, Lance J Klingler, Gregory S Okin, Stuart G Santee, and Thomas L Volkert. Magnetic Circular Dichroism Spectroscopy as a Probe of Geometric and Electronic Structure of Cobalt (II) -Substituted Proteins : Ground-State Zero-Field Splitting as a Coordination Number Indicator. *Journal of the American Chemical Society*, 119(Ii):4182–4196, 1997.

[26] Lc Kuo and Mw Makinen. Ground term splitting of high-spin cobalt (2+) ion as a probe of coordination structure. 2. The ligand environment of the active site metal ion of carboxypeptidase A in. *Journal of the American Chemical Society*, 6(8):5255–5261, 1985.

[27] Paul G. Blommel and Brian G. Fox. A combined approach to improving large-scale production of tobacco etch virus protease. *Protein Expression and Purification*, 55(1):53–68, 2007.

[28] Frank Neese and Edward I. Solomon. MCD C-Term Signs, Saturation Behavior, and Determination of Band Polarizations in Randomly Oriented Systems with

Spin S > 1/2. Applications to S = 1/2 and S = 5/2. *Symposium A Quarterly Journal In Modern Foreign Literatures*, 52(4):1847–1865, 1999.

[29] Mark J. Nilges. *No Title*. PhD thesis, University of Illinois, Urbana-Champaign, IL, 1979.

[30] Edward Solomon, Jill Rawlings, Ib David R Mcmillin, P J Stephens, and Harry B Gray. Infrared and Visible Circular Dichroism and Magnetic Circular Dichroism Studies. 519(20):8046–8048, 1976.

[31] Mark T Werth, Syou-fen Tang Grazyna, and Formicka Michael. Magnetic Circular Dichroism and Electron Paramagnetic Resonance Studies of Cobalt-Substituted Horse Liver Alcohol Dehydrogenase. *Inorganic Chemistry*, 34(10):218–228, 1995.

[32] S W May and J Y Kuo. Preparation and properties of cobalt(II) rubredoxin. *Biochemistry*, 17(16):3333–3338, 1978.

[33] H Eklund, J P Samma, L Wallén, C I Brändén, A Akeson, and T a Jones. Structure of a triclinic ternary complex of horse liver alcohol dehydrogenase at 2.9 A resolution. *Journal of molecular biology*, 146(4):561–587, 1981.

[34] J. Krzystek, S. a. Zvyagin, Andrew Ozarowski, Adam T. Fiedler, Thomas C. Brunold, and Joshua Telser. Definitive Spectroscopic Determination of Zero-Field Splitting in High-Spin Cobalt(II). *Journal of the American Chemical Society*, 126(7):2148–2155, 2004.

[35] Kiyoung Park, Paola E. Mera, Theodore C. Moore, Jorge C. Escalante-Semerena, and Thomas C. Brunold. Unprecedented Mechanism Employed by the Salmonella enterica EutT ATP:Co ^I rrinoid Adenosyltransferase Precludes Adenosylation of Incomplete Co ^{II} rrinoids. *Angewandte Chemie International Edition*, pages n/a–n/a, 2015.

[36] Dennis W. Darnall and Ralph G. Wilkins, editors. *Methods for Determining Metal Ion Environments in Proteins*. Elsevier/Noth-Holland, New York, New York, 1980.

[37] Edward I Solomon, Robert K Szilagyi, Serena Debeer George, and Lipika Basumallick. Electronic Structures of Metal Sites in Proteins and Models : Contributions to Function in Blue Copper Proteins Electronic Structures of Metal Sites in Proteins and Models : Contributions to Function in Blue Copper Proteins. *Chemical reviews*, 104(January):419–458, 2004.

[38] S J Yoo, J Meyer, C Achim, J Peterson, M P Hendrich, and E Münck. Mössbauer, EPR, and MCD studies of the C9S and C42S variants of Clostridium pasteurianum rubredoxin and MDC studies of the wild-type protein. *Journal of biological inorganic chemistry : JBIC : a publication of the Society of Biological Inorganic Chemistry*, 5(4):475–487, 2000.

[39] S. Sri Krishna, Indraneel Majumdar, and Nick V. Grishin. Structural classification of zinc fingers. *Nucleic Acids Research*, 31(2):532–550, 2003.

[40] Marcel J. Lachenmann, John E. Ladbury, Jian Dong, Kun Huang, Paul Carey, and Michael a. Weiss. Why zinc fingers prefer zinc: Ligand-field symmetry and

the hidden thermodynamics of metal ion selectivity. *Biochemistry*, 43(44):13910–13925, 2004.

[41] Edyta Kopera, Tanja Schwerdtle, Andrea Hartwig, and Wojciech Bal. Co(II) and Cd(II) substitute for Zn(II) in the zinc finger derived from the DNA repair protein XPA, demonstrating a variety of potential mechanisms of toxicity. *Chemical Research in Toxicology*, 17(11):1452–1458, 2004.

[42] Todor Dudev and Carmay Lim. Metal Binding and Selectivity in Zinc Proteins. *Journal of the Chinese Chemical Society*, 50:1093–1102, 2003.

[43] Heribert Cypionka. Oxygen respiration by Desulfovibrio species. *Annu. Rev. Microbiol.*, 54:827–848, 2000.

[44] Jacques Meyer. Iron-sulfur protein folds, iron-sulfur chemistry, and evolution. *Journal of Biological Inorganic Chemistry*, 13(2):157–170, 2008.

[45] Satya Prakash, Monica Sundd, and Purnananda Guptasarma. The key to the extraordinary thermal stability of P. furiosus holo-rubredoxin: Iron binding-guided packing of a core aromatic cluster responsible for high kinetic stability of the native structure. *PLoS ONE*, 9(3), 2014.

[46] Vikas Nanda, Michael M. Rosenblatt, Artur Osyczka, Hidetoshi Kono, Zelleka Getahun, P. Leslie Dutton, Jeffery G. Saven, and William F. DeGrado. De novo design of a redox-active minimal rubredoxin mimic. *Journal of the American Chemical Society*, 127(16):5804–5805, 2005.

[47] Peng Zheng, Shin-ichi J Takayama, a Grant Mauk, and Hongbin Li. Hydrogen Bond Strength Modulates the Mechanical Strength of. *Journal of the American Chemical Society*, 2012.

[48] ABHISHEK DEY EDWARD I. SOLOMON, SERGE I. GORELSKY. Metal–Thiolate Bonds in Bioinorganic Chemistry EDWARD. *Journal of computational chemistry*, 27:1415–1428, 2006.

[49] Z Dauter, K S Wilson, L C Sieker, J M Moulis, and J Meyer. Zinc- and iron-rubredoxins from Clostridium pasteurianum at atomic resolution: a high-precision model of a ZnS4 coordination unit in a protein. *Proceedings of the National Academy of Sciences of the United States of America*, 93(17):8836–8840, 1996.

[50] Helen K. Leech, Evelyne Raux, Kirsty J. McLean, Andrew W. Munro, Nigel J. Robinson, Gilles P M Borrelly, Marco Malten, Dieter Jahn, Stephen E J Rigby, Peter Heathcote, and Martin J. Warren. Characterization of the cobaltochelatase CbiXL: Evidence for a 4Fe-4S center housed within an MXCXXC motif. *Journal of Biological Chemistry*, 278(43):41900–41907, 2003.

[51] Tatiana Svetlitchnaia, Vitali Svetlitchnyi, Ortwin Meyer, and Holger Dobbek. Structural insights into methyltransfer reactions of a corrinoid iron-sulfur protein involved in acetyl-CoA synthesis. *Proceedings of the National Academy of Sciences of the United States of America*, 103(39):14331–14336, 2006.

[52] S. W. Ragsdale, P. a. Lindahl, and E. Münck. Mössbauer, EPR, and optical studies of the corrinoid/iron-sulfur protein involved in the synthesis of acetyl

coenzyme A by Clostridium thermoaceticum. *Journal of Biological Chemistry*, 262(29):14289–14297, 1987.

[53] Karl a. P. Payne, Carolina P. Quezada, Karl Fisher, Mark S. Dunstan, Fraser a. Collins, Hanno Sjuts, Colin Levy, Sam Hay, Stephen E. J. Rigby, and David Leys. Reductive dehalogenase structure suggests a mechanism for B12-dependent dehalogenation. *Nature*, 517(7535):513–516, 2014.

[54] Martin Bommer, Cindy Kunze, Jochen Fesseler, Torsten Schubert, and Gabriele Diekert. Structural basis for organohalide respiration. *Science*, 2871(2010):2741–2745, 2014.

[55] Sandra E. Hennig, Sebastian Goetzl, Jae-Hun Jeoung, Martin Bommer, Friedhelm Lendzian, Peter Hildebrandt, and Holger Dobbek. ATP-induced electron transfer by redox-selective partner recognition. *Nature communications*, 5:4626, jan 2014.

[56] Matthew D. Liptak, Supratim Datta, Rowena G. Matthews, and Thomas C. Brunold. Spectroscopic study of the cobalamin-dependent methionine synthase in the activation conformation: Effects of the Y1139 residue and S-adenosylmethionine on the B12 cofactor. *Journal of the American Chemical Society*, 130(48):16374–16381, dec 2008.

[57] Jeffrey Green and Mark S Paget. Bacterial redox sensors. *Nature reviews. Microbiology*, 2(12):954–966, 2004.

[58] F Wayne Outten and Elizabeth C Theil. Iron-based redox switches in biology. *Antioxidants & redox signaling*, 11(5):1029–1046, 2009.

Chapter 6

Outlook

6.1 Concluding Remarks

B_{12} cofactors are employed by a variety of enzymes catalyze unique chemical transformations. These include the formation of an organometallic bond between the Co ion of cobalamin and substrate in the case of ATP:Co(I)rrinoid adenosyltransferases (ACATs) and methyltranferases, and the mediation of radical-mediated rearrangement of substrates (e.g. Ethanolamine Ammonia Lyase (EAL) and related AdoCbl-dependent enzymes). These enzymes require the formation of "activated" cobalamin species for catalysis, such as the formation of a highly reduced Co(I) cobalamin (Co(I)Cbl) "supernucleophile" in the active site for the case of ACATs. Other enzyme bound species of cobalamins are implicated in the acceleration of the homolytic cleavage of the Co–C(Ado) bond of AdoCbl to generate an 5‘-deoxyadenosyl-based radical and Co(II) cobalamin (Co(II)Cbl). This is a critical first step in the mechanism of AdoCbl-dependent enzymes. More recently, reductive dehalogenases (RDases), enzymes implicated in the bioremediation of organohalides, have been postulated to employ unique cobalamin intermediates in a novel reaction mechanism. However, little is known about the particular cobalamin species involved, and their role in catalysis.

Thus, despite their biochemical importance, many unresolved issues remain in the proposed mechanisms of many B_{12} utilizing enzymes, in particular with the role of the enzyme scaffold on promoting catalysis. For instance, reactive Co(I)Cbl species are postulated in various enzyme mechanisms, in particular for that of ACATs, however spectroscopic characterization of Co(I)Cbl bound to enzyme ac-

tives site during turnover has been difficult due to the high reactivity of this species and its quick oxidation in the presence of oxygen. This has limited the understanding how enzymes stabilize Co(I)rrinoids species in their active sites and how they are able to control the nucleophillicity of this transiently generated species. In the case of AdoCbl-dependent enzymeslittle is known about the mechanism of Class II enzymes, such as the ethanolamine ammonia lyase (EAL) from *Salmonella enterica*, which bind their cofactors in a base-on conformation (or Class 2 enzymes). Unlike Class I enzymes, which are present with their cofactors bound to a protein-derived histidine moiety, Class II enzymes are expected to employ a distinct mechanism to facilitate the homolysis of the Co–C(Ado) bond of their AdoCbl cofactors. Lastly, very little is known about the cobalamin species involved in the mechanism of reductive dehalogenases (RDases). Recent crystallographic and spectroscopic results have suggested the presence of halogenated cobalamin species relevant for the catalytic cycle of these enzymes; however the role of these in mediating the overall reaction remains to be determined. Spectroscopic and computational methods can provide a powerful tool for the study of these enzymes. In many cases, spectroscopic and biochemical approaches may be the sole source of information available to study the properties of relevant intermediates generated along the catalytic cycle. For instance, the spectroscopic and biochemical date reported on the EutT ACAT from *Salmonella enterica* have been the first to elucidate the approach by which this enzyme generates AdoCbl from Co(II)Cbl and ATP. Notably, in the absence of any structural information of the structure of this enzyme, these methods provide the only available information about the role of the EutT active site in modulating the

reactivity of its substrates. By comparison to the structures and spectroscopic properties of known cobalamin species as well as computational models, spectroscopic methods are thus well suited to the study of systems of unknown structure by providing a direct probe into their reactivity. From these observations, the following studies are proposed.

I. Biosynthesis of Coenzyme B_{12}: Previous spectroscopic studies of ACATs have provided compelling evidence that 4c Co(II)rrinoid species are generated in the catalytic cycle of these enzymes (Chapters 2 and 3). However, details regarding subsequent steps in the proposed mechanism remain unclear. Subsequence reduction of these species to generate Co(I)rrinoids has been implicated as a critical step in the adenosylation step. However, a direct characterization of these "supernucleophilic" species during enzymatic turnover has not yet been accomplished. Due to distinct spectroscopic properties of Co(I) and Co(II) corrinoids, electronic absorption and circular dichroism (CD) spectroscopies are uniquely suited to monitor the Co(II)→Co(I)rrinoid reduction in the CobA and EutT active sites complexed with ATP, in the presence of biological reductants (e.g. the FldA/Fpr reducing system and FMN and NADHP).[1] These experiments would also conform the identity of the reducible Co(II) species generated in the ACAT active sites. While MCD and EPR studies of ACATs have revealed that enzyme-bound Co(II)rrinoids can be present in base-on, base-off, and 4c conformations, it has been suggest that only 4c Co(II) species can be converted to Co(I) by reducing agents available in the cell, based on the chemical properties of these species. Because the room-temperature (RT) CD spectra of base-off Co(II)Cbl (or Co(II)Cbi^+) and 4c Co(II)rrinoid species are

strikingly different,[2] CD studies in particular are uniquely suited to monitor the generation of this species in aqueous solution. Furthermore, shifts observed for the LF transitions of the subsequently transient Co(I)Cbi species relative to free Co(I)Cbl can be used to monitor perturbations Co $3d_{z^2}$-based molecular orbital in the enzyme intermediate. Notably, perturbations to this orbital reflect changes in the nucleophillicity of the Co(I) species, as it holds the valance electrons that are involved in the S_{N^2} attack of the 5'C atom of ATP. Based on the results presented in Chapters 2 and 3, absorption and CD experiments of the *Salmonella enterica* CobA and EutT(Zn) ACATs are promising targets for these studies. In the case of CobA, several variants have been identified that generate variable amounts of base-on, base-off, and 4c Co(II)rrinoids. By collecting absorption and CD spectra as a function of reducing equivalents added, the reducible fraction of Co(II)rrinoids generated in the CobA active site can be characterized. Similarly, MCD studies of the air-stable EutT(Zn) presented in Chapter 3 identify several variants suitable for absorption and CD studies. Since the relative populations of base-on, base-off, and 4c Co(II)Cbl species vary considerably as a function of ATP incorporation into the enzyme active site, the effect of the concentration of this co-substrate on the formation of Co(I)Cbl can he further characterized. The ability of ACATs to generate Co(I)rrinoid species under aerobic conditions is remarkable. However, these species have been difficult to characterize spectroscopically, as their rapid reaction with co-substrate ATP prevents them from accumulating in high yield. Based on the results presented in Chapter 2, $CobA^{F91W}$ variant appears to be a good candidate to study these Co(I) species, as this enzyme it generates significant amounts of 4c

Co(II)Cbi$^+$, but produces AdoCbi$^+$ at more than a 10-fold reduced rate than the wild-type enzyme.[3] Likely, a large build-up of Co(I)Cbi$^+$ occurs in the active site of the CobA^{+F91W}/ATP complex following the addition of a reducing agent, which will permit a characterization of this species by various spectroscopic methods. In the absence of structural data for EutT, it is difficult to identify specific amino acid residues that could modulate the nucleophillic properties of the Co(I)Cbl intermediate. However, absorption and CD studies of EutT in the presence of ATP analogues are a promising route. EutT is capable of generating AdoCbl when presented with ADP (with retention of 80% of specific activity) and dATP (31% activity), while no activity was observed with AMP.[4,5] Although it is not currently known if the binding of ATP analogues to EutT suppresses the formation of enzyme-bound 4c Co(II)Cbl, it seems more likely that changes to the native substrate primarily affect the adenosylation step due to an inadequate positioning of the 5‘ carbon of the substrate analogues. These hypotheses can be tested with the spectroscopic approach presented in Chap 3.

II. Mechanism of B_{12}-dependent dehalogenation: Spectroscopic and computational studies of the PceA RDase from *S. multivorans* are well suited to examine the interaction between the corrinoid cofactor and the active site of RDases and to characterize key intermediates in the catalytic cycle. In the proposed mechanism for RDases, the corrinoid species involved in the elimination of the halide moiety from substrates is in the Co(I) state, while in the resting state of the enzymes the cofactor is present in the Co(II) state. The in vivo reducing agent that supplies electrons to these enzymes remains unidentified, although it has been suggested that a

ferrodoxin/NAPDH system may be involved. Using the spectroscopic approach presented in earlier chapters and outlined above, studies of Co(II) and Co(I) species bound to PceA can be employed to establish the coordination environment of the norpseudo-Co(II)Cbl cofactor in PceA, determine if the binding of substrate triggers any conformational changes of the cofactor, and quantify the relative populations of different species if the cofactor adopts numerous conformations. Specifically these studies can be used to identify the nature of the Co–X(halide) interaction postulated in the mechanism of NprdhA and related RDases.[6,7] The spectroscopic data obtained in these studies will also provide valuable information for the generation of models of the putative intermediates in the catalytic cycle of PceA via whole-protein QM/MM geometry optimizations. Viable models of these intermediates can be generated on the basis of the crystal structure of PceA in the presence of TCE and using the insights gained in our spectroscopic studies aimed at discriminating between pathways involving homolytic or heterolytic C–X(Halide) bond cleavage. Validation of the computational models can be carried by my comparison to compute spectroscopic observables of the QM regions these to spectroscopically characterized enzyme species. These models can help identify key active site residues that will become the target of subsequent site-directed mutagenesis experiments, as well as providing a experimentally-validated molecular model for the mechanism of these enzymes.

6.2 References

[1] Mathew D Liptak and Thomas C Brunold. Spectroscopic and computational studies of Co1+cobalamin: spectral and electronic properties of the "superreduced" B12 cofactor. *Journal of the American Chemical Society*, 128(28):9144–56, jul 2006.

[2] Kiyoung Park. *Spectroscopic and Computational Studies of Corrinoids*. Ph.d., University of Wisconsin Madison, 2010.

[3] Theodore C. Moore, Sean a. Newmister, Ivan Rayment, and Jorge C. Escalante-Semerena. Structural insights into the mechanism of four-coordinate cob(II)alamin formation in the active site of the salmonella enterica ATP:Co(I)rrinoid adenosyltransferase enzyme: Critical role of residues Phe91 and Trp93. *Biochemistry*, 51(48):9647–9657, 2012.

[4] Nicole R Buan, Sang-jin Suh, and Jorge C Escalante-semerena. The eutT Gene of Salmonella enterica Encodes an Oxygen-Labile, Metal-Containing ATP:Corrinoid Adenosyltransferase Enzyme. *Journal of Bacteriology*, 186(17):5708–5714, 2004.

[5] Nicole R. Buan and Jorge C. Escalante-Semerena. Purification and initial biochemical characterization of ATP:Cob(I)alamin adenosyltransferase (EutT) enzyme of Salmonella enterica. *Journal of Biological Chemistry*, 281(25):16971–16977, 2006.

[6] Karl a. P. Payne, Carolina P. Quezada, Karl Fisher, Mark S. Dunstan, Fraser a. Collins, Hanno Sjuts, Colin Levy, Sam Hay, Stephen E. J. Rigby, and David Leys. Reductive dehalogenase structure suggests a mechanism for B12-dependent dehalogenation. *Nature*, 517(7535):513–516, 2014.

[7] Martin Bommer, Cindy Kunze, Jochen Fesseler, Torsten Schubert, and Gabriele Diekert. Structural basis for organohalide respiration. *Science*, 2871(2010):2741–2745, 2014.

DISCARD THIS PAGE

COLOPHON

Additional content available from the University of Wisconsin Library, and online at pubs.acs.org.

Written in Madison, Wisconsin, at 313 N. Livingston during the summer of 2015. Typesetting done with LaTeX and the Wisconsin thesis template, at Brenham, Texas. 8443 Woodlands Rd on December 2015. Sent from the museum of 4 in the morning.

qtπ, here is to nothing but blue skies,
wind at your back, and a clear path ahead.